

V030000917

GJO-98-39-TAR  
GJO-HAN-18

Hanford Tank Farms Vadose Zone

# C Tank Farm Report

July 1998



U.S. Department  
of Energy

**GRAND JUNCTION OFFICE**

*Work Performed Under DOE Contract No. DE-AC13-96GJ87335 for the U.S. Department of Energy  
Approved for public release; distribution is unlimited.*

This report was prepared as an account of work sponsored by an agency of the United States Government. Neither the United States Government nor any agency thereof, nor any of their employees, makes any warranty, express or implied, or assumes any legal liability or responsibility for the accuracy, completeness, or usefulness of any information, apparatus, product, or process disclosed in this report, or represents that its use would not infringe privately owned rights. Reference herein to any specific commercial product, process, or service by trade name, trademark, manufacturer, or otherwise, does not necessarily constitute or imply its endorsement, recommendation, or favoring by the United States Government or any agency thereof. The views and opinions of authors expressed herein do not necessarily state or reflect those of the United States Government or any agency thereof.

MEMO TO: Distribution  
FROM: Jim Bertsch, Project Manager  
MACTEC-ERS  
DATE: July 9, 1998  
SUBJECT: C Tank Farm Report (Final)

Please find enclosed a copy of the subject report. The official letter will be coming from DOE-GJO Project Manager, Mr. Joel Berwick.

Should you have any questions or comments, please contact me at (509) 946-3635.

JFB:jmm  
Enclosure

cc: JFB LB

Distribution:

C. Abraham, GAO	S. Narbutovskih, PNNL
S. Agnew, LANL	PNNL Technical Library
C. Babel, DOE-RL	J. Poppiti, DOE-RL
D. Barnes, LMHC	D. Powaukee, Nez Perce Indian Nation
J. Berwick, DOE-GJO	C. Ruud, WDOE
C. Brevick, LMHC	D. Shafer, DOE-RL
M. Butherus, MACTEC-ERS	D. Sherwood, EPA
Central Files, LMHC ✓	W. Steele, MACTEC-ERS
G. deBruler, Columbia River United	S. Stokes, DNFSB, (2)
M. Dexter, LMHC	M. Thompson, DOE-RL
D. Dunning, Oregon Office of Energy	T. Traub, PNNL
E. Fredenburg, LMHC	C. West, DOE-RL
M. Gossett, MACTEC-ERS (3)	J. Wilkinson, Umatilla Indian Nation
M. Graham, BHI	J. Williams, FDH
Hanford File	
Jacobs Engineering Group	
R. Jim, Yakama Indian Nation	
S. Leja, WDOE	
R. Lober, DOE-RL	
S. McKinney, WDOE	
D. Myers, LMHC	

C:\MyFiles\Letterbook\FY98\98-110

**Hanford Tank Farms Vadose Zone**

**C Tank Farm Report**

**July 1998**

Prepared for  
U.S. Department of Energy  
Richland Operations Office  
Richland Washington

Prepared by  
U.S. Department of Energy  
Albuquerque Operations Office  
Grand Junction Projects Office  
Grand Junction, Colorado

# Contents

	Page
<b>Signature Page</b> .....	xi
<b>Executive Summary</b> .....	xiii
<b>1.0 Introduction</b> .....	1
<b>2.0 Purpose and Scope</b> .....	2
2.1 Purpose of the Project .....	2
2.2 Scope of the Project .....	2
2.3 Regulatory Basis .....	3
2.4 Purpose of the Report .....	4
<b>3.0 Radionuclides of Interest</b> .....	5
3.1 Cesium-137 ( <sup>137</sup> Cs) .....	6
3.2 Cobalt ( <sup>60</sup> Co) .....	6
3.3 Europium-152 ( <sup>152</sup> Eu) and Europium-154 ( <sup>154</sup> Eu) .....	7
3.4 Strontium-90 ( <sup>90</sup> Sr) .....	8
3.5 Antimony-125 ( <sup>125</sup> Sb) .....	9
3.6 Technetium-99 ( <sup>99</sup> Tc) .....	9
3.7 Uranium .....	10
3.8 Plutonium, Americium-241 ( <sup>241</sup> Am), Iodine, Neptunium-237 ( <sup>237</sup> Np), and Ruthenium-106 ( <sup>106</sup> Ru) .....	11
<b>4.0 Geology and Hydrogeology</b> .....	12
4.1 Regional Geology .....	12
4.1.1 Geologic Structure of the Pasco Basin .....	13
4.1.2 Stratigraphy of the Pasco Basin .....	13
4.1.2.1 Columbia River Basalt Group .....	14
4.1.2.2 Ringold Formation .....	14
4.1.2.3 Plio-Pleistocene Unit .....	15
4.1.2.4 Early Palouse Unit .....	15
4.1.2.5 Pre-Missoula Gravels .....	15
4.1.2.6 Hanford Formation .....	16
4.1.2.7 Holocene Surficial Sediments .....	17
4.2 C Tank Farm Geology Description .....	17
4.3 C Tank Farm Hydrogeology .....	18
4.4 Groundwater Monitoring and Contamination in the C Tank Farm Area .....	21
<b>5.0 C Tank Farm Background</b> .....	22
5.1 Construction .....	22
5.2 History and Tank Contents .....	23

## Contents (continued)

	Page
5.3 Current Status .....	25
5.4 Unplanned Releases .....	26
5.5 Leak-Detection Monitoring .....	29
5.6 Vadose Zone Monitoring Boreholes .....	29
5.7 Gross Gamma Logging .....	31
5.8 Previous Spectral Gamma-Ray Characterizations .....	33
<b>6.0 Adjacent Waste Handling Facility Information .....</b>	<b>35</b>
6.1 216-C-8 French Drain .....	35
6.2 244-CR Vault .....	35
6.3 241-C-301C Catch Tank .....	35
6.4 241-C-801 Cesium Loadout Facility .....	36
<b>7.0 Spectral Gamma Logging Measurements .....</b>	<b>36</b>
7.1 Equipment .....	36
7.2 Calibrations .....	37
7.3 Logging Process and Procedures .....	39
7.4 Data Management .....	40
7.5 Data Analysis .....	41
<b>8.0 Log Data Results .....</b>	<b>42</b>
8.1 Instrumentation Performance .....	42
8.2 Radionuclides Detected .....	43
8.3 Log Plots .....	43
8.4 Tank Summary Data Reports .....	44
8.5 Shape Factor Analysis .....	44
8.5.1 Specific Shape Factors .....	45
8.5.2 Interpretation of Shape Factors .....	46
8.5.3 Uncertainties of Shape Factor Analysis .....	47
8.6 Interpreted Data Set Used for the Development of the Visualizations .....	47
8.6.1 Boreholes Surrounding Tank C-101 .....	49
8.6.2 Boreholes Surrounding Tank C-103 .....	49
8.6.3 Boreholes Surrounding Tank C-104 .....	50
8.6.4 Boreholes Surrounding Tank C-105 .....	50
8.6.5 Boreholes Surrounding Tank C-106 .....	51
8.6.6 Boreholes Surrounding Tank C-107 .....	51
8.6.7 Boreholes Surrounding Tank C-108 .....	52
8.6.8 Boreholes Surrounding Tank C-109 .....	52
8.6.9 Boreholes Surrounding Tank C-110 .....	52
8.6.10 Boreholes Surrounding Tank C-111 .....	53
8.6.11 Boreholes Surrounding Tank C-112 .....	53

## Contents (continued)

	Page
<b>9.0 Development of the Geostatistical Model and the Three-Dimensional Contaminant Visualizations</b> .....	53
9.1 Introduction .....	53
9.2 Geostatistical Structural Model .....	55
9.3 Three-Dimensional Plume Calculations and Creation of the Visualizations .....	56
9.4 Potential Geostatistical Model and Visualization Uncertainties and Inaccuracies .....	57
<b>10.0 Discussion of Results</b> .....	59
10.1 Surface and Near-Surface Contamination .....	59
10.2 Tank-by-Tank Discussion .....	62
10.2.1 Tank C-101 .....	63
10.2.2 Tank C-102 .....	64
10.2.3 Tank C-103 .....	65
10.2.4 Tank C-104 .....	66
10.2.5 Tank C-105 .....	67
10.2.6 Tank C-106 .....	69
10.2.7 Tank C-107 .....	71
10.2.8 Tank C-108 .....	71
10.2.9 Tank C-109 .....	73
10.2.10 Tank C-110 .....	74
10.2.11 Tank C-111 .....	75
10.2.12 Tank C-112 .....	75
10.2.13 200 Series Tanks .....	76
10.3 Significant Contamination Plumes in the C Tank Farm .....	76
10.3.1 Vadose Zone Plumes Associated With Known Leakers in the C Tank Farm .....	77
10.3.1.1 Vadose Zone Plume from the Tank C-101 Leak .....	77
10.3.1.2 Vadose Zone Plume from the Tank C-110 Leak .....	77
10.3.1.3 Vadose Zone Plume from the Tank C-111 Leak .....	77
10.3.2 Vadose Zone Plumes Not Related to Known Leaks from Tanks or Ancillary Equipment .....	78
10.3.2.1 Vadose Zone Contaminant Plumes Beneath Tanks C-104, C-105, and C-106 .....	78
10.3.2.2 Vadose Zone Contaminant Plumes Beneath Tanks C-108 and C-109 .....	80
10.4 Potential Effect of Adjacent Waste Facilities on the C Tank Farm Vadose Zone Contaminant Plumes .....	80
<b>11.0 Impacts and Implications of the Vadose Zone Contamination</b> .....	80
11.1 Nature of Contamination .....	80
11.2 Extent of Migration .....	80
11.3 Stability of Contamination .....	81

## Contents (continued)

	Page
11.4 Impacts to Groundwater .....	81
<b>12.0 Conclusions</b> .....	<b>82</b>
<b>13.0 Recommendations</b> .....	<b>83</b>
13.1 Tank and Farm Characterization Data .....	83
13.2 Additional Vadose Zone Characterizations .....	85
13.3 Future Vadose Zone Monitoring .....	85
<b>14.0 Figures for the C Tank Farm</b> .....	<b>85</b>
Figure 14-1. Map Showing the Location of the C Tank Farm, RCRA and Non-RCRA Wells, and Adjacent Waste Sites .....	87
14-2. Landforms of the Pasco Basin in the Vicinity of the Hanford Site .....	88
14-3. Geologic Structure Map of the Hanford Site and Surrounding Area .....	89
14-4. Surface Geology of the Hanford Site and Surrounding Area .....	90
14-5. Generalized Cross Section of the Hanford Site .....	91
14-6. General Stratigraphy of the Hanford Site .....	92
14-7. Geologic and Hydrogeologic Column Beneath the C Tank Farm .....	93
14-8. Geomorphology of the 200 East and 200 West Areas .....	94
14-9. 1996 Water Table Elevations .....	95
14-10. Estimated Natural Recharge for the Hanford Site .....	96
14-11. Plan View of the C Tank Farm Showing Borehole Locations .....	97
14-12. One of the Spectral Gamma Logging Systems During Logging Operations ....	97
14-13. Logging Sonde Used by the Spectral Gamma Logging System .....	98
14-14. Example of an Efficiency Curve for Gamma 1 .....	99
14-15. Interpreted <sup>137</sup> Cs Contamination Distribution Around the C Tank Farm Boreholes .....	100
14-16. Interpreted <sup>60</sup> Co Contamination Distribution Around the C Tank Farm Boreholes .....	101
14-17. Visualization of the Contaminant Plumes in the C Tank Farm Viewed From the South .....	102
14-18. Visualization of the <sup>137</sup> Cs and <sup>60</sup> Co Plumes in the C Tank Farm Viewed From the Southeast .....	103
14-19. Visualization of the <sup>137</sup> Cs and <sup>60</sup> Co Plumes in the C Tank Farm Viewed From the East .....	104
14-20. Visualization of the <sup>137</sup> Cs and <sup>60</sup> Co Plumes in the C Tank Farm Viewed From the Northeast .....	105
14-21. Visualization of the <sup>137</sup> Cs and <sup>60</sup> Co Plumes in the C Tank Farm Viewed From the North .....	106

## Contents (continued)

	Page
Figure 14-22. Visualization of the $^{137}\text{Cs}$ and $^{60}\text{Co}$ Plumes in the C Tank Farm Viewed From the Northwest .....	107
14-23. Visualization of the $^{137}\text{Cs}$ and $^{60}\text{Co}$ Plumes in the C Tank Farm Viewed From the West .....	108
14-24. Visualization of the $^{137}\text{Cs}$ and $^{60}\text{Co}$ Plumes in the C Tank Farm Viewed From the Southwest .....	109
14-25. Visualization of the $^{137}\text{Cs}$ Contamination at the Ground Surface of the C Tank Farm .....	110
14-26. Visualization of the $^{137}\text{Cs}$ Contamination 5 ft Below the Surface of the C Tank Farm .....	111
14-27. Visualization of the $^{137}\text{Cs}$ Contamination 10 ft Below the Surface of the C Tank Farm .....	112
14-28. Visualization of the $^{137}\text{Cs}$ and $^{60}\text{Co}$ Contamination 15 ft Below the Surface of the C Tank Farm .....	113
14-29. Visualization of the $^{137}\text{Cs}$ and $^{60}\text{Co}$ Contamination 20 ft Below the Surface of the C Tank Farm .....	114
14-30. Visualization of the $^{137}\text{Cs}$ Contamination 25 ft Below the Surface of the C Tank Farm .....	115
14-31. Visualization of the $^{137}\text{Cs}$ and $^{60}\text{Co}$ Contamination 30 ft Below the Surface of the C Tank Farm .....	116
14-32. Visualization of the $^{137}\text{Cs}$ and $^{60}\text{Co}$ Contamination Around Tanks C-101, C-102, and C-103 Viewed From the South .....	117
14-33. Visualization of the $^{137}\text{Cs}$ and $^{60}\text{Co}$ Contamination Around Tanks C-101, C-102, and C-103 Viewed From the Northwest .....	118
14-34. Visualization of the $^{137}\text{Cs}$ and $^{60}\text{Co}$ Contamination Around Tanks C-101, C-102, and C-103 Viewed From the Southeast .....	119
14-35. Visualization of the $^{137}\text{Cs}$ and $^{60}\text{Co}$ Contamination Around Tanks C-103, C-106, and C-109 Viewed From the South .....	120
14-36. Visualization of the $^{137}\text{Cs}$ and $^{60}\text{Co}$ Contamination Around Tanks C-101, C-104, and C-107 Viewed From the East .....	121
14-37. Visualization of the $^{137}\text{Cs}$ and $^{60}\text{Co}$ Contamination Around Tanks C-101, C-104, and C-107 Viewed From the Southwest .....	122
14-38. Visualization of the $^{137}\text{Cs}$ and $^{60}\text{Co}$ Contamination Around Tanks C-102, C-105, and C-108 Viewed From the Southwest .....	123
14-39. Visualization of the $^{137}\text{Cs}$ and $^{60}\text{Co}$ Contamination Around Tanks C-102, C-105, and C-108 Viewed From the East .....	124
14-40. Visualization of the $^{137}\text{Cs}$ and $^{60}\text{Co}$ Contamination Around Tanks C-102, C-105, and C-108 Viewed From the Northeast .....	125

## Contents (continued)

	Page
Figure 14-41. Visualization of the $^{137}\text{Cs}$ and $^{60}\text{Co}$ Contamination Around Tanks C-102, C-105, and C-108 Viewed From the North . . . . .	126
14-42. Visualization of the $^{137}\text{Cs}$ and $^{60}\text{Co}$ Contamination Around Tanks C-104, C-105, and C-106 Viewed From the South . . . . .	127
14-43. Visualization of the $^{137}\text{Cs}$ and $^{60}\text{Co}$ Contamination Around Tanks C-104, C-105, and C-106 Viewed From the North . . . . .	128
14-44. Visualization of the $^{137}\text{Cs}$ and $^{60}\text{Co}$ Contamination Around Tanks C-103, C-106, and C-109 Viewed From the West . . . . .	129
14-45. Visualization of the $^{137}\text{Cs}$ and $^{60}\text{Co}$ Contamination Around Tanks C-106, C-109, and C-112 Viewed From the Northeast . . . . .	130
14-46. Visualization of the $^{137}\text{Cs}$ and $^{60}\text{Co}$ Contamination Around Tanks C-106, C-109, and C-112 Viewed From the Southwest . . . . .	131
14-47. Visualization of the $^{137}\text{Cs}$ and $^{60}\text{Co}$ Contamination Around Tanks C-104, C-107, and C-110 Viewed From the Northeast . . . . .	132
14-48. Visualization of the $^{137}\text{Cs}$ and $^{60}\text{Co}$ Contamination Around Tanks C-104, C-107, and C-110 Viewed From the Southwest . . . . .	133
14-49. Visualization of the $^{137}\text{Cs}$ and $^{60}\text{Co}$ Contamination Around Tanks C-105, C-108, and C-111 Viewed From the North . . . . .	134
14-50. Visualization of the $^{137}\text{Cs}$ and $^{60}\text{Co}$ Contamination Around Tanks C-105, C-108, and C-111 Viewed From the West . . . . .	135
14-51. Visualization of the $^{137}\text{Cs}$ and $^{60}\text{Co}$ Contamination Around Tanks C-107, C-108, and C-109 Viewed From the South . . . . .	136
14-52. Visualization of the $^{137}\text{Cs}$ and $^{60}\text{Co}$ Contamination Around Tanks C-107, C-108, and C-109 Viewed From the West . . . . .	137
14-53. Visualization of the $^{137}\text{Cs}$ and $^{60}\text{Co}$ Contamination Around Tanks C-106, C-109, and C-112 Viewed From the East . . . . .	138
14-54. Visualization of the $^{137}\text{Cs}$ and $^{60}\text{Co}$ Contamination Around Tanks C-106, C-109, and C-112 Viewed From the West . . . . .	139
14-55. Visualization of the $^{137}\text{Cs}$ and $^{60}\text{Co}$ Contamination Around Tanks C-110, C-111, and C-112 Viewed From the West . . . . .	140
14-56. Visualization of the $^{137}\text{Cs}$ and $^{60}\text{Co}$ Contamination Around Tanks C-110, C-111, and C-112 Viewed From the North . . . . .	141
<b>15.0 References . . . . .</b>	<b>143</b>
<b>Appendix A. C Tank Farm Correlation Plots . . . . .</b>	<b>A-1</b>
<b>Appendix B. Shape Factor Analysis for Tanks C-101, C-103, C-104, C-105, and C-106 . . . . .</b>	<b>B-1</b>

# Contents (continued)

Page

## Tables

Table 1. General C Tank Information .....	25
2. Spectral Shape Factors .....	46

**This page intentionally left blank.**

**Hanford Tank Farms Vadose Zone**

**C Tank Farm Report**

**Prepared by:**

*S.E. Kos*

S.E. Kos  
MACTEC-ERS, Hanford

*6/29/98*

Date

**Concurrence:**

*J.R. Brodeur*

J.R. Brodeur, Technical Lead  
MACTEC-ERS, Hanford

*6/30/98*

Date

*Carl J. Koizumi*

C.J. Koizumi, Technical Lead  
MACTEC-ERS, Grand Junction Office

*07/02/98*

Date

**Approved by:**

*J.F. Beutsch*

J.F. Beutsch, Project Manager  
MACTEC-ERS, Hanford

*6/30/98*

Date

*M.C. Butherus*

M.C. Butherus, Task Order Manager  
MACTEC-ERS, Grand Junction Office

*7/6/98*

Date

*Joel Berwick*

J. Berwick, Project Manager  
U.S. Department of Energy  
Grand Junction Office

*7/7/98*

Date

*David S. Shafer*

D. Shafer, Project Manager  
U.S. Department of Energy  
Richland Operations Office

*7/9/98*

Date

This page intentionally left blank.

## Executive Summary

The U.S. Department of Energy Grand Junction Office (DOE-GJO) was tasked by the DOE Richland Operations Office (DOE-RL) to perform a baseline characterization of the gamma-ray-emitting radionuclides that are distributed in the vadose zone sediments beneath and around the single-shell tanks (SSTs) at the Hanford Site. The intent of this characterization is to determine the nature and extent of the contamination, to identify potential contamination sources when possible, and to develop a baseline of the contamination distribution that will permit future data comparisons. The results of this initial baseline will provide the information necessary to plan and prioritize more comprehensive characterization efforts. This characterization work also allows an initial assessment of the impacts of the vadose zone contamination as required by the Resource Conservation and Recovery Act (RCRA). This characterization effort is limited to the use of existing boreholes; no new boreholes were constructed for this project.

The scope of this characterization project involves acquiring information regarding vadose zone contamination with borehole geophysical logging methods and documenting that information in a series of reports. The borehole geophysical logging methods are presently limited to detection of gamma-emitting radionuclides from both natural and anthropogenic sources. Data from boreholes surrounding each tank are compiled into individual Tank Summary Data Reports. The data from each tank in a tank farm are then compiled and summarized in a Tank Farm Report. This document is the Tank Farm Report for the C Tank Farm.

The C Tank Farm Report is the final document produced as a result of this initial characterization of the C Tank Farm. This report discusses the vadose zone contamination in the entire C Tank Farm as well as the relationship of the natural radionuclide log plots to the geology beneath the tank farm. This report also presents the results of the shape factor analysis method that was applied to the SGLS data acquired in the C Tank Farm boreholes.

The spectral-gamma logging operations are described with references made to all pertinent documentation related to data acquisition, data analysis and log preparation, data management, and quality assurance. Particular emphasis is placed on descriptions of the technical aspects of the measurements, including instrumentation calibration and data reduction.

This report also describes the vadose zone contamination with empirically derived three-dimensional models (visualizations) that are based on a geostatistical model of the log data. Because the geostatistical modeling software assumes all of the data represent contamination distributed in the formation, the resulting visualizations may potentially show false plumes. In order for the model and visualizations to best represent the actual contaminant distribution in the C Tank Farm vadose zone, intervals of SGLS log data that were interpreted to be localized to the borehole were removed from the data set used by the modeling software.

The C Tank Farm was constructed between 1943 and 1944 and is located in the central portion of the 200 East Area. This tank farm consists of 12 first-generation 530,000-gallon (gal) steel-lined single-shell tanks and four smaller 200-series 55,000-gal tanks designed to store high-level nuclear waste. The C Tank Farm currently stores approximately 1.976 million gal of high-level

waste. Tanks C-101, C-110, C-111, C-201, C-202, C-203, and C-204 are currently designated as assumed leakers; these tanks are estimated to have leaked approximately 29,000 gal of high-level waste. The accuracy of these estimates is unknown.

The C Tank Farm is defined by extensive low-level gamma-ray-emitting contamination. The majority of this contamination cannot be directly tied to documented leaks from either tanks or subsurface ancillary equipment. The contaminant distribution, as measured by the SGLS, does appear to indicate that some tanks that are currently considered sound may in fact have leaked. Conversely, there was not much contamination around some of the known "leakers" such as tanks C-110 and C-111. Contamination resulting from leakage from these tanks may have migrated downward and did not reach the lateral extent necessary to be intersected by the vadose zone monitoring boreholes.

Two scenarios could explain the contamination detected beneath tanks C-104, C-105, and C-106, which are all presently designated sound tanks. The first scenario is based on an apparent overfilling of tank C-105 (a review of liquid-level data did not support this conclusion). If the tank was overfilled, then the contamination most likely resulted from leaks in the cascade lines between tanks C-104, C-105, and C-106.

Between 1963 and 1967, tank C-105 experienced a 36-inch (in.) liquid-level drop. An investigation attributed the liquid-level drop to evaporation. However, the investigators acknowledge that there were no data to support this conclusion. Tank C-105 contained a significant amount of heat-generating radionuclides; therefore, it is reasonable to expect a significant amount of liquid was evaporated during that time. However, if tank C-105 was not overfilled, as supported by the liquid-level data, then it is possible the contamination beneath these tanks is the result of a leak from tank C-105. It is also possible that both of these events occurred.

Extensive  $^{60}\text{Co}$  and  $^{137}\text{Cs}$  contamination was measured beneath tanks C-108 and C-109, which are presently designated sound tanks. This contamination may have resulted from leaks from tanks C-108 and/or C-109, from a leak in the cascade line between these two tanks, or from a leak over the dome top of either tank that migrated downward along the tank sides and accumulated at the interface of the backfill materials and undisturbed Hanford Formation sediments. It is also possible some of the deeper  $^{60}\text{Co}$  (below 80 feet [ft]) beneath tanks C-108 and C-109 originated from another nearby tank such as tank C-105. Regardless, positive identification of the source(s) of this contamination has not been determined and additional investigation is warranted.

There are no boreholes around tanks C-201, C-202, C-203, and C-204; therefore, the vadose zone around these tanks cannot be characterized. However, because these four tanks are estimated to have leaked only 1,750 gal of waste, their contribution to the total vadose zone contamination in the C Tank Farm is probably relatively small.

On the basis of published groundwater monitoring data, waste from the C Tank Farm tanks does not appear to have reached groundwater.

## 1.0 Introduction

The C Tank Farm is located in the central portion of the 200 East Area of the Hanford Site (Figure 14-1). The C Tank Farm consists of 12 first-generation 100-series single-shell underground waste storage tanks and four 200-series tanks. Each 100-series tank has a capacity to store 530,000 gallons (gal) of high-level waste, and each 200-series tank has a capacity to store 55,000 gal; therefore, the C Tank Farm has a capacity to store a total of 6,580,000 gal of waste. These tanks currently store a total of 1,976,000 gal of high-level nuclear waste that was generated primarily from the chemical processing of irradiated uranium fuel. Tanks C-101, C-110, C-111, C-201, C-202, C-203, and C-204 are currently listed in Hanlon (1997) as "assumed leakers." These tanks are estimated to have leaked a total of 29,250 gal of high-level radioactive liquid into the vadose zone sediments at the C Tank Farm (Hanlon 1997). The basis for this leak estimate, or lack thereof, is discussed in the appropriate sections of this report.

In 1994, the Department of Energy Richland Operations Office (DOE-RL) requested the DOE Grand Junction Office (DOE-GJO), Grand Junction, Colorado, to conduct a baseline characterization of gamma-emitting radionuclide contamination in the vadose zone at all of the Hanford Site single-shell tank farms. The baseline characterization of the C Tank Farm was accomplished by logging each of the boreholes surrounding the tanks with spectral gamma logging systems. The results of this baseline characterization for the C Tank Farm are presented in this report.

This characterization project was undertaken to begin the process of determining the nature and extent of gamma-emitting contamination in the vadose zone around the SSTs. Existing monitoring boreholes in the C Tank Farm were logged with high-purity germanium (HPGe) spectral gamma-ray logging systems (SGLSs). Data acquired during this characterization work establish a limited baseline of the current vadose zone contamination conditions and present a limited assessment of the impacts of this contamination. The limited baseline is available to identify areas for further characterization. This work may be utilized to establish a vadose zone monitoring program, to identify areas for further characterization, and to determine the implications or impacts of the contamination.

Radionuclide concentration logs for individual boreholes were compiled and presented in 12 individual Tank Summary Data Reports (DOE 1997i, 1997j, 1997k, 1997l, 1997m, 1997n, 1997o, 1997p, 1997q, 1997r, 1998a, and 1998b). These data were analyzed to produce assays of the gamma-emitting radionuclides in the sediment surrounding the boreholes. A three-dimensional geostatistical model of the distribution of these radionuclides within the vadose zone around the C Tank Farm tanks was developed based on interpretations from the SGLS log data. On the basis of a geostatistical model of the interpreted data set, visualizations of the contaminant distribution were generated and are presented in this report.

Section 14.0, "Figures for the C Tank Farm," contains figures in the order they are presented in the report text.

## 2.0 Purpose and Scope

### 2.1 Purpose of the Project

The purpose of this baseline characterization is to quantify the gamma-emitting radionuclides and, if possible, to determine the nature and extent of this contamination. Because only passive gamma logging methods are used, only gamma-emitting radionuclides are assayed. The gamma-ray signatures of the radionuclides that are deposited in the vadose zone around the SSTs can be detected through the existing steel-cased monitoring boreholes (referred to at Hanford as "drywells") that surround the tanks.

This characterization project provides a baseline measurement of the gamma-emitting radionuclide concentrations around the individual boreholes and a baseline of the gamma-emitting contamination distribution within the C Tank Farm in general. This baseline consists of the individual borehole logs or the log database and the contamination distribution model. These data can be used for future data comparisons in order to determine whether the contamination has remained stable. The data can also be used to confirm and characterize potential future tank leaks.

The gamma-emitting radionuclide data can be used to identify areas for future characterization efforts. Recommendations on future characterization efforts for the C Tank Farm are presented in Section 13.

An additional objective of this project is to provide more site-specific geologic information by generating geophysical logs of the naturally occurring potassium-40 ( $^{40}\text{K}$ ), uranium-238 ( $^{238}\text{U}$ ), and thorium-232 ( $^{232}\text{Th}$ ) (KUT) concentrations, which can be used to identify changes in the lithology that can influence moisture and contaminant migration. These KUT data are correlated in this report with published analyses of sediment sample data from nearby groundwater monitoring wells.

### 2.2 Scope of the Project

The primary scope of this project involves spectral gamma logging of existing vadose zone monitoring boreholes within the single-shell tank farms. No boreholes were drilled in the C Tank Farm during the course of this project; therefore, the assessments of the vadose zone contamination are based on the limited distribution and depths of existing boreholes. These boreholes extend to between 100 to 150 feet (ft) down into the vadose zone, while on the basis of 1996 data, the groundwater is approximately 248 ft below the ground surface (PNNL 1997b).

A major portion of this project involves assessment of historical or existing data, such as the gross gamma logs, drilling logs, groundwater monitoring information, tank leak documentation, and tank operations information. Much of this information had not previously been comprehensively compiled, reviewed, and analyzed to understand its significance in relation to the C Tank Farm vadose zone contamination. The historical information helps to identify

potential sources of contamination and to understand and explain the nature and extent of the contamination identified by the spectral gamma log data.

Visualizations of the three-dimensional distribution of the contamination in the C Tank Farm are a primary product of this initial characterization effort. These visualizations correlate the individual borehole logs in three dimensions and allow identification of contaminant plumes, depict relationships between plumes, and sometimes help to determine the source of the contamination.

This project is limited in scope to passive spectral gamma-ray logging data acquisition methods. As a result, radionuclides that do not decay with the emission of gamma-ray photons are not assayed, nor are other regulated chemical constituents that may have been present in the tank waste that leaked into the vadose zone.

The scope of the project also includes preparation of reports that provide the results to current and future Hanford Site personnel and identification of the quality of the data in terms of precision and accuracy as well as quality assurance. Documentation of procedures, instrument calibration, quality assurance, and data analysis methods has been prepared (DOE 1995a, 1995b, 1995c, 1996c, 1996d, 1997a, 1997b, 1997c, 1997d, 1997e, 1997f, and 1997g). All reports are available from Hanford document control centers and from the project files. Currently, log data are only available in the project databases; upon completion of the project the log data will be stored by current and future Hanford contractors.

## 2.3 Regulatory Basis

The operation and eventual closure of the SST farms are regulated by both Federal and State laws. The mixed waste in the SSTs is regulated through the Resource Conservation and Recovery Act of 1976 (RCRA) and the Washington Hazardous Waste Management Act of 1976 (HWMA) for the hazardous waste component, and through the Atomic Energy Act of 1954 (AEA) as amended for the radioactive waste component. For purposes of this vadose zone characterization project, RCRA and the HWMA are the environmental laws of primary importance.

Under RCRA and the HWMA, the Washington State Department of Ecology (Ecology) regulates the SSTs as hazardous waste storage-tank systems under Washington Administrative Code (WAC) 173-303 (DOE 1996b). The SSTs are a treatment, storage, and/or disposal (TSD) unit, and, therefore, part of the larger Hanford Facility that consists of all TSD units at the Hanford Site.

TSD units of the Hanford Facility are regulated as either interim status or final status units. A final status permit, *Dangerous Waste Portion of the Resource Conservation and Recovery Act Permit for the Treatment, Storage, and Disposal of Dangerous Waste* (Ecology 1994), was issued for the Hanford Facility in 1994. Under a negotiated permitting approach, additional TSD units will be added to this permit as the units are evaluated through the RCRA permitting process. Eventually all TSD units of the Hanford Facility, which will continue dangerous waste

management, will be converted from interim status to final status and included in Ecology (1994).

According to the *Hanford Federal Facility Agreement and Consent Order* (Ecology et al. 1996), also known as the Tri-Party Agreement or TPA, closure of the SSTs will be pursuant to WAC 173-303-610. DOE is required to remove or decontaminate all waste residues, contaminated containment system components, contaminated soils, and contaminated equipment at the time of closure; closure of the SSTs as landfills is allowed if all the contaminated soil cannot be practicably decontaminated or removed (DOE 1996b). In either case, characterization of the nature and extent of the leaked waste is needed to evaluate remedial action alternatives for closure of the soils contaminated by waste leaked from the SSTs. Without appropriate data on the nature and extent of contamination, it will not be possible to develop or assess the risk associated with various closure options for the SSTs.

In addition to providing necessary information to support closure of the SSTs, the vadose zone characterization will provide a baseline of gamma-ray activity in boreholes surrounding the SSTs. Newly acquired spectral gamma-ray data can be compared to this baseline to help identify any new or continuing leaks. Monitoring of the SSTs is required under a number of regulations, including DOE orders and interim status requirements of RCRA. The existence of a defensible baseline will reinforce the effectiveness of future monitoring activities.

## 2.4 Purpose of the Report

This report presents a compilation of the results of the spectral gamma logging characterization at the C Tank Farm that were originally reported in individual Tank Summary Data Reports and provides visualizations of the cesium-137 ( $^{137}\text{Cs}$ ) and cobalt-60 ( $^{60}\text{Co}$ ) contamination distributions that are based on a geostatistical model for these radionuclides. The visualizations of the contaminant distributions correlate the individual borehole logs in three dimensions and help to identify contamination plumes, to develop relationships between the plumes, and to determine or confirm the potential sources of the contamination. Section 8.6 describes how the SGLS data set was interpreted to produce the data set used by the geostatistical model. Section 9.0 documents the geostatistical model and visualization development, identifies assumptions and model parameters, and explains the uncertainty associated with the visualizations.

Implementation of the spectral shape factor analysis occurred after half of the Tank Summary Data Reports for the C Tank Farm were completed. Therefore, spectral shape factor analysis was completed for the appropriate tank monitoring boreholes in the C Tank Farm during the preparation of this report. The details of the shape factor analysis process are presented in Section 8.5 and the results are presented in Appendix B.

This report provides brief introductory information regarding the C Tank Farm, including a history of the tank farm, summaries of geologic and hydrogeologic information, and descriptions of the waste sites and facilities adjacent to the C Tank Farm. Information regarding these subjects was obtained from published Hanford Site documents.

### 3.0 Radionuclides of Interest

Radionuclide contamination distributions and their impacts or implications relative to contamination sources are the primary focus of this project. Although an assay of all radionuclide contamination and non-radionuclide contamination in the vadose zone is desirable, the technology used in this project (passive gamma logging) allows an assay of only gamma-emitting radionuclides.

The radionuclide contamination in the vadose zone can be considered to present both a short-term occupational exposure risk to operations workers and a long-term risk to the public and the environment. The types of possible risks depend on a variety of factors that are specific to each radionuclide, including the decay half-life of the nuclide, its mobility in the vadose zone (and ultimately in the groundwater), and its specific activity and/or biological toxicity.

Long-term human health risks arise primarily from a potential pathway whereby an individual is exposed by ingesting contaminated groundwater and from a pathway involving direct exposure of an individual to contaminated sediment that is uncovered or otherwise brought to the surface in the distant future, after the end of an institutional control period. Long-term risk scenarios are usually evaluated by using vadose zone contaminant-transport modeling to produce performance assessments that estimate potential doses for different pathways. Radionuclides of concern would be those with long half-lives and those that are mobile in the vadose zone and could contribute to groundwater contamination.

Short-term risk scenarios involve inhalation of radionuclides or direct exposure to workers during remediation or other operations that would uncover or bring the vadose zone contamination to the surface in the near future. The radionuclides of greatest concern are those that are easily suspended in air and the high specific-activity radionuclides that present an exposure problem.

Boothe (1996) presents a review of the radionuclide inventory of the tank wastes and the risk levels associated with each radionuclide. Many radionuclides in the original tank wastes that have short half-lives have since decayed and are no longer detectable.

Some of the radionuclides of interest are identified in the following sections. These radionuclides include those that are detectable with the SGLS, those whose occurrences can be inferred from the SGLS data, and radionuclides that are related to those detected with the SGLS.

The information in the following sections was obtained from a variety of sources, including National Low-Level Waste Management Program documents (Rudin and Garcia 1992a, 1992b; Rudin et al. 1992), nuclear physics references including Lederer and Shirley (1978), GE (1989), Erdtmann and Soyka (1979), and Hanford Site contractor documents including Dresel et al. (1995) and Johnson (1993).

### 3.1 Cesium-137 (<sup>137</sup>Cs)

<sup>137</sup>Cs is one of the highest specific-activity radionuclides ( $8.7 \times 10^4$  Ci/g) in the tank wastes and is present at high concentrations. This radionuclide is a man-made isotope that originated as a high-yield fission product and accounted for a high percentage of the total radioactivity in irradiated fuel assemblies. <sup>137</sup>Cs was a major component of the process waste stream generated by the plutonium and uranium separations processes.

<sup>137</sup>Cs has a half-life of 30.2 years and is the longest-lived high-yield fission-product. It decays with the emission of beta particles (511 and 1176 kilo-electron-volts [keV]) to produce barium-137 (<sup>137m</sup>Ba), which in turn produces a 661.6-keV gamma-ray photon with an intensity of 84.62 gamma photons per 100 decays of <sup>137</sup>Cs (Erdtmann and Soyka 1979). As a result of the gamma photon emission, <sup>137</sup>Cs is easily detected and quantified with HPGe spectral gamma-ray detection equipment. The minimum detectable level (MDL) of <sup>137</sup>Cs for the SGLS when logging with 100-second (s) counting times is about 0.1 picocurie per gram (pCi/g).

Because of its long half-life and relatively high concentration in the tank waste, <sup>137</sup>Cs is the most abundant radionuclide in the vadose zone around the SSTs. This contaminant is easy to detect and quantify with passive gamma logging and was detected in every borehole in the C Tank Farm. <sup>137</sup>Cs is reported to have a high sorptive capacity in sediment. However, in the presence of competing positive ions such as from the dissolved radioactive salts present in the SSTs, the sorption of <sup>137</sup>Cs decreases (Carboneau et al. 1994b). At low concentrations, <sup>137</sup>Cs is more strongly adsorbed to the sediment, particularly if pH values are greater than 4.0, as is typical of the Hanford sediment.

<sup>137</sup>Cs is absorbed by humans and animals through the digestive tract and behaves chemically in the body similar to potassium (Carboneau et al. 1994b). The EPA-mandated maximum contaminant level (MCL) for <sup>137</sup>Cs in groundwater is 200 picocuries per liter (pCi/L).

### 3.2 Cobalt-60 (<sup>60</sup>Co)

<sup>60</sup>Co is generated in nuclear reactors by neutron activation of stable <sup>59</sup>Co. <sup>60</sup>Co occurs in relatively high concentrations in the cladding of irradiated reactor fuel elements and was present in the waste stream products sent to the SSTs from the plutonium and uranium separation processes. <sup>60</sup>Co was originally present in the tanks at significant activities, but much of the <sup>60</sup>Co has since decayed away because it has a short half-life of 5.27 years.

<sup>60</sup>Co decays via beta emission to create stable nickel-60 (<sup>60</sup>Ni). About 95 percent of the beta particles emitted during the decay of <sup>60</sup>Co have energies equal to or below 314 keV, but beta particle energies as high as 1480 keV can be generated. During the decay to stable <sup>60</sup>Ni, <sup>60</sup>Co also emits two high-energy gamma rays: one at 1173 keV and the other at 1333 keV. The production of these gamma rays is 99.8 and 99.9 percent, respectively (Erdtmann and Soyka 1979). These gamma rays make the presence of <sup>60</sup>Co easy to detect and quantify with passive gamma measurement equipment. The MDL of <sup>60</sup>Co is about 0.15 pCi/g with the present logging acquisition rates of 100 seconds utilized for this vadose zone characterization project.

The human exposure risk for  $^{60}\text{Co}$  is relatively high because this radionuclide emits both beta particles and gamma rays during decay that are relatively high-energy and because it has a high specific activity ( $1.1 \times 10^3$  curies per gram [Ci/g]).

Adams (1995) provides a good review of studies on the mobility of  $^{60}\text{Co}$  in soils and sediment, including laboratory experiments and actual site investigations. The ability of soil and sediment to retain  $^{60}\text{Co}$  is quantified by the solid/liquid partition or the solid versus aqueous ratio (in micrograms of cobalt per gram of sediment) and is designated as  $K_d$ . The  $K_d$  value for  $^{60}\text{Co}$  is reported to vary over 4 orders of magnitude and is strongly dependent on the type of sediment in which it was measured or calculated (Adams 1995).

$^{60}\text{Co}$  is usually present as a divalent cation in the subsurface sediments and is strongly adsorbed onto sediment, particularly to the surface of clay minerals. However, dilute acid or chelating compounds such as ethylenediaminetetraacetic acid (EDTA) interfere with this adsorption. At the other extreme, the noncationic form of  $^{60}\text{Co}$  is not adsorbed by the sandy soils that are prevalent at Hanford.

When  $^{60}\text{Co}$  comes in contact with groundwater, it generally becomes fixed in the soil and does not migrate appreciably from the original source site.  $^{60}\text{Co}$  is generally immobile and does not present a long-term health-and-safety risk from a groundwater pathway because of its short half-life. The EPA-mandated MCL for  $^{60}\text{Co}$  in drinking water is 100 pCi/L.

$^{60}\text{Co}$  is considered an exposure risk to workers because of the energetic gamma rays emitted during decay but does not need to be considered in long-term performance assessments because of its short half-life. Nevertheless, this contaminant is monitored in the vadose zone because it can be mobile and because it is easily detected and assayed. The presence of  $^{60}\text{Co}$  in the subsurface provides an indication of the location and extent of a contamination plume; monitoring for changes in  $^{60}\text{Co}$  concentrations would indicate changing conditions of a plume that are due to recharge from precipitation or to new or additional tank releases.

### 3.3 Europium-152 ( $^{152}\text{Eu}$ ) and Europium-154 ( $^{154}\text{Eu}$ )

Europium radionuclides in the tank wastes include the isotopes  $^{152}\text{Eu}$  and  $^{154}\text{Eu}$ .  $^{154}\text{Eu}$  originates from the activation of europium-153 ( $^{153}\text{Eu}$ ), which is a fission product.  $^{154}\text{Eu}$  is not as abundant in the irradiated fuel or the processing waste streams as  $^{137}\text{Cs}$ , but it is present in irradiated fuel at high enough concentrations that it contributes a significant amount to the total radiation flux from the fuel.

$^{154}\text{Eu}$  decays by emission of a beta particle to stable gadolinium-154 ( $^{154}\text{Gd}$ ) and has a half-life of 8.59 years. The most intense gamma rays emitted during decay include 123 keV (40.5 percent), 723 keV (19.7 percent), 1004 keV (17.6 percent), and 1274 (35.5 percent) (Erdtmann and Soyka 1979).

$^{152}\text{Eu}$ , with a half-life of 13.5 years, decays by electron capture and positron emission to samarium-152 ( $^{152}\text{Sm}$ ) and by beta particle emission to gadolinium-152 ( $^{152}\text{Gd}$ ) with the release

of a large number of possible gamma rays, the most intense of which include 344 keV (27 percent), 779 keV (13 percent), 964 keV (14.6 percent), 1112 keV (13.6 percent), and 1408 keV (21 percent) (Erdtmann and Soyka 1979).

<sup>154</sup>Eu presents a short-term exposure risk because of the gamma radiation, but it is not considered a long-term risk because of its relatively short half-life. The EPA-mandated MCL for <sup>154</sup>Eu in drinking water is 200 pCi/L.

### 3.4 Strontium-90 (<sup>90</sup>Sr)

<sup>90</sup>Sr is similar to <sup>137</sup>Cs because it is also a high-yield, long-lived fission product with a half-life of 29 years. Unlike <sup>137</sup>Cs, <sup>90</sup>Sr decays with the emission of a beta particle but no gamma-ray photons. <sup>90</sup>Sr decays to yttrium-90 (<sup>90</sup>Y), which has a short half-life (64 hours), and decays to stable zirconium-90 (<sup>90</sup>Zr). The beta particle emitted in the decay of <sup>90</sup>Y has a high energy (up to 2.2 million-electron-volts [MeV]) and is usually associated with the parent radionuclide <sup>90</sup>Sr.

Some beta particles from <sup>90</sup>Sr are so energetic that when <sup>90</sup>Sr is present in the subsurface at high concentrations (greater than about 2,000 pCi/g), bremsstrahlung radiation or braking radiation may be measured in a borehole with the gamma-ray detectors. Bremsstrahlung radiation is characterized in a gamma-ray spectrum by a low-energy continuum that decreases in intensity with increasing energy, in a log-linear manner, and covers an energy range from the x-ray region to about 300 keV. If <sup>90</sup>Sr is present at about 2,000 pCi/g or greater, it can be positively identified but not readily quantified with the spectral gamma-ray detection equipment (Section 8.5).

Because of its long half-life, the inventory of <sup>90</sup>Sr in a reactor increases linearly with fuel fission, and essentially all the <sup>90</sup>Sr produced still remains in the fuel when it is extracted from the reactor and processed. At the end of processing, <sup>90</sup>Sr represents only about 0.05 percent of the total fission product activity but accounts for 20 percent of the total remaining radioactivity after 100 years.

Strontium is a divalent (Sr<sup>2+</sup>) element that mimics the chemistry of calcium. It forms an ionic bond with negatively charged elements and is easily dissolved in water. When released, dissolved in liquid effluent and into the sediment, it will readily adsorb onto sediment grains or clay particles and can replace Ca<sup>2+</sup> in CaCO<sub>3</sub>.

<sup>90</sup>Sr is the second most abundant radionuclide in the tank waste material. In the high-heat and self-boiling tanks (typical of the A and SX Tank Farms), the decay of <sup>90</sup>Sr generates more heat than all other radionuclides combined. This heat is the result of the release of high-energy beta particles from the decay of <sup>90</sup>Y. <sup>90</sup>Sr is dissolved easily during the fuel dissolution process, the first stage of fuel rod processing, and it stays in solution throughout the separation process. Consequently, <sup>90</sup>Sr is always a component in the effluent waste products of the separation processes.

<sup>90</sup>Sr has a large  $K_d$  value for clay or organic soil, but the  $K_d$  value is much less than for <sup>137</sup>Cs (Carboneau et al. 1994a). The <sup>90</sup>Sr  $K_d$  value for sand or loam sediment typical of the Hanford

formation is about 1 order of magnitude lower than the  $K_d$  value for clay soil.  $^{90}\text{Sr}$  is also sensitive to the presence of calcium, and it apparently can replace calcium in carbonate sediment. This chemical relationship has particular significance where calcium carbonate rich zones are present in the Hanford formation and Ringold Formation sediments, as these zones may effectively inhibit the vertical migration of  $^{90}\text{Sr}$ .  $^{90}\text{Sr}$  retention in soil increases with an increasing pH value.

$^{90}\text{Sr}$  is a significant health risk because it replaces calcium and is deposited in bone material, where it becomes fixed. Once deposited in the body, damage is caused by the high-energy beta radiation emitted during decay.

In groundwater,  $^{90}\text{Sr}$  tends to stay in soluble form and migrates farther than other fission products such as  $^{137}\text{Cs}$ .  $^{90}\text{Sr}$  is often a risk-limiting radioisotope because of the relatively high mobility of  $^{90}\text{Sr}$  in both the vadose zone sediment and the groundwater and because of its high health risk relative to other nuclides. The EPA-mandated MCL for  $^{90}\text{Sr}$  in drinking water is 8 pCi/L.

### 3.5 Antimony-125 ( $^{125}\text{Sb}$ )

$^{125}\text{Sb}$  is another fission product, but its yield from slow neutron fission of uranium-235 ( $^{235}\text{U}$ ) or plutonium-239 ( $^{239}\text{Pu}$ ) is only about 0.02 percent (out of 200 percent of the fission atoms) and does not account for a large percentage of the total fission product. However, its percentage of abundance in the waste products increases as the waste ages because it has a long half-life (2.8 years) relative to other more abundant fission and activation products (excluding  $^{137}\text{Cs}$  and  $^{90}\text{Sr}$ ).

$^{125}\text{Sb}$  decays with the emission of a beta particle to tellurium-125 ( $^{125}\text{Te}$ ), which is stable. Gamma rays emitted during the decay of  $^{125}\text{Sb}$  include 428 keV (29.6 percent), 600 keV (18 percent), and 636 keV (11 percent) (Erdtmann and Soyka 1979).

$^{125}\text{Sb}$  is an important radionuclide for vadose zone characterization and monitoring work because it can be abundant, it is easily measured, and it is more mobile than some of the other gamma-emitting radionuclides. It poses minimal risk because of its generally low abundance, but it is easily monitored and tracked for contaminant migration studies because it is a gamma-emitter.

$^{125}\text{Sb}$  presents a short-term exposure risk because it can be inhaled. The EPA-mandated MCL for  $^{125}\text{Sb}$  in drinking water is 300 pCi/L.

### 3.6 Technetium-99 ( $^{99}\text{Tc}$ )

$^{99}\text{Tc}$  is an abundant fission product that is long-lived and can be very mobile in the environment. It is an important radionuclide in long-term risk assessments and its presence can yield high calculated risk values.

$^{99}\text{Tc}$  has a fission yield from fissionable isotopes of uranium and plutonium of about 6 percent (out of 200 percent), which is equivalent to that of  $^{137}\text{Cs}$ . As a result, it is as abundant in terms of

mass content as  $^{137}\text{Cs}$  in effluent streams and SST wastes at Hanford. However,  $^{99}\text{Tc}$  is present in the tank waste at a lower curie content (by many orders of magnitude) because  $^{137}\text{Cs}$  has a much higher specific activity.

$^{99}\text{Tc}$  has a half-life of  $2.1 \times 10^5$  years, which is one of the reasons for its high risk rating in long-term performance assessments. It decays by beta emission to stable ruthenium-99 ( $^{99}\text{Ru}$ ) without the emission of gamma rays that are detectable with the logging system; therefore, it cannot be detected or assayed through the boreholes.

The mobility of  $^{99}\text{Tc}$  in soil is highly dependent on its chemical form, which is governed by the oxidation-reduction potential of the soil. Rudin et al. (1992) state that if sufficient reducing conditions exist in the sediment, technetium will precipitate out of solution as a sulfide or hydrated oxide. If oxidizing conditions exist, technetium will be present as a pertechnetate ion, which studies have shown will migrate at a rate of 88 percent of the groundwater velocity or greater.

### 3.7 Uranium

Uranium isotopes are long-lived and can be mobile in both the groundwater and vadose zone. Boothe (1996) lists uranium isotopes as a groundwater hazard that should be included in a performance assessment.

Uranium isotopes in tank wastes primarily include  $^{238}\text{U}$  and  $^{235}\text{U}$ , with minute quantities of  $^{232}\text{U}$ ,  $^{233}\text{U}$ ,  $^{234}\text{U}$ , and  $^{236}\text{U}$ . In the initial bismuth-phosphate separation process, uranium was not separated from the fission and activation products. However, after 1952, a separate batch process was added to the bismuth-phosphate process to recover uranium from the waste stream. Also, all of the accumulated waste in the tanks was eventually processed to remove the uranium. The REDOX and PUREX processes that were developed after the bismuth-phosphate process removed more than 95 percent of the uranium from the fission and activation products.

$^{238}\text{U}$ , by far the most abundant uranium isotope in the waste, occurs naturally in the Earth's crust and is assayed for stratigraphic correlation purposes. It decays through a long and complex decay chain that results in the emission of alpha and beta particles as well as gamma rays.  $^{238}\text{U}$  has a long half-life ( $4.7 \times 10^9$  years) and is easily assayed by gamma spectroscopy methods when in secular equilibrium with its short-lived, gamma-emitting daughter products bismuth-214 ( $^{214}\text{Bi}$ ) and lead-214 ( $^{214}\text{Pb}$ ).

When  $^{238}\text{U}$  is not in secular equilibrium with its post-radium daughter nuclides, such as when uranium is chemically separated from them, it can be assayed with gamma spectroscopy methods with the 1001-keV gamma ray from the second daughter product metastable protactinium ( $^{234\text{m}}\text{Pa}$ ). This gamma ray is not as intense as the gamma rays from  $^{214}\text{Bi}$  and  $^{214}\text{Pb}$ , but when necessary, the logging data acquisition parameters can be enhanced to obtain adequate assay statistics.

$^{235}\text{U}$ , the second most abundant uranium isotope, is the fissile isotope present in enriched reactor fuel. It is also long-lived, with a half-life of  $7.0 \times 10^8$  years. The presence of  $^{235}\text{U}$  can be detected from an intense low-energy gamma ray of 185.7 keV at 54 photons per 100 decays (Erdtmann and Soyka 1979). Although photons at this energy are indistinguishable from those emitted at the same energy from other nuclides, the existence of  $^{235}\text{U}$  can be confirmed with other gamma rays if necessary.

The chemistry and geochemistry of uranium have been widely studied, and the behavior of uranium in the vadose zone and in groundwater is well known, as are remediation processes. Uranium can exist in several oxidation states, and the uranium Eh-pH diagram is well understood. Uranium is highly mobile in an acidic hydrologic regime or an oxidizing environment. The sediments of the Hanford and Ringold Formations are calcareous and typically result in high pH and moderate Eh values. As a result, uranium has a lower mobility than in other environments but is still one of the more mobile radionuclides at Hanford, and a large quantity of water will flush it through the vadose zone sediments. An extensive uranium/technetium-contaminated groundwater plume associated with uranium recovery operations at U Plant in the Hanford Site 200 West Area is currently undergoing remediation through a pump and treat system. This system removes the contaminants from groundwater with an ion-exchange column.

In terms of a long-term performance assessment, uranium is often one of the higher risk radionuclides for groundwater contamination. The proposed EPA-mandated MCL for uranium in groundwater is 20 micrograms per liter ( $\mu\text{g/L}$ ) or about 13 pCi/L.

### **3.8 Plutonium, Americium-241 ( $^{241}\text{Am}$ ), Iodine, Neptunium-237 ( $^{237}\text{Np}$ ), and Ruthenium-106 ( $^{106}\text{Ru}$ )**

Other nuclides and elements of interest and/or concern with this project include plutonium,  $^{241}\text{Am}$ , iodine,  $^{237}\text{Np}$ , and  $^{106}\text{Ru}$ . None of these nuclides or elements were detected in the vadose zone at the C Tank Farm, and will not be discussed in this report, but a short summary of each is provided.

Plutonium isotopes are an inhalation exposure risk. These isotopes are reported to be strongly adsorbed onto the sediment, but in some cases, organic compounds may enhance their mobility (Carboneau and Garcia 1994). Several plutonium isotopes are present in small quantities in the tank waste, and most can be detected and assayed to some degree with gamma spectroscopy measurements if these isotopes are present at high enough concentrations.

$^{241}\text{Am}$  has a long half-life (433 years) and can be mobile under low pH conditions. It has an intense gamma ray with an energy of 59.5 keV, which is too low in energy to be detected and assayed with the SGLS.  $^{241}\text{Am}$  decays by alpha particle emission to  $^{237}\text{Np}$ , which is more mobile than americium. Both of these nuclides may pose a high long-term risk mainly because of the mobility of neptunium (Winberg and Garcia 1995).

$^{237}\text{Np}$  is produced from the decay of  $^{241}\text{Am}$  and in a reactor by fast neutron interactions with  $^{238}\text{U}$  and subsequent decay to  $^{237}\text{Np}$ .  $^{237}\text{Np}$  emits a gamma ray with an energy of 311 keV and can be detected with the SGLSs to a lower level of about 2.0 pCi/g. The presence of  $^{237}\text{Np}$  would be an indication that  $^{241}\text{Am}$  might also be present.

Most of the iodine isotopes generated in nuclear reactors are short lived and may be a short-term exposure problem. However, iodine-129 ( $^{129}\text{I}$ ) is a long-lived isotope with a half-life of  $1.6 \times 10^7$  years that is mobile in the vadose zone and groundwater, and it can be a significant long-term risk.  $^{129}\text{I}$  cannot be detected with gamma spectroscopy equipment. This isotope does emit an x-ray during decay that can be detected with another type of photon detector. The EPA-mandated MCL for  $^{129}\text{I}$  is 1 pCi/L.

$^{106}\text{Ru}$  is a fission product that was abundant in the nuclear waste.  $^{106}\text{Ru}$  decays to rhodium-106 ( $^{106}\text{Rh}$ ), which in turn immediately decays to palladium-106 ( $^{106}\text{Pd}$ ) and emits intense gamma rays at 512 keV and 622 keV. When the waste was first placed in the tanks,  $^{106}\text{Ru}$  was a major contributor to the total gamma flux of the waste. However, because  $^{106}\text{Ru}$  has a half-life of only 368 days, it has now decayed to low levels and is probably not detectable.  $^{106}\text{Ru}$  was thought to have been a primary target nuclide for vadose zone leak-detection schemes, but spectral gamma data show that in many cases,  $^{137}\text{Cs}$ ,  $^{60}\text{Co}$ , or  $^{238}\text{U}$ , and not  $^{106}\text{Ru}$  were detected with the gross gamma logging systems. The EPA-mandated MCL for  $^{106}\text{Ru}$  in groundwater is 30 pCi/L.

## 4.0 Geology and Hydrogeology

The following sections provide a basic summary of geologic information that is necessary for the discussions in later sections of this report. For more detailed information about the geology and hydrogeology below C Tank Farm, the reader is referred to the following documents. Price and Fecht (1976) first described the lithology beneath the C Tank Farm. Reidel et al. (1989) provide a discussion of the geologic evolution of the Columbia Plateau. Lindsey (1992) provides a description of the geology specific to the 200 West Area. Caggiano and Goodwin (1991) reviewed historical data and current lithologic data from newly drilled groundwater monitoring wells and compiled geologic cross sections from these data. Lindsey (1993) provides detailed information about the stratigraphy and hydrologic characteristics of the sediments forming the vadose zone beneath the SST farms. The *200 East Groundwater Aggregate Area Management Study Report* (DOE 1993a) provides a detailed analysis of the geologic and hydrogeologic conditions in the 200 East Area. Lindsey (1995) provides a detailed description of Miocene to Pliocene Aged sediments of the Hanford Site.

### 4.1 Regional Geology

The Hanford Site is located in the Pasco Basin, which is a physical and structural depression in the Columbia Plateau created by tectonic activity and folding of the Columbia River basalts. Figure 14-2 presents the position of the Hanford Site within the Pasco Basin and identifies major landforms. The Pasco Basin is bounded on the north by the Saddle Mountains; on the east by the Palouse Slope, on the west by the Umtanum Ridge, the Yakima Ridge, and the Rattlesnake Hills;

and on the south by Rattlesnake Mountain and the Rattlesnake Hills. All these uplifts are major structural anticlines within the basalt bedrock. The eastern boundary of the Pasco Basin is a structural monocline with the bedrock dipping to the west and covered with the sediment that constitutes the Palouse Slope. The Hanford Site is underlain by Miocene Age basalt of the Columbia River Basalt Group and Miocene to Pleistocene suprabasalt sediments.

#### **4.1.1 Geologic Structure of the Pasco Basin**

The Columbia Plateau is a part of the North American continental plate and lies in a back-arc setting east of the Cascade Range. It is bordered on the east by the Rocky Mountains and Idaho Batholith, on the north by the Okanogan Highlands, and on the south by the High Lava and Snake River Plains. The Columbia Plateau is divided into three informal structural subprovinces: the Blue Mountains, the Palouse, and the Yakima Fold Belt (Tolan and Reidel 1989). The Hanford Site lies within the Pasco Basin, one of the largest structural basins in the Columbia Plateau, near the junction of the Yakima Fold Belt and the Palouse subprovinces. Figure 14-3 shows the Hanford Site relative to the major structural features of the Pasco Basin.

Distinctive features of the Yakima Fold Belt are a series of segmented, narrow, asymmetrical anticlines that are generally east-west trending. The northern limbs generally dip steeply to the north and are vertical or overturned. The southern limbs generally dip to the south at shallow angles. The anticlinal ridges are separated by broad synclines or basins that may contain thick accumulation of sediments. The Umtanum-Gable Mountain anticline divides the Pasco Basin into the Wahluke and Cold Creek synclines. The Cold Creek syncline is asymmetrical and is a relatively flat-bottomed structure. The Hanford Site 200 Areas are located on the northern limb of the Cold Creek syncline where the bedrock dips to the south at an angle of approximately 5 degrees. Anticlines to the north and south create topographic high areas with outcropping basalt flows of Gable Mountain and Rattlesnake Mountain, respectively.

#### **4.1.2 Stratigraphy of the Pasco Basin**

Figure 14-4 shows the surface geology of the Hanford Site and surrounding areas, and Figure 14-5 shows a generalized cross section of the Hanford Site. A generalized stratigraphic column of the Hanford Site is shown in Figure 14-6, and a stratigraphic column specific to the C Tank Farm that provides details on hydrogeologic conditions is shown in Figure 14-7. These figures show the relative position of various formations that are discussed in the following sections.

The gently sloping surface on which the 200 East Area is situated resulted from Pleistocene cataclysmic flooding and Holocene eolian activity. Flooding resulted when glacially created dams failed and drainage from the dammed lakes flowed across the Columbia Plateau. These floods led to the deposition of sand and gravel in the waters that were impounded (with the formation of Lake Lewis) behind Wallula Gap. Deposition of sand and gravel created Cold Creek bar, a prominent feature on which the 200 Areas (both East and West) are located (Figure

14-8). Since the Pleistocene, winds have locally reworked the surface of the glacio-fluvial sediments, depositing a thin veneer of eolian sand in places.

#### **4.1.2.1 Columbia River Basalt Group**

The bedrock at the Hanford Site consists of a series of basalt flows that are a part of the Columbia River Basalt Group. These flows are continental flood basalts of Miocene Age that extend from north-central Washington, south into Oregon, and east into Idaho, covering an area of more than 63,000 square miles. They are generally of tholeiitic composition. The thickest flows are more than 100 ft thick, with sedimentary interbeds occurring between some of the lava flows.

#### **4.1.2.2 Ringold Formation**

The Ringold Formation is the most extensive suprabasalt sedimentary unit at the Hanford Site. This formation is as much as 600 ft thick south of the 200 West Area. It is absent in the north and northeastern portions of the 200 East Area and adjacent areas to the north, and it pinches out against structural highs.

The Ringold Formation is best described if divided on the basis of sediment facies associations and their distribution. Facies associations in the Ringold Formation (defined by lithology, petrology, stratification, and pedogenic alteration) include fluvial gravel, fluvial sand, overbank deposits, lacustrine deposits, and alluvial fan. The facies associations are as follows:

**Fluvial gravel.** Clast-to-matrix-supported granule-to-cobble gravel with a sandy matrix dominates the fluvial gravel facies association. Lithologic features observed in outcrop include low angle to planar stratification, massive bedding, wide shallow channels, and large-scale cross-bedding. Sediments of this association were deposited in a gravelly fluvial braidplain characterized by wide, shallow, shifting channels.

**Fluvial sand.** Quartzo-feldspathic sand that displays cross-bedding and cross-lamination in outcrop dominates this association. Intercalated strata consist of lenticular silty sands and clays as much as 3 meters (m) thick and thin (less than 0.5 m) gravels. Fining upwards sequences less than 1 m to several meters are common. Sediments of this association were deposited in wide, shallow channels.

**Overbank-Paleosol deposits.** This association consists predominantly of laminated to massive silt, silty fine-grained sand, and paleosols containing variable amounts of pedogenic calcium carbonate. Sediments of this association were deposited in proximal levee to more distal floodplain conditions.

**Lacustrine deposits.** Sediments consisting of well-stratified silt and silty sand that display some soft-sediment deformation characterize this association. These sediments were deposited in lakes under standing water to deltaic conditions.

**Basaltic Alluvium.** Massive to crudely stratified, weathered to unweathered, basaltic detritus dominates this association. These deposits are generally present around the periphery of the Pasco Basin, and record debris flow in an alluvial fan environment and sidestream drainage into the basin.

The lower half of the Ringold Formation is informally referred to as the Wooded Island member and contains four different stratigraphic intervals known as units A, B/D, C, and E. These units are dominated by fluvial gravels interbedded by the overbank-paleosol and lacustrine facies. The lowermost fine-grained unit is commonly referred to as the lower mud sequence and overlies unit A.

Above the Wooded Island member lies another informal member of the Ringold Formation called the Taylor Flats member. The Taylor Flats member consists of mixed fluvial sand and overbank deposits. The sand and overbank units are commonly referred to as the Ringold Formation upper unit.

Overlying the Taylor Flats member is the Savage Island member. The Savage Island member consists primarily of the lacustrine facies.

The Ringold Formation was most likely deposited in three stages. The first stage is defined by alternating periods of Columbia and Salmon/Clearwater fluvial gravel deposition and lacustrine and paleosol deposits; this stage defines the deposits of the Wooded Island member. The second phase is characterized by a mix of sandy fluvial and overbank deposits and defines the deposits of the Taylor Flats member. The third depositional phase, which is defined by lacustrine-fill deposits, is known as the Savage Island member.

#### **4.1.2.3 Plio-Pleistocene Unit**

The Plio-Pleistocene unit is not present near the C Tank Farm; therefore, it is not included in this discussion.

#### **4.1.2.4 Early Palouse Unit**

The Early Palouse unit is not present near the C Tank Farm; therefore, it is not included in this discussion.

#### **4.1.2.5 Pre-Missoula Gravels**

The Pre-Missoula Gravels are not present near the C Tank Farm; therefore, they are not included in this discussion.

#### 4.1.2.6 Hanford Formation

The Hanford formation consists of pebble-to-boulder gravel, fine- to coarse-grained sand, and silt. The gravel deposits range from well sorted to poorly sorted. These deposits are divided into three facies. Ordered from the top of the formation these facies are: gravel-dominated, sand-dominated, and silt-dominated. These facies are commonly referred to as the coarse-grained deposits (generally referred to as the Pasco Gravels), the plane-laminated sand facies, and the rhythmite facies (commonly referred to as the Touchet Beds), respectively (Baker et al. 1991). The Hanford formation is thickest in the 200 East and 200 West Areas, where it is as much as 350 ft thick, and it is absent on ridges more than 1,160 ft above sea level. These sediments were deposited during numerous episodes of cataclysmic flooding that resulted from multiple drainages of glacial lake Missoula in the Pleistocene Age (Baker et al. 1991).

The gravel-dominated facies generally consists of coarse-grained basaltic sand and granule-to-boulder gravel. In outcrop, these sediments display massive bedding, plane to low-angle bedding, and large-scale planar cross-bedding. Gravels dominate the Hanford formation in the 100 Areas north of Gable Mountain, the northern portion of the 200 East Area, and the eastern portion of the Hanford Site. The gravel-dominated facies was deposited by high-energy flood waters in or immediately adjacent to the main flood channel.

The sand-dominated facies consists of fine- to coarse-grained sand and granule gravel. In outcrop, these sediments display plane lamination and bedding and, less commonly, plane bedding and channel-fill sequences. These sands may contain small pebbles or pebble-gravel interbeds less than 8 inches (in.) thick. The silt content of the sands is variable, but where it is low, open framework texture occurs. The sands are typically basaltic, displaying a salt-and-pepper appearance. The sand-dominated facies is transitional between the gravel-dominated facies to the north and the rhythmite facies to the south, and it is present in the 200 Areas. The laminated-sand facies was deposited adjacent to the main flood channelway as it spilled out of the main channel, or it was deposited during the diminishing stages of flooding.

The rhythmite facies sediments were deposited under slack water conditions and in back-flooded areas remote from the main flood channelway. These sediments consist of thinly bedded, plane-laminated and ripple cross-laminated silt and fine- to coarse-grained sand and commonly display normally graded rhythmites a few centimeters to several tens of centimeters thick. This facies dominates the Hanford formation occurrence along the western, southern, and northern margins of the Pasco Basin, within and south of the 200 Areas.

Clastic dikes are present in the Hanford formation as well as in other sedimentary units in the Pasco Basin (Black 1980). Locally, these dikes normally cross-cut bedding, although they do parallel bedding. They usually consist of thin alternating vertical to subvertical layers of silt, sand, and granules. Clastic dikes are more common in the finer grained facies and rare in the open-framework gravels (Connelly et al. 1992). Where the dikes intersect the ground surface, distinctive patterned ground is observed.

#### 4.1.2.7 Holocene Surficial Sediments

Holocene surficial deposits consist of silt, sand, and gravel that form a thin layer across much of the Hanford Site. These sediments were deposited by a combination of aeolian and alluvial processes.

### 4.2 C Tank Farm Geology Description

Price and Fecht (1976) provided the initial geologic information about the C Tank Farm geology on the basis of data collected during the construction of the first monitoring boreholes surrounding the tanks. Cross sections were prepared on the basis of analytical results obtained from these samples and from information documented on the drilling logs (on which drilled materials were recorded at 5-ft intervals). Caggiano and Goodwin (1991), Lindsey (1993), and Lindsey et al. (1992) present detailed descriptions and interpretations of the geologic formations in the vicinity of the C Tank Farm. This section is a summary of these documents.

When possible, the  $^{40}\text{K}$ ,  $^{238}\text{U}$ , and  $^{232}\text{Th}$  log plots were used to identify changes in the lithologic units. The  $^{40}\text{K}$ ,  $^{238}\text{U}$ , and  $^{232}\text{Th}$  log plots, as well as details regarding the interpretations of these plots, are presented in the individual Tank Summary Data Reports (DOE 1997i, 1997j, 1997k, 1997l, 1997m, 1997n, 1997o, 1997p, 1997q, 1997r, 1998a, and 1998b).

The most current and highest quality geologic information specific to the C Tank Farm is obtained from the most recently drilled groundwater monitoring wells. Caggiano and Goodwin (1991) consider well 299-E27-14 upgradient of the C Tank Farm, and wells 299-E27-12, 299-E27-13, and 299-E27-15 are downgradient. Figure 14-1 shows the locations of these and other non-RCRA-compliant groundwater monitoring wells in relation to the C Tank Farm and other adjacent facilities. These four wells constitute the RCRA-compliant groundwater monitoring network. All of these wells were completed during the drilling program for installation of RCRA-standard monitoring wells for SSTs in 1989. The RCRA-standard monitoring wells are distinguished from the non-RCRA-standard monitoring boreholes in Figure 14-1.

The RCRA groundwater well construction data packages were reviewed for lithology information. Caggiano and Goodwin (1991) and Lindsey (1993) provide interpretations of the geology and hydrogeology of the region below the C Tank Farm. Figure 14-7 shows the general stratigraphy and interpreted hydrologic conditions beneath the C Tank Farm. The geologic interpretations and the groundwater well construction data packages were used for interpreting the KUT log plots to identify the geologic contacts as well as for describing the geology below the C Tank Farm.

The surface of the basalt beneath the C Tank Farm is the eroded surface of the Elephant Mountain member of the Saddle Mountains Basalt. The basalt lies at a depth of about 300 ft below the surface of the C Tank Farm and dips gradually to the south.

Overlying the basalt is about 75 ft of Ringold Formation sediments consisting of gravels of Ringold unit A and the fine-grained sediments of the Ringold lower mud sequence. The top of the unconfined aquifer beneath the C Tank Farm is contained either in the Ringold unit A or the Ringold Formation Lower Mud unit (Figure 14-7). The C Tank Farm vadose zone monitoring boreholes do not extend to a depth necessary to intercept the contact between the Hanford formation and the Ringold Formation.

Overlying the Ringold Formation is about 225 ft of sediments of the Hanford formation. The upper 70 ft of the Hanford formation consists of the gravel-dominated facies (sometimes referred to as the Upper Coarse unit). Below the gravel-dominated facies lies approximately 155 ft of Hanford formation sand-dominated facies containing numerous laterally discontinuous silt-rich interbeds (sometimes referred to as the Hanford Fine unit) (see Figure 14-7).

The <sup>40</sup>K log plots for many of the boreholes show one or more intervals of elevated concentration values between the base of the tank farm excavation (about 40 to 45 ft) and at about 70 to 75 ft. The increases in concentration values generally ranged from 1 to 5 pCi/g.

The interval between the base of the tank farm excavation (at a depth of about 45 ft) and a depth of about 70 ft is interpreted to represent the Hanford formation gravel-dominated facies with some inter-bedded sands. Below a depth of about 70 to 75 ft, the <sup>40</sup>K concentration values increase and no other variations are identified; the contact at 70 to 75 ft is interpreted to represent the Hanford formation sand-dominated facies (Figure 14-7).

The excavation for the C Tank Farm tanks was constructed entirely in Hanford formation sediments, specifically gravel-dominated facies. The backfill placed around the completed tanks was the excavated materials that were stockpiled next to the tank farm during tank construction. When the tank construction reached a certain level, backfill material was added to raise the level of the excavation floor.

The contact between the backfill material and the undisturbed Hanford formation can be identified on the KUT log plots for most of the boreholes by a small increase in the <sup>40</sup>K concentration values. This increase typically occurred at depths of between 40 and 45 ft.

### **4.3 C Tank Farm Hydrogeology**

The following discussion is summarized from PNNL (1997a), Lindsey (1993), and DOE (1993b).

The Hanford Site is underlain by a multi-aquifer system consisting of four hydrologic units that correspond to the three uppermost formations of the Columbia River Basalt Group and the suprabasalt sediments (Delaney et al. 1991). The groundwater beneath the Hanford Site occurs under confined, semiconfined, and unconfined conditions. Figure 14-9 shows the water table elevations of the unconfined aquifer for 1996.

The confined aquifers are located in the sedimentary interbeds of the Ellensburg Formation, flow-top breccias, and in permeable interflow zones that occur between basalt flows (Figure 14-7). The shallow basalt flows are generally located in the Saddle Mountains and upper Wanapum Basalts. Recharge to these shallow basalt aquifers occurs through infiltration of precipitation and runoff along the margins of the Pasco Basin. Groundwater from the shallow basalt aquifers most likely discharges to the overlying sediments and to the Columbia River. Dense regions within the interior of the basalt flows of the Columbia River Basalt Group separate the flow tops and interflow zones and act as aquitards in the confined system.

At the C Tank Farm, the upper portion of the uppermost aquifer is contained in the Ringold Formation, which consists of variably cemented pebble-cobble gravel with a sand matrix with the finer grained material increasing with depth (Figure 14-7). In some places beneath the C Tank Farm, the top of the aquifer may be overlain by the Ringold Formation Lower Mud unit. The thickness of the Ringold unit A aquifer is approximately 50 ft thick beneath the C Tank Farm. In the vicinity of the C Tank Farm, the top of the saturated zone is about 247 ft below the ground surface, and the base, which is the top surface of the uppermost basalt flow (the Elephant Mountain Member of the Columbia River Basalt Group), is about 300 ft below the ground surface.

The elevation of the groundwater beneath the 200 East Area has varied significantly since the 1940s, when artificial recharge of the aquifers occurred through liquid discharges to several sites in the 200 East Area. At the present time, the surface of the groundwater is about 247 ft below the ground surface of the C Tank Farm. Figure 14-9 presents a groundwater map of the 200 East Area compiled from 1996 data.

Artificial recharge from the nearby 216-B-3 Pond System (B Pond) has altered the natural groundwater flow directions in the 200 East Area by producing a mound beneath this pond. This resulted in the development of a "saddle" that causes the groundwater beneath the 200 East Area to be partitioned into two flow directions, north through Gable Gap and to the southeast. Discharges to the B Pond have ceased, and the influence of these discharges on the 200 East Area groundwater flow is diminishing.

The direction of groundwater flow before Hanford Site operations is postulated to have been from west to east. As the groundwater mounded beneath pond and crib disposal sites, radial flow patterns developed that disrupted the natural west-to-east flow. The groundwater flow for the past several years in the 200 East Area was southeasterly (eventually turning east to the river) or north through Gable Gap.

Hydraulic properties for the unconfined aquifer have been determined from aquifer testing that was conducted in a number of boreholes in the 200 East Area, the details of which are provided in PNNL (1997a). These data indicate the hydraulic conductivity ranges between 48.7 and 119 meters per day (m/d) for unconfined aquifer beneath the C Tank Farm. However, because the hydraulic gradient is nearly non-existent beneath the C Tank Farm, the rate of groundwater flow is only approximately 0.01 to 0.06 m/d. Even though the gradient is barely measurable beneath the C Tank Farm (see Figure 14-9), the groundwater is thought to flow to the west.

Vadose zone conditions across the Hanford Site show variations similar to those observed in the uppermost aquifer system. Sediments in the C Tank Farm vadose zone vary from open-framework gravels of the gravel-dominated facies to interbedded sand and silt of the silt-dominated facies of the Hanford formation. These sediments are characterized by numerous lateral discontinuities, such as pinchouts and erosion truncations. If clastic dikes are present, they may enhance vertical flow of liquids. Therefore, there are numerous possible avenues for contamination-laden moisture to migrate through the vadose zone.

At the Hanford Site, recharge of the unconfined aquifer by precipitation is highly variable depending on seasons, vegetative cover, and surface and near-surface soil types. Figure 14-10 presents a natural recharge map from *Hanford Site Groundwater Monitoring for 1996* (PNNL 1997b). Natural recharge of the uppermost aquifer is through rainfall and runoff from the hills bordering the Hanford Site, infiltration from small ephemeral streams, water infiltration through faults and fractures in the underlying basalts, and from the Columbia and Yakima Rivers. Moisture movement through the unsaturated (vadose) zone has been studied at various locations at the Hanford Site. The most recent attempt at estimating recharge rates at the Hanford Site is documented in Fayer and Walters (1995). Fayer and Walters (1995) estimate average long-term recharge rates at the Hanford Site can vary from 2.6 millimeters per year (mm/yr) to 127 mm/yr (annual amounts of precipitation at the Hanford Site range from 76 to 291 mm). According to Fayer and Walters (1995), recharge is highest in coarse-grained sediments with little to no vegetative cover; this is the current surface configuration at the C Tank Farm.

The surface of the C Tank Farm has been altered significantly from its original natural state. The tank farm surface covers are designed to limit radiation dose by controlling surface contamination, which is accomplished by removing all vegetation, applying a gravel cover, and in some cases by applying a surface sealant to control dust. These measures may be increasing the potential for infiltration of meteoric water.

Artificial recharge of the uppermost aquifer occurs from the disposal of wastewater at the Hanford Site and from large-scale agricultural irrigation that surrounds the Site. Currently, large-scale waste water disposal occurs only at the Treated Effluent Disposal Facility located southeast of the 200 East Area and the Effluent Treatment Facility State Approved Land Disposal System located just north of the 200 West Area. Small-scale discharges are found in the form of numerous miscellaneous streams (as defined by WAC 173-216) and constitute only a small amount of the total site discharge.

Vadose zone hydraulic properties are an important factor in understanding the effects of the fate and transport of contaminants and the potential recharge of the vadose zone through precipitation. Laboratory results indicated a high degree of variability in moisture retention; however, there was a sparsity of data for some of the lithologic units encountered in the vadose zone beneath the 200 East Area. The reader is referred to DOE (1993a) and Connelly et al. (1992) for details regarding these analyses, as well as for the results of the analyses performed on samples of the vadose zone sediments from the Hanford and Ringold Formations.

#### 4.4 Groundwater Monitoring and Contamination in the C Tank Farm Area

The 200 East Area of the Hanford Site was used to chemically process irradiated nuclear fuel, to separate and purify plutonium, and to manufacture plutonium metal. Facilities associated with these operations include processing plants, manufacturing plants, and waste disposal facilities, including tank farms, landfills, injection wells, impoundments, cribs, ponds, and ditches. Figure 14-1 shows the location of the C Tank Farm relative to nearby adjacent waste handling and discharge facilities.

Groundwater beneath several facilities in the 200 East Area is monitored under a RCRA groundwater monitoring program currently administered by Pacific Northwest National Laboratories (PNNL). Included in the monitoring program, which was initiated in 1989, is Waste Management Area (WMA) C, an area that is defined by the C Tank Farm.

The *Interim Status Groundwater Monitoring Plan for Single Shell Tanks* (Caggiano and Goodwin 1991), the *200 East Groundwater Aggregate Area Management Study Report* (DOE 1993a), *Hanford Site Groundwater Monitoring for Fiscal Year 1996* (PNNL 1997b), and the *Hanford Site Environmental Monitoring Report for Calendar Year 1996* (PNNL 1997a) were reviewed during the preparation of this section. Brief summaries of groundwater data and previously published assessments of groundwater contamination are included so that the reader can place the vadose zone contamination in the C Tank Farm in context with known nearby contamination conditions. Inclusion of the groundwater contamination data also illustrates the need for additional vadose zone characterization data in order to confirm or refute the C Tank Farm as a source of groundwater contamination. All data and interpretations of the groundwater contamination presented in this section were derived from the documents listed above. Additional interpretations of the groundwater contamination were not performed as part of the Hanford tank farms vadose zone characterization project. The reader is referred to those documents for details regarding contaminant distributions, for discussions regarding methods and quality assurance of sample analyses, and for further interpretations of the results.

RCRA-compliant interim status groundwater monitoring for the SSTs was initiated in 1989. Groundwater is sampled semiannually in the WMA-C monitoring wells. These samples are analyzed for comparison to drinking water standards, general contamination indicators, and water quality parameters.

The RCRA groundwater monitoring network for WMA C consists of one upgradient and three downgradient wells. Well 299-E27-14 is upgradient of C WMA, and wells 299-E27-12, 299-E27-13, and 299-E27-15 are downgradient (Figure 14-1). The most recent groundwater level measurements indicate the depth to groundwater in wells monitoring the C Tank Farm is about 247 ft. These measurements also indicate the depth to groundwater is increasing. This increase is attributable to the cessation of liquid effluent discharges to nearby facilities.

The only contaminant to exceed groundwater quality standards is iodine-129. Contaminant levels were exceeded in all four RCRA monitoring wells. Contaminant levels in upgradient well 299-E27-14 were slightly higher than the downgradient wells. According to PNNL (1997a),

critical mean values of the indicator parameters specific conductance, pH, total organic carbon, and total organic halogen were not exceeded in fiscal year 1996.

Low levels of  $^{99}\text{Tc}$  (maximum of 88 pCi/L in upgradient well 299-E27-14) were detected in both the upgradient and downgradient RCRA wells around the C Tank Farm. However, there is no evidence of a plume upgradient of the tank farm (PNNL 1997a).

Tritium and nitrates were detected in the C Tank Farm RCRA wells in 1996, but did not exceed regulatory limits. These contaminants appear to be part of larger plumes that are extensive throughout the 200 East Area groundwater.

## 5.0 C Tank Farm Background

The following sections are summarized from Brevick et al. (1994), Agnew (1995, 1996), Hanlon (1997), and Anderson (1990). The reader is referred to these documents for more detailed descriptions of the C Tank Farm construction, tank waste history, and the current status regarding tank monitoring and waste content.

### 5.1 Construction

The C Tank Farm was constructed at the Hanford Site to store high-level radioactive waste generated by chemical processing of irradiated uranium fuel. Located in the central portion of the 200 East Area, about 2,000 ft north of the PUREX Plant, the C Tank Farm was constructed during 1943 and 1944. The C Tank Farm consists of 12 first-generation 100-series single-shell underground waste storage tanks and four 200-series tanks. Each 100-series tank has a capacity to store 530,000 gal of high-level waste and each 200-series has a capacity to store 55,000 gal; therefore, the C Tank Farm has a capacity to store 6,580,000 gal of waste. Tanks C-101, C-110, C-111, C-201, C-202, C-203, and C-204 are suspected to have leaked approximately 29,250 gal of high-level waste into the vadose zone. Figure 14-11 shows the relative positions of the C Tank Farm tanks and the vadose zone monitoring boreholes around them. The seven tanks in the C Tank Farm designated as assumed leakers are also noted on Figure 14-11.

The construction of the twelve 530,000-gal tanks and four 55,000-gal tanks in the C Tank Farm is discussed in Brevick et al. (1994). The twelve 530,000-gal tanks are steel lined and are 75 ft in diameter, with a maximum operational height (cascade overflow level) of 16 ft above the center of the dished tank base; the center of the dished base is 1 ft lower than the base perimeter. The tanks are covered by a 1.25-ft-thick reinforced concrete domed top that extends about 13 ft above the tank operating level. The tanks are entirely below the ground surface and are covered with about 8 to 12 ft of backfill material. The maximum operating level of the tank is about 21 to 23 ft below the ground surface. Allowing space for footings and other construction requirements, the base of the C Tank Farm excavation is about 40 ft below the ground surface.

The C tanks are connected in four three-tank cascade series: tanks C-101, -102, -103, tanks C-104, -105, -106, tanks C-107, -108, -109, and tanks C-110, -111, -112. The cascade tanks are

arranged with each successive tank sited at a lower elevation (with the receiving tank 1 ft lower than the feed tank), creating a gradient that allowed fluids to flow from one tank to another as they were filled. Allowing for the gradient, the cascade-line connections between the tanks are approximately 22 to 24 ft below the ground surface. The inside bottom of the first tank of the series is approximately 40 ft below the ground surface, with the other tank bottoms successively lower by 1 ft. The wastes from the 100-series tanks were apparently not cascaded to cribs, but wastes from the 200-series tanks were.

Various measuring devices such as FIC gauges (liquid surface measuring device), ENRAF gauges (liquid surface measuring device), thermocouple trees (for measuring waste temperatures), and liquid observation wells (used to measure the liquid levels in the tanks with geophysical logging tools) are used to monitor the tank wastes. These devices are discussed in Section 5.5 of this report.

Also installed in the tanks is equipment used to transfer waste to and from the tank, including various sized pumps and sluicing equipment.

Each tank is surrounded by several boreholes in which radiometric instruments were used to detect changes in activity levels in the sediments surrounding the borehole. Seventy boreholes were constructed between 1944 and 1978 to monitor for leaks from the 12 SSTs of the C Tank Farm. These boreholes have served as both primary and secondary leak-detection devices and are shown in Figure 14-11.

## **5.2 History and Tank Contents**

High-level radioactive waste generated at Hanford from 1945 to 1989 was derived predominantly from the chemical dissolution and extraction of plutonium and uranium from irradiated reactor fuel elements. The extractions during these years evolved through three basic processes: the bismuth phosphate ( $\text{BiPO}_4$ ) process, the reduction-oxidation (REDOX) process, and the plutonium uranium extraction (PUREX) process. These processes were used for the extraction of plutonium. A fourth process, the tributyl phosphate (TBP) process, was designed for the recovery of uranium from the  $\text{BiPO}_4$  waste. The wastes from these processes were neutralized and discharged to the underground waste-storage tanks, cribs, and ponds.

Anderson (1990) provides general information about the contents of the C Tank Farm tanks. More information specific to this farm and each tank is provided in a recent compilation of historical monitoring information assembled in several volumes of reports by ICF Kaiser Hanford Company and Los Alamos National Laboratory. The volumes prepared by Brevick et al. (1994) specifically address the C Tank Farm; these documents present historical waste inventories for each of the C Tank Farm tanks. The authors of those documents have compiled most of the available monitoring information on the tanks and provided detailed summaries of tank construction and configuration, interior tank photographs, and other data. Agnew (1995, 1997) provide an estimate of the chemical and radionuclide composition of the tank waste in the C Tank Farm (as well as all tank farms). The information provided in this section is a summary of information from those documents; the reader is referred to those documents for a more

detailed description of the tank contents. A sampling program is underway to determine the current radionuclide content and chemistry of the waste; results of that campaign were not used in the preparation of this report.

The C Tank Farm received a variety of wastes types primarily from B Plant, U Plant, the Strontium Semiworks Plant, and the PUREX Plant. These waste streams included metal waste, byproduct cake solution, first-cycle decontamination waste, cladding waste, PUREX organic wash waste, various waste streams from the thorium campaigns, and Evaporator/Chrystalizer waste streams. Some of the principal radionuclides in the C Tank Farm wastes include  $^{137}\text{Cs}$ ,  $^{134}\text{Cs}$ ,  $^{60}\text{Co}$ ,  $^{89-90}\text{Sr}$ ,  $^{125}\text{Sb}$ ,  $^{106}\text{Ru}$ ,  $^{144}\text{Ce}$ ,  $^{95}\text{Zr}$ , and  $^{154}\text{Eu}$  (Brevick et al. 1994).

The C Tank Farm tanks were scavenged to recover uranium in the early to mid-1950s. In the 1960s,  $^{137}\text{Cs}$  and  $^{90}\text{Sr}$  (the primary heat producers) were removed from the tank waste in order to facilitate safer storage of the waste. A large amount of strontium remains in tank C-106 and has caused a high heat load in the tank. A lesser amount of these heat-generating radionuclides remains in tank C-105. Water is added to these tanks in order to promote cooling of the waste. In the past, data used to calculate the evaporation rate in these tanks apparently did not exist. Therefore, it is possible that if one of these tanks leaked, it would have been masked by liquid loss through evaporation.

The waste sent to the C Tank Farm tanks in the mid to late-1950s resulted from the later part of the bismuth phosphate plutonium extraction process. During this time, the fuel rods were "burned" longer to cause a higher percentage of transmutation of uranium to plutonium in the reactors. The longer burning fuel times also created higher concentrations of activation products that were carried into the process feed material.  $^{60}\text{Co}$  in particular was an activation product of concern because it is a high activity nuclide that emits high-energy gamma rays.  $^{60}\text{Co}$  was generated from that activation of stable  $^{59}\text{Co}$  that was present as either an impurity or as an intentional additive in the steel used as components of the fuel rods (DOE 1997m).

The high gamma flux from  $^{60}\text{Co}$  became a problem during processing operations in the mid-1950s, until the specifications were changed to limit the amount of  $^{59}\text{Co}$  present in the fuel rods. As a result, the waste stored in the tanks contained a relatively higher concentration of  $^{60}\text{Co}$ . In addition, the tanks were used in the ferrocyanide scavenging campaigns, which solidified the  $^{137}\text{Cs}$  and  $^{90}\text{Sr}$  and further increased the concentration of  $^{60}\text{Co}$  in the supernatant liquid. Therefore, if a tank leaked, it is more than likely to have leaked a substantial amount of  $^{60}\text{Co}$ ; the  $^{60}\text{Co}$  should then be found in abundance in the vadose zone sediments (DOE 1997m).

Liquid levels in the tanks were highly variable during the next 20 years until the tanks were eventually filled with solids. The fluctuating liquid levels would have made accurate in-tank leak detection nearly impossible.

The wastes in the C Tank Farm consist mainly of sludge, salt cake, and liquid. Sludge is composed of solid (hydrous metal oxides) precipitate that results from the neutralization of acid waste. The wastes were neutralized before being transferred to the waste tanks. Salt cake is composed of salts formed by the evaporation of water from the waste. Sludge and salt cake form

the "solids" component of the tank waste. Liquids are present as supernatant and interstitial liquids. Supernatant is found on the top of the solid waste surface, and interstitial liquid fills the interstitial spaces within the waste solids. Interstitial liquid may be drainable if it is not held in the void spaces by capillary forces.

General tank content (liquid and solid levels) data and some tank monitoring data are summarized monthly in the *Waste Tank Summary Report*. Hanlon (1997) is an example of one of those reports. Table 1 shows current tank waste quantities, current monitoring methods, and some historical information. The drainable liquid is the total estimated liquid in the tank. The leak volumes are based on estimates that are summarized in Hanlon (1997).

Table 1. General C Tank Information

Tank	Total Waste Volume (1,000 gal)*	Drainable Liquid (1,000 gal)*	Current Primary Leak Detection Method*	Other Available Tank Monitoring Methods*	Leaker (Y/N)*	Estimated Leak Volume (gal)*	Original Leak Indication
C-101	88	3	None	Manual tape	Y	20,000	Liquid-level decrease
C-102	316	30	None	FIC			
C-103	195	133	ENRAF				
C-104	295	11	None	FIC			
C-105	134	32	None	Manual ENRAF			
C-106	229	48	ENRAF				
C-107	237	24	ENRAF				
C-108	66	0	None	Manual tape			
C-109	66	4	None	Manual tape			
C-110	178	29	Manual tape		Y	2,000	Historical gross gamma log data
C-111	57	0	None	Manual tape	Y	5,500	Liquid-level decrease
C-112	104	32	None	Manual ENRAF			
C-201	2	0	None	Manual tape	Y	550	Liquid-level decrease
C-202	1	0	None	Manual tape	Y	450	Liquid-level decrease
C-203	5	0	None	Manual tape	Y	400	Liquid-level decrease
C-204	3	0	None	Manual tape	Y	350	Liquid-level decrease
TOTAL	1,976	346			7	29,250	

\* Information from Hanlon (1997).

### 5.3 Current Status

Tanks C-102, C-103, and C-106 have been identified as Watch List Tanks in accordance with Public Law 101-510, Section 3137 (commonly referred to as the Wyden Amendment). These

tanks have been identified as high priority safety issues at the Hanford Site. Tanks C-102 and C-103 are listed on the Organics Watch List and tank C-106 is listed on the High Heat Load Watch List. Tanks are added to the Organics Watch List because they contain greater than 3 weight-percent of total organic carbon. Tank C-106 is on the High Heat Load Watch List because the tank contains a significant amount of heat-producing strontium and without periodic water additions the tank could reach temperatures that could result in structural damage to the tank.

Seven of the 16 C Tank Farm tanks are classified as a leakers: tanks C-101, C-110, C-111, C-201, C-202, C-203, and C-204. These tanks are currently estimated to have leaked a total of 29,250 gal of waste. For tanks C-101, C-111, C-201, C-202, C-203, and C-204, the basis for the assumed leaker designation was apparently due to in-tank liquid-level measurements. The assumed leaker designation for tank C-110 was based on anomalous activity in the vadose zone boreholes.

Liquid-level increases occur in most of the tanks in the C Tank Farm. The C Tank Farm tanks have been out of service for almost 20 years, and since then no waste products have been added to the tanks. Liquid-level increases can generally be attributed to intrusion of precipitation or shifting or settling solid wastes.

## **5.4 Unplanned Releases**

Fourteen unplanned releases (UPRs) are located within or immediately adjacent to the C Tank Farm. Figure 14-1 shows the locations of the unplanned releases within and around the C Tank Farm. The information contained in this section was obtained from the *PUREX Source Aggregate Area Management Study Report* (DOE 1993b).

### **UPR-200-E-137**

This UPR is associated with the leak from tank C-203. Over a period of 2 to 3 years precipitation entered the tank and migrated through or became entrained in the salt cake. Approximately 400 gal of waste eventually leaked from the tank. The leak estimate is based on in-tank liquid-level measurements.

Because no monitoring boreholes are located around tank C-203, the nature and extent of the tank leak cannot be determined.

### **UN-200-E-91**

This UPR, which is located approximately 100 ft from the northeast side of the tank farm, is the result of surface contamination that has migrated from the C Tank Farm. The occurrence date, the areal extent, and the nature of the contamination were not specified.

The contaminated sediment was removed and the area was released from radiological controls.

### **UN-200-E-118**

This UPR, which is located in the northeast portion of the farm and extends north up to 300 yards beyond the fence line, is the result of an airborne release from tank C-107 that occurred in April 1957. The highest exposure rate was estimated at 50 millirem/hour at the ground surface.

### **UPR-200-E-136**

This UPR is associated with a leak from tank C-101 and the resulting contaminated vadose zone sediments. The tank was classified as "questionable integrity" in 1970. According to DOE (1993b), the tank leaked between 17,000 and 24,000 gal of waste containing 2,000 Ci of unknown radionuclides.

### **UN-200-E-27**

This UPR is located just east of the 244-CR Vault and extends generally east several hundred feet beyond the tank farm fence line. DOE (1993b) indicates the surface contamination was deposited in 1960, but does not specify the source or potential sources of the contamination.

### **UN-200-E-72**

This UPR is located south of the C Tank Farm and occurred in 1985. According to DOE (1993b), the source of the contamination was buried contaminated waste, but posed little release potential because the contamination was fixed in place. The source of contamination was stabilized (the source was not specified) and the area posted as a radiologically controlled area.

The volume of the contamination was not specified, but was measured at 7 roentgen/hr.

### **UN-200-E-100**

This UPR is a surface spill of unknown proportions and constituents that occurred in 1986. It is located about 200 ft south and east of the C Tank Farm and surrounds the 244-A Lift Station.

### **UN-200-E-99**

This UPR is defined as surface contamination that occurred as a result of numerous piping changes associated with the 244-CR Vault. It is located west of the 244-CR Vault and was established as a release site in 1980. The site was apparently decontaminated in 1981.

### **UN-200-E-68**

This UPR is surface contamination that resulted from wind-borne contamination spread from the 241-C-151 Diversion Box. The surface contamination occurred in 1985 and was subsequently decontaminated or covered with clean sediment.

#### **UN-200-E-107**

This UPR is a surface spill that is located at the 244-CR Vault, inside the C Tank Farm fence. DOE (1993b) is unclear as to the cause of the contamination. The document claims a spill occurred on November 26, 1952 when a pump discharged liquid to the ground surface during operation as the result of a pump installation. The proportions of the spill and any cleanup actions were not documented.

#### **UN-200-E-81**

This UPR is located between tank C-104 and the 244-CR Vault and occurred as a result of a leak in an underground transfer pipeline in October 1969.

The waste leaked from the pipeline consisted of PUREX coating waste and contained 360 Ci of <sup>90</sup>Sr, 720 Ci of <sup>137</sup>Cs, 360 Ci of <sup>144</sup>Ce, 1,080 Ci of <sup>95</sup>Zr/Nb, and 1,080 Ci of <sup>106</sup>Ru (apparently measured at the time of the leak). The site was covered with gravel.

#### **UN-200-E-82**

This UPR is located between a C Tank Farm diversion box and tank C-105 and is the result of a leak from an underground pipeline that occurred in December 1969.

The leak spilled an unknown volume of waste containing an estimated 100 Ci of <sup>134</sup>Cs, 11,300 Ci of <sup>137</sup>Cs, 260 Ci of <sup>144</sup>Ce, 260 Ci of <sup>95</sup>Zr, and 130 Ci of <sup>106</sup>Ru (apparently measured at the time of the spill). The contaminated site was covered with clean gravel.

#### **UN-200-E-86**

This UPR is a spill that resulted from a leak in a transfer line, approximately 8 ft below the ground surface. It occurred in March 1971 and is located just outside the west corner of the tank farm.

DOE (1993b) indicates the spill consisted of 25,000 Ci of <sup>137</sup>Cs (apparently measured at the time of the spill). The sediments surrounding the pipeline were sampled and it was determined the contamination had not penetrated below 20 ft. The contamination plume volume was estimated at 1,300 cubic feet.

#### **UN-200-E-16**

This UPR is defined as a surface spill that occurred as a result of a leak in an overground transfer pipeline located between tanks C-105 and C-108. The surface spill associated with this UPR is located approximately 60 ft northeast of tank C-105 and occurred in 1959.

The spilled liquid was classified as PUREX coating waste. The contaminated pipe was buried in a trench near the C Tank Farm fence.

## 5.5 Leak-Detection Monitoring

The SSTs have been monitored for leak-detection purposes throughout the years using either liquid-level measurements, solid-level measurements, or direct detection of contamination in the vadose zone with gross gamma logging. Section 5.7, "Gross Gamma Logging," presents a discussion of previous gross gamma logging programs used to detect contamination in the vadose zone.

Solid- and liquid-level measurements continue to be made by direct access to the surface of the waste inside the tanks through surface riser ports built into the tank's domed tops. Instruments lowered to the waste surface to determine the level include simple instruments like weighted hand-held measuring tapes, conductivity probes, electronic tapes, and, more recently, automated ENRAF ATG 854 (manufactured by ENRAF, Inc.) liquid-level measuring instruments. The precision of the measurements or potential problems likely to be encountered are described in Welty (1988), Scott (1993), and Catlin (1980).

Sealed fiberglass and TEFZEL (trade name) casings were also inserted into the waste solids (sludge and salt cake) in a majority of the tanks to allow access for geophysical logging tools. These sealed casings are called liquid observation wells or LOWs at the Hanford Site. The monitoring tools used in the LOWs include very low-efficiency gamma-ray detection probes (Geiger-Mueller detectors) to measure the variations in gamma flux and neutron-neutron probes to measure variations in the hydrogen content profile. These tools are intended to detect changes in the solid-to-liquid interface level, and, thus, changes in the liquid level. They are particularly important for detecting leaks because most tanks now have relatively solid sludge and salt cake waste components and the liquid is only found in the interstices or pores of the solid material. Therefore, a surface-level measurement will not detect changes in the interstitial liquid level. Scott (1993), Isaacson (1982), and Catlin (1980) describe the instrumentation used to measure interstitial liquid levels in the tanks.

New LOW liquid-level measurement instrumentation has recently been procured at Hanford and reportedly will soon be used to monitor the interstitial liquid level.

Currently, the in-tank solid- and liquid-level measurements provide the primary method of detecting leaks from the tanks (see Table 5.1). Work is in progress to install liquid-level-measuring ENRAF gauges and to perform LOW liquid-level measurements on a regular basis for all of the tanks (Hanlon 1997).

## 5.6 Vadose Zone Monitoring Boreholes

All the SST farms, including the C Tank Farm, have monitoring boreholes installed around the tanks. These boreholes were installed and used as a part of a tank leak-detection monitoring program where gamma-ray detectors were lowered into the boreholes to detect the presence of gamma-ray-emitting radionuclides in the sediments surrounding the tanks. The locations and identifications of the boreholes surrounding tanks in the C Tank Farm are shown on

Figure 14-11. Details regarding the construction and current configuration of the boreholes can be found in the individual Tank Summary Data Reports.

The construction of most boreholes is documented in the form of drilling logs. The drilling logs provide varying degrees of detail and description regarding the drilling operations, geologic descriptions of sediments penetrated by the drilling, and explanations of the construction configurations of the boreholes. Although the information provided in the drilling logs is limited in scope in most instances, the drilling logs provide information on when and how the boreholes were drilled and sometimes document the occurrences of radiological contamination when it was encountered during drilling. All the drilling logs are available in borehole archive files maintained by Waste Management Federal Services, Inc., Northwest Operations.

All the vadose zone monitoring boreholes were drilled with a cable-tool drill rig. This type of drill rig uses a drill stem suspended from a cable to drive an open-ended drive barrel into the sediments. The filled drive barrel is removed from the borehole and struck to remove the sediments. When sediments are encountered that do not remain in the drive barrel as the drive barrel is removed from the borehole, water is added to the borehole to wet the drilled sediments and to improve cohesion within the drive barrel.

As the drive barrel is driven downward and the drill cuttings are removed to create the borehole, the borehole is open along the drilling interval, which can be from about 4 to 10 ft, depending on the competency of the sediments being drilled. A carbon-steel casing is then driven down into the slightly undersized, open portion of the borehole, and the drilling process then proceeds over another drilling interval. The first sediments drilled after casing advancement are those materials sheared off the formation wall into the borehole as the casing was advanced.

During cable tool drilling, there is a possibility that the borehole wall will collapse along the "open hole" portion of the borehole, before the steel casing is driven into place. If formation material sloughs from the borehole wall into the borehole, the sloughed material will be removed with the drive barrel; however, a void is created in the borehole. Once the casing is driven into place, the void may remain behind the borehole casing.

When a borehole is drilled through a zone of contamination with a cable tool rig, contamination could be carried down to at least the maximum extent of the drilling interval (4 to 10 ft) if sloughing were to occur in the open portion of the borehole as it is being drilled. However, because most of the sediment is removed from the hole by the drive barrel after the casing is driven into place, only a relatively small amount of contaminated sediment would be left at the bottom of a drilled interval around the outside of the casing.

Voids behind the casing or a highly rugose borehole can create a pathway for migration of contaminants down the outside of the borehole casing. Minor contamination movement could occur as sloughed material sifted downward within the gap between the outside of the casing and the formation. The pounding action of the cable tool drilling process would significantly amplify the sifting action along the casing and thus minimize the amount of void space behind the casing at the completion of the borehole.

Small concrete collars were installed at the ground surface at the completion of the construction of the boreholes. These collars may have been designed to prevent water from migrating down the interface of the outside of the casing and the sediments if this interface was exposed at ground surface. However, these collars would be insignificant barriers if considerable water was present at the surface, such as from ponding from rain or snowmelt.

Surface sealants have been applied to the C Tank Farm ground surface to inhibit contaminant migration. The surface sealants also enhance surface runoff. The C Tank Farm surface contains many small depressions where the runoff accumulates and evaporates or infiltrates through breaks in the surface sealant.

All of the borehole casings were cut off at the top of the surface collars. Plugs or caps were put into the boreholes to keep dust, contaminants, and objects out of the boreholes, but the caps are not watertight. If ponding occurred at the surface, there is potential for water and contaminated sediments to enter and migrate down the inside of the borehole casings even though the cap is on the top of the casing. If a borehole cap is removed for a significant amount of time, contaminated sand or silt can be blown into the borehole and settle at the bottom of the hole. This is seen as slightly elevated contamination activity at the bottom of the borehole. When low-level contamination is present at the bottom of a borehole with contamination-free regions above it, it is usually assumed that the contamination is on the inside of the borehole casing and is not present in the formation sediments.

The potential for contamination either being carried down during the drilling process or being driven down by ponded water from the ground surface has been considered when the SGLS data for each borehole were interpreted in the Tank Summary Data Reports and in this report.

Log Data Reports accompany the log plots in the Tank Summary Data Reports. The borehole data presented in the Log Data Reports contain information regarding borehole drilling details, geological information, well construction configuration, and other pertinent information found in the documentation on file. Additional information on the individual boreholes is provided in each Tank Summary Data Report.

## **5.7 Gross Gamma Logging**

A gross gamma logging program was the primary means of detecting leaks from the SSTs for many years. The intent of the logging program was to detect a leak front that was thought to produce high concentrations of radionuclides in the formation intersected by tank monitoring boreholes. Gross gamma logs were acquired for all the C Tank Farm boreholes according to a schedule specified in Welty and Vermeulen (1989) and Welty (1988). In the past, logging was performed more frequently because it was often the only leak-detection method available or in-tank measurement precision was poor. More recently, this program has been discontinued in favor of upgraded and more accurate in-tank measurements, and reliance on the gross gamma logging for leak detection was eliminated for all of the SSTs.

Gross gamma logging of some fashion began at Hanford in the 1960s by making station measurements with Geiger-Mueller detectors that were lowered by hand into the boreholes. Almost no documentation is available about this work, other than references to the monitoring in some daily operations logs of the health physics technicians.

In the mid-1970s, the gross gamma logging program was upgraded to more automated systems installed in vans; description of this equipment is documented in Isaacson (1982). These logging systems were used to create a large monitoring database. The systems used three different downhole gamma-ray detector probes that sent pulses up a cable to a pulse counter. The counter tallied the pulses and output a total count value to a computer every second. The downhole probes were withdrawn from the hole at a set rate, thereby summing the counts throughout an interval in the borehole.

The three downhole probes consisted of a 1-in.-diameter by 1-in.-long sodium-iodide detector, a lower efficiency probe containing three Geiger-Mueller tubes, and a low-efficiency probe containing a small, shielded Geiger-Mueller tube. The intent of the three probes was to be able to cover a large gamma-ray flux range without saturating the instrumentation. These systems were effective at covering the high range of activity but were not effective at detecting lower radionuclide concentrations (less than 10 pCi/g equivalent  $^{137}\text{Cs}$ ).

Boreholes were logged at a set rate of 45 feet per minute (ft/min). With a counting time of 1 s and a delay required to save the data, the resulting data acquisition interval was 1 ft. These logging systems recorded the total number of gamma-ray photons detected throughout the 1-ft intervals and recorded the top depth of the data acquisition interval.

Data were presented as plots of the gross count rate in counts per second (cps) as a function of depth. Spatial count-rate activity peaks were compared visually with previous data to determine, in a qualitative manner, if changes had occurred. No additional processing or analysis was performed on the data. If a change was suspected, the borehole was relogged or the monitoring frequency was increased. An increasing count-rate activity trend in the data was used to identify a leak from a tank.

Determinations of contaminant migration were made on the basis of changes in gamma-ray flux instead of on radionuclide concentrations because the logging instrumentation was not calibrated to a radionuclide concentration response. Relative changes in detected count rate were sometimes related to leaks from tanks.

Review and visual comparison of gross gamma log profiles over time have been useful to determine if contamination has moved downward or changed in intensity. However, because of the poor spatial resolution of the data (1 ft), tabulation of the maximum spatial peak count rates and comparison of those count rates over time are not recommended. Small changes in the position of the borehole probe between log runs cause large variations in the spatial peak count rates. Review of the gross gamma logs over time has shown depth variations of several feet for some boreholes.

When evaluating any gross gamma log data, the sensitivity of the instruments to the presence of  $^{137}\text{Cs}$  must be considered. Comparison of the Tank Farms gross gamma log data to the  $^{137}\text{Cs}$  concentration plots has shown that a positive gross gamma response can only be expected when  $^{137}\text{Cs}$  is present at concentrations of 10 pCi/g or more.  $^{60}\text{Co}$  and other lower specific activity nuclides each have higher minimum detection levels.

Despite its limitations, the gross gamma logging database is the best historical record of the vadose zone contamination around the SSTs. Because the boreholes were consistently logged, an extensive and fairly comprehensive library of gross gamma activity is available for many of the boreholes. Once the limitations of these data are understood, the data library may be useful for assessing some of the history of the vadose zone contamination.

At the present time, no gross gamma-ray logging is being conducted in the monitoring boreholes surrounding the tanks in the C Tank Farm. Leak detection is conducted through acquisition of in-tank measurements within LOWs and/or by measurements of waste surfaces using the ENRAF measuring device. The most recent procedures for leak detection are outlined in the *Operating Specifications for Tank Farm Leak Detection* (WHC 1994).

## 5.8 Previous Spectral Gamma-Ray Characterizations

A study of the gamma-ray-emitting radionuclide contaminant distribution surrounding tanks C-105 and C-106 was undertaken in response to Washington State Department of Ecology concerns that RL and the existing Hanford Site contractor could not provide conclusive evidence that tank C-106 had not leaked. Ecology contended the liquid-level data, temperature data, and evaporative cooling calculations did not meet the regulatory requirements needed to assure them the tank had not leaked. Several actions were identified that would ultimately provide conclusive evidence as to the true integrity status of tank C-106; one of these actions was to characterize the gamma-ray-emitting radionuclides that should be present in the sediments surrounding the tank if the tank had in fact leaked.

*Assessment of Unsaturated Zone Radionuclide Contamination Around Single-Shell Tanks 241-C-105 and 241-C-106* (Brodeur 1993) provides an assessment of the data acquired from an 18-percent HPGe detector mounted on a system known as the Radionuclide Logging System (RLS) (the SGLS uses a 35-percent HPGe and is discussed in Section 7.0), with the intent of determining if there was evidence that tanks C-105 or C-106 had leaked. In support of this assessment, the WHC Geophysics group analyzed tank farm gross gamma log data, tank construction records, in-tank measurement records, and the local geology.

Brodeur (1993) identified three zones of subsurface contamination. The first zone was between tanks C-104 and C-105 and was attributed to a leak in the cascade pipeline that runs between the two tanks. The second zone is located at a depth of about 50 ft around borehole 30-05-05 and was attributed to the leak in the C-104-to-C-105 cascade line or a leak from tank C-105. The third zone is located between tanks C-103 and C-105 at a depth of about 27 ft and was attributed to a leak in a subsurface pipeline or a leak from either tank C-103 or C-106. According to

Brodeur (1993), data from the RLS as well as a review of historical information did not provide direct evidence that tank C-105 or tank C-106 had leaked.

The investigation conducted by the WHC Geophysics group relied heavily on gross gamma log data. Attempts were made to correlate between boreholes with spectral gamma log data and boreholes with only historical gross gamma log data in order to provide a greater understanding of the subsurface contaminant distribution. Based on interpretations of these correlations, Brodeur (1993) proposed tanks C-103 and C-109 may have leaked.

In response to preliminary conclusions and recommendations in Brodeur (1993), a study was conducted of gamma-ray-emitting radionuclides around tank C-103. As discussed in Section 10.2.5, analysis done by the WHC Geophysics group and documented in Brodeur (1993) suggested leaks from tanks C-103 and C-109 may have been the cause of subsurface contamination around these tanks. Characterization of the vadose zone around tank C-103 was considered a higher priority because it held 133,000 gal of liquid and tank C-109 had been interim stabilized. The vadose zone around tank C-109 was not characterized by the WHC Geophysics group.

*Assessment of Vadose Zone Radionuclide Contamination Around Single Shell Tank 241-C-103* (Kos 1995) provides an assessment of the data acquired from an 18-percent HPGe detector mounted on the RLS, with the intent of determining if there was evidence that tank C-103 had leaked. In support of this assessment, the WHC Geophysics group analyzed historical tank farm gross gamma log data, tank construction records, in-tank measurement records, and the local geology.

Kos (1995) identified three zones of contamination around tank C-103: one near the surface, another at the base of the tank farm excavation, and a third at a depth of 80 ft. The RLS logging campaign for tank C-103 identified  $^{137}\text{Cs}$  and  $^{60}\text{Co}$  in the boreholes surrounding the tank. Kos (1995) proposed two scenarios to explain the contaminant distribution around the tank.

Kos (1995) concludes the  $^{137}\text{Cs}$  contamination from the ground surface to the base of the tank farm excavation is the result of a large undocumented surface spill. The surface spill apparently migrated through the backfill material until it reached the tank dome. Upon reaching the tank dome the contamination ran along the outside of the tank structure to the base of the tank farm excavation. The  $^{137}\text{Cs}$  appears to have remained stable since 1974 (the earliest available gross gamma log data) (Kos 1995).

The  $^{60}\text{Co}$  contamination at 80 ft was attributed to a source near tanks C-108 and C-109. Kos (1995) concludes the RLS log data, neutron moisture probe data, and tank farm gross gamma log data show a clear "trail" from the vicinity of tanks C-108 and C-109. Neutron-moisture probe data show an interval of elevated moisture at a depth of about 80 ft. The tank farm gross gamma log data show the contamination migrating as late as the mid-1980s. Also, the RLS data do not identify  $^{60}\text{Co}$  above 80 ft as would be expected if the contamination came from tank C-103.

## 6.0 Adjacent Waste Handling Facility Information

Several waste disposal facilities are located in the vicinity of the C Tank Farm, and brief descriptions of these facilities are provided in the following sections. Figure 14-1 shows the locations of these waste sites. Only sites that could potentially have affected the vadose zone contamination at the C Tank Farm are considered.

The information presented in the following sections is summarized from the *PUREX Source Aggregate Area Management Study Report* (DOE 1993b) and the *Handbook of the 200 Areas Waste Sites* (Maxfield 1979).

### 6.1 216-C-8 French Drain

The 216-C-8 French Drain, which is located about 75 ft south of the southeast perimeter fence of the C Tank Farm, is a 6-ft-diameter by 8-ft-long concrete culvert placed vertically into the ground (see Figure 14-1). The culvert is filled with gravel and resides in an 8-ft-diameter by 16-ft-long excavation. The excavation is filled with gravel and backfill material to the surface grade. The surface area is currently stabilized with sand.

The french drain was active from June 1962 to June 1965 and received an unknown amount of ion-exchange regenerant waste from the 271-CR Control House. A definition of "ion exchange regenerant waste" is not known.

### 6.2 244-CR Vault

The 244-CR Vault, which is located inside the C Tank Farm just south of the tanks, is a concrete structure that is 102 ft long, 26 ft wide, and 55 ft deep and operated from 1946 to 1988 (see Figure 14-1). It is a 2-level structure, the lower level contains process vessels and the upper cells contain the ancillary piping and equipment. The lower cell contains four tanks, two 20 ft in diameter by 19 ft tall and the other two 14 ft in diameter by 12 ft tall. The 244-CR Vault was used to transfer various waste streams between the C Tank Farm tanks and processing and decontamination operations.

### 6.3 241-C-301C Catch Tank

The 241-C-301C Catch Tank is located in the north corner of the C Tank Farm and is adjacent to tank C-112 (see Figure 14-1). This unit is associated with the 241-C-151, 241-C-152, 241-C-153, and 241-C-252 Diversion Boxes and was used for the transfer of waste streams from various processing and decontamination operations. The catch tank was constructed in 1946 and is currently inactive. The dates when this unit was operating were not documented. The tank currently holds 10,470 gal of 207-A Retention Basin condensate.

## 6.4 241-C-801 Cesium Loadout Facility

The 241-C-801 Cesium Loadout Facility is located within the C Tank Farm (see Figure 14-1). This facility operated between 1962 and 1976. Trucks equipped with ion-exchange casks were backed into the facility and supernate was pumped from tank C-105. The casks were then sent to Oak Ridge, Tennessee to recover cesium.

# 7.0 Spectral Gamma Logging Measurements

## 7.1 Equipment

Logging operations were accomplished with two SGLSs (designated for identification purposes as Gamma 1 and Gamma 2). These systems were manufactured in 1993 by Greenspan, Inc., of Houston, Texas. They are a custom assemblage and adaptation of laboratory-quality spectroscopy instrumentation and were designed specifically to perform laboratory-quality assays in boreholes. Complete documentation, including plans, system schematics, software documentation, and specific component manuals, is available in the DOE-GJO archive files.

Both logging units are completely self-contained systems composed of a downhole probe, a logging cable and delivery system, and surface computer electronics mounted in a cabin on a heavy-duty truck chassis. Figure 14-12 shows one of the SGLSs in a typical logging setup over a borehole.

These systems use HPGe gamma-ray detectors with efficiencies of 35 percent relative to a 3-in. by 3-in. cylindrical sodium-iodide detector standard. Germanium detectors are used because they provide a high-energy resolution that allows unique identification of the radioisotope source. Use of germanium detectors for both laboratory and field work is practical because of advances in portable electronic systems and because of developments by the manufacturers of the detection systems that made production of higher efficiency detectors more economical.

The detectors, which are housed in cylindrical probes, are mounted in a portion of the housing with a decreased housing wall thickness that reduces the attenuation of the gamma-ray signal. The downhole probes also contain a high-voltage supply, a preamplifier, and a liquid nitrogen dewar and cryostat assembly. The liquid nitrogen dewar system is needed to cool the detector diode to liquid nitrogen temperatures. The dewar holds a quantity of liquid nitrogen that allows 10 hours of logging between refills.

The sonde is delivered downhole on a Kevlar-reinforced, multiconductor cable. The cable transmits the preamplified detector pulses and timing pulses uphole to the truck-mounted instrumentation. Conductors provide low-voltage power to the downhole power supply. The cable also has a vent tube for releasing nitrogen gas as the liquid nitrogen in the dewar vaporizes. The vent tube allows the downhole probe to be used in water-filled boreholes. Figure 14-13 shows a complete logging sonde suspended over a calibration borehole.

Sonde movement within a borehole is governed by a servo-controlled hydraulic winch that receives its control signal from the uphole system computer. The probe position in the borehole is measured with a digital rotary encoder mounted on a sheave wheel hanging from a boom (Figure 14-12). The boom is used to position the detector over the borehole.

The surface instrumentation, which is mounted in standard instrument racks inside the rear cabins of the logging trucks, consists of a high-count-rate nuclear spectroscopy amplifier interfaced to a computer-controlled multichannel analyzer. Spectral log data are recorded by computers onto hard disks.

All instrumentation control, winch control, tool positioning, safety interlocks, and other functions are under computer control using a data acquisition and control program written by the manufacturer of the system and known as "LOG." The extensive computer control and automation of the system allow it to operate much faster than a nonautomated system, thus making the characterization operation cost effective.

## 7.2 Calibrations

The calibration of the SGLSs is specified in a calibration plan (DOE 1997a) and reported in a calibration report (DOE 1995a). Koizumi et al. (1991), Brodeur et al. (1991), and Koizumi et al. (1994) provide more general information on calibration methods and procedures for germanium logging systems.

The logging systems are calibrated by several processes that include a base calibration, biannual field calibrations, and daily field verifications.

The base calibration completed in the spring of 1995 included initial testing and qualification of the logging systems. This calibration was performed using the DOE borehole calibration models at the DOE-GJO as standards. These models are concrete cylinders or monoliths with large homogeneous regions where the concrete is enriched with known concentrations of the naturally occurring radionuclides  $^{40}\text{K}$ ,  $^{238}\text{U}$ , and  $^{232}\text{Th}$ . Boreholes pass through the enriched zones so the logging sonde could be lowered into these zones. When a logging tool is placed in the middle of the zone of enriched concrete, the measurement geometry is such that a homogeneous, isotropic medium of known radionuclide concentration is simulated. The response of the detector to the medium of the calibration zone is recorded, and the mathematical relationships between radionuclide concentration and count rate response are computed. The mathematical relationships constitute the system calibration factors.

During the base calibration, calibration factors were calculated to enable direct conversion of specific photon peak count rate responses to KUT concentration in picocuries per gram. In addition, the efficiency versus energy curve was calculated. This so-called efficiency curve allows direct calculation of the efficiency of the system at a specified photon energy, thus allowing determination of the concentration of man-made radionuclides that are not present in the calibration models, such as  $^{137}\text{Cs}$  or  $^{60}\text{Co}$ . Figure 14-14 presents an example of an efficiency calibration function.

The calculated radionuclide concentrations derived with these conversion factors may be as much as 14 percent higher than the actual in situ concentrations because the concentrations of the calibration models are expressed in terms of gamma-ray activity per unit-sample mass of *dry* bulk material. However, the measurements made in the calibration models were in a water-saturated environment. The conversion factors in the calibration reports are strictly applicable only when the logged formation has the same water content as the calibration-model test zones. The vadose zone contains pore-space water in various percentages of saturation from near 0 percent to near 100 percent, and the boreholes are logged dry. Corrections for pore-space water cannot presently be applied to the vadose zone measurements because the in situ water content is not being measured.

The base calibration also determined the environmental corrections that are used to correct for logging in a nonstandard borehole environment. For instance, steel casing installed in a borehole attenuates the gamma-ray signal from the formation to the detector. As a result, the detected count rate is lower than it would have been in an open (uncased) borehole measurement. An environmental correction is applied to the spectral peak intensities to correct for casing attenuation.

Environmental corrections were determined in the base calibration for a large range of casing thicknesses and for the effect of water in the borehole. Because the environmental corrections do not change with changes in the detection system, they need to be determined only once.

The base calibration also determined the response of the system to high gamma-ray flux. This test enabled determination of a count-rate correction equation, sometimes called a dead-time correction, that is applied to all of the spectra data during data analysis.

During the initial acceptance and base calibration, the cable systems were tested in order to determine accuracy in depth measurements and cable stretch. The results of the tests can be found in the acceptance test records. No discernable cable stretch was noted.

Field calibrations are performed biannually at the DOE borehole calibration models at the Hanford Site. The field calibration models are identical in status as calibration standards to the national standards in Grand Junction. They were constructed at the GJO and eventually moved to the Hanford Site in the late 1980s for use in Hanford environmental logging work. Koizumi (1993) presents descriptions of these calibration models. These calibrations provide periodic confirmation of proper system performance, and also "close the loop" by ensuring that every borehole measurement is bracketed in time by system calibrations.

Biannual field calibrations are used to quantify any small changes in the performance of the logging systems over time. The first field calibration was completed immediately after the base calibration was completed, before any logging operations began. This first field calibration is documented in the base calibration report (DOE 1995a). The first biannual calibration (second field calibration) was performed in October 1995 and is reported in DOE (1996c). The second biannual calibration (third field calibration) was performed in April 1996 and May 1996 and is

reported in DOE (1996d). The data acquired during the second field calibration demonstrate there was no statistically significant change in the performance of the system.

The efficiency of the logging systems is checked in the field calibrations by recalculating the direct conversion factors for KUT and by recalculating the energy versus efficiency functions shown on Figure 14-14. The dead-time correction is confirmed by measuring the system response in calibration zones that have successively increasing radionuclide concentrations. Calibration uncertainties are calculated and incorporated in the analysis of borehole log data.

In addition to the base and field calibrations, the performance of each logging system is verified daily in the field, before and after acquiring log data. These field verifications are performed by recording the system response when the detector is surrounded by a cylindrical-shaped gamma-ray source. By placing the detectors in a consistent geometrical relationship with a large, cylindrical field verification photon source, it is possible to verify the efficiency of the system, as well as other performance factors (i.e., the energy resolution and system gain).

The field verifications are designed to quantify the system efficiency and energy resolution, because these performance factors are subject to small changes over time and could be appreciably affected in the event of a logging-system malfunction.

During the performance of the C Tank Farm logging, an extensive database tracking the response of the SGLSs to the field verification sources was developed, and system performance guidelines were established on the basis of these data. These criteria are now being used as a quality-assurance measure that verify system performance in the field.

The field verification data have been analyzed and are reported in DOE (1996c) and DOE (1997g), respectively. The data show no statistically significant trend over time, verifying the stability of the systems and consistent performance.

### **7.3 Logging Process and Procedures**

Data acquisition or logging work is performed according to a logging procedure (DOE 1997d). Adherence to this procedure ensures consistent and documented operation of the logging systems. This procedure does not specify actual data acquisition parameters because those parameters may vary in the field according to the borehole environment encountered during the logging process. Parameters such as data acquisition interval, logging mode, logging speed, or counting time may be varied by the engineer in an effort to extract as much information from the borehole as possible. Requirements specify that all data acquisition parameters are recorded on Log Data Sheets so the borehole-specific data acquisition parameters are documented and available for data processing, analysis, and interpretation. Log Data Sheets are completed as the borehole is being logged and are transferred from the field site to the office upon completion of logging. Log Data Reports are created from data on the Log Data Sheets, and the Log Data Reports are provided with the log plots in the Tank Summary Data Reports for each tank.

Logging operations commence after an initial instrumentation warm-up time period and after completion of the pre-survey field verification. Under normal conditions with moderate to low man-made radionuclide concentrations, data acquisition is initiated with 100-s detector live time at 0.5-ft depth intervals along the borehole. This spatial resolution is adequate to properly define thin zones of contamination, yet it is not overly time consuming or costly.

If high concentrations of contamination are encountered and the detector dead-time increases to a level greater than about 80 percent, the logging engineer will generally change to a real-time (clock time) logging mode. A real-time logging mode is used through zones of high radionuclide concentrations, but even then the system sometimes become saturated and unable to record data. Above a  $^{137}\text{Cs}$  concentration of about 8,000 pCi/g, the SGLS becomes saturated and log data cannot be obtained using the current high-efficiency detectors. These zones are identified on the log plots.

The SGLSs have digital spectrum stabilizers that automatically adjust the gain and maintain the natural  $^{40}\text{K}$  peak at 1460 keV within an established spectrum channel range. Occasional fine adjustments of the gain may be required throughout an 8-hour (hr) logging period to keep the 1460-keV peak in the established range; these adjustments are recorded on the Log Data Sheets. However, this adjustment does not affect the system's efficiency or the calculated radionuclide concentrations.

Each time the computer is set with specified data acquisition parameters and an automated data acquisition process is executed, it is defined as a separate log run. If the process is interrupted for any reason, such as when a high count-rate region is encountered or operations cease for the day, a new log run is established. The logging parameters for each log run are recorded on Log Data Sheets.

The spectra recorded at each depth in the borehole are automatically transferred by the LOG program to nonvolatile memory on the computer hard disk as each spectrum recording is completed. At the end of the day, another field verification spectrum is recorded.

Upon completion of the logging of a borehole, the spectra recorded on hard disk are transferred to an optical disk. These optical disks are then transported into the field office, and the data are transferred to the main computer database maintained in the office according to the Vadose Zone Characterization Project Working File Index. Log Data Sheets are completed as the borehole is being logged and also transferred from the field to the office. The data on the Log Data Sheets are entered into a Paradox database created specifically for the log data; the Log Data Sheets are then copied and filed.

## 7.4 Data Management

All data and records are managed as specified in the *General Administrative Procedures Manual* (MACTEC-ERS 1996). Section 3.0, "Records Management," of that manual should be used in conjunction with the current revision of the Vadose Zone Characterization Project Working File Index for complete records management guidance.

The Vadose Zone Characterization Project Working File Index specifies management requirements for all project data, reports, memoranda, and miscellaneous information and governs recording and retention of data and records, copying the data to the computer database, and management and retention of the database.

## 7.5 Data Analysis

Data analysis can begin after logging of a borehole is completed and the log data are transferred to the office computer. Data analysis is the process of reducing the spectra data to individual peak count rates and converting those raw count rates to radionuclide concentrations. The radionuclide concentration data are put into a log profile format and then plotted.

The data analysis work is accomplished with Pentium microprocessor-equipped personal computers and a combination of commercial and custom software. The data analysis process, instructions, software, and procedures are documented in the data analysis manual (DOE 1997b). All computer programs that are not commercial programs are verified and validated according to DOE standards.

Statistical uncertainties derived from the logging and calibration data by standard uncertainty propagation methods are converted in the analysis software to equivalent concentrations to produce an estimation of the uncertainty of the concentration determination. The estimated uncertainties provide a measure of the quality of the data and are shown on the log plots as error bars at the concentration data points. Discussion of the uncertainty estimation calculation method is provided in detail in the base calibration report (DOE 1995a).

The MDL is also plotted with the concentration values. Calculation of the MDL is described in the data analysis manual (DOE 1997b). The MDL represents the minimum concentration at which the radionuclide would have to be present for it to be represented by a statistically significant peak in the spectrum. It also represents the lowest radionuclide concentration that could be detected using the data acquisition parameters used to acquire the spectra.

Preparation of a Log Data Report is the final step of the data analysis process. The Log Data Report is created to document the analysis of the borehole log data. It is created using the Paradox database program with data from the vadose zone characterization database.

The Log Data Report provides information about the borehole construction and casing configuration and how the borehole was logged (log run information). It also includes information regarding data analyses and provides a description of the accompanying log plots. The Log Data Report is provided with the log plots so that others may independently interpret the results.

Upon completion of the data analysis, the original spectra data, the analyzed spectra data, the individual nuclide concentration versus depth data, and the log plots are archived in permanent data storage as specified in the data analysis manual.

This brief synopsis of the data analysis process describes the complexities of the data analyses. The data analysis process is documented in greater detail in the data analysis manual.

## 8.0 Log Data Results

### 8.1 Instrumentation Performance

The two logging systems (Gamma 1 and Gamma 2) logged a total of 70 boreholes within the C Tank Farm. An optimum production rate of one 100-ft of borehole per day was logged, generally using a counting time of 100-s live time at 0.5-ft depth intervals.

Field verification spectra were recorded before and after each day's work. The verification data were analyzed before the commencement of logging. All data were recorded on the computer as spectra, and logging information was recorded by the logging engineers on the Log Data Sheets. The entries on the Log Data Sheets were later entered into a Paradox database and used in the analysis of the spectra.

Some assumptions regarding the borehole casing thicknesses were used in data analysis. Often the surface of the casings were obscured by a small concrete pad placed around each borehole, making field measurements of the casing thickness impossible. Therefore, the thickness was assumed to be the standard thickness for casing of the documented or observed inner diameter. The casing thicknesses used to correct the data were recorded on the individual Log Data Reports (provided with the logs in Appendix A of the individual Tank Summary Data Reports). The original spectral data are saved in the data archive; therefore, the conversion from count rate to concentration can be recalculated for any borehole if the true casing thickness is determined to be different from the value assumed for data analysis.

A maximum radiation flux from  $^{137}\text{Cs}$  from which a meaningful spectrum could be recorded was associated with a concentration of about 8,000 pCi/g. However, data acquisition procedures have been refined to raise that maximum to a slightly higher value.

For a counting time of 100 s, the MDL for  $^{137}\text{Cs}$  is consistently between 0.1 and 0.2 pCi/g. The MDL differs slightly for each spectrum depending on the concentrations of other radionuclides at the individual spectrum depth region, including the naturally occurring nuclides. In regions of higher man-made radionuclide concentrations, the Compton background continuum becomes elevated, increasing the MDL value.

The MDL for  $^{60}\text{Co}$  is about 0.15 pCi/g; the MDL for  $^{154}\text{Eu}$ ,  $^{238}\text{U}$ , and  $^{235}\text{U}$  is about 0.2 pCi/g. These values represent the lower limit of detection for the system when it is operated with a 100-s counting time. The detector can be operated at much longer counting times, but more time would be required to log a borehole. The assay capability for these nuclides down to the levels reported is well within any health and safety risk levels.

## 8.2 Radionuclides Detected

Detection of a nuclide is considered positive when the peak identification routine of the spectrum analysis software detects a peak associated with a gamma ray known to be emitted by the radionuclide and the intensity of the peak is statistically above the MDL. Radionuclides that emit multiple photons are confirmed by detection of two or more peaks associated with the characteristic gamma rays. When a peak is detected and the source radionuclide is identified, custom software converts the peak count rate to an equivalent concentration in picocuries per gram.

In the C Tank Farm, the most abundant gamma-emitting radionuclide contaminants in the vadose zone were  $^{137}\text{Cs}$  and  $^{60}\text{Co}$ . A small amount of  $^{154}\text{Eu}$  was also detected in the subsurface.  $^{235}\text{U}$ ,  $^{152}\text{Eu}$ , and  $^{154}\text{Eu}$  were detected at the ground surface around several boreholes.

In many instances, a small photon peak was measured or suspected, but because the peak did not satisfy the above detection criteria established for this project, it was not reported. However, only extremely low concentrations of man-made radionuclides (generally less than 0.1 pCi/g) are undetected and unreported.

## 8.3 Log Plots

Log data results are presented in the Tank Summary Data Reports as log plots showing concentration relative to depth in the boreholes. A set of logs for each borehole consists of a separate log plot of any man-made radionuclides detected, a log plot of the KUT concentrations, and a combination plot showing logs of the man-made and naturally occurring radionuclides with the total gamma log and the historical gross gamma-ray log from the Tank Farms logging system. Where a significant anomaly in the gamma-ray activity was identified in the historical gross gamma-ray logs, a time-sequence plot was created and included with the suite of SGLS log plots.

Each set of logs also includes a Log Data Report. The Log Data Reports provide all the information required to analyze and interpret the log data, including explanations of any anomalies or peculiarities in the data or the analysis process. The logs themselves do not provide enough information with which to assess the data; consequently, anyone looking at the data should also review the Log Data Reports. The Log Data Reports are retained with the log plots as a part of the project quality assurance program.

The log plots for the boreholes surrounding each of the tanks are provided in the appendix of the Tank Summary Data Reports for the individual tanks. These plots were used for correlation purposes. The plots of the man-made radionuclides for the boreholes surrounding each tank are provided in Appendix A of this report.

The log plots and the nuclide-specific data files for each borehole are maintained in the vadose zone characterization computer database. These data will eventually be transferred to other Hanford databases to make the information more readily available.

## 8.4 Tank Summary Data Reports

A Tank Summary Data Report was prepared for each of the 100-series tanks in the C Tank Farm. Each report provides a mechanism for reporting the results of the spectral gamma logging and allows the analyst to place the data into the context of the documented tank history and local geology. The purpose of the Tank Summary Data Report is to provide an understanding of the effects that the particular tank had on the condition of the vadose zone.

In addition to the log plots for the boreholes surrounding the tank, the Tank Summary Data Report provides a discussion of each borehole and the spectral gamma data analysis and interpretation for each borehole.

The Tank Summary Data Report provides a correlation and discussion of the contamination around the tank and identifies any geologic correlations. The correlation plot provided in the Tank Summary Data Report shows the contamination concentration plots from each borehole around the tank in a single figure to aid in the cross-borehole correlation of the gamma-ray-emitting contamination. The analysts also make conclusions, where appropriate, about the sources of the contamination in the vadose zone. If the analysis indicates that a particular tank is the source of contamination, this is stated in the Tank Summary Data Report.

In general, the Tank Summary Data Report provides a summary of the logging data, an assessment of the conditions of the vadose zone, and an analysis of the relationship between the vadose zone contamination and the tank. The reader is referred to the individual Tank Summary Data Reports listed in Section 15.0 of this report for detailed information and in-depth analysis of specific boreholes.

## 8.5 Shape Factor Analysis

The shape factor analysis method described in this section was not available for use on the SGLS log data prior to issuance of the individual Tank Summary Data Reports for the C Tank Farm. Therefore, shape factor analysis of the log data was conducted during the preparation of this report and the results of the data analyses are presented in Appendix B.

Insights into the distribution of the radionuclides identified by the SGLS can be provided by using an analytical method known as shape factor analysis (Wilson 1997, 1998). Shape factor analysis takes advantage of 1) the SGLSs ability to record the specific energies of detected gamma rays, and 2) the Compton downscattering caused by the interaction of gamma rays with matter between the gamma-ray source and the detector.

Compton scattering results in higher energy photons being converted to lower energy photons; hence, Compton scattering within and outside of the detector accounts for the low-energy continuum in a pulse height spectrum. Many factors exterior to the detector influence the low-energy portion of the spectrum of gamma rays incident on the detector and thereby affect the low-energy continuum in the pulse height spectrum. Wilson (1997, 1998) have shown that variations in gamma-ray source distribution relative to a borehole produce measurable changes in

the shapes of the pulse height spectra recorded by logging the boreholes. The spectral shape changes are quantified by ratios of counts from defined portions of the pulse height spectrum, and these ratios are used to assess the distribution of the source.

Shape factor analysis can also be used to identify the presence of bremsstrahlung radiation from the beta-emitting radionuclide  $^{90}\text{Sr}$ . Beta particles, emitted from the radioactive decay of  $^{90}\text{Sr}$ , interact with the electromagnetic fields within the substances they traverse. The deflection and resulting deceleration of the beta particles produce x-rays, known as bremsstrahlung radiation, which are detected in the lower energy portion of the gamma-ray spectrum. In instances of high total gamma-ray activity, a preponderance of lower energy gamma radiation may be due to the presence of beta emitters such as  $^{90}\text{Sr}$ .

Additional information on shape factor analysis theory is provided in Wilson (1997, 1998).

### 8.5.1 Specific Shape Factors

As stated previously, the ratios of gamma-ray counts from defined portions of a spectrum are indicators of gamma-ray source distribution. Three ratios are used in shape factor analysis. These ratios, known as shape factors, are designated CsSF1, CoSF1, and SF2.

- CsSF1 is the ratio of the total number of counts in the continuum window (60 to 650 keV) to the counts in the  $^{137}\text{Cs}$  peak. This shape factor is useful for evaluating the distribution of the radionuclide  $^{137}\text{Cs}$ .
- CoSF1 is the ratio of the total number of counts in the continuum window (60 to 650 keV) to the sum of the counts in the two  $^{60}\text{Co}$  peaks (1173 and 1332 keV). This shape factor is useful for evaluating the distribution of the radionuclide  $^{60}\text{Co}$ .
- SF2 is the ratio of the total number of counts in the lower energy portion of the continuum window (60 to 350 keV) to the counts in the higher energy portion of the continuum window (350 to 650 keV). This parameter is somewhat sensitive to the radionuclide distribution, but is most applicable to the identification of the beta emitter  $^{90}\text{Sr}$  and in distinguishing remote  $^{137}\text{Cs}$  or  $^{60}\text{Co}$  from  $^{90}\text{Sr}$ .

At low concentrations, high uncertainties in the  $^{137}\text{Cs}$  and  $^{60}\text{Co}$  peak count rates and in the net continuum count rates cause large errors in the calculated values of CsSF1 and CoSF1, respectively. A minimum  $^{137}\text{Cs}$  peak count rate of 1 cps (approximately 1.6 pCi/g) must be present for the calculated CsSF1 to be meaningful, and a minimum  $^{60}\text{Co}$  peak count rate of 2 cps must be present for CoSF1 (Wilson 1998).

It is not possible to compute CsSF1 and CoSF1 when these contaminants occur together unless the spatial distribution is known for one of the radionuclides so its contribution can be subtracted from the continuum counts. Then SF1 can be computed for the other radionuclide.

The values of CsSF1, CoSF1, and SF2 also become less reliable as the radionuclide concentrations and count rates become very high and the dead time increases. Inaccuracies in the measurement of the spectral regions occur when system dead time increases to above about 20 percent. However, the effect on shape factors is relatively small for dead times up to 40 percent. For measurements made at dead times below 20 percent, distortion of the spectrum is negligible (Wilson 1998).

### 8.5.2 Interpretation of Shape Factors

Values of CsSF1, CoSF1, and SF2 that can be expected for radionuclides in various distributions were established from investigations by Wilson (1997, 1998). These distributions are:

1) contamination confined to the borehole region, such as when contaminants occur on the borehole casing, 2) contamination uniformly distributed throughout the formation around the borehole, and 3) contamination in the formation but at discrete locations remote from the detector. The expected CsSF1, CoSF1, and SF2 values for various distributions of <sup>137</sup>Cs or <sup>60</sup>Co are summarized below.

Table 2. Spectral Shape Factors

<sup>137</sup> Cs or <sup>60</sup> Co Source Distribution	Spectral Shape Factor			
	CsSF1	CoSF1	CsSF2	CoSF2
Inside of 6-in. casing	4.5	5.5	2.8	2.7
Outside of 6-in. casing	6.8	7.4	2.8	3.0
Uniformly distributed in formation	13	14.6	3.5	3.2
Discrete source 10 centimeter (cm) radial distance	~ 19	15	~ 3.8	3.3
Discrete source 30 cm radial distance	~ 37	38	~ 4.2	3.3
Discrete source more than 50 cm radially distant	80 - 100	68	4.4	3.1

When CsSF1, CoSF1, and SF2 values exceed those listed, the presence of <sup>90</sup>Sr is suggested. However, photons from intense gamma-ray sources remote from the borehole can also produce spectra with high CsSF1 and CoSF1 values, indicating that elevated values of these two shape factors alone are not sufficient for a <sup>90</sup>Sr identification. The presence of <sup>90</sup>Sr can be inferred with confidence when SF2 significantly exceeds the extreme value (about 5.0) for a distant source. The interpretation may be aided by an SF2-SF1 cross plot. If <sup>90</sup>Sr is absent, then as the distance between the borehole and the inner edge of a (cylindrically symmetric) <sup>137</sup>Cs source increases, the points on the SF2-SF1 cross plot define a "trend line." <sup>90</sup>Sr is indicated if the SF2 values are so high that the points on the cross plot lie well above the trend line. However, a <sup>90</sup>Sr concentration of about 1,000 pCi/g is necessary to produce a noticeable increase in count rates (DOE 1997a). Radiation transport computer simulations have shown the SF2 value will exceed 10 when no

other contaminants are present and the  $^{90}\text{Sr}$  concentrations are 1,000 pCi/g, or higher. The presence of  $^{90}\text{Sr}$  was not identified in any of the C Tank Farm vadose zone monitoring boreholes.

### 8.5.3 Uncertainties of Shape Factor Analysis

The counts resulting from  $^{137}\text{Cs}$  and  $^{60}\text{Co}$  in the continuum windows are corrected for background by subtracting (stripping) the counts contributed by the naturally occurring radionuclides  $^{40}\text{K}$ ,  $^{238}\text{U}$ , and  $^{232}\text{Th}$  from the continuum windows. Counting statistics for the gamma rays associated with  $^{238}\text{U}$  and  $^{232}\text{Th}$  are poor for the 100-s counting time typically used by the SGLS in borehole logging; accordingly, there may be a considerable relative statistical uncertainty in the peak intensity that is used to calculate any background correction. To minimize the effects of statistical counting uncertainties in the calculated background corrections, the corrections are calculated at each depth point, then filtered with a Gaussian smoothing function. The correction at a particular depth point is the average over a 5-ft interval that extends 2.5 ft above and 2.5 ft below the point. The other source of experimental uncertainty is systematic uncertainty in the stripping factors. Errors in these constants have been minimized with an heuristic approach, but in general, the stripping constant errors are the ultimate limitation on the accuracy of the background corrections.

The use of shape factor analysis is currently limited to evaluating the distributions of  $^{137}\text{Cs}$  and  $^{60}\text{Co}$  and to identifying the presence of  $^{90}\text{Sr}$ . At this stage of the method's development, other gamma-ray-emitting radionuclides (i.e.,  $^{125}\text{Sb}$ ,  $^{154}\text{Eu}$ , and  $^{152}\text{Eu}$ ) interfere with shape factor analysis. The number of other radionuclides present in a borehole is a quality indicator. Non-zero values of this indicator may mark intervals of a borehole that are unsuitable for the application of shape factor analysis.

### 8.6 Interpreted Data Set Used for the Development of the Visualizations

Visualizations in most of the past tank farm reports have shown all of the SGLS log data, even data that were interpreted to be local to the borehole casing and not part of a subsurface plume. Inclusion of all the SGLS log data in the geostatistical model represents the most conservative interpretation of the contaminant distribution in the vadose zone. However, this caused numerous false plumes to be shown on the tank farm visualizations. These false plumes were identified and discussed in the text of the tank farm report, but the visualizations still did not depict the most accurate representation of the contaminant distribution in the tank farm vadose zone.

To rectify this situation, intervals where the log data show the contamination is localized to the borehole casing were removed from the data set analyzed by the visualization software. Because the geostatistical modeling software assumes all the data represent contamination distributed in the formation, the resulting visualizations will better represent the actual contaminant distribution after the borehole localized contaminant data are removed. Contamination that was interpreted to be localized to the borehole was removed from the geostatistical modeling data set prior to developing the three-dimensional visualizations.

In cases where the contaminant occurs as intermittent or isolated cases and in low concentrations, the geostatistical model will typically not identify that contamination as correlatable between boreholes; thus, a plume will not be formed from that data point. Therefore, in developing the interpreted data set, an emphasis was placed on removing data that were interpreted to be local to the borehole casing, either by shape factor analysis or other means, that would have resulted in a false plume in the visualizations.

The geostatistical model is used to determine if two points are statistically correlatable. On the basis of the geostatistical model, three-dimensional visualizations of the contaminant plumes are developed. However, the geostatistical model treats the SGLS data as actual data points and does not have the capability for inputting apparent distribution based on shape factor analysis.

The interpreted data set represents contamination that is interpreted to be in the formation. In some cases, the contaminant distribution around the borehole is not well understood. In these cases, the interval was conservatively interpreted to be deposited in the formation sediments and remains in the model data set.

The intervals of  $^{137}\text{Cs}$  data that were left in the model data set are interpreted to represent contamination that is distributed in the formation sediments around the borehole. Shape factor analysis has revealed that the contaminant is not always uniformly distributed around the borehole. Shape factor analysis for the C Tank Farm boreholes has revealed numerous intervals of contaminants that are non-uniformly distributed in the formation sediments or are remote from the borehole. These data were also left in the interpreted data set.

The basis for removing intervals of log data can be found in the individual Tank Summary Data Reports (DOE 1997i, 1997j, 1997k, 1997l, 1997m, 1997n, 1997o, 1997p, 1997q, 1997r, 1998a, and 1998b) and the shape factor analysis results presented in Appendix B of this report. Intervals where data were removed are identified on the correlation plots in Appendix A. Contamination localized to the borehole in the C Tank Farm can be described by three basic categories: 1) surface contamination in the vicinity of the borehole or direct gamma rays from nearby contaminated equipment, 2) contamination that was dragged down during borehole construction, or 3) contamination that fell into the bottom of the borehole (inside the casing).

In many cases  $^{137}\text{Cs}$  was identified at or just above the MDL. Typically, the geostatistical model will ignore these data. However, to ensure the accuracy of the model and resulting visualizations, these data were removed.

Interpretations of contaminant distribution is based on observed relationships. Therefore, it is possible that intervals where the contamination is interpreted to be localized to the borehole casing are in fact distributed in the formation sediments. Only if the contaminated materials were exhumed would the distribution of the contamination in these intervals be more fully understood.

The categories of contaminant distribution that are interpreted to be local to the borehole casing were removed from the visualization data set because they are thought to represent contamination

that is not distributed in the vadose zone sediments. The following sections describe the data that were removed from the data set for each borehole and also include a discussion of the reason why the data were removed. The boreholes are organized by individual tanks as they appear in the Tank Summary Data Reports (refer to the borehole logs included in Appendix A).

The data that remain for each borehole constitute the database from which the model of the contamination was developed and the visualizations were prepared.

### **8.6.1 Boreholes Surrounding Tank C-101**

The contamination detected near the surface of borehole 30-00-06 was removed from the data set because the contamination is actually located in a hillside above the C Tank Farm. The  $^{137}\text{Cs}$  and  $^{60}\text{Co}$  contamination detected in the perforated interval of this borehole was not removed due to its proximity to tank C-101, a known leaker.

$^{137}\text{Cs}$  was detected in isolated occurrences at or just above the MDL around borehole 30-01-12 at 45, 60, and 66.5 ft. If the  $^{137}\text{Cs}$  is truly present, then it represents contamination that is most likely localized to the borehole casing and it was removed from the data set.

Isolated occurrences of  $^{137}\text{Cs}$  were detected in the bottom of boreholes 30-01-01, 30-01-06, 30-01-09, and 30-01-12. This contamination is interpreted to be from particulate matter that has fallen into the bottom of the borehole.

### **8.6.2 Boreholes Surrounding Tank C-103**

The contamination detected from 8 to 17 ft around borehole 30-00-03 was removed from the data set because this contamination is interpreted to have been carried down during borehole construction.  $^{137}\text{Cs}$  was detected nearly continuously in the perforated interval (54 ft to bottom of borehole); the pattern of  $^{137}\text{Cs}$  contamination being directly associated with the perforations is common to many perforated boreholes. The reason for this correlation and the mechanism that caused this contamination to be associated with the perforations is not known. Regardless, it is doubtful that contamination in the perforated interval represents contamination that is distributed in the formation sediments and it was removed from the data set.

The shape factor analysis for borehole 30-03-09 indicates the  $^{137}\text{Cs}$  from 25 to 30 ft is local to the borehole casing. Therefore, these data were removed from the modeling data set.

Isolated occurrences of  $^{137}\text{Cs}$  were detected in the bottom of boreholes 30-03-05 and 30-03-07. This contamination is interpreted to be from particulate matter that has fallen into the bottom of the borehole.

### **8.6.3 Boreholes Surrounding Tank C-104**

According to the Tank Summary Data Report for tank C-104 (DOE 1997), the  $^{137}\text{Cs}$  detected around borehole 30-04-04 from 22 to 45 ft and from 58 ft to the bottom of the logged interval

was carried down during the construction of this borehole or later migrated down the outside of the casing. These intervals of contamination were removed from the data set.

The  $^{137}\text{Cs}$  detected around borehole 30-04-05 from 69 ft to the bottom of the logged interval was carried down during borehole construction or later migrated down the outside of the casing. This interval was removed from the visualization data set.

$^{137}\text{Cs}$  was detected in isolated occurrences at or just above the MDL in borehole 30-04-12 at 67 and 88 ft. If the  $^{137}\text{Cs}$  is truly present, then it represents contamination that is most likely localized to the borehole casing and it was removed from the data set.

Isolated occurrences of  $^{137}\text{Cs}$  were detected in the bottom of boreholes 30-04-02 and 30-04-12. This contamination is interpreted to be from particulate matter that has fallen into the bottom of the borehole. These occurrences were removed from the visualization data set.

#### **8.6.4 Boreholes Surrounding Tank C-105**

It was originally speculated that the  $^{137}\text{Cs}$  and  $^{60}\text{Co}$  detected together around boreholes 30-05-02, 30-05-03, and 30-05-04 were not deposited at the same time even though they shared the same origin. However, shape factor analysis for borehole 30-05-04 indicates the  $^{137}\text{Cs}$  is distributed in the formation sediments to a depth of at least 70 ft; below 70 ft the  $^{137}\text{Cs}$  is below the threshold for calculating shape factors. Also, in other nearby boreholes it is apparent the  $^{60}\text{Co}$  and  $^{137}\text{Cs}$  may have similar origins. Because the possibility that the contaminants co-exist can no longer be ruled out, the data remain in the visualization data set. This will have little impact because the concentration levels are less than 1 pCi/g and are limited in extent to the west side of tank C-105.

According to the Tank Summary Data Report for tank C-105, the  $^{137}\text{Cs}$  from 65 ft to the bottom of the logged interval of borehole 30-05-09 was carried down during borehole construction activities or later migrated down the outside of the casing. Therefore, these data were removed from the visualization data set.

$^{137}\text{Cs}$  was detected in isolated occurrences at or just above the MDL in borehole 30-05-10 at 64, 74, and 103 ft. If the  $^{137}\text{Cs}$  is truly present, then it represents contamination that is most likely localized to the borehole casing; therefore, this contamination was removed from the data set. According to the Tank Summary Data Report for tank C-105 (DOE 1997m), the  $^{137}\text{Cs}$  from 114 to 120 ft was carried down during borehole construction activities or later migrated down the outside of the casing; therefore, this contamination was also removed from the data set.

Isolated occurrences of  $^{137}\text{Cs}$  were detected in the bottom of boreholes 30-05-09 and 30-05-10. This contamination is interpreted to be from particulate matter that has fallen into the bottom of the borehole.

Borehole 30-05-07 had zones of  $^{137}\text{Cs}$  concentrations high enough to saturate the detector. A value of 8,000 pCi/g was placed in the visualization data set for the saturated intervals.

## 8.6.5 Boreholes Surrounding Tank C-106

According to the Tank Summary Data Report for tank C-106 (DOE 1997n), the contamination around borehole 30-06-02 from 16 to 36 ft and from 41 ft to the bottom of the borehole is localized to the borehole casing. However, shape factor analysis indicates that at least some of the  $^{137}\text{Cs}$  from 41 to 61 ft is distributed in the Hanford formation sediments; therefore, this entire interval remains in the interpreted data set.

The interpretation for the  $^{137}\text{Cs}$  detected around borehole 30-00-01 between 25 and 45 ft is that the contamination was carried down during borehole construction activities or later migrated down the outside of the casing. This interval of contamination was removed from the visualization data set.

The  $^{137}\text{Cs}$  detected between 10 and 40 ft around borehole 30-06-10 is interpreted to be the result of borehole construction activities or contamination that later migrated down the outside of the casing wall. This interval of contamination was removed from the visualization data set.

Isolated occurrences of  $^{137}\text{Cs}$  were detected in the bottom of boreholes 30-06-02, 30-06-03, 30-06-04, 30-06-09, and 30-06-10. This contamination is interpreted to have resulted from particulate matter that has fallen into the bottom of the borehole. These intervals of contamination were removed from the visualization data set.

## 8.6.6 Boreholes Surrounding Tank C-107

Interpretations presented in the Tank Summary Data Report for C-107 (DOE 1997o) for borehole 30-07-05 suggested the contamination from 5 to 45 ft and from 55 to 78 ft was local to the borehole casing. However, this contamination appears to correlate with contamination detected in other nearby boreholes that were not considered in the Tank Summary Data Report; therefore, the contamination remains in the visualization data set.

According to the Tank Summary Data Report for tank C-107, the  $^{137}\text{Cs}$  detected from 70 to 88 ft around borehole 30-07-01 and from 16.5 to 37 ft around borehole 30-07-11 was carried down during borehole construction activities or later migrated down the outside of the casing. These intervals of contamination were removed from the visualization data set.

$^{137}\text{Cs}$  was detected in isolated occurrences at or just above the MDL in borehole 30-07-08 at depths of 37.5, 49, and 53 ft and at a depth of 77.5 ft around borehole 30-07-10. If the  $^{137}\text{Cs}$  is truly present, then it represents contamination that is most likely localized to the borehole casing; therefore, this contamination was removed from the data set.

Isolated occurrences of  $^{137}\text{Cs}$  were detected in the bottom of boreholes 30-07-02, 30-07-07, and 30-07-11. This contamination is interpreted to be from particulate matter that has fallen into the bottom of the borehole and it was removed from the visualization data set.

Zones of  $^{137}\text{Cs}$  concentrations high enough to saturate the detector were detected in borehole 30-07-11. A value of 8,000 pCi/g was placed in the visualization data set for the saturated intervals.

### **8.6.7 Boreholes Surrounding Tank C-108**

An isolated occurrence of  $^{137}\text{Cs}$  was detected in the bottom of borehole 30-08-02. This contamination is interpreted to be from particulate matter that has fallen into the bottom of the borehole and it was removed from the visualization data set.

The original interpretation of the  $^{137}\text{Cs}$  from 9 to 36 ft around borehole 30-08-12 suggested with the support of shape factor analysis that the contamination was local to the borehole casing. However, the shape factor results are greater than expected for borehole casing contamination, indicating some Compton scattering is occurring. These results are not yet well understood and could represent any number of scenarios that result in a non-uniform distribution. Therefore, this interval remains in the visualization data set.

### **8.6.8 Boreholes Surrounding Tank C-109**

According to the Tank Summary Data Report for tank C-109 (DOE 1997q), the  $^{137}\text{Cs}$  from 15 to 35 ft around borehole 30-09-07 was carried down during the drilling process or later migrated down the outside of the casing.

Isolated occurrences of  $^{137}\text{Cs}$  were detected in the bottom of boreholes 30-09-01, 30-09-02, 30-09-06, and 30-09-11. This contamination is interpreted to be from particulate matter that has fallen into the bottom of the borehole.

### **8.6.9 Boreholes Surrounding Tank C-110**

The contamination detected near the surface of borehole 30-00-09 was removed from the data set because the contamination is actually located in a hillside above the C Tank Farm.

Boreholes 30-00-11, 30-00-22, and 30-00-24 are located 100 to 200 ft from the nearest C Tank Farm tank. The data obtained from these boreholes are not in the visualizations because they would provide no meaningful insight as to the contaminant distribution in the C Tank Farm.

An isolated occurrence of  $^{137}\text{Cs}$  was detected in the bottom of borehole 30-10-02. This contamination is interpreted to be from particulate matter that has fallen into the bottom of the borehole.

### **8.6.10 Boreholes Surrounding Tank C-111**

According to the Tank Summary Data Report for tank C-111 (DOE 1998a), the  $^{137}\text{Cs}$  from 32 to 66 ft around borehole 30-11-01 was carried down during the construction of this borehole or later migrated down the outside of the casing. This contamination was removed from the visualization data set.

$^{137}\text{Cs}$  was detected in isolated occurrences at or just above the MDL in borehole 30-11-05 at about 12 ft and in borehole 30-11-06 at about 13 ft. If the  $^{137}\text{Cs}$  is truly present, then it represents contamination that is most likely localized to the borehole casing; therefore, this contamination was removed from the data set.

The  $^{137}\text{Cs}$  detected at the surface of borehole 30-11-11 is most likely direct gamma rays from nearby contaminated equipment.

Isolated occurrences of  $^{137}\text{Cs}$  were detected in the bottom of boreholes 30-11-01 and 30-11-06. This contamination is interpreted to be from particulate matter that has fallen into the bottom of the borehole.

### **8.6.11 Boreholes Surrounding Tank C-112**

Borehole 30-00-13 is located 100 ft from the nearest C Tank Farm tank. The data obtained from this borehole are not in the visualizations because they would provide no meaningful insight as to the contaminant distribution in the C Tank Farm.

The  $^{137}\text{Cs}$  detected at the surface of borehole 30-12-09 is most likely direct gamma rays from nearby contaminated equipment.

An isolated occurrences of  $^{137}\text{Cs}$  was detected in the bottom of borehole 30-12-13. This contamination is interpreted to be from particulate matter that has fallen into the bottom of the borehole.

Borehole 30-12-13 had zones of  $^{137}\text{Cs}$  concentrations high enough to saturate the detector. A value of 8,000 pCi/g was placed in the visualization data set for the saturated intervals.

## **9.0 Development of the Geostatistical Model and the Three-Dimensional Contaminant Visualizations**

### **9.1 Introduction**

One objective of this characterization project is to produce three-dimensional visualizations of the major contaminant plumes within the C Tank Farm. These visualizations can be used for

many aspects of tank farm operations and management, as well as for the tank remediation studies.

Creating the visualizations required developing a geostatistical model of the interpreted  $^{137}\text{Cs}$  and  $^{60}\text{Co}$  distributions, which were the major contaminants detected in the vadose zone in the C Tank Farm. The geostatistical model is considered to be an empirical model, as contrasted with a conceptual model or a model developed from predictive calculations such as contaminant transport calculations. The geostatistical model is considered an empirical model because it is based on data obtained by measuring the contamination concentrations at discrete points in the subsurface.

The development of a geostatistical model requires a determination of the mathematical relationship or correlation between discrete data points. It is necessary to determine if two data points can be correlated. A visualization is only as good or as accurate as the relationship defining the correlation between two data points in three-dimensional space.

The best way to correlate discrete data points is to use the process provided by geostatistics. Geostatistics is simply an analysis and application of the spatial variability of data. It is an empirical analysis of the data and application of the results to the estimation of the contamination concentration at unsampled points in three-dimensional space.

A geostatistical structural model was developed for the man-made radionuclides  $^{137}\text{Cs}$  and  $^{60}\text{Co}$  that used a process called "kriging" to estimate the grade or contaminant concentration at points on a defined three-dimensional grid. Adaptive gridding was utilized in kriging the C Tank Farm data. In this mode, the modeling software automatically refines gridding in each cell(s) surrounding the measured samples to ensure that the interpolated results and isosurfaces accurately honor measured sample data. Once this concentration grid was developed, visualizations of the contamination could be produced that resulted in a solid surface model of the contamination.

A geostatistical model was developed for the purpose of creating the visualizations of the  $^{137}\text{Cs}$  and  $^{60}\text{Co}$  distributions in the C Tank Farm. The empirical model is not intended to be used for quantitative calculations because the geostatistical structures are not well understood. However, they are adequate to provide a basic understanding of the  $^{137}\text{Cs}$  and  $^{60}\text{Co}$  distributions.

A more rigorous geostatistical structural analysis would be desirable. The existing data samples are 0.5 ft apart in the vertical dimension, creating an ideal database for a geostatistical assessment. However, in the horizontal dimension, an ideal structural analysis would require drilling (and logging) several lines of closely spaced boreholes and constructing variograms that are based only on those data. Future assessments may help to refine and validate the variograms that are the basis of the geostatistical structure of the data.

The software package from C Tech Development Corporation called "Environmental Visualization Systems" (EVS) was used to perform the geostatistical analysis and to create the

visualizations. Journel and Huijbregts (1978) and David (1977) explain the theory and application of geostatistics as applied to the development of a geostatistical structural model.

The radionuclide concentration data that constitute the spectral gamma-ray log data reported in the Tank Summary Data Reports for the C Tank Farm were interpreted and only data believed to represent contamination distributed in the formation sediments were placed in geostatistical model data files. This data file contains data on the position in space of each data sample point and the nuclide-specific concentration for that point.

## 9.2 Geostatistical Structural Model

The initial stage in developing a geostatistical model of the contamination was to assess the geostatistical structure of the interpreted data set by performing a geostatistical structural analysis. A geostatistical structural analysis determines if two data points can be correlated and quantifies the quality of the correlation.

The EVS software performs the geostatistical structural analysis by calculating three-dimensional variograms which are plots of the variance of the concentration values relative to the distance between data points. The EVS software is an "expert" system that automatically determines optimum parameter settings for the geostatistical structural model and for the kriging operation. These optimum settings were used as a starting point for refinement of the structural model. Parameters were initially calculated by the software and then refined to create the geostatistical structures for the contamination.

A drawback of the "expert" system is that the software does all of the geostatistical structural analysis. As a result, an extensive structural analysis of the data was not completed. This limited analysis is adequate for the intended purpose, which is to create visualizations of the contaminant plumes. The models are not adequate for any type of quantitative endeavors.

The total data domain of the calculations included all vadose zone boreholes within the C Tank Farm. The domain was extended in the north-south and east-west directions to include the maximum and minimum borehole coordinate values. Borehole depths were converted to elevations, and the vertical parameter of the domain was set to include the highest and lowest sample points.

The calculated variogram for  $^{137}\text{Cs}$  contamination that was used to represent the geostatistical structure in the horizontal direction had a range value of 229 ft and a sill value of 1.22. The range for the vertical variogram was also calculated to be 229 ft, but it had a lower sill value of 1.16. The range shows that a spatial relationship exists between two data points up to 229 ft, such that the knowledge of one point will decrease the mean estimation uncertainty of the other.

The calculated variogram for  $^{60}\text{Co}$  contamination that was used to represent the geostatistical structure in the horizontal direction had a range value of 230 ft and a sill value of 0.80. The range for the vertical variogram was also calculated to be 230 ft and had a sill value of 0.80. The

range shows that a spatial relationship exists between two data points up to 230 ft, such that the knowledge of one point will decrease the mean estimation uncertainty of the other.

The geostatistical structural analysis produced the equations for the variograms that were used to define the contamination concentration models for each of the radionuclides.

### 9.3 Three-Dimensional Plume Calculations and Creation of the Visualizations

The kriging process calculates mean grade, or, in this case, radionuclide concentrations of a volume of sediment by using the information from nearby sample points. The influence of each sample point or the weighting of the point in the calculation is determined by the geostatistical structure or the variogram model and is dependent on the proximity of the data sample point to the volume being investigated. Each sample point is combined in such a way that the kriging operation minimizes the error of the radionuclide concentration for the volume being investigated.

The kriging software applies a horizontal-to-vertical anisotropy ratio that allows the user to apply the effects of anisotropy in the conductivity of soil matrices in fluid flow. The anisotropy ratio tells the kriging algorithm what multiplication factor to use for applying a biased weighting on data points in the horizontal and vertical direction away from a given model node. The program default is 10, which results in data points a given distance in a horizontal direction from a data point node to influence the data node 10 times more than data points the same distance away in the vertical direction. This emphasis helped decrease reliance on data from the same borehole and more appropriately depicts the horizontal migration of the contaminants. Review of SGLS data and trial and error analyses yielded an anisotropy value of 10 for the  $^{137}\text{Cs}$  and  $^{60}\text{Co}$ .

The kriging process was set to clip data points from the calculations that had concentration values of less than 0.1 pCi/g. With this setup, the software calculates the radionuclide concentration on the basis of the knowledge that the data samples are less than 0.1 pCi/g, rather than ignore those data points. The lowest  $^{137}\text{Cs}$  and  $^{60}\text{Co}$  concentration that is visualized and presented in Section 10.0, "Discussion of Results," is 0.2 pCi/g.

Similarly, in regions where the radionuclide concentration was so high that the detection system became saturated, a value of 8,000 pCi/g was placed in the database for the kriging operation. This value was chosen by interpolating the concentration values on the  $^{137}\text{Cs}$  concentration plot profile. This setup has minimal effect on the C Tank Farm data because there were only three boreholes (30-05-07, 30-07-11, and 30-12-13) that had zones of  $^{137}\text{Cs}$  concentrations high enough to saturate the detector.

As discussed in Section 8.6, the SGLS log data were interpreted and the concentration values from the intervals where the contamination was localized to the borehole were removed from the geostatistical model data set. To remove the SGLS data at a specific point, a value of 0 replaced the actual concentration value. This caused the software to calculate the geostatistical model as if no contamination existed at that data point.

The kriging process calculated the individual radionuclide concentrations for each block bound by grid nodes. Each block was assigned a concentration, a concentration uncertainty, and minimum and maximum concentrations that were based on the uncertainty. These data were input into the visualization component of the program.

The visualizations were constructed to include the highest and lowest node values in three-dimensional space. Because nodes were set up at all data sampling points, the horizontal extent of the model and the visualizations are governed by the positions of the boreholes. The model does not extrapolate beyond the extent of either the sill distance or the kriging extent. As a result, both the model and the visualizations can extend only to the maximum depth of the boreholes and the extent of the geostatistical range unless other deeper boreholes are nearby.

In the visualization process, solid surfaces were created by connecting the three-dimensional points in space that had equal concentrations. Depending on the view angle and the isolevel, the outermost solid surface of a plume is viewed. To view an inner surface, a cut section is inserted through the solid model. If the isolevel is increased, progressively higher radionuclide concentration surfaces can be visualized. Where a low concentration medium exists surrounding a higher concentration medium, a cut in the three-dimensional plume is necessary to visualize the high-concentration zone.

Tanks were visualized by creating solid three-dimensional surfaces at the location of the tank. In regions at the surface of the tanks, the model does not insert a contamination barrier; therefore, a borehole directly across a tank can have some influence on a node point concentration calculation. This is a shortcoming of the calculation method, but it only applies to the region of the vadose zone above the base of the tanks.

#### **9.4 Potential Geostatistical Model and Visualization Uncertainties and Inaccuracies**

The visualizations presented in this report are based on assignments of individual  $^{137}\text{Cs}$  and  $^{60}\text{Co}$  concentration values to blocks bound by data point nodes. The software program does not include a mechanism to factor in the estimation uncertainty associated with each data point used in the model development (as depicted in the individual borehole concentration plots). The estimation uncertainty calculation is discussed in the base calibration report (DOE 1995a) and is calculated by combining the uncertainties of the calibration efficiency determination, the calibration-model grade assignments, and the individual spectrum photon-peak counting statistics from the field measurements. The spherical variogram model does not allow input of uncertainties associated with the individual assays into the structural model. However, that error is relatively small compared to the sill values and the rate of rise in the variogram curve with distance from the source. It would be advantageous to include this error in the variogram model and reflect that particular error in the concentration estimation uncertainty.

There are numerous cases where the SGLS log data are suspected of representing contamination that is localized to the borehole. To improve the accuracy of the geostatistical model and the resulting visualizations, concentration values were removed where it was interpreted the

contamination is localized to the borehole as opposed to distributed in the formation sediments. Also, much of the bias of the borehole log data that is due to borehole migration effects is removed from the plume visualizations because of the high horizontal-to-vertical anisotropy emphasis applied by the software in the modeling process, as discussed previously.

Potential model uncertainties and inaccuracies associated with zones of high  $^{137}\text{Cs}$  concentrations are not significant in the C Tank Farm because of the limited occurrence of these zones. The method utilized when these zones are encountered was described previously. Interpolated values are entered into the concentration database for all 0.5-ft intervals within the high count-rate zone. The problem with this method is that it puts a bias in the variogram because the variance between two data points in a borehole suddenly becomes zero. The result is a variogram (particularly the variogram in the vertical direction) that may not represent the true spatial structure of the data.

At the other extreme, there may be low-intensity radionuclides that were not detected by the current logging methods and equipment. The 35-percent efficiency detectors used in the SGLSs are considered to be a good compromise between performing the data acquisition for all the boreholes in the C Tank Farm in a cost-effective manner and detecting contamination at low concentrations while still doing a reasonable job of characterizing the high-contamination zones. The current visualizations do not include gamma-emitting radionuclides in concentrations that are less than the detection levels realized with the data acquisition configuration explained in Section 7.3, "Logging Process and Procedures."

The calibration of the logging system assumes a homogeneous medium of contamination that is effectively infinite in extent with respect to gamma-ray transport in horizontal and vertical extents. This assumption is valid for all situations except at the very top and the bottom of the boreholes, where the concentration changes rapidly with depth, or where the contamination is localized to the borehole. The data acquisition interval used to log the C Tank Farm boreholes (0.5 ft) provides adequate spatial resolution to characterize the situations where the contamination is not homogeneous in the vertical dimension. Contamination-zone edge effects can be removed if desired by spatial deconvolution methods described by Conaway and Killeen (1978).

Near the ground surface, the source distribution is no longer an infinite medium; the inaccuracies associated with that distribution are discussed in Section 10.1, "Surface and Near-Surface Contamination."

Most of the boreholes are open at the bottom and in direct contact with the sediment or with contamination that migrated down the inside of the borehole casing. As a result, the gamma rays emitted from the borehole bottom sediments are not attenuated by a casing, but a casing attenuation factor is applied to these data. Therefore, the reported apparent concentrations are most likely slightly high at the bottom of the borehole.

The reader is cautioned not to extrapolate beyond the intended purpose of the visualizations and should not assume the visualizations represent contaminant migration pathways or that they

represent quantitative distributions. The current visualizations should also not be used for developing or demonstrating theories on how the contaminants migrate through the vadose zone.

These visualizations are intended only to provide the reader with an understanding of approximately how the contamination that has leaked from the tanks is distributed in the vadose zone. Once a general understanding of the contaminant distribution is obtained, areas of concern can become the focus of comprehensive and quantitative characterizations.

## 10.0 Discussion of Results

The historical information discussed in the following sections has been summarized from the individual Tank Summary Data Reports. The reader is referred to the individual Tank Summary Data Reports for specifics regarding the sources of the historical information.

The following sections are related to the results of the visualizations that were created using the interpreted data set of the spectral log data acquired by the SGLS in the 70 C Tank Farm boreholes. These visualizations represent the interpreted data set discussed in Section 8.6. The visualizations are provided in Section 14.0 in the order in which they are discussed.

Figure 14-15 shows the interpreted data set used in the geostatistical models and is included to let the reader compare the individual borehole  $^{137}\text{Cs}$  concentration data with the visualizations depicting this radionuclide. The data are presented as spheres that are colored and sized according to the  $^{137}\text{Cs}$  concentration values and are presented in the spatial position in which the data were collected. Figure 14-16 shows the interpreted data set for the radionuclide  $^{60}\text{Co}$ .

Visualizations were prepared that show the  $^{137}\text{Cs}$  and  $^{60}\text{Co}$  contamination plumes with concentration isolevels at 0.2 pCi/g. Figures 14-17, 14-18, 14-19, 14-20, 14-21, 14-22, 14-23, and 14-24 present these visualizations from various viewpoints at the farm level.

The farm-level visualizations show the majority of contamination is located in the central and southern regions of the tank farm. These regions of contamination are discussed in detail in the following sections.

Several minor regions of subsurface contamination also exist in the C Tank Farm vadose zone sediments. These regions will also be discussed in detail.

### 10.1 Surface and Near-Surface Contamination

The logging operations measured gamma-emitting radionuclide concentrations at the ground surface when the detector was centered at the 0-ft depth location in the boreholes. Radionuclide concentration values measured at the ground surface are not accurate for two reasons. The calibration of the logging systems makes the assumption of a homogeneous infinite medium; however, this is not the case when the detector is located at the ground surface. Instead, there is only an infinite geometrical half space with gamma rays originating from the sediments in only

the lower half space. From the upper surface, gamma rays can originate from contamination far from the borehole, such as nearby contaminated equipment, because they are not attenuated by the sediments or borehole casing materials. If there is an appreciable amount of contamination on the surface, the reported radionuclide concentrations would be higher than is actually present in the formation.

The other reason the concentrations are not valid is because most of the boreholes were constructed with a small concrete surface collar. This collar, which is about 6 in. deep and 12 in. in diameter, surrounds the borehole, effectively attenuating the gamma rays. This collar attenuation will cause the reported concentrations to be lower than what is actually present in the formation.

Because the contamination model was developed without attempting to correct for this attenuation, the visualization of the surface contamination is not correct in terms of the actual concentration of the  $^{137}\text{Cs}$  in the sediment. The  $^{137}\text{Cs}$  concentration may be higher or lower by an unknown amount.

In nearly all the C Tank Farm boreholes,  $^{137}\text{Cs}$  was detected at the ground surface. Because half of the SGLS detector is located outside the borehole when at the ground surface measuring point, the detector is most likely measuring direct gamma rays from  $^{137}\text{Cs}$  that is actually located on nearby contaminated equipment or is localized to the top of the borehole casing. Where it is interpreted the  $^{137}\text{Cs}$  is due to nearby contaminated equipment or is localized to the top of the borehole casing, the  $^{137}\text{Cs}$  concentration value was removed from the geostatistical model data set.

Not all contamination measured at the ground surface is related to nearby contaminated equipment. Around many boreholes,  $^{137}\text{Cs}$  contamination was detected not only at the ground surface, but also for a short interval directly below the ground surface. This contamination is most likely the result of surface spills that occurred in the C Tank Farm.  $^{137}\text{Cs}$  from known and potential surface spills was left in the data set used to develop the geostatistical model.

Areas of surface  $^{137}\text{Cs}$  contamination were observed throughout the C Tank Farm. Figure 14-25 presents a visualization of the  $^{137}\text{Cs}$  data measured by the SGLS at the ground surface. Figure 14-25 shows the surface contamination with the highest concentrations over tanks C-105 and C-106 and over the southwest portion of tank C-108. Unplanned releases UN-200-E-82, UN-200-E-118, and UN-200-E-16 (see Section 5.4) describe surface contamination above or near tanks C-105, C-106, and C-108. The surface contamination detected by the SGLS is most likely the results of the surface contamination described in Section 5.4.

Minor amounts of surface contamination were detected above tanks C-102, C-103, C-110, C-111, and C-112. A review of historical records did not provide documented sources for this contamination. Therefore, this surface contamination may be the result of one or more undocumented surface spills or surface contamination documented as unplanned releases UN-200-E-82, UN-200-E-118, and UN-200-E-16 that have spread or are larger than originally believed.

Figure 14-26 shows a horizontal slice of the C Tank Farm contamination at a depth of 5 ft. This figure shows that most of the  $^{137}\text{Cs}$  contamination discussed above has migrated to this depth. A review of the "as-built" drawings for the C Tank Farm piping shows numerous pipelines at this depth. Therefore, it is possible some the contamination at this depth is from leaks in those pipelines. A review of historical operating records did not reveal any information that could substantiate the conclusion that these shallow subsurface pipelines had leaked.

Figure 14-27 shows a horizontal slice of the C Tank Farm contamination at a depth of 10 ft. This figure shows that some of the  $^{137}\text{Cs}$  contamination that originated from the surface or near the surface appears to have continued migrating to this depth. Higher levels of contamination are still present above tanks C-103, C-105, and C-106.

Figures 14-28 and 14-29 show a horizontal slice of the C Tank Farm contamination at depths of 15 and 20 ft, respectively. Figures 14-30 and 14-31 show a horizontal slice of the C Tank Farm contamination at depths of 25 and 30 ft, respectively. These figures show the  $^{137}\text{Cs}$  discussed above has continued to migrate and the concentration values appear to have decreased. These figures also show that some of the  $^{137}\text{Cs}$  appears to have cascaded across the tops of the tank domes.

While some of the contamination between the depths of 15 and 30 ft is from dome runoff, it most likely does not account for all of the near-surface contamination. The C Tank Farm contains numerous subsurface pipelines that are used to transfer the waste from facility to facility. The pipelines within the tank farm are generally connected to pump pits, diversion boxes, and as cascade overflows. The pipelines range from about 5 to 25 ft below the tank farm ground surface and are generally 3 to 6 in. in diameter. Each tank has at least two nozzles constructed into the side wall of the tank; these nozzles are used for cascade overflows and for adding waste to the tanks. Brevick et al. (1994) provide a summary of the tank access points. Potential leaks from these pipelines may have contributed to the subsurface contamination shown in the visualizations. A review of the as-built drawings for the C Tank Farm piping shows numerous pipelines at these depths. Therefore, it is possible that some the contamination shown in Figures 14-28, 14-29, 14-30, and 14-31 is from leaks in those pipelines. Except as noted below, a review of historical operating records did not reveal any information that could substantiate the conclusion that these subsurface pipelines had leaked.

The one exception is the recent interpretation in Brodeur (1993) that indicates the cascade line between tanks C-104 and C-105 leaked. The  $^{137}\text{Cs}$  and  $^{60}\text{Co}$  contamination shown on Figures 14-29 and 14-31 between tanks C-104 and C-105 clearly shows a leak described in Brodeur (1993) where a cascade line is located (see Section 5.8), or more specifically, a leak from the cascade line connection to the tank.

The correlation plots, and, to a limited extent, the visualizations show that the surface contamination has migrated primarily downward to about 10 to 30 ft below the ground surface and that it has diminished in intensity. This distribution is not as apparent on the visualizations as it is on the borehole correlation plots provided in Appendix A, because the  $^{137}\text{Cs}$  concentration

values are low (in many cases below the 0.2-pCi/g isopleth used in the visualizations) and intermittent.

A majority of the boreholes have a small circular concrete pad around the borehole casing at the ground surface. The only exceptions are those boreholes that are located within berms. Because the berms were installed subsequent to the completion of these boreholes, casing extensions were welded to the original borehole casings.

In a few cases, an 8-in. starter casing was installed to a depth of between 15 and 20 ft; after the permanent 6-in. casing was installed, the starter casing was removed and grout was generally added to the remaining annular space.

Other than the surface pad and starter casing modifications, there was no other seal between the casing and formation to prevent migration along the interface between casing and formation. In the event of a surface spill, leak of contaminated material, or precipitation at the tank farm surface, contamination could have migrated downward or previously deposited contamination may have been remobilized and driven down the borehole-created pathway within the sediments.

Due to the low sensitivity of the gross gamma logging equipment, regions where contamination was actively migrating downward from the ground surface could not be identified in the gross gamma log data recorded from the early 1970s to the late 1980s.

In summary, the most likely scenarios for the contamination from the ground surface to a depth of about 30 ft are downward migration of surface contamination from spills or leakage from pipelines and ancillary equipment. Some contaminated sediments below the ground surface may have been carried downward during borehole drilling as casing was advanced in the borehole. The contamination believed to be on the borehole casing was removed from the visualization data set.

## 10.2 Tank-by-Tank Discussion

The following sections provide a discussion of the contaminant distribution on a tank by tank basis. Historical and current tank content data are summarized from the individual Tank Summary Data Reports and Hanlon (1997). Information regarding the KUT log plots is provided in the individual Tank Summary Data Reports.

A geophysical logging campaign was conducted by the WHC Geophysics group in 1992 and 1994 in the boreholes surrounding tanks C-103, C-105, and C-106 (see Section 5.8 of this report). The geophysical logging campaign was limited strictly to spectral gamma logging methods; therefore, the focus of the investigations was limited strictly to gamma-ray-emitting radionuclides. The logging campaigns are documented in two reports: *Assessment of Unsaturated Zone Radionuclide Contamination Around Single-Shell Tanks 241-C-105 and 241-C-106* (Brodeur 1993) and *Assessment of Vadose Zone Radionuclide Contamination Around Single Shell Tank 241-C-103* (Kos 1995). The WHC Geophysics group reports were billed as a

“comprehensive assessment of the radionuclide concentration data” and are similar to the Tank Summary Data Reports published by this characterization effort.

Summaries of the WHC Geophysics group findings and conclusions as well as data comparisons are detailed in the individual Tank Summary Data Reports, Section 5.8 of this report, and the appropriate sections below. The reader is referred to Brodeur (1993) and Kos (1995) for detailed descriptions of the data acquisition methods, discussion of findings, conclusions, and recommendations from these investigations. For a detailed discussion of a comparison of the SGLS data and the spectral gamma data from Brodeur (1993) and Kos (1995), the reader is referred to the individual Tank Summary Data Reports (DOE 1997k, 1997m, and 1997n).

### 10.2.1 Tank C-101

Tank C-101 was placed into service in 1946. Throughout its service life, this tank received and stored metal waste, uranium recovery waste, PUREX cladding waste, and decontamination waste (DOE 1997i).

In the late 1960s, the tank experienced a liquid-level decrease and was subsequently taken out of service. The tank was classified as having questionable integrity in 1970 and a confirmed leaker in 1980. The tank is assumed to have leaked 20,000 gal of waste containing 2,000 Ci of unknown radionuclides. A review of historical operations records did not reveal information regarding the liquid-level decrease or the basis for the leak estimate.

Interim stabilization for tank C-101 was completed in 1983. The present inventory of tank C-101 is 88,000 gal of waste consisting of 88,000 gal of sludge; 3,000 gal drainable interstitial liquid is contained within the sludge. The current waste level is approximately 27 in. above the dished tank bottom (Hanlon 1997; DOE 1997i).

Six monitoring boreholes are associated with tank C-101; five were drilled in the early to mid-1970s and one (30-00-06) was drilled in 1944 (see Figure 14-11). All of these boreholes were logged with the SGLS. The concentration plots for the contaminants detected in these boreholes are presented in Appendix A. Figures 14-32 and 14-33 show the  $^{137}\text{Cs}$  and  $^{60}\text{Co}$  distribution in the vadose zone sediments surrounding tank C-101. The views are from the south and northwest, respectively.

The visualizations show  $^{137}\text{Cs}$  plumes at various depths surrounding tank C-101. Figure 14-33 shows  $^{60}\text{Co}$  at a depth of about 30 ft that is most likely associated with tank C-104.

According to the Tank Summary Data Report for tank C-101, the tank is suspected to have leaked somewhere near borehole 30-01-09 at a depth of about 27.5 ft (DOE 1997i). The visualizations show two  $^{137}\text{Cs}$  plumes at the base of the backfill material (one to the southwest and the second to the southeast) that appear to have resulted from the leak in tank C-101. The gap between the  $^{137}\text{Cs}$  plumes shown in Figure 14-32 may be the result of double casing and grout of borehole 30-00-06 having effectively masked any potential contamination around that borehole that would have connected the two plumes.

Both Figures 14-32 and 14-33 show a  $^{137}\text{Cs}$  plume and a  $^{60}\text{Co}$  plume north of tank C-101. This plume most likely consists of commingled contaminants from the leak in tank C-101 and from the cascade line leak between tanks C-104 and C-105 (see Section 10.2.5).

The visualizations show a  $^{137}\text{Cs}$  plume beneath tank C-101 starting at a depth of about 70 ft. This plume is defined by data from borehole 30-00-06 and other boreholes near tanks C-103 and C-105. Borehole 30-00-06 is perforated from about 57 ft to the bottom of the logged interval (111 ft) and is double cased and possibly grouted from about 4 to 57 ft. If the grout is present, it could be effectively shielding any gamma rays being emitted from contamination that may be present. It is possible the perforations have allowed contamination present at the base of the backfill to migrate deeper into the vadose zone.

The visualizations show the  $^{137}\text{Cs}$  appears to spread horizontally from the perforated borehole (30-00-06) to the north. Even though every effort has been made to remove data that will cause the geostatistical model to create "false plumes," it is possible the model has overestimated the horizontal extent of this plume. However, due to a lack of vadose zone boreholes that extend below a depth of 100 ft, the total horizontal extent of this plume cannot be accurately determined.

Details regarding the data acquired in the boreholes surrounding tank C-101 are provided in the Tank Summary Data Report for tank C-101 (DOE 1997i).

## 10.2.2 Tank C-102

Tank C-102 was placed into service in 1946. Throughout its service life, this tank received and stored metal waste, uranium recovery waste, waste water, and various PUREX waste streams. Tank C-102 was removed from service and declared inactive in 1977. Interim stabilization of the tank was completed in 1995. Tank C-102 is currently on the Organic Salts Watch List (DOE 1997j).

The current inventory of tank C-102 consists of 316,000 gal of sludge and 30,000 gal of drainable interstitial liquid. The waste level is approximately 150 in. above the lowest point of the dished tank base (Hanlon 1997; DOE 1997j).

There are no vadose zone monitoring boreholes specifically associated with tank C-102. This large gap in the database creates a high degree of uncertainty in the plumes around tank C-102. However, five monitoring boreholes that are associated with adjacent tanks are in positions relative to tank C-102 to provide information regarding vadose zone contamination in the vicinity of the tank. The concentration plots for the contaminants detected around these boreholes are provided in Appendix A. Figures 14-32 (viewed from the south), 14-33 (viewed from the northwest), and 14-34 (viewed from the southeast) show the  $^{137}\text{Cs}$  and  $^{60}\text{Co}$  contaminant distribution in the vadose zone sediments surrounding tank C-102.

Figures 14-32, 14-33, and 14-34 show  $^{137}\text{Cs}$  nearly surrounds tank C-102. A review of historical operations records does not provide evidence this tank has leaked. The contamination shown in the visualizations is most likely associated with other nearby tanks and their associated

subsurface pipelines as well as with the pipelines associated with tank C-102. The  $^{60}\text{Co}$  beneath the tank is most likely associated with leak events from adjacent tanks or nearby subsurface pipelines. The  $^{137}\text{Cs}$  plume that is located approximately 70 ft below tank C-102 is associated with leak events from nearby tanks and their associated subsurface pipelines. Discussions regarding the origin of the  $^{137}\text{Cs}$  and  $^{60}\text{Co}$  that surround tank C-102 are provided in the appropriate sections.

Details regarding the data acquired in the boreholes surrounding tank C-102 are provided in the Tank Summary Data Report for tank C-102 (DOE 1997j).

### 10.2.3 Tank C-103

Tank C-103 was placed into service in 1953. Throughout its operating history, tank C-103 received and stored metal waste, U Plant waste streams, PUREX waste streams, and B Plant evaporator bottoms. The tank was removed from service and declared inactive in 1979. The tank has not been interim stabilized (DOE 1997k).

This tank currently contains 62,000 gal of sludge and 133,000 gal of supernatant. The present surface of the waste is about 66 in. above the lowest point of the dished tank base. The tank is currently listed as sound (Hanlon 1997; DOE 1997k).

Seven monitoring boreholes are associated with tank C-103; borehole 30-00-03 was constructed in 1945 and the rest were drilled in the 1970s (see Figure 14-11). All of these boreholes were logged with the SGLS. The concentration plots for the contaminants detected around these boreholes are provided in Appendix A. Visualizations of the contamination detected by the SGLS are presented in Figures 14-33 (viewed from the northwest), 14-34 (viewed from the southeast), and 14-35 (viewed from the east).

As discussed in Section 5.8, Kos (1995) identified three zones of contamination around tank C-103: one near the ground surface, another at the base of the tank farm excavation, and a third at a depth of 80 ft. Kos (1995) concludes that the  $^{137}\text{Cs}$  contamination from the ground surface to the base of the tank farm excavation is the result of a large undocumented surface spill. The surface spill apparently migrated through the backfill material until it reached the tank dome and ran along the outside of the tank structure to the base of the tank farm excavation.

The  $^{60}\text{Co}$  contamination at 80 ft was attributed by Kos (1995) to a source near tanks C-108 and C-109. Kos (1995) concludes the RLS log data, neutron moisture probe data, and tank farm gross gamma log data show a "trail" of contamination from tanks C-108 and C-109. Neutron-moisture probe data show an interval of elevated moisture at a depth of about 80 ft. The tank farm gross gamma log data show the contamination migrating as late as the mid-1980s. Also, the RLS data do not identify  $^{60}\text{Co}$  above 80 ft as would be expected if the contamination came from tank C-103.

The SGLS acquired data in the C-103 boreholes 3 years after the RLS. The Tank Summary Data Report for tank C-103 provides a detailed comparison of the spectral data. Some general

statements can be made. The SGLS and RLS data show good correlation for the  $^{137}\text{Cs}$ . The profiles of the  $^{137}\text{Cs}$  are very similar, suggesting the contaminants are stable. The comparison for  $^{60}\text{Co}$  shows an apparent increase and may indicate the  $^{60}\text{Co}$  is continuing to migrate.

The visualizations show  $^{137}\text{Cs}$  completely surrounds tank C-103 from the ground surface to a depth of about 50 ft. This distribution is most likely the result of one or more surface and/or more subsurface pipeline leaks that have occurred in the vicinity of tank C-103 (a review of operational records did not identify a documented occurrence of a surface spill or pipeline leak). It is possible this contamination migrated from the surface or near surface to the tank dome and then migrated along the tank dome and wall and collected at the base of the tank farm excavation. It is also possible that some of the contamination is the result of a leak from tank C-103.

The  $^{60}\text{Co}$  beneath the tank is most likely associated with leak events from adjacent tanks or associated subsurface pipelines. The  $^{137}\text{Cs}$  plume that is located approximately 80 ft below tank C-103 is associated with leak events from nearby tanks and their associated subsurface pipelines.

Details regarding the data acquired in the boreholes surrounding tank C-103 are provided in the Tank Summary Data Report for tank C-103 (DOE 1997k).

#### **10.2.4 Tank C-104**

Tank C-104 was placed into service in 1946. Throughout its service life, this tank received and stored metal waste, U Plant waste streams, coating waste, and PUREX waste streams. The tank was removed from service in 1980. Tank C-104 was interim stabilized in 1989 and is currently listed as sound.

The present waste inventory for tank C-104 consists of 295,000 gal of sludge that includes 11,000 gal of potentially drainable liquid. The waste level is about 100 in. above the tank's dished bottom.

In 1974, historical gross gamma logs for borehole 30-04-02 (located between tanks C-104 and C-105) began to show an anomalous zone of activity at a depth of about 40 ft. Boreholes 30-05-05, 30-05-06, 30-05-08, and 30-05-09 were installed in an effort to identify the source of the anomalous activity. The investigation concluded the contamination was the result of overfilling tank C-105 and the subsequent leakage from the subsurface cascade line connections. It is not known when the overfill occurred.

A review of historical operating records for tank C-104 revealed three deviation reports between 1982 and 1983 regarding decreases in liquid level. In all three cases, the engineering evaluation concluded the liquid loss was due to evaporation.

In 1993, WHC logged borehole 30-05-06, which is located between tanks C-104 and C-105. In 1997 the borehole was logged by the SGLS. Comparison of the data suggests the  $^{137}\text{Cs}$

contamination between tanks C-104 and C-105 has remained fixed in the vadose zone since 1993.

Ten vadose zone monitoring boreholes, all drilled in the early to mid-1970s, surround tank C-104 (Figure 14-11). All of these boreholes were logged with the SGLS. The concentration plots for the contaminants detected in these boreholes are provided in Appendix A. Figures 14-36 (shown from the east) and 14-37 (shown from southwest) show the  $^{137}\text{Cs}$  and  $^{60}\text{Co}$  contaminant distribution around tank C-104.

The visualizations show  $^{137}\text{Cs}$  contamination nearly surrounds tank C-104. The depth of the  $^{137}\text{Cs}$  contamination is limited to about 70 ft or about 25 ft below the base of the tanks.  $^{60}\text{Co}$  is present in a plume that is localized to the immediate area between tanks C-104 and C-105. The depth of the  $^{60}\text{Co}$  contamination is limited to about 65 ft or about 25 ft below the base of the tanks.

The  $^{137}\text{Cs}$  and  $^{60}\text{Co}$  located between tanks C-104 and C-105 is most likely the result of overfilling and subsequent leak from the cascade line (or cascade line connection) between tanks C-104 and C-105. Contamination from this leak appears to have migrated at least 25 ft below the base of the tank. The horizontal extent cannot be determined because the  $^{137}\text{Cs}$  appears to commingle with contamination from other sources.

The  $^{137}\text{Cs}$  contamination detected around the rest of tank C-104 is most likely the result of surface spills and subsurface pipeline leaks that have migrated through the backfill sediments and about 15 ft into the Hanford formation.

Details regarding the data acquired in the boreholes surrounding tank C-104 are provided in the Tank Summary Data Report for tank C-104 (DOE 1997i).

### **10.2.5 Tank C-105**

Tank C-105 was placed into service in 1946. Throughout its service life, this tank received and stored metal waste, uranium recovery waste streams, U Plant waste streams, PUREX waste streams, B Plant low-level waste and strontium sludge, waste water, REDOX high-level waste and supernatant, B Plant cesium ion-exchange waste, and noncomplexed and complexed waste.

The present inventory for tank C-105 consists of 132,000 gal of sludge. The waste contains an estimated 33,000 gal of drainable interstitial liquids and 2,000 gal of supernate. The present level of the waste surface in tank C-105 is about 50 in. above the lowest point of the dished tank base. The tank was interim stabilized in October 1995 and is currently categorized as sound (DOE 1997m; Hanlon 1997).

A review of historical operating documents revealed tank C-105 experienced a 36-in. waste level decrease between 1963 to 1967. An investigation of the incident concluded the level loss was due to evaporation. However, the investigation also acknowledges there were no data to support this conclusion.

In March 1974, historical gross gamma logs for borehole 30-04-02 (located between tanks C-104 and C-105) began to show an anomalous zone of activity at a depth of about 40 ft. Boreholes 30-05-05, 30-05-06, 30-05-08, and 30-05-09 were installed in an effort to identify the source of the anomalous activity. The investigation concluded the contamination was the result of overfilling tank C-105 and the subsequent leakage from the subsurface pipeline connections.

It is not known when the overflow occurred, but it is assumed to have occurred shortly before the anomalous activity in borehole 30-04-02 was detected. It is also not known by how much the tank was overfilled. A review of historical operating records indicates the waste level in tank C-105 from June 1973 to March 1974 was 30 to 100 in. below the cascade lines. Therefore, the contention the tank was overfilled cannot be confirmed.

As discussed in Section 5.8, Brodeur (1993) identified three zones of subsurface contamination. The first zone was between tanks C-104 and C-105 and was attributed to a leak in the cascade pipeline that runs between the two tanks. The second zone is located at a depth of about 50 ft around borehole 30-05-05 and was attributed to the leak in the C-104-to-C-105 cascade line or a leak from tank C-105. The third zone is located between tanks C-103 and C-105 at a depth of about 27 ft and was attributed to leak in a subsurface pipeline or a leak from either tank C-103 or C-106. According to Brodeur (1993), data from the RLS as well as a review of historical information did not provide direct evidence that tank C-105 or C-106 had leaked.

The SGLS acquired data in the C-105 and C-106 boreholes 4 years after the RLS. The Tank Summary Data Reports for tanks C-105 and C-106 provide a detailed comparison of the spectral data. However, some general statements can be made. The SGLS and RLS data show good correlation for the  $^{137}\text{Cs}$ . The profiles of the  $^{137}\text{Cs}$  are very similar, suggesting the contaminants are stable. The comparison for  $^{60}\text{Co}$  shows changing concentration profiles, reflecting the radioactive decay of this radionuclide.

Ten vadose zone monitoring boreholes surround tank C-105, all of which were drilled in the 1970s (Figure 14-11). All of the boreholes were logged with the SGLS. The concentration plots for the contaminants detected in these boreholes are provided in Appendix A.

Figures 14-38 (shown from the southwest), 14-39 (shown from the east), 14-40 (shown from the northeast), and 14-41 (shown from the north) are visualizations with northwest- to southeast-trending cut planes that show the  $^{137}\text{Cs}$  and  $^{60}\text{Co}$  distribution in the vadose zone sediments surrounding tank C-105. Figures 14-42 (shown from the south) and 14-43 (shown from the north) are visualizations with northeast- to southwest-trending cut planes applied.

The visualizations show  $^{137}\text{Cs}$  contamination surrounding tank C-105. The  $^{137}\text{Cs}$  appears to have originated between tanks C-104 and C-105 and migrated into the backfill and Hanford formation sediments to a depth of at least 120 ft, or about 80 ft below the base of the tank. The  $^{60}\text{Co}$  appears to have migrated to a depth of at least 80 ft, or about 40 ft below the base of the tank. The actual horizontal migration cannot be determined because the contaminant plumes most likely contain waste from more than one source that in many cases is undeterminable.

The potential sources for the  $^{137}\text{Cs}$  and  $^{60}\text{Co}$  contaminant plumes include surface spills, leaks from one or more nearby subsurface pipelines, and leaks from one or more tanks. A review of historical operating records did reveal two documented sources for the contamination. The first potential source is the contamination that resulted from unplanned release UN-200-E-16. This unplanned release was the result of a leak from an overground transfer line located between tanks C-105 and C-106. It is unknown what volume of waste was spilled or its radionuclide content. This unplanned release could only have contributed to the vadose zone contamination between tanks C-105 and C-106 if a sufficient volume of waste was leaked from the transfer line.

As stated previously, tank C-105 experienced a 36-in. waste-level decrease in the mid-1960s that was attributed solely to evaporation. Historical operating records acknowledge temperature data and liquid-level decrease studies were not available to substantiate this conclusion. Therefore it is possible, although not verifiable, that a leak from tank C-105 is the second potential source for at least some of the  $^{137}\text{Cs}$  and  $^{60}\text{Co}$  contamination.

Unverifiable sources for the contamination include leaks from nearby subsurface pipelines (other than related to the overflow event) and leaks from nearby tanks. The potential for leaks in nearby tanks is discussed in the appropriate sections of this report.

The visualizations show a  $^{137}\text{Cs}$  plume between tanks C-105 and C-106 that extends to a depth of about 120 ft. The anthropogenic radionuclide  $^{60}\text{Co}$  is also found in this plume. The source of this plume is most likely a leak event from tanks C-105 or C-106 or from the cascade line that runs between them. However, as discussed previously, this interpretation cannot be verified with historical operating records.

Details regarding the data acquired in the boreholes surrounding tank C-105 are provided in the Tank Summary Data Report for tank C-105 (DOE 1997m).

### **10.2.6 Tank C-106**

Tank C-106 was placed into service in 1947. Throughout its service life, this tank received and stored metal waste, U Plant waste streams, PUREX Waste streams B Plant low-level waste, decontamination waste, strontium sludge, uranium recovery waste, coating waste, and waste water. The tank was removed from service in 1979. The present inventory for tank C-106 is 197,000 gal of sludge and approximately 32,000 gal of supernate. This tank has not been interim stabilized and is currently considered sound (DOE 1997n; Hanlon 1997).

In 1971, waste temperatures in tank C-106 reached 212 °F, a temperature the waste tank was not designed for. Since this occurrence, water has been added periodically to the tank to promote cooling. The evaporation of the water makes in-tank leak detection difficult.

As discussed in Sections 5.8 and 10.2.5, tank C-106 was part of the investigation that is described in *Assessment of Unsaturated Zone Radionuclide Contamination Around Single-Shell Tanks 241-C-105 and 241-C-106* (Brodeur 1993). The intent of this investigation was to determine if there was evidence that tanks C-105 or C-106 had leaked.

Eight vadose zone monitoring boreholes surround tank C-106; borehole 30-00-01 was installed in 1944 and the rest were drilled in the 1970s (Figure 14-11). All of these boreholes were logged with the SGLS. The concentration plots for the contaminants detected in these boreholes are provided in Appendix A.

Figures 14-35 (viewed from the east), 14-43 (viewed from the north), 14-44 (viewed from the west), 14-45 (viewed from the northeast), and 14-46 (viewed from the southwest) show the  $^{137}\text{Cs}$  and  $^{60}\text{Co}$  distribution around tank C-106. The visualizations show  $^{137}\text{Cs}$  nearly surrounds the tank.  $^{60}\text{Co}$  is also present beneath the tank.

The  $^{137}\text{Cs}$  between the ground surface and the base of the backfill material is most likely the result of surface spills and leaks in nearby subsurface pipelines. It is possible the increased runoff from the tank dome may have carried the  $^{137}\text{Cs}$  contamination along the outside of the tank, where it accumulated at the base of the excavation and within the top 10 ft of the Hanford formation sediments (total depth of 50 ft).

A review of historical operating records revealed two unplanned releases (see Section 5.4) in the vicinity of tank C-106 that could have contributed to the  $^{137}\text{Cs}$  contamination. The first unplanned release (UN-200-E-118) was an airborne release from tank C-107 that occurred 1957. It is doubtful that an airborne release would have sufficient radionuclide content for a significant contribution to the subsurface contamination around tank C-106.

The second unplanned release (UN-200-E-16) is a surface spill that resulted from a leak of an overground transfer line located between tanks C-105 and C-106. It is unknown what volume of waste was spilled or its radionuclide content. This unplanned release could only have contributed to the vadose zone contamination between tanks C-105 and C-106 if a sufficient volume of waste was leaked from the transfer line.

It is possible the  $^{137}\text{Cs}$  from 40 to about 50 ft has commingled with  $^{137}\text{Cs}$  from the overground transfer line leak, a leak in tank C-105, or the cascade line that runs between tanks C-105 and C-106. It is also possible another unidentified leak event could have contributed to this contamination.

The visualizations show a  $^{137}\text{Cs}$  plume between tanks C-105 and C-106 that extends to a depth of about 120 ft; some  $^{60}\text{Co}$  is also present in this plume which is located beneath and to the southeast of tank C-106. It is possible that the source of the plume is a leak from tanks C-105 or C-106 or a cascade line associated with one of these tanks. Due to the addition of water to the tank to promote cooling, accurate in-tank leak detection in tank C-106 is not possible. Therefore, tank C-106 cannot be ruled out as a potential source.

The  $^{60}\text{Co}$  contamination detected in the boreholes below and to the northwest of tank C-106 is probably from a nearby tank or subsurface pipeline leak, not tank C-106.

As discussed in Section 10.2.5, the boreholes were logged by WHC with a spectral system (the RLS) in 1993 and again as part of this characterization effort (with the SGLS) in 1997.

Generally, the SGLS and RLS data show good correlation for the  $^{137}\text{Cs}$ . The profiles of the  $^{137}\text{Cs}$  are very similar, suggesting the contaminants are stable. The differences in the  $^{60}\text{Co}$  profiles reflect its radioactive decay. However, the  $^{60}\text{Co}$  in borehole 30-06-10 showed some apparent downward migration, indicating that at least the  $^{60}\text{Co}$  contamination may be actively migrating.

Details regarding the data acquired in the boreholes surrounding tank C-106 are provided in the Tank Summary Data Report for tank C-106 (DOE 1997n).

### **10.2.7 Tank C-107**

Tank C-107 was placed into service in 1946. Throughout its service life, this tank received and stored first-cycle decontamination waste, uranium recovery waste, and Strontium Semiworks waste streams. The tank was removed from service in 1978. The present inventory for tank C-107 is 237,000 gal of sludge that includes 24,000 gal of drainable interstitial liquids. The present level of the waste in tank C-107 is about 108 in. above the tank base. The tank is currently considered sound and was interim stabilized in September 1985 (DOE 1997o; Hanlon 1997).

Eight vadose zone monitoring boreholes surround tank C-107, all of which were drilled in the 1970s (Figure 14-11). All of the boreholes were all logged with the SGLS. The concentration plots for the contaminants detected in these boreholes are provided in Appendix A.

Figures 14-47 (viewed from the northeast) and 14-48 (viewed from the southwest) show the  $^{137}\text{Cs}$  contaminant distribution in the vadose zone sediments surrounding tank C-107. The visualizations show a  $^{137}\text{Cs}$  plume to the north of tank C-107 that extends to a depth of about 70 ft (about 30 ft below the base of the tank). This contamination is most likely from a leak in a nearby tank such as tanks C-110 or C-111 (known leakers).

The KUT log data indicate the contact between the Hanford formation gravel facies and the Hanford formation sand facies is approximately 55 ft (DOE 1997o, 1997r). The distribution of the  $^{137}\text{Cs}$  contamination appears to have been controlled by this contact.

Details regarding the data acquired in the boreholes surrounding tank C-107 are provided in the Tank Summary Data Report for tank C-107 (DOE 1997o).

### **10.2.8 Tank C-108**

Tank C-108 was placed into service in 1947. Throughout its service life, this tank received and stored first-cycle waste, U Plant waste streams, evaporator bottoms, ferrocyanide waste, coating waste, PUREX cladding waste, strontium recovery waste, Strontium Semiworks waste, organic wash waste, and ion-exchange waste. The tank was removed from service and declared inactive in 1977. The present inventory for tank C-108 is 68,000 gal of sludge. The present level of the waste in tank C-108 ranges between 18.25 and 20 in. above the dished tank base. The tank was interim stabilized in March 1984 and is currently considered sound (DOE 1997p; Hanlon 1997).

Eight vadose zone monitoring boreholes surround tank C-108; borehole 30-08-03 was drilled in 1944, borehole 30-09-07 was drilled in 1982, and the rest of the boreholes were drilled in the 1970s (Figure 14-11). All of these boreholes were logged with the SGLS. The concentration plots for the contaminants detected in these boreholes are provided in Appendix A. Figures 14-49 (viewed from the north), 14-50 (viewed from the west), 14-51 (viewed from the south), and 14-52 (viewed from the west) show the  $^{137}\text{Cs}$  and  $^{60}\text{Co}$  distribution in the vicinity of tank C-108. Figures 14-49 and 14-50 show the contamination around tank C-108 with cut planes placed to the southwest and northeast of the tank. Figures 14-51 and 14-52 show the contamination around tank C-108 with cut planes placed northwest and southeast of the tank.

The KUT log data indicate the contact between the Hanford formation gravel facies and the Hanford formation sand facies is between approximately 60 and 70 ft (DOE 1997p). Figure 14-49 shows  $^{137}\text{Cs}$  and  $^{60}\text{Co}$  in the Hanford formation gravel facies beginning at the base of the tank farm excavation and extending to the top of the Hanford formation sand facies (approximately 70 ft below the ground surface). The contamination appears to extend from beneath the center of tank C-108, underneath and to the north and east of tank C-109.

The source of the contamination below tank C-108 cannot be positively identified. The continuous distribution of the  $^{60}\text{Co}$  contamination between depths of 47 and 80 ft in borehole 60-08-02 and the absence of  $^{60}\text{Co}$  contamination above this interval suggest this contamination originated from a subsurface source such as from leakage from tank C-108, or some other subsurface source such as a leak in the cascade line between tanks C-108 and C-109.  $^{60}\text{Co}$  contamination was detected below a depth of 45 ft in several boreholes surrounding tank C-109, and this  $^{60}\text{Co}$  contamination may be indicative of a possible leak from tank C-109 that migrated into the vicinity of tank C-108 or vice versa (contamination from a leak from tank C-108 that migrated into the region beneath tank C-109) along some undetermined pathway. Regardless, positive identification of the source(s) of this contamination has not been determined and additional investigation is warranted.

A distinct zone of  $^{137}\text{Cs}$  and  $^{154}\text{Eu}$  contamination was detected around borehole 30-08-02 (located between tanks C-108 and C-109) between the depths of 19 and 25 ft. Shape factor analysis indicates this contamination is remote from the borehole, indicating this contamination is from a leak in a subsurface pipeline that has not migrated far or is contamination that is contained in the pipeline itself.

Figure 14-50 shows the  $^{137}\text{Cs}$  contamination that is located between tanks C-107 and C-108 and extends to a depth of about 60 ft. This contamination could be the result of a leak in tanks C-110 and C-111 (known leakers) or possibly tank C-108 or its associated subsurface pipelines.

Figure 14-51 shows the  $^{137}\text{Cs}$  located to the southeast side of tank C-108 that extends to a depth of about 70 ft below the ground surface. This contamination is most likely associated with leak events (tank leaks or subsurface pipeline leaks) from the vicinity of tanks C-104 and C-105.

Figure 14-52 shows the  $^{137}\text{Cs}$  contamination on the southwest side of tank C-108 that extends to a depth of about 80 ft below the ground surface. This contamination is most likely associated with leaks from nearby tanks C-110 and C-111.

Details regarding the data acquired in the boreholes surrounding tank C-108 are provided in the Tank Summary Data Report for tank C-108 (DOE 1997p).

### 10.2.9 Tank C-109

Tank C-109 was placed into service in 1948. Throughout its service life, this tank received and stored first-cycle waste, U Plant waste streams, evaporator bottoms waste, coating waste, fission product waste, waste water, Strontium Semiworks waste, and ion-exchange waste. In 1956 and 1957 the tank was used as a primary settling tank for the ferrocyanide-scavenging program. The tank was removed from service and declared inactive in 1978. Tank C-109 is presently designated a sound tank. The tank was interim stabilized in November 1983. The present inventory for tank C-109 is 62,000 gal of sludge, 4,000 gal of supernate, and apparently no drainable interstitial liquids. The present level of the waste in tank C-109 is about 18 in. above the lowest point of the dished tank base (DOE 1997q; Hanlon 1997).

Eight vadose zone monitoring boreholes surround tank C-109, borehole 30-09-07 was drilled in 1982 and the rest were installed in the 1970s (Figure 14-11). The concentration plots for the contaminants detected around these boreholes are provided in Appendix A. Figures 14-51 (viewed from the south), 14-53 (viewed from the east), and 14-54 (viewed from the west) show the  $^{137}\text{Cs}$  and  $^{60}\text{Co}$  distribution in the vadose zone sediments surrounding tank C-109. The visualizations show  $^{137}\text{Cs}$  and  $^{60}\text{Co}$  plumes beneath tank C-109. These plumes appear to extend to a depth of about 100 ft below the ground surface.

The visualizations show  $^{60}\text{Co}$  contaminant plumes, the tops of which are at a depth of 45 ft; this is the approximate depth of the tank base. A review of the log plot data (see Appendix A) shows large contaminant-free intervals immediately above the intervals of  $^{60}\text{Co}$ . Shape factor analysis of the  $^{60}\text{Co}$  indicates the contamination is distributed in the formation sediments. This distribution, along with the absence of  $^{60}\text{Co}$  in the upper regions (above depths of 45 ft) of the tank C-109 monitoring boreholes, suggests the contamination originated from a subsurface source such as leakage from either tank C-108 or C-109, or possibly from both of these tanks (see Section 10.2.8). A review of historical tank operating records for tank C-109 did not reveal liquid-level losses that could be attributed to a tank leak. This tank was once used as a primary settling tank for the ferrocyanide-scavenging program, and this process would have increased concentrations of  $^{60}\text{Co}$  in the tank waste, particularly the supernatant liquid (DOE 1997q).

The  $^{60}\text{Co}$  distribution beneath tank C-109 defined by the SGLS data acquired in the monitoring boreholes indicates several possible sources. The  $^{60}\text{Co}$  contamination around borehole 30-08-02 originated from a leak in tank C-108 or C-109 or a leak in the cascade line connecting these two tanks. The  $^{60}\text{Co}$  contamination around 30-09-02 indicates the original or possibly a second leak point on tank C-109, and the  $^{60}\text{Co}$  contamination beginning at a depth of 70 ft originated from a leak in tank C-108, C-109, or another nearby tank such as C-105. On the basis of the

contaminant distribution, one or more of these proposed scenarios is the most likely source for the contamination around tank C-109. However, positive source(s) of the  $^{60}\text{Co}$  contamination that was detected in the tank C-109 monitoring boreholes could not be determined.

Another possible source is a leak that occurred above the tank dome and migrated along the top of the tank dome and down the tank walls, where it accumulated at the base of the tank farm excavation. Sources for this contamination include leaks from ancillary equipments such as pump pits, shallow subsurface pipelines, and surface spills. The boreholes around tank C-109 are not in a position to verify these sources. A review of historical records did not reveal a leak event from any of these sources. Therefore, while it is possible the contamination resulted from a leak above the tank that migrated along the tank dome and walls, it cannot be proven at this time.

Details regarding the data acquired in the boreholes surrounding tank C-109 are provided in the Tank Summary Data Report for tank C-109 (DOE 1997q).

### **10.2.10 Tank C-110**

Tank C-110 was placed into service in 1946. Throughout its service life, this tank received and stored first-cycle waste, uranium recovery waste, organic wash waste, ion-exchange waste and evaporator bottoms. The tank was removed from service in 1976 and interim stabilized in May 1995. The current inventory for tank C-110 is 177,000 gal of sludge and 1,000 gal of supernate. The drainable interstitial liquids volume is estimated at 28,000 gal. The present level of the waste in tank C-110 is about 63 in. above the lowest point of the dished tank base (DOE 1997r; Hanlon 1997).

The tank is presently designated as an assumed leaker and is estimated to have leaked approximately 2,000 gal of waste. The basis of the assumed leaker designation was apparently elevated activities in the historical gross gamma log data from boreholes 30-10-02 and 30-10-09. These boreholes are located on opposite sides of the tank. The basis for the leak volume estimate was not located.

Ten vadose zone monitoring boreholes surround tank C-110, borehole 30-00-09 was drilled in 1944, the rest were drilled in the 1970s (Figure 14-11). All of the boreholes were logged by the SGLS. The concentration plots for the contaminants detected in these boreholes are provided in Appendix A.

Figures 14-48 (viewed from the southwest) and 14-55 (viewed from the west) show the  $^{137}\text{Cs}$  contaminant distribution around tank C-110 (defined by data from borehole 30-10-02). The visualizations show a  $^{137}\text{Cs}$  plume on the north side of the tank. This plume extends from the ground surface to a depth of about 60 ft. The origin of this plume is a combination of surface spills that have migrated into the backfill sediments and the leak from tank C-110.

Details regarding the data acquired in the boreholes surrounding tank C-110 are provided in the Tank Summary Data Report for tank C-110 (DOE 1997r).

### 10.2.11 Tank C-111

Tank C-111 was placed into service in 1946. Throughout its service life, this tank received and stored first-cycle waste, ferrocyanide scavenged waste, PUREX organic wash waste, coatings waste, evaporator bottoms, and Strontium Semiworks waste streams.

This tank was declared an assumed leaker in 1968, apparently on the basis of a liquid-level decrease. The tank is estimated to have leaked 5,500 gal; this leak estimate is apparently based on liquid-level data.

The present inventory for tank C-111 is 57,000 gal of sludge. The present level of the waste in tank C-111 is about 16 in. above the lowest point of the dished tank base (DOE 1998a; Hanlon 1997). Tank C-111 was administratively interim stabilized in March 1984.

Nine vadose zone monitoring boreholes surround tank C-111; borehole 30-00-10 was constructed in 1944 and the rest were drilled in the early to mid-1970s (Figure 14-11). All the boreholes were logged with the SGLS. The concentration plots for the contaminants detected in these boreholes are provided in Appendix A.

Figures 14-50 (viewed from the west) and 14-55 (also viewed from the west) show the <sup>137</sup>Cs contamination around tank C-111. The visualizations show <sup>137</sup>Cs contamination on the east and south sides of the tank that extends to a depth of about 70 ft below the ground surface.

There is no indication in the data obtained from the SGLS, historical gross gamma-ray logs, and other available information of residual radionuclide contamination from a past or present leak from tank C-111. Data leading to the determination that this tank leaked in the past should be re-evaluated.

However, the data considered in this report indicate that surface spills have occurred in the past and that minor leaks from pipelines or other service facilities may have also occurred. The contamination detected at and below the base of the tank farm excavation in boreholes 30-08-12 and 30-10-02 probably originated from tanks C-108 and C-110.

Details regarding the data acquired in the boreholes surrounding tank C-111 are provided in the Tank Summary Data Report for tank C-111 (DOE 1998a).

### 10.2.12 Tank C-112

Tank C-112 was placed into service in 1946. Throughout its service life, this tank received and stored first-cycle bismuth phosphate process waste, U Plant waste streams, cladding waste, ion-exchange waste, organic wash waste, and evaporator bottoms. Tank C-112 was removed from service in 1976. Tank C-112 was administratively interim stabilized in 1990 and is presently designated as sound. The present inventory for tank C-112 is 104,000 gal of sludge containing 32,000 gal of drainable interstitial liquids. The present level of the waste in tank C-112 is about 45 in. above the lowest point of the dished tank base (DOE 1998b; Hanlon 1997).

Nine vadose zone monitoring boreholes surround tank C-112; borehole 30-00-12 was drilled in 1944, and the rest were drilled in the 1970s (Figure 14-11). All the boreholes were logged with the SGLS. The concentration plots for the contaminants detected in these boreholes are provided in Appendix A.

Figure 14-56 (as viewed from the north) shows the  $^{137}\text{Cs}$  distribution in the vadose zone sediments surrounding tank C-112. The visualization shows two subsurface regions of  $^{137}\text{Cs}$ : one on the north side and the other on the south side of the tank. The  $^{137}\text{Cs}$  on the south side of the tank is most likely associated with leak events from nearby tanks such as tank C-111 (a designated leaker) or subsurface pipelines. The  $^{137}\text{Cs}$  on the north side of tank C-112 is most likely the result of a leak in the salt well pump pit (DOE 1998b).

Details regarding the data acquired in the boreholes surrounding tank C-112 are provided in the Tank Summary Data Report for tank C-112 (DOE 1998b).

### **10.2.13 200-Series Tanks**

Tanks C-201, -202, -203, and -204 were placed into service in 1947 and 1948. Throughout their service lives, they received and stored metal waste and Strontium Semiworks waste. All four tanks are classified as assumed leakers and are estimated to have leaked a total of 1,750 gal of waste to the vadose zone sediments. The leak estimates were apparently derived from in-tank liquid-level measurements. All of the tanks have been interim stabilized.

The outer shells of the 200-series tanks and the 100-series tanks are separated by a distance of approximately 60 ft. Only borehole 30-00-12 is located close enough to the 200-series tanks to detect any potential plumes from these tanks. The visualizations show the vadose zone in the vicinity of the borehole is relatively contaminant free. However, this is based strictly on the fact that there are no vadose zone monitoring boreholes surrounding the 200-series tanks. Therefore, the nature and extent of the vadose zone contamination around tanks could not be characterized.

## **10.3 Significant Contamination Plumes in the C Tank Farm**

The C Tank Farm vadose zone is defined by extensive low-levels of gamma-ray-emitting contamination, the majority of which cannot be directly associated with a known leak from either a tank or subsurface pipeline. The following discussion describes, to the extent known, the vadose zone contamination that can be directly related to a known subsurface leak event (or events) as well as contamination that cannot. Where the contamination cannot be directly tied to a source, candidate sources are presented. Candidate sources were selected based on the contaminant distribution in the vadose zone as well as anomalous in-tank data. Section 13 provides recommendations that, if implemented, may help identify the sources.

### **10.3.1 Vadose Zone Plumes Associated With Known Leakers in the C Tank Farm**

The following discussion describes the C Tank Farm vadose zone plumes that are associated with known tank leaks.

#### **10.3.1.1 Vadose Zone Plume from the Tank C-101 Leak**

Tank C-101 apparently experienced a liquid-level decrease in the late 1960s that ultimately led to the tank to become classified as an assumed leaker. The tank is assumed to have leaked 20,000 gal of waste into the vadose zone. The vadose zone contamination that resulted from the C-101 tank leak is defined by the  $^{137}\text{Cs}$  that is located south of tank C-101 at the base of the tank farm excavation and by the  $^{137}\text{Cs}$  located southeast of tank C-101 beginning at a depth of 70 ft that extends underneath the tank to the north (see Figures 14-18, 14-32, and 14-33).

The  $^{137}\text{Cs}$  plume below 100 ft appears to extend horizontally to the north. Most of the boreholes in this region of the tank farm do not extend below a depth of 100 ft, making it impossible to define the total horizontal extent of the plume at that depth. Therefore, it is possible the geostatistical model overestimated the horizontal extent of this plume.

#### **10.3.1.2 Vadose Zone Plume from the Tank C-110 Leak**

The designation of tank C-110 as an assumed leaker resulted from anomalous activity measured in boreholes 30-10-02 and 30-10-09. These boreholes are on opposite sides of the tank. The tank is assumed to have leaked 2,000 gal to the vadose zone. The vadose zone contamination that resulted from the leak in tank C-110 is defined by the  $^{137}\text{Cs}$  plume on the north side of the tank (see Figure 14-22, 14-48, and 14-55). It is not known where the anomalous activity in borehole 30-10-09 originated, but it is assumed to be a leak from tank C-110.

The visualizations show  $^{137}\text{Cs}$  contamination on the north side of the tank that extends from the ground surface to a depth of about 60 ft. The origin of this plume is most likely a combination of surface spills and the leak from tank C-110.

#### **10.3.1.3 Vadose Zone Plume from the Tank C-111 Leak**

The designation of tank C-111 as an assumed leaker resulted from a liquid-level decrease. The tank is estimated to have leaked 5,500 gal of waste to the vadose zone. The visualizations show  $^{137}\text{Cs}$  contamination on the east and south sides of tank that extends to a depth of about 70 ft below the ground surface (see Figures 14-22, 14-55, and 14-56).

There is no indication in the data obtained from the SGLS, historical gross gamma-ray logs, and other available information of residual radionuclide contamination from a past or present leak

from tank C-111. Data leading to the determination that this tank leaked in the past should be re-evaluated. However, the data considered in this report indicate that surface spills have occurred in the past and that minor leaks from pipelines or other service facilities may have also occurred.

### **10.3.2 Vadose Zone Plumes Not Related to Known Leaks From Tanks or Ancillary Equipment**

The contaminant plumes described in Sections 10.1 and 10.3.1 do not account for all of the contamination detected by the SGLS and shown in the visualizations. Significant amounts of contamination remain unaccounted for beneath tanks C-104, C-105, C-106, C-108, and C-109. The following section describes this contamination and provides candidate sources.

#### **10.3.2.1 Vadose Zone Contaminant Plumes Beneath Tanks C-104, C-105, and C-106**

Figures 14-9 and 14-21 show there is substantial  $^{137}\text{Cs}$  and  $^{60}\text{Co}$  contamination below tanks C-104, C-105, and C-106. The contamination extends horizontally from the northeast side of tank C-104 to the north side of tank C-106. The plumes extend vertically into the vadose zone to about 120 ft below the ground surface (80 ft below the base of the tanks).

There are two potential sources that can be identified as sources for the contaminant plumes around tanks C-104, C-105, and C-106. First, it is apparent there have been one or more significant surface spills. The contamination appears to have infiltrated into the backfill sediments, and upon reaching the tank, migrated along the tank dome and walls where it collected at the base of the tank farm excavation.

The second potential source is a leak from the cascade lines between tanks C-104 and C-105 and between tanks C-105 and C-106. The visualizations show  $^{137}\text{Cs}$  and  $^{60}\text{Co}$  contamination between tanks C-104 and C-105 extends to a depth of about 65 ft below the ground surface and at least 75 ft horizontally, and the  $^{60}\text{Co}$  contamination extends to a depth of about 65 ft below the ground surface and at least 30 ft horizontally (see Figure 14-36). The visualizations show the  $^{137}\text{Cs}$  and  $^{60}\text{Co}$  contamination between and below tanks C-105 and C-106 (see Figures 14-42 and 14-43). The  $^{137}\text{Cs}$  around tanks C-105 and C-106 extends to a depth of about 120 ft below the ground surface, and the  $^{60}\text{Co}$  appears to have migrated to a depth of about 80 ft below the ground surface. Due to the potential for commingling of plumes from other nearby sources, the total horizontal extent of the contamination cannot be determined.

The leak in the cascade lines most likely resulted when tank C-105 was overfilled. However, a review of liquid-level data does not show the tank was overfilled. If both plumes resulted from the alleged tank overfill, it is possible each cascade line (or cascade line connection) experienced different leak rates. This would have resulted in two different volumes being leaked to the vadose zone, creating two different sized plumes.

Even though the sources discussed above provide plausible explanations for the contamination around tanks C-104, C-105, and C-106, it cannot be ruled out that a leak from tanks C-105 and C-106 contributed to the subsurface plume. A review of historical operating documents revealed tank C-105 experienced a 36-in. waste-level decrease between 1963 to 1967. An investigation of the incident concluded the level loss was due to evaporation. However, the investigation also acknowledges there were no data to support the conclusion. If one of these tanks leaked in the past, the comparison between the RLS and SGLS data indicates they are not continuing to leak.

### **10.3.2.2 Vadose Zone Contaminant Plumes Beneath Tanks C-108 and C-109**

The visualizations show extensive  $^{60}\text{Co}$  and  $^{137}\text{Cs}$  contamination beneath tanks C-108 and C-109 (Figures 14-20, 14-49, and 14-54). A review of historical operating records did not provide direct evidence or reveal investigations that indicated either of these tanks had leaked. However, the contaminant distribution appears to indicate one or both of the tanks had leaked.

The visualizations show a  $^{60}\text{Co}$  plume beginning at a depth of about 45 ft. The SGLS log plots show extended contaminant-free intervals immediately above the  $^{60}\text{Co}$ . This indicates shallower sources such as subsurface pipelines are most likely not the source of the  $^{60}\text{Co}$  beneath these tanks. Also,  $^{60}\text{Co}$  was not detected in boreholes around nearby assumed leakers tanks C-110 and C-111, indicating these tanks are not the source of the  $^{60}\text{Co}$  contamination.

As discussed in Section 5.2, the C Tank Farm tanks received waste that was high in  $^{60}\text{Co}$  (relative to other tank farms). This is particularly true for tank C-109, which was used as a primary settling tank for the ferrocyanide-scavenging program. Tank C-108 also received some form of waste from the ferrocyanide-scavenging process. Therefore, tanks C-108 and C-109 would probably have contained a relatively higher concentration of  $^{60}\text{Co}$ .

Several possible scenarios could explain the contaminant distribution shown on the visualizations beneath tanks C-108 and C-109. The  $^{60}\text{Co}$  contamination around borehole 30-08-02 originated from a leak in tank C-108 or C-109 or from leakage from the cascade line connecting these tanks. The  $^{60}\text{Co}$  contamination around 30-09-02 indicates the original or possibly a second leak point on tank C-109, and the  $^{60}\text{Co}$  contamination beginning at a depth of 80 ft originated from a leak in tanks C-108, C-109, or another nearby tank such as tank C-105. It is also possible that some of the contamination resulted from a leak that occurred over the top of tank C-108 and/or C-109 that migrated along the tank dome and down the sides and accumulated at the interface of the backfill and undisturbed Hanford formation sediments. Regardless, positive identification of the source(s) of the  $^{60}\text{Co}$  contamination beneath tanks C-108 and C-109 could not be determined.

## **10.4 Potential Effect of Adjacent Waste Facilities on the C Tank Farm Vadose Zone Contaminant Plumes**

The plumes of the gamma-ray-emitting radionuclides in the vadose zone within the C Tank Farm are, in general, clearly defined both horizontally and vertically. The maximum extent of the contaminant plumes are within the C Tank Farm boundary and are explained by the tank leaks, subsurface pipeline leaks, and surface spills. Therefore, based on the SGLS data, it does not appear the adjacent waste facilities contributed to the contamination within the vadose zone of the C Tank Farm.

## **11.0 Impacts and Implications of the Vadose Zone Contamination**

### **11.1 Nature of Contamination**

The primary gamma-emitting contaminants detected in the vadose zone beneath the C Tank Farm were  $^{137}\text{Cs}$  and  $^{60}\text{Co}$ .  $^{154}\text{Eu}$ ,  $^{152}\text{Eu}$ , and uranium contamination was detected in small quantities around several boreholes in the C Tank Farm. Much of the  $^{152}\text{Eu}$  and uranium contamination was detected only at the ground surface. Other gamma-emitting radionuclides may have been present at the time the tanks leaked, but they have since decayed to such low levels that they can no longer be detected using current logging methods. Clearly defined plumes of  $^{137}\text{Cs}$  and  $^{60}\text{Co}$  were identified within the C Tank Farm boundary.

Other contaminants are most likely present in the vadose zone beneath the C Tank Farm that do not emit detectable gamma rays. On the basis of process knowledge of the waste streams stored in the tanks, it is reasonable to expect  $^{99}\text{Tc}$ ,  $^{90}\text{Sr}$ , isotopes of plutonium,  $^3\text{H}$ , and other more mobile radionuclides and RCRA-regulated constituents to have leaked to the vadose zone. Only a comprehensive characterization effort using other data collection and analysis methods will help define the distribution of the nongamma-emitting radionuclides and RCRA constituents.

### **11.2 Extent of Migration**

The characterization of the C Tank Farm upper vadose zone revealed extensive contamination. Analysis of the KUT log plots showed relatively small changes in concentration at the interpreted formation contacts. This may indicate the difference in the sediment composition and grain size is not great, potentially allowing contaminants to migrate easier and further through the vadose zone sediments.

The SGLS data indicate the anthropogenic radionuclide contamination has migrated at least 120 ft into the vadose zone sediments. Due to the strong potential of individual waste plumes commingling beneath the tanks, the extent of horizontal migration cannot be estimated.

However, as the visualizations show, the C Tank Farm vadose zone is contaminated beneath most of the farm.

### **11.3 Stability of Contamination**

The boreholes surrounding tanks C-105 and C-106 were logged by the RLS in 1993 and the boreholes surrounding tank C-103 were logged by the same system in 1994. All of these boreholes were logged using the SGLS in 1997. Comparison of the data (as reported in the Tank Summary Data Reports for tanks C-103, C-105, and C-106) provided an accurate means to determine whether the contaminants had migrated during that time period.

Comparing the RLS data to the SGLS data showed the  $^{60}\text{Co}$  around borehole 30-06-10 below 110 ft has migrated. The SGLS data indicated the  $^{60}\text{Co}$  contamination was slightly deeper in 1997. It is possible the contamination simply migrated down the outside of the casing. However, the contamination most likely has migrated vertically through the formation or horizontally as the plume continues to move through the region. Regardless of how or where the contamination is moving, the change in the contaminant profile between 1993 and 1997 indicates the  $^{60}\text{Co}$  is not fixed or adsorbed on the sediment.

Historical gross gamma log data from the mid-1970s through the mid-1990s were reviewed during the preparation of individual Tank Summary Data Reports. In the past, contaminant movement was identified with the gross gamma-ray system, sometimes many years after the original leak event. However, no trends were identified in the historical gross gamma logs that could indicate the contamination was continuing to migrate. Because of the low sensitivity of the historical gross gamma logging system and the poor spatial control, small changes in the contamination distribution cannot be quantified.

No data are available to accurately quantify or determine the long-term stability of the contamination in the vadose zone beneath the rest of the C Tank Farm tanks.

The stability of radionuclides that do not emit gamma rays cannot be addressed in this report because they were not assessed in this project. Nongamma-emitting radionuclides and other non-radioactive waste constituents must be studied by alternative sampling methods.

### **11.4 Impacts to Groundwater**

The groundwater beneath the C Tank Farm has been monitored by a RCRA-compliant groundwater monitoring system since 1989. One groundwater well, 299-E-27, was installed in 1982 but was not in a position to monitor for potential contaminant sources from the C Tank Farm. Therefore, the C Tank Farm groundwater has only been accurately monitored for 9 of the approximately 52 years the tank farm has actively stored waste. Since inception of the RCRA groundwater monitoring program, there has apparently been no indication that waste from the C Tank Farm tanks has reached groundwater. Because the vadose zone boreholes do not reach groundwater, there is no direct trace of contamination down to the water table.

## 12.0 Conclusions

Seventy vadose zone boreholes in the C Tank Farm were logged with the SGLSs, and gamma-emitting radionuclide concentration data were generated at 0.5-ft intervals. The data from these logging activities were used to create a gamma-ray-emitting radionuclide contaminant baseline database for this tank farm. Log plots were prepared and published in individual Tank Summary Data Reports. These Tank Summary Data Reports provide a history of each tank and put the SGLS log data into an appropriate format so they can be used for future tank farm operations and remediation.

Empirical contaminant distribution models were created for the man-made radionuclides  $^{137}\text{Cs}$  and  $^{60}\text{Co}$  with the geostatistical tools available in a commercial software package. These models were used to create visualizations of the contaminant distribution that were reviewed and interpreted in this report. The geostatistical model and the resulting visualizations presented in this report are based on an interpreted data set. The interpreted data set does not contain concentration values in intervals where it is interpreted the contamination is local to the borehole casing. Therefore, the contaminant distribution shown in the visualizations represents only contamination that is believed to be distributed in the vadose zone sediments.

The C Tank Farm is defined by significant and extensive gamma-ray-emitting contamination. The majority of this contamination cannot be directly tied to a documented leak from either a tank or subsurface ancillary equipment. The contaminant distribution, as measured by the SGLS, does appear to indicate that some tanks that are currently considered sound (i.e., tanks C-108 and C-109) may in fact have leaked. Conversely, there was not much contamination around some of the known "leakers" such as tanks C-110 and C-111. This may reflect that contamination resulting from leakage from these tanks migrated downward and did not reach the lateral extent necessary to be intersected by the vadose zone monitoring boreholes.

Tanks C-101, C-110, C-111, C-201, C-202, C-203, and C-204 are known or suspected to have leaked an estimated 29,250 gal into the C Tank Farm vadose zone sediments. There are no boreholes around tanks C-201, C-202, C-203, and C-204; therefore, the potential vadose zone contamination around these tanks cannot be characterized. However, these four tanks are estimated to have leaked only 1,750 gal of waste, making their contribution to the vadose zone contamination less significant.

The source of significant amounts of contamination remains unaccounted for beneath tanks C-104, C-105, and C-106 and beneath tanks C-108 and C-109. There are two scenarios that could explain the contamination beneath tanks C-104, C-105, and C-106. The first scenario is based on the apparent overfilling of tank C-105 (a review of liquid-level data did not support the conclusion that tank C-105 was overfilled). If the tank was overfilled, then the contamination most likely resulted from leaks in the cascade lines between tanks C-104, C-105, and C-106.

Between 1963 and 1967, tank C-105 experienced a 36-in. liquid-level drop. An investigation into the liquid-level drop determined evaporation was the cause. However, the investigators acknowledge there were no data to support this conclusion. Tank C-105 contains a significant

amount of heat-generating radionuclides; therefore, it is reasonable to expect a significant amount of water was most likely evaporated during that time. However, if tank C-105 was not overfilled, as supported by the liquid-level data, then it is possible the contamination beneath these tanks is the result of a leak from tank C-105. It is also possible both of these events occurred.

Extensive  $^{60}\text{Co}$  and  $^{137}\text{Cs}$  contamination was measured beneath tanks C-108 and C-109. The contamination may have resulted from leaks in tanks C-108 and/or C-109, or both. However, it is possible that some or all of the contamination resulted from leakage from the cascade line between tanks C-108 and C-109, or from a leak that occurred over the tank tops, migrated along the tank sides, and accumulated at the interface of the backfill and undisturbed Hanford formation sediments. Positive identification of the source(s) of this contamination could not be determined.

Although this is a vadose zone characterization of the C Tank Farm, less than half of the volume of the vadose zone was investigated. Therefore, the full extent of the vadose zone contamination has not been determined.

On the basis of recent groundwater monitoring data, it does not appear waste from the C Tank Farm tanks has reached groundwater.

Interpretation of the logging data was not always conclusive, and questions remain about the true nature and extent of the contamination. However, a database has been established for the distribution of the gamma-ray-emitting contaminants within the C Tank Farm. Comparison of the RLS and SGLS data has shown that accurate borehole logging techniques can show small changes in the contaminant distribution. Future monitoring can be conducted to determine if the contamination is continuing to move, where the contamination is going, and if additional contamination sources are present. In addition, the data provided in this characterization may be used to determine if future characterization projects are required, what type of data are required, and how these characterization endeavors may be conducted.

## **13.0 Recommendations**

Recommendations regarding specific boreholes can be found in the individual Tank Summary Data Reports. The following sections provide recommendations in the context of the C Tank Farm as a whole and the major subsurface plumes.

### **13.1 Tank and Farm Characterization Data**

Identification of the sources for the contaminant plumes beneath tanks C-104, C-105, C-106, C-108, and C-109 is based mostly on the contaminant distribution. It is not known whether historical records currently exist that could confirm or refute whether these tanks have leaked. Therefore, it is recommended that work to collect, catalog, assess, and analyze historical documents, publications, and records pertaining to the tanks and tank farms be continued. Some

comprehensive work on collecting historical data was performed and is presented in a multivolume publication (Brevick et al. 1994). It is also recommended this effort be expanded to include more information that is not directly tied to tank contents information, such as some of the significant operational records.

## 13.2 Additional Vadose Zone Characterizations

This report presents an initial characterization of the vadose zone at the C Tank Farm. Because of the limited scope of this project, additional characterization activities should be accomplished before the baseline characterization can be considered comprehensive. There is some degree of uncertainty and skepticism, in some cases, about conclusions regarding the actual distribution of contamination around the boreholes. This uncertainty and skepticism must be resolved. Therefore, it is recommended that additional characterization of the vadose zone be performed. Many of the recommendations cited in this section are similar to the recommendations for the SX Tank Farm found in the *TWRS Vadose Zone Contamination Issue Expert Panel Status Report* (DOE 1997h).

The geostatistical methods and software that produced the visualizations can be used in the future to develop models of the contamination distributions that are refined to the point that they can depict the various theories on the migration of contaminants and they can be used for quantitative calculations. Extensive characterizations would be required to quantify the contamination concentrations and the actual spatial variability, and an adequate understanding of the contaminant migration mechanisms would need to be developed.

In many cases, the boreholes do not appear to penetrate to the bottom of the contaminant plume. Therefore, it is recommended the boreholes be deepened in order to determine the true vertical extent of the contaminant plume. This is particularly important in the region around tanks C-104 and C-105.

The current distribution of boreholes near the 200-series tanks is insufficient for characterizing the plumes from these tanks. It is recommended boreholes be installed around these tanks so that the characterization of the C Tank Farm vadose zone can be completed.

Because of the existing distribution of boreholes in the C Tank Farm and the lack of data on nongamma-emitting contaminants, the true maximum extent of the contaminant plumes was not identified. Future vadose zone characterization efforts should attempt to determine the true maximum extent of the plumes (DOE 1997h).

Distributions of much of the contaminants in the C Tank Farm were determined to be related to lithologic features in the sediments beneath the tank farm. These features were defined by the properties of the sediment materials and can be identified by variations in the  $^{40}\text{K}$  concentrations. Correlation of the  $^{40}\text{K}$  concentration data with the actual lithologic samples acquired when the boreholes were drilled could provide greater insight into the lithology of the vadose zone beneath the C Tank Farm. Therefore, it is recommended such a correlation be performed.

Other borehole geophysical methods, such as density, moisture, temperature logging, high-flux spectral gamma measurements, and possibly resistivity-through-casing techniques should be developed and implemented at the C Tank Farm in order to provide needed characterization data. These techniques should be part of an overall vadose zone characterization program.

### **13.3 Future Vadose Zone Monitoring**

A program should be implemented for routine monitoring against the baseline documented in this initial characterization effort. The comparison between the RLS and SGLS data clearly illustrates how highly accurate data can be used to measure changes in the contaminant distribution. It is highly recommended the plumes identified in Section 10.3 be monitored using a spectral gamma logging system to determine the stability of the individual plumes.

## **14.0 Figures for the C Tank Farm**

The following section presents the figures cited in this report in the order in which they were presented.

This page intentionally left blank.

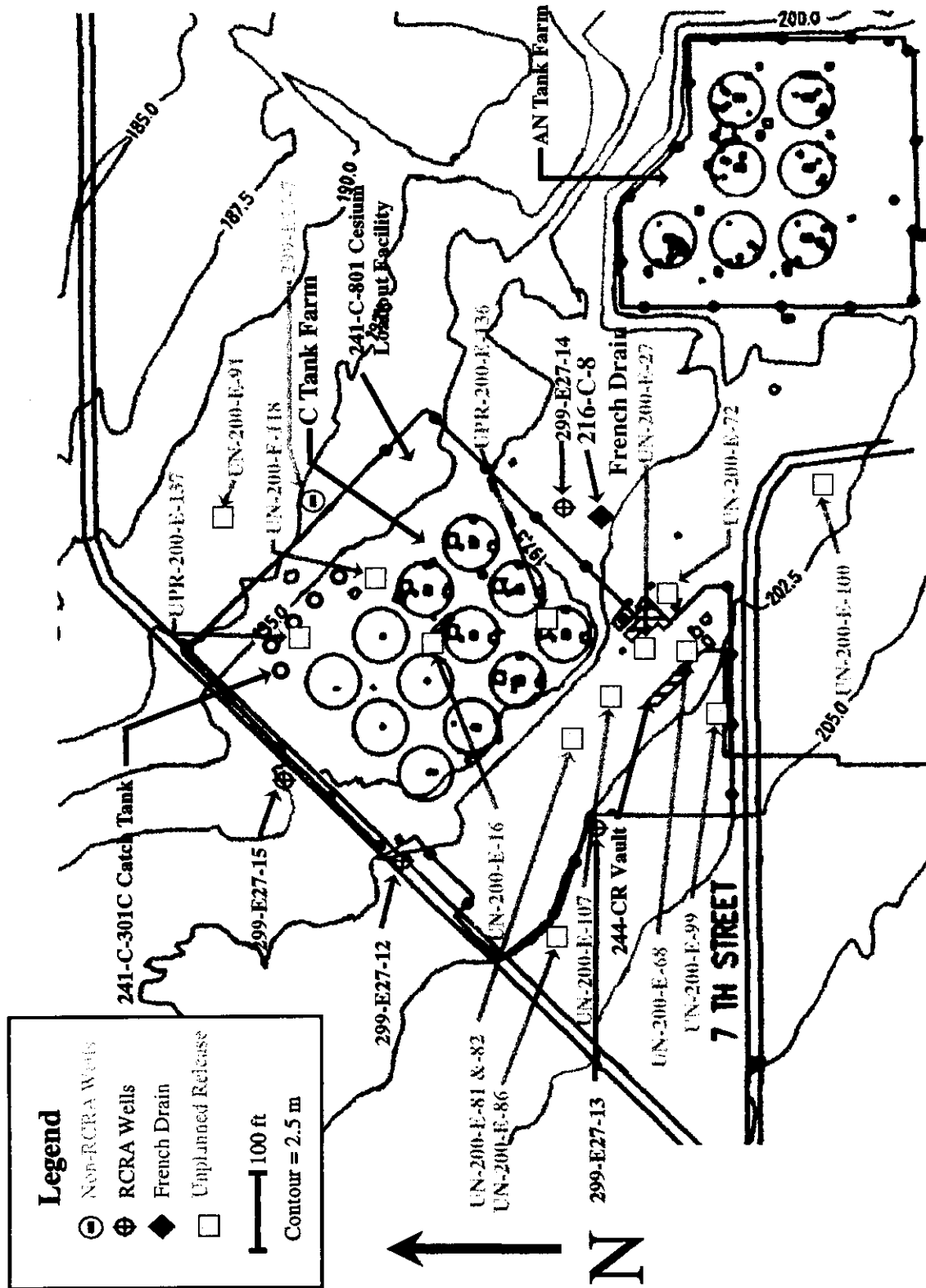
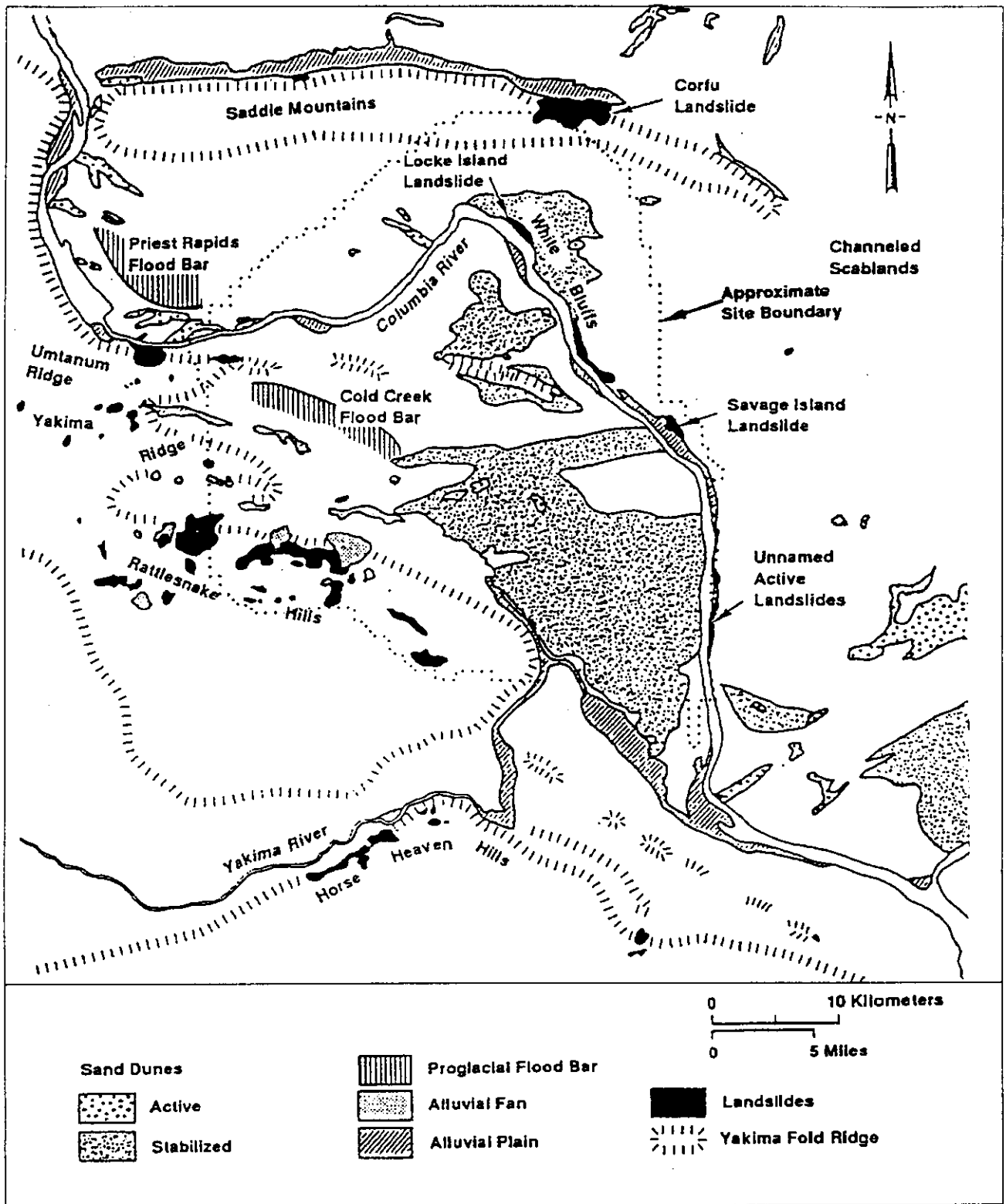
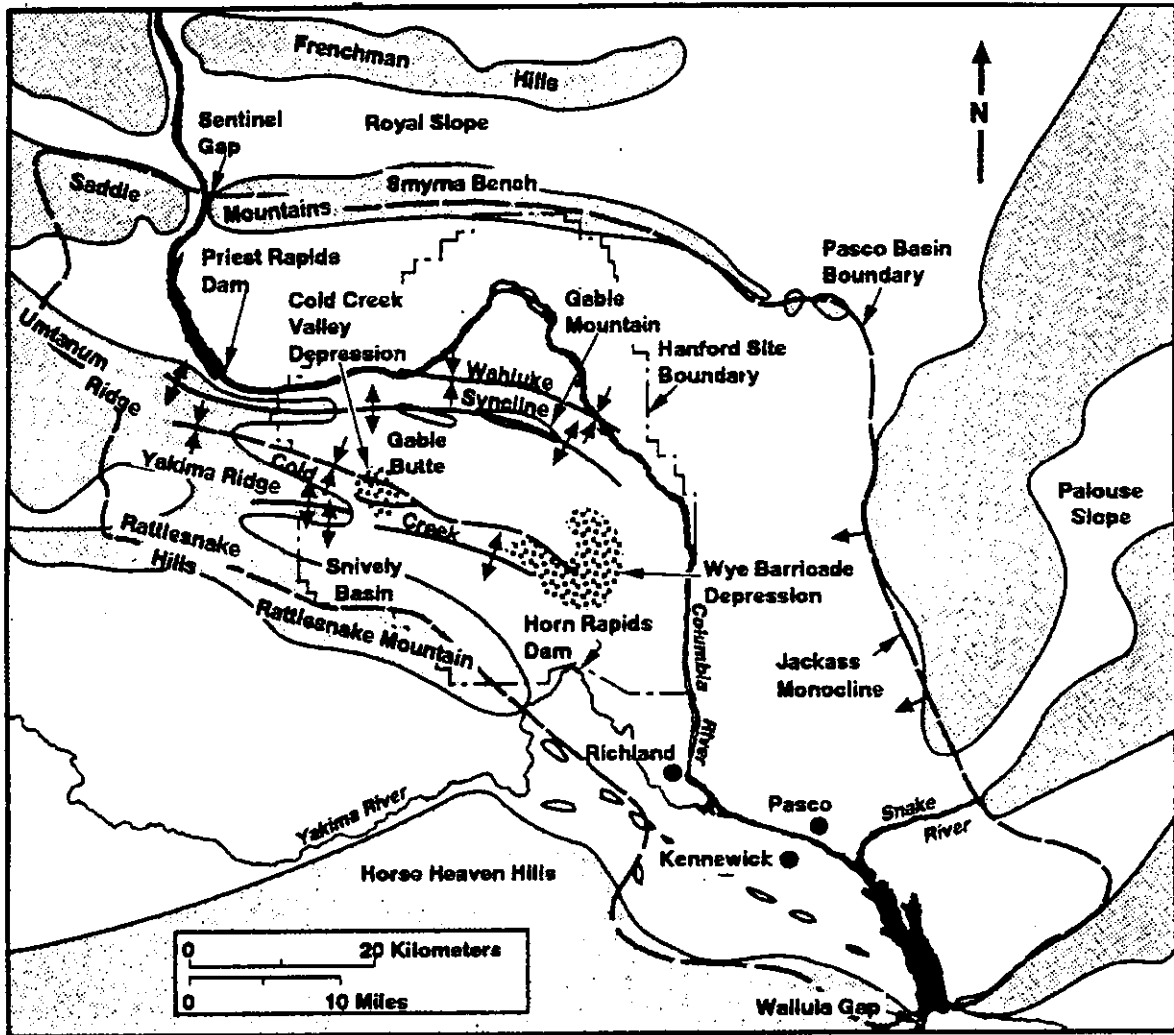


Figure 14-1. Map Showing the Location of the C Tank Farm, RCRA and Non-RCRA Wells, and Adjacent Waste Sites



From DOE (1993b)

Figure 14-2. Landforms of the Pasco Basin in the Vicinity of the Hanford Site



From DOE (1993b)

Figure 14-3. Geologic Structure Map of the Hanford Site and Surrounding Areas

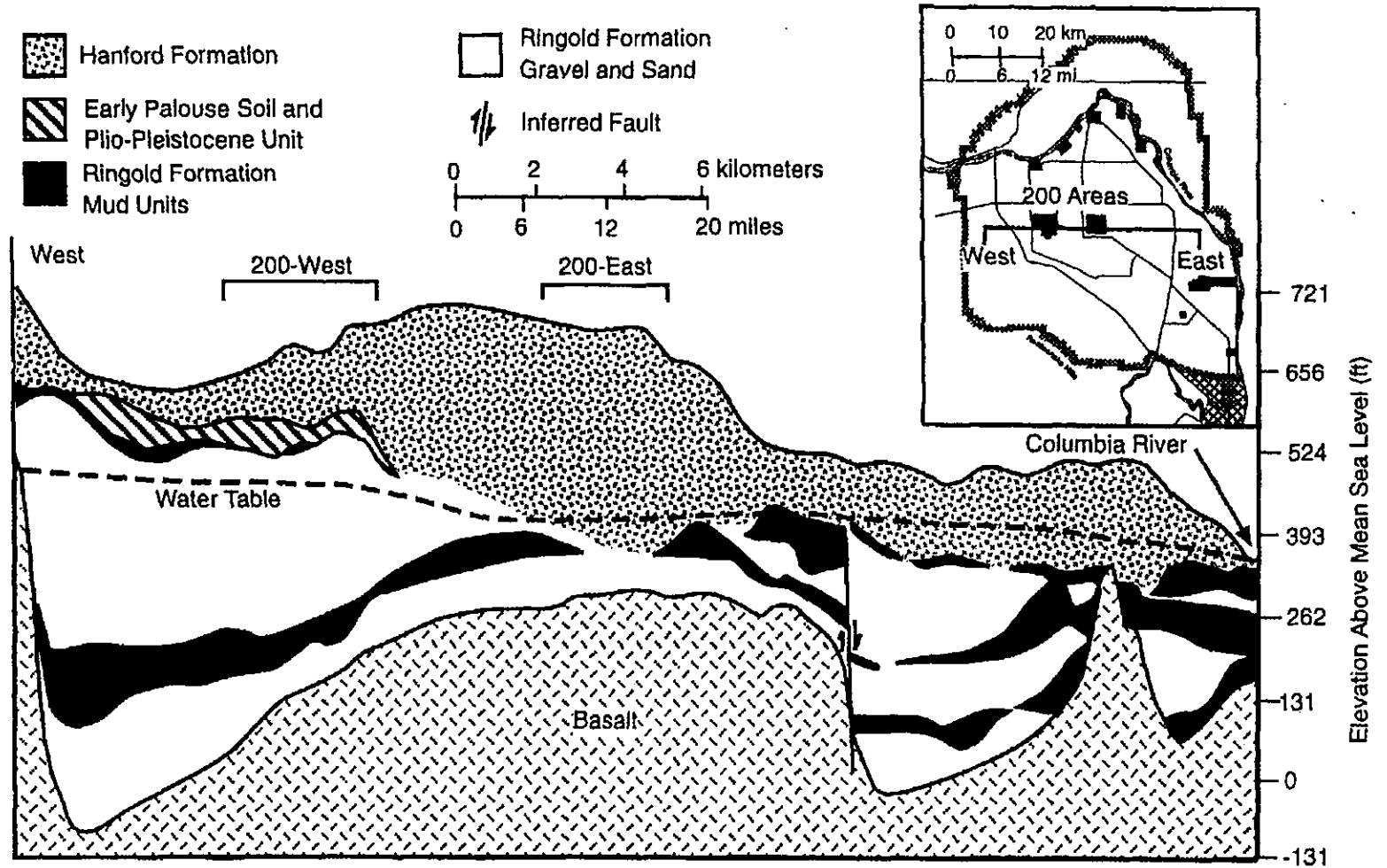


- |                                     |                                |                                     |                         |   |                              |
|-------------------------------------|--------------------------------|-------------------------------------|-------------------------|---|------------------------------|
| <input type="checkbox"/>            | Surficial Quaternary Sediments | <input checked="" type="checkbox"/> | Saddle Mountains Basalt | — | Anticline or Syncline        |
| <input checked="" type="checkbox"/> | Hanford Formation              | <input type="checkbox"/>            | Wanapum Basalt          | — | Fault (exposed or concealed) |
| <input checked="" type="checkbox"/> | Plio-Pleistocene Sediments     | <input checked="" type="checkbox"/> | Grande Ronde Basalt     | — | Hanford Site Boundary        |
| <input type="checkbox"/>            | Ringold Formation              | <input type="checkbox"/>            | Surface Water           |   |                              |



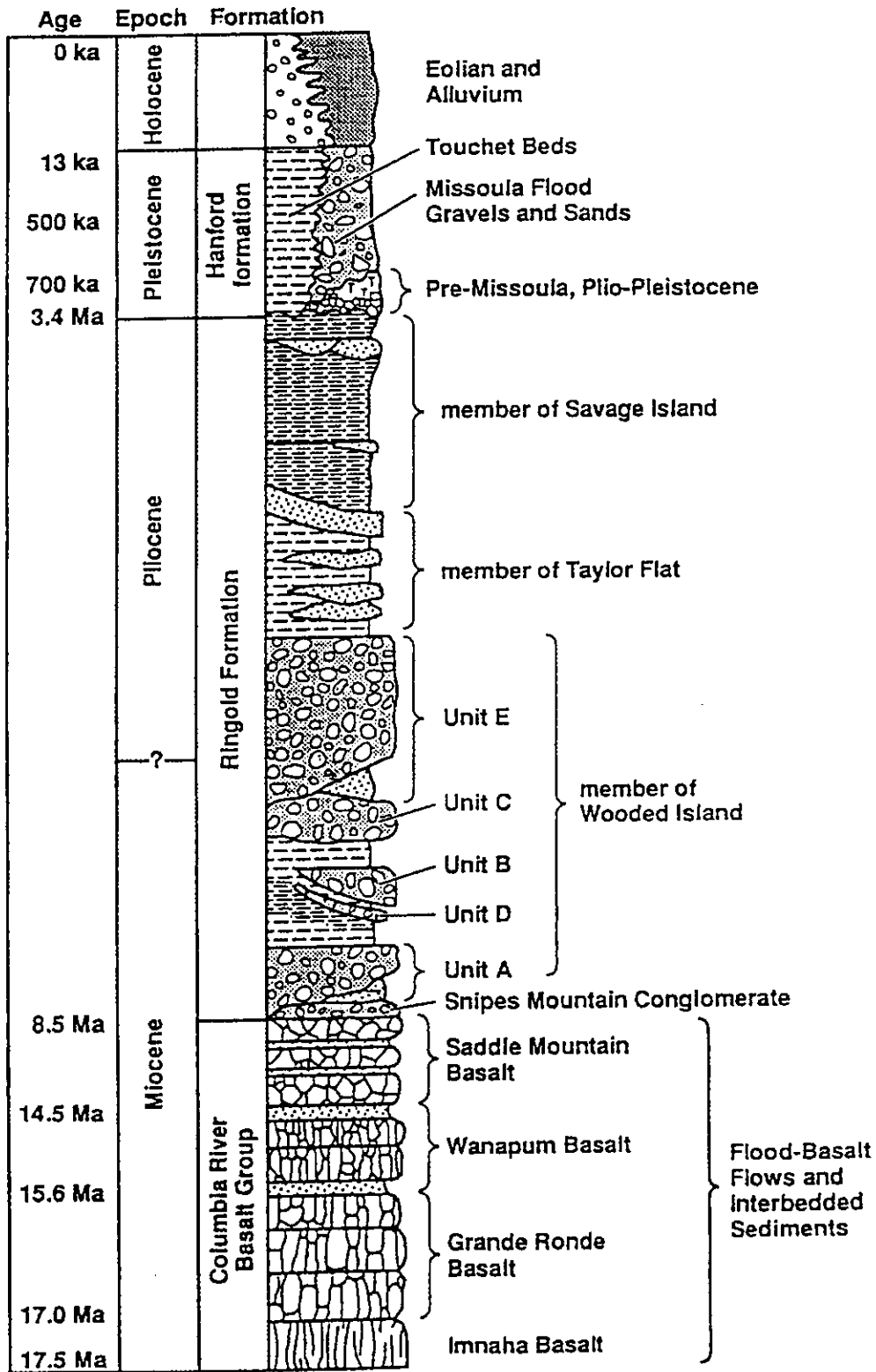
From PNNL (1997)

Figure 14-4. Surface Geology of the Hanford Site and Surrounding Areas



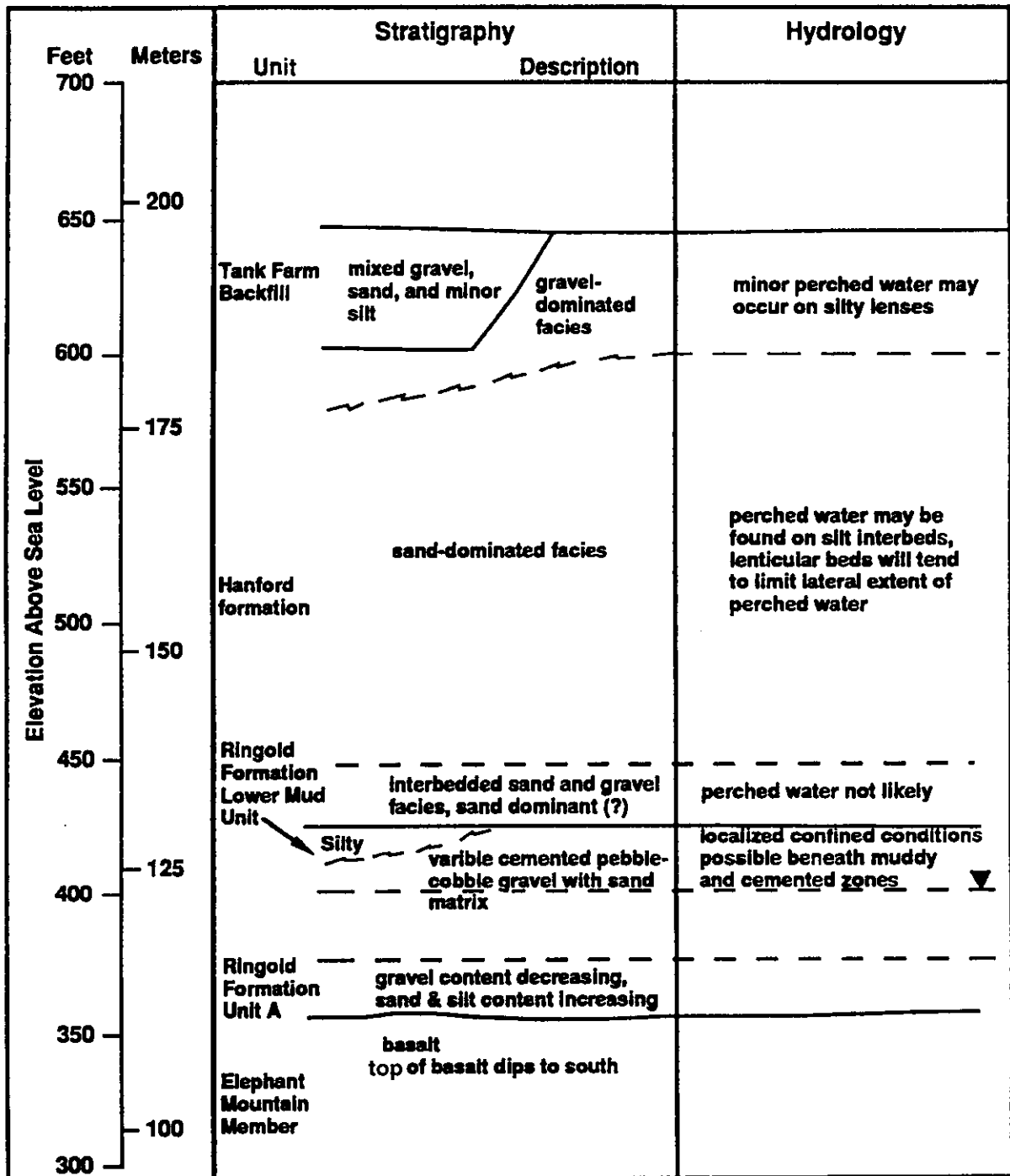
From PNNL (1997)

Figure 14-5. Generalized Cross Section of the Hanford Site



From Lindsey (1995)

Figure 14-6. General Stratigraphy of the Hanford Site



From Lindsey (1993)

Figure 14-7. Geologic and Hydrogeologic Column Beneath the C Tank Farm

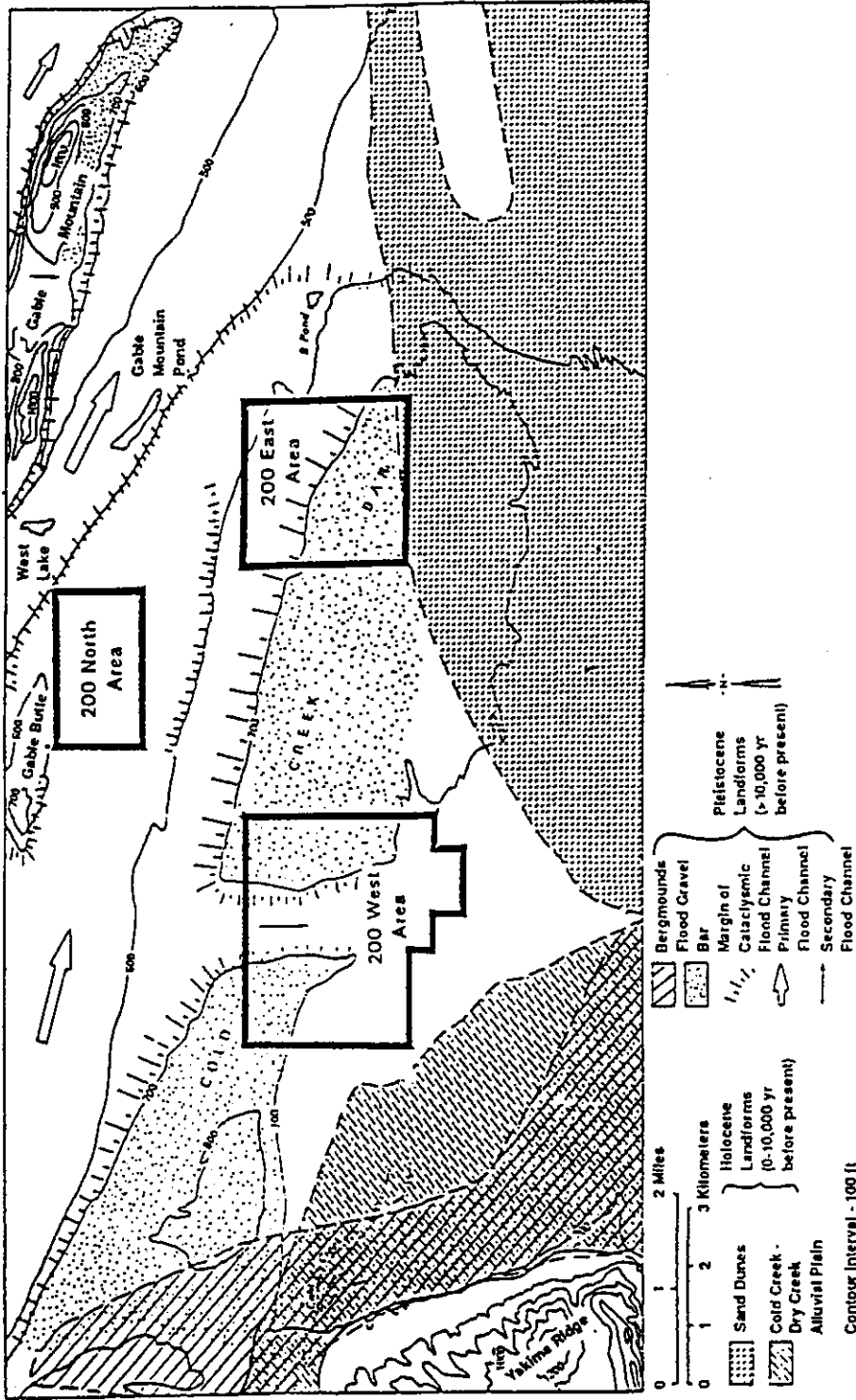
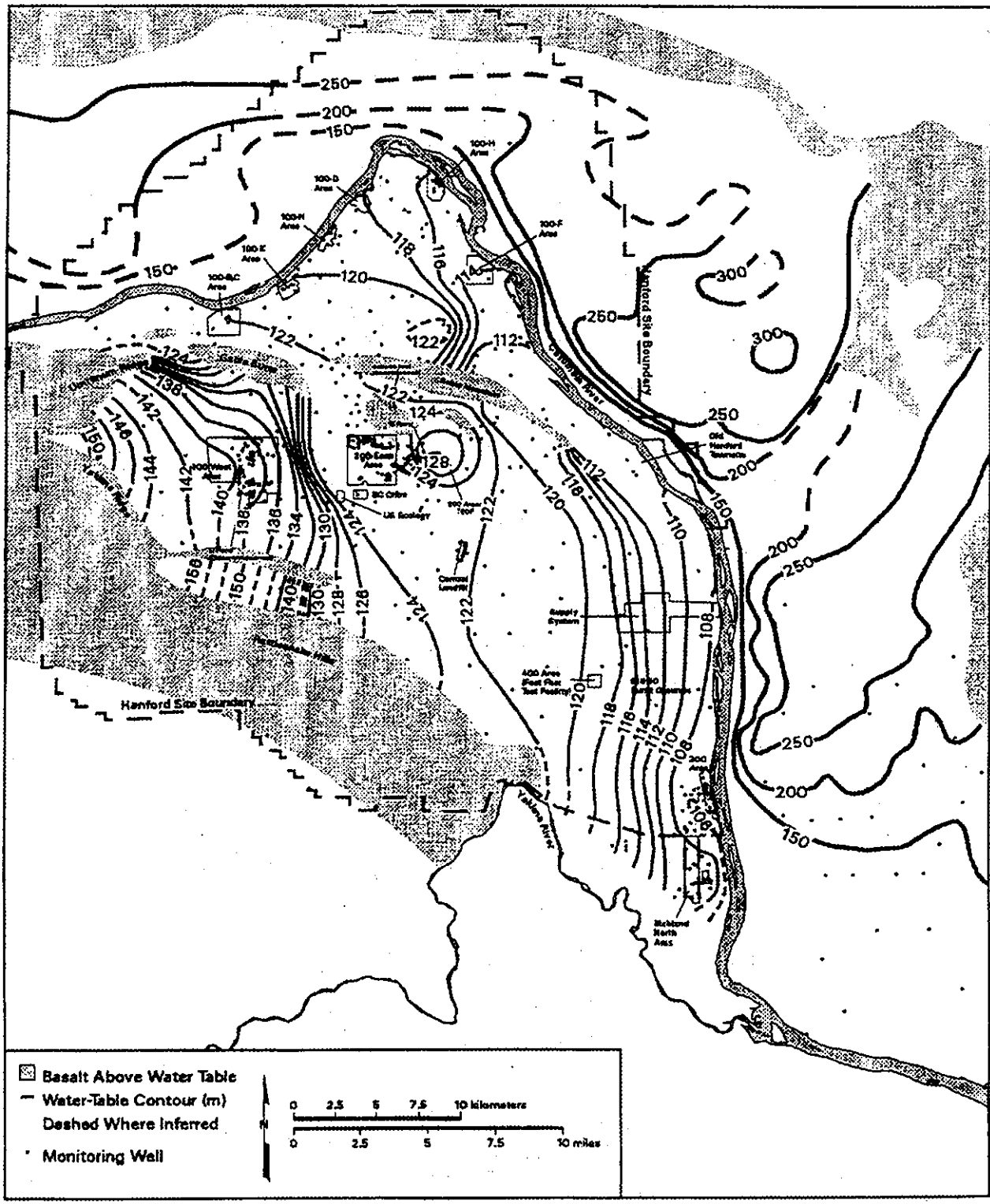


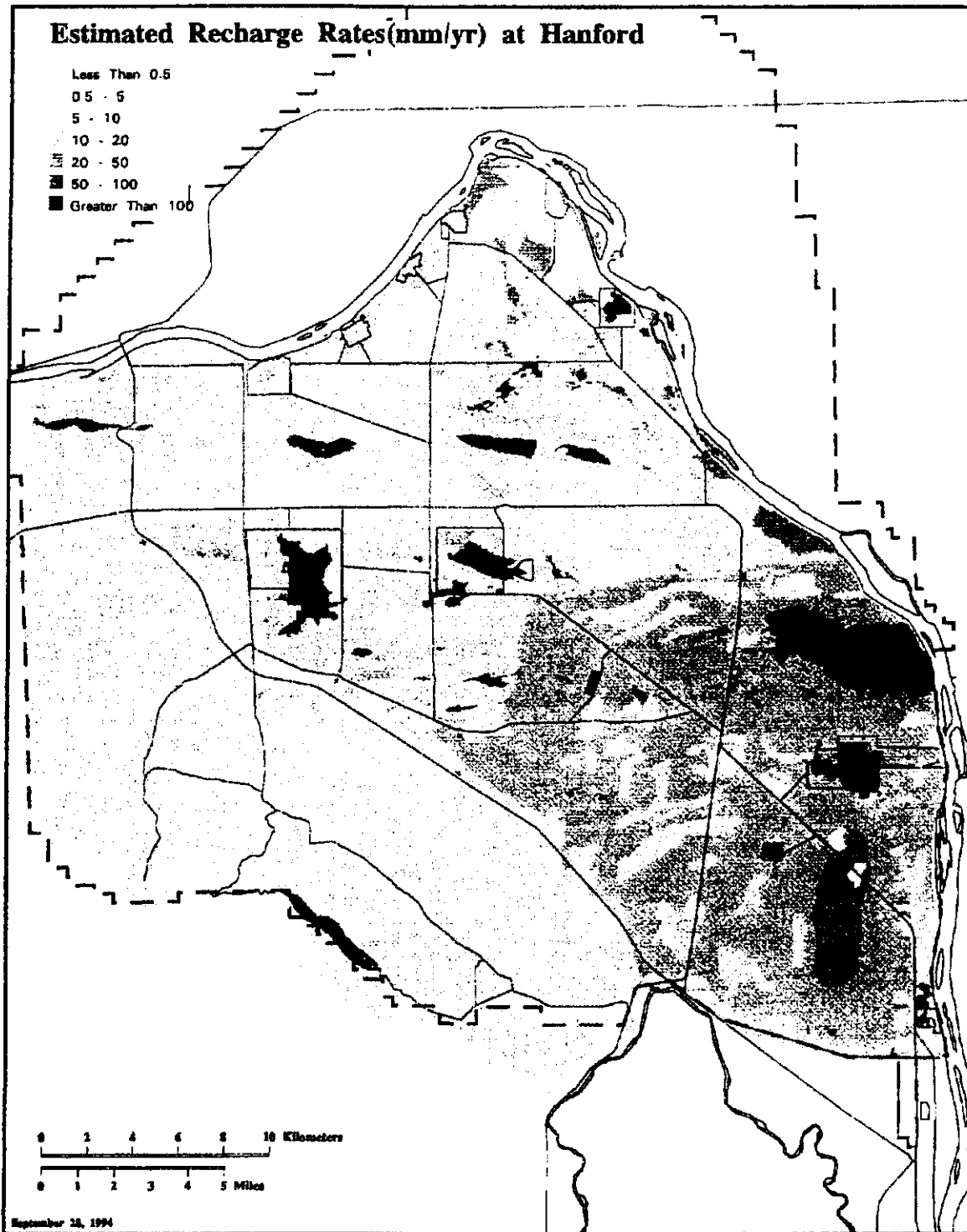
Figure 14-8. Geomorphology of the 200 East and 200 West Areas

From DOE (1993b)



From PNNL (1997)

Figure 14-9. 1996 Water Table Elevations



From PNNL (1997)

Figure 14-10. Estimated Natural Recharge for the Hanford Site

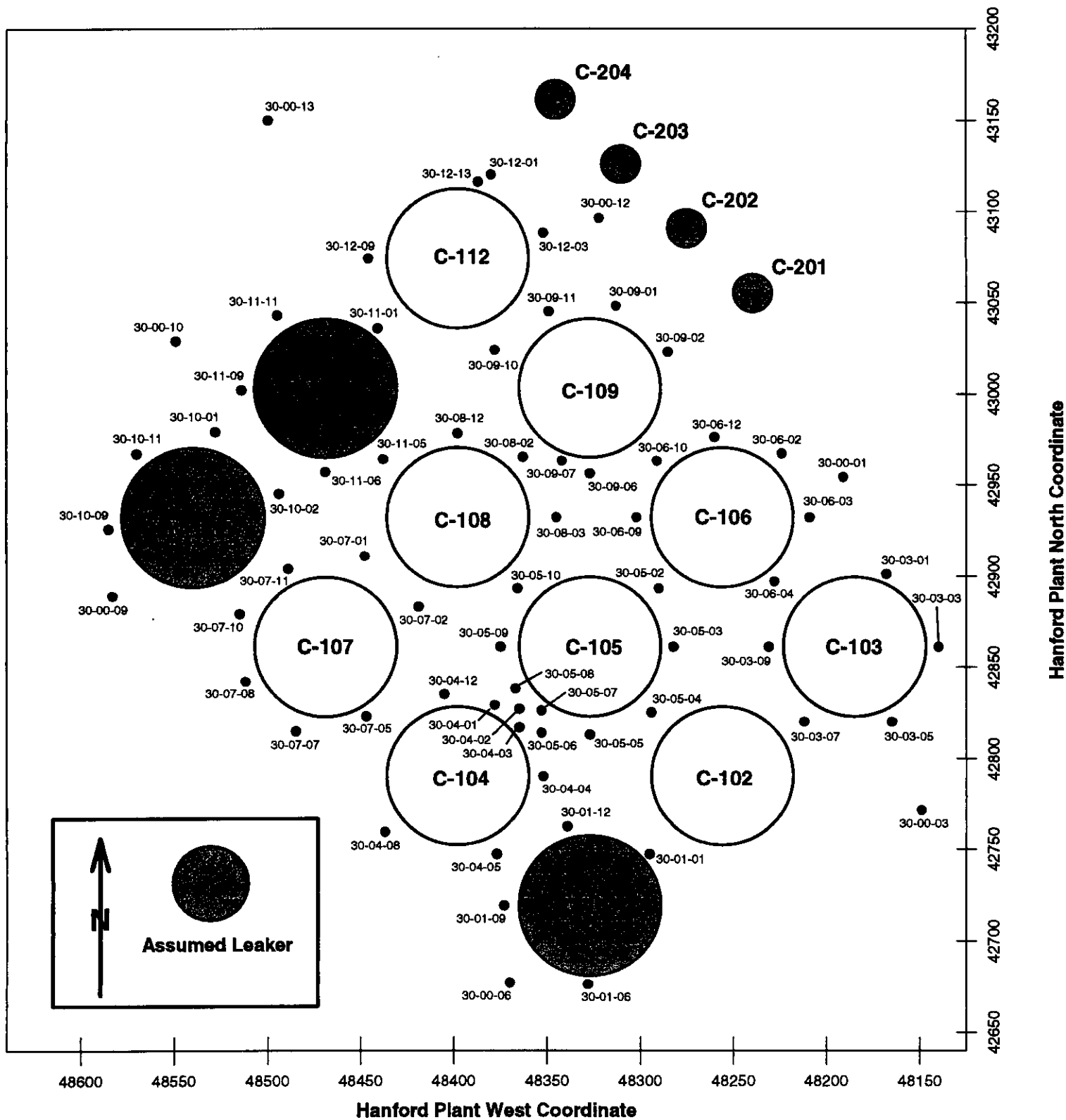
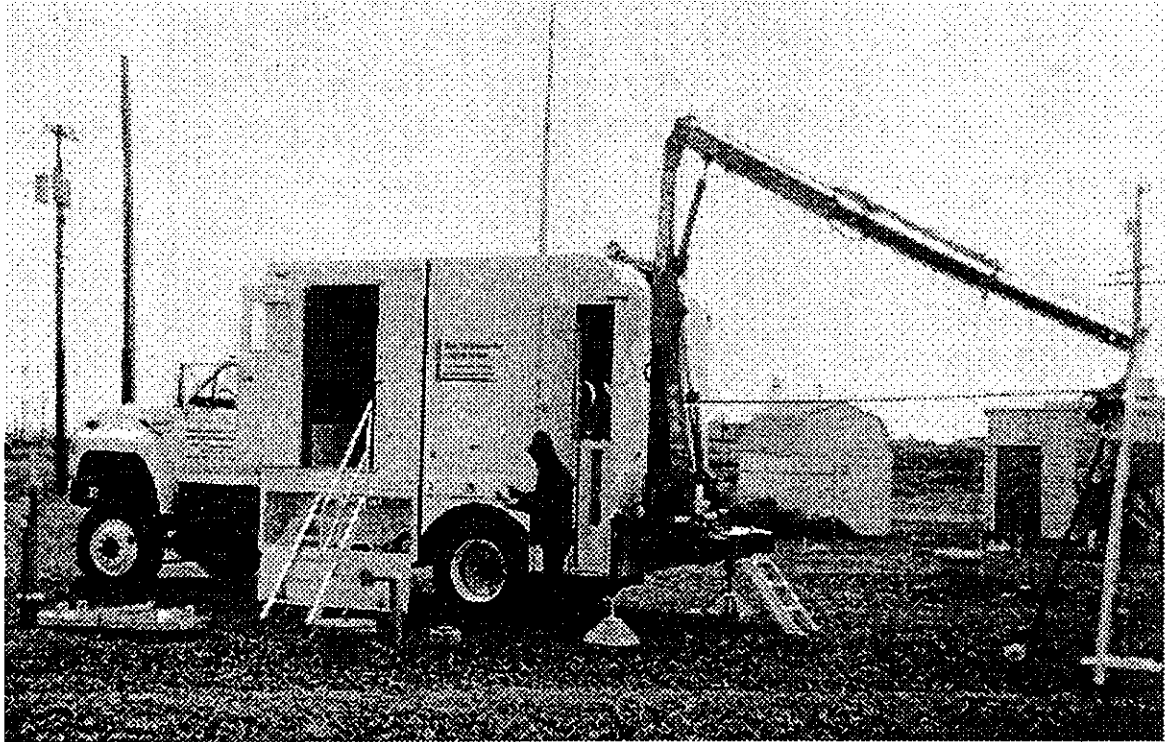
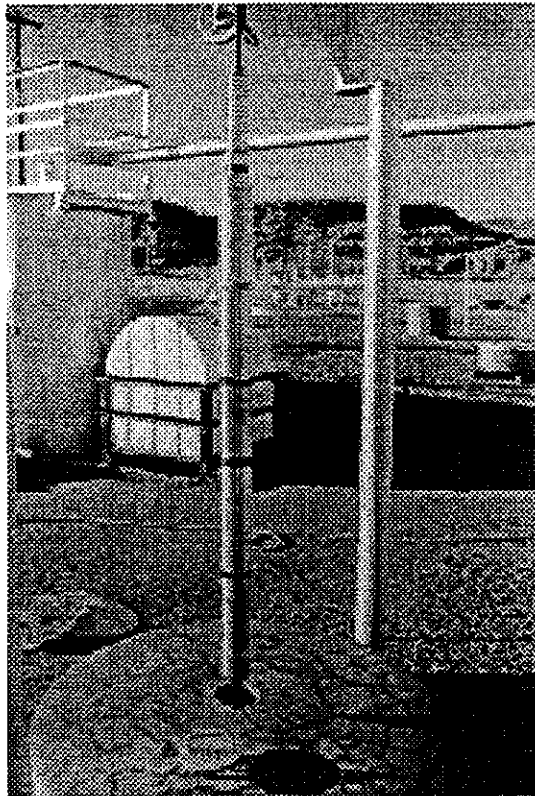


Figure 14-11. Plan View of the C Tank Farm Showing Borehole Locations



*Figure 14-12. One of the Spectral Gamma Logging Systems During Logging Operations*



*Figure 14-13. Logging Sonde Used by the Spectral Gamma Logging System*

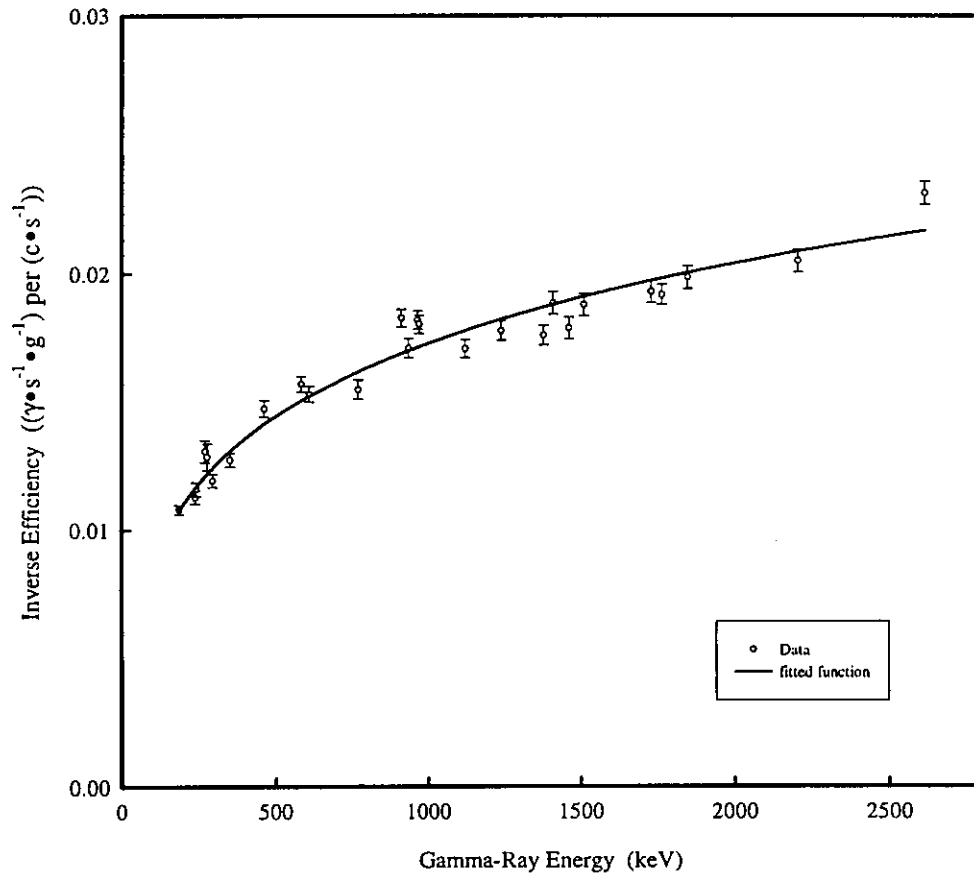
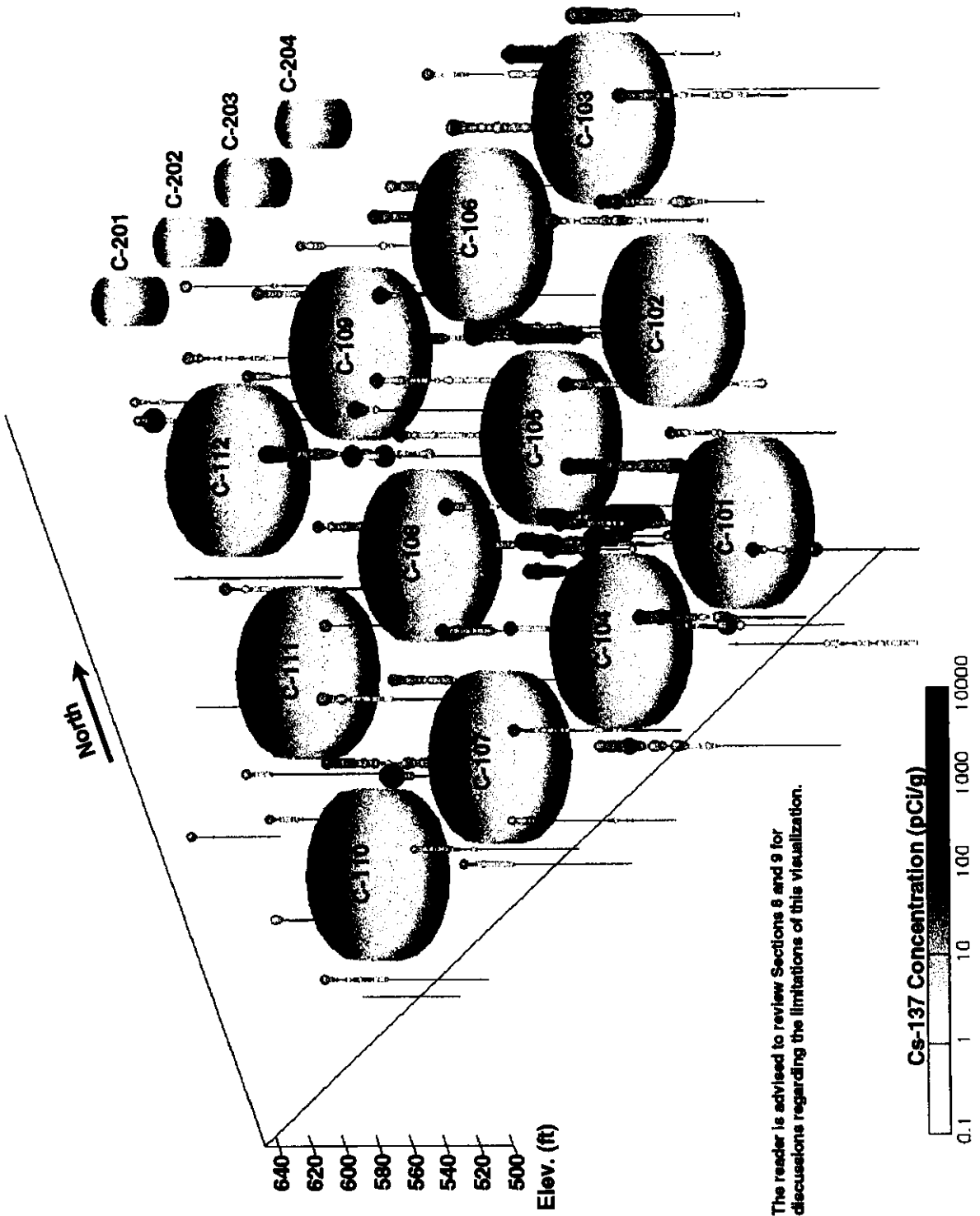
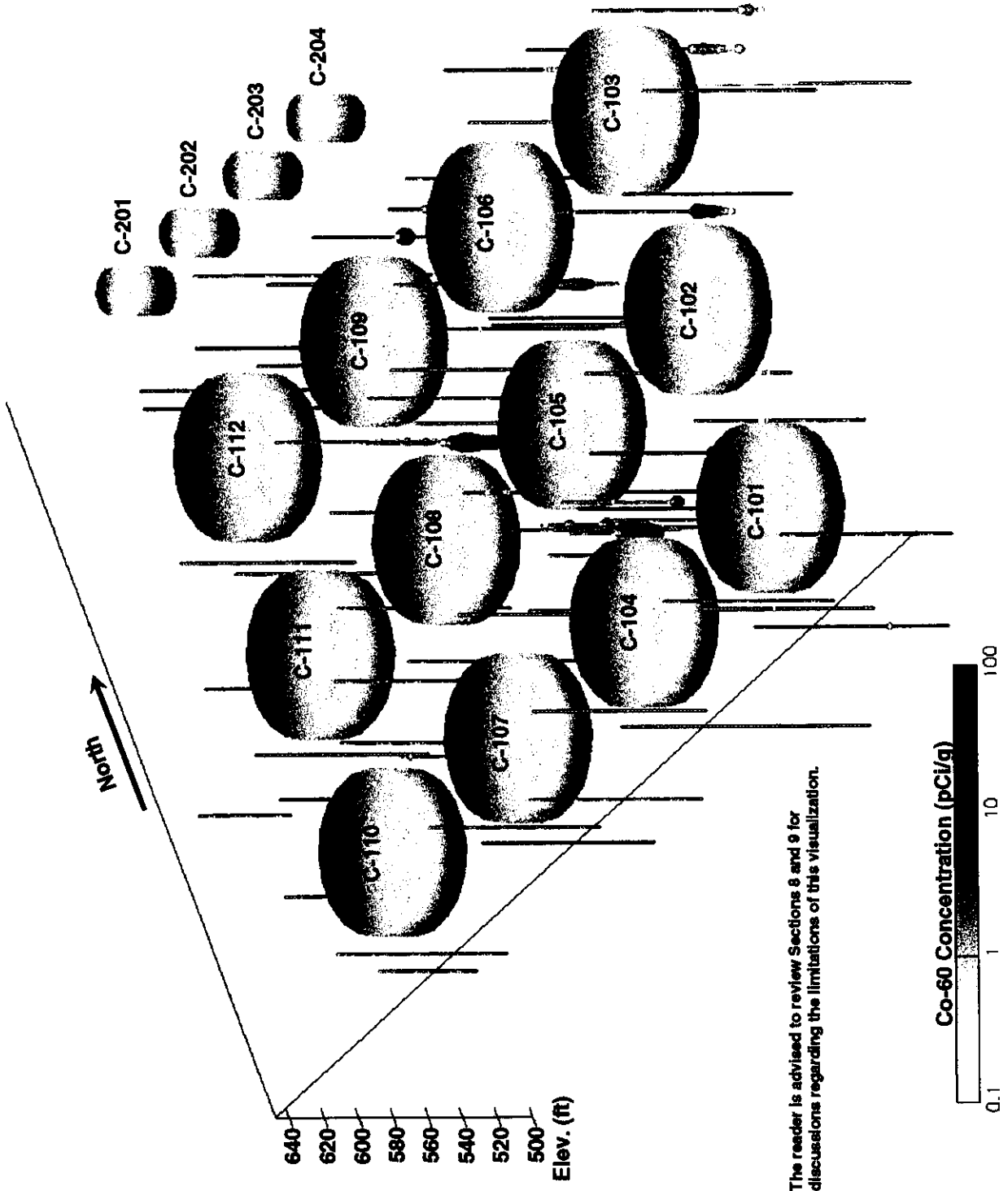


Figure 14-14. Example of an Efficiency Curve for Gamma 1



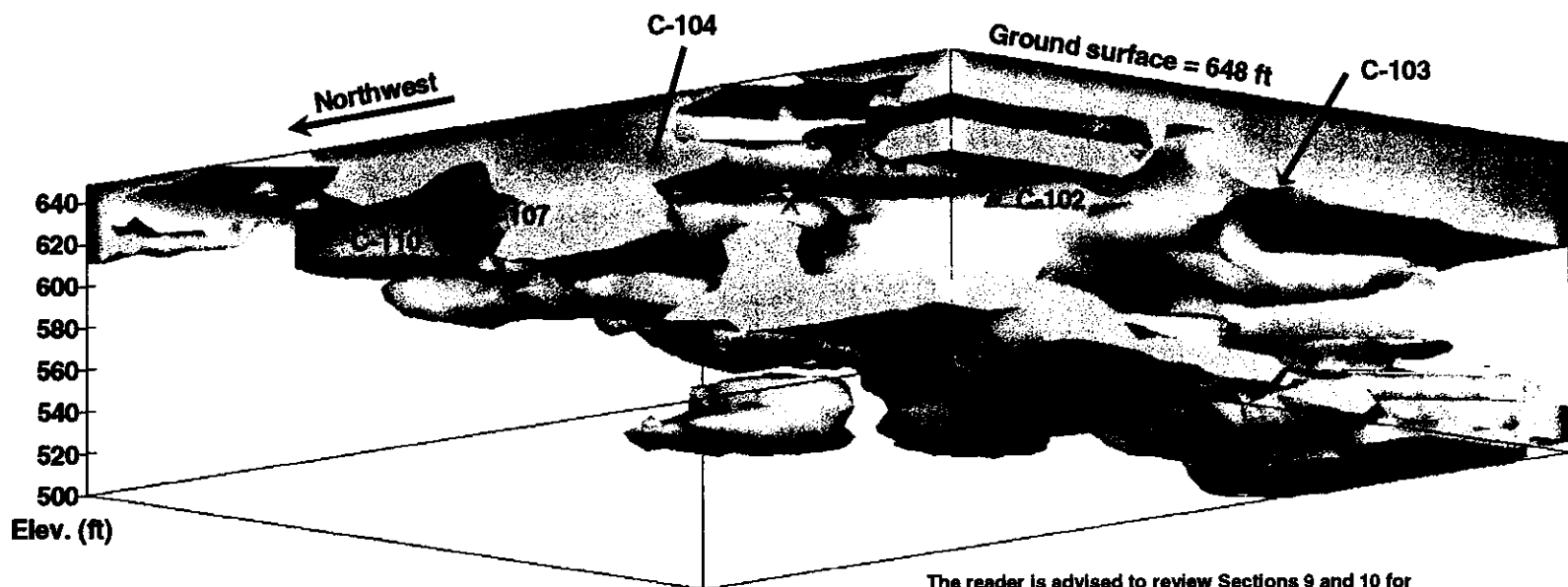
The reader is advised to review Sections 8 and 9 for discussions regarding the limitations of this visualization.

Figure 14-15. Interpreted <sup>137</sup>Cs Contamination Distribution Around the C Tank Farm Boreholes



The reader is advised to review Sections 8 and 9 for discussions regarding the limitations of this visualization.

Figure 14-16. Interpreted <sup>60</sup>Co Contamination Distribution Around the C Tank Farm Boreholes



The reader is advised to review Sections 9 and 10 for discussions regarding the limitations of this visualization.

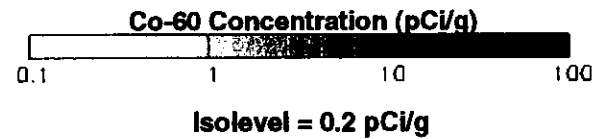
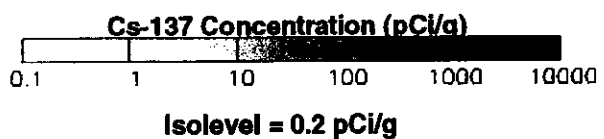


Figure 14-17. Visualization of the Contaminant Plumes in the C Tank Farm Viewed From the South

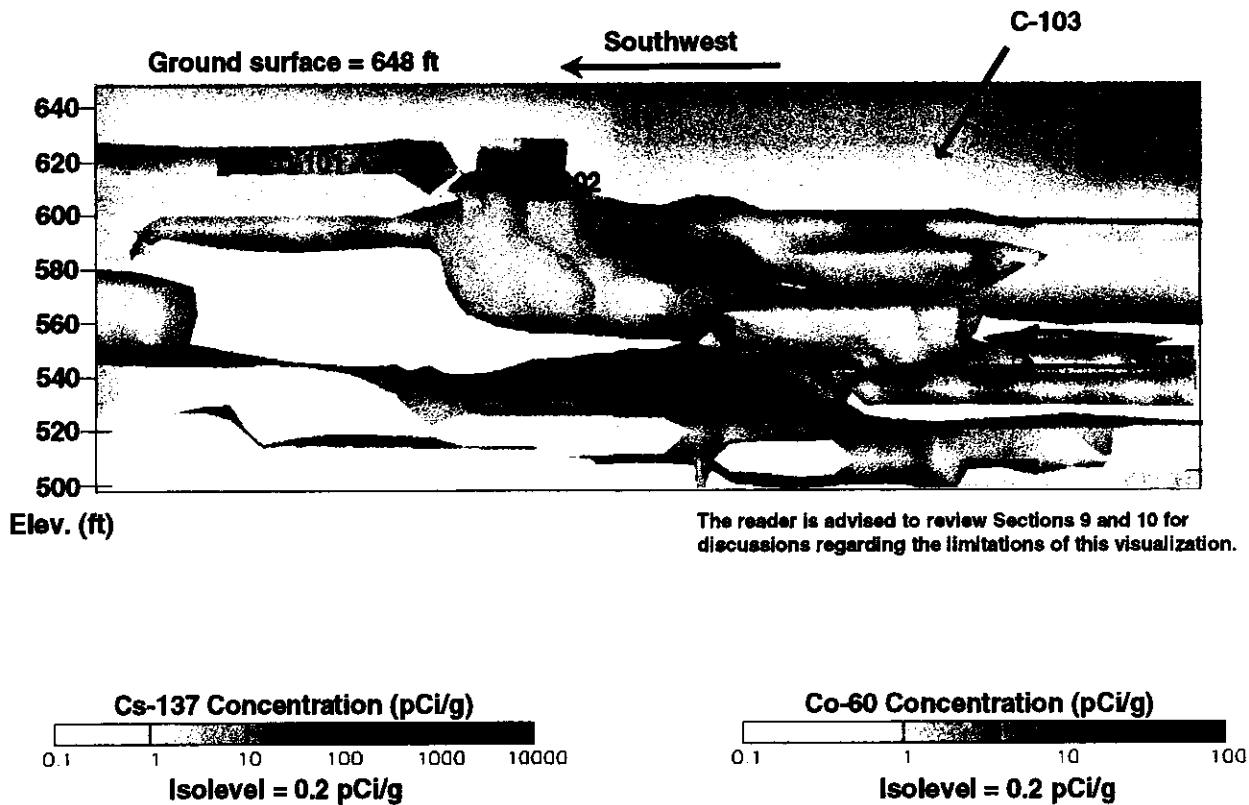
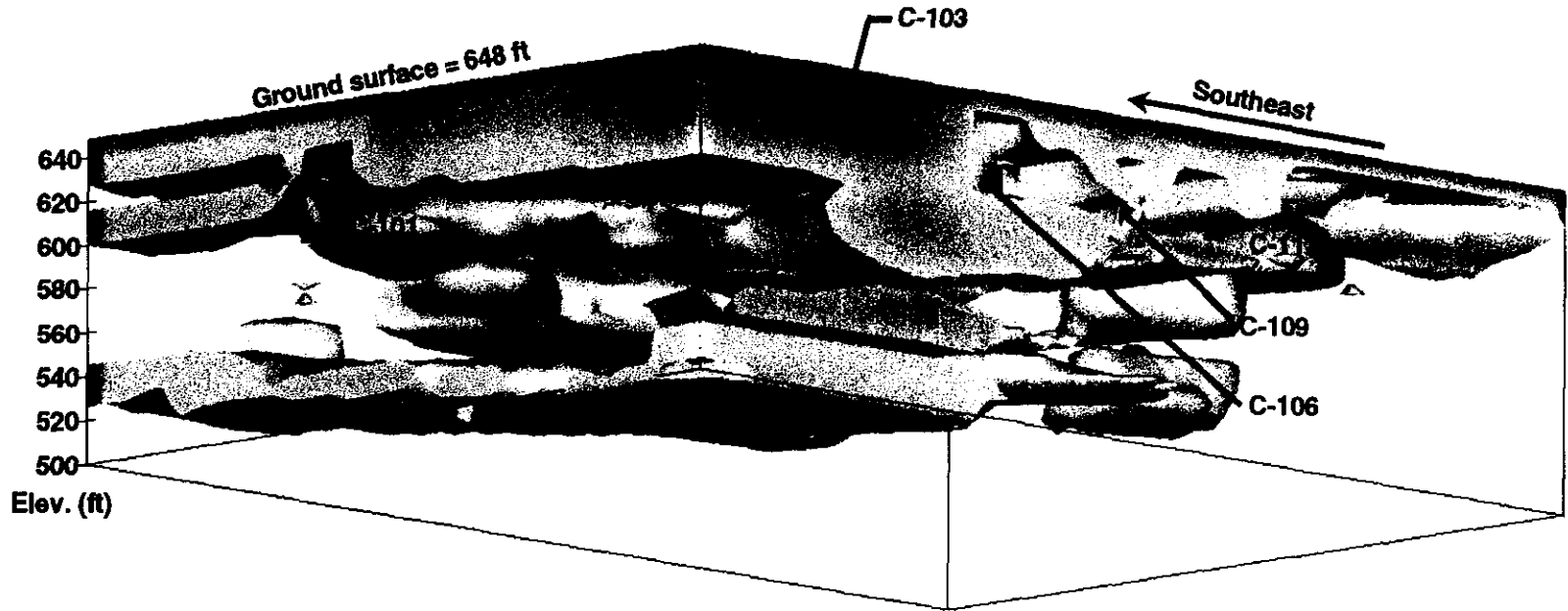


Figure 14-18. Visualization of the <sup>137</sup>Cs and <sup>60</sup>Co Plumes in the C Tank Farm Viewed From the Southeast



The reader is advised to review Sections 9 and 10 for discussions regarding the limitations of this visualization.

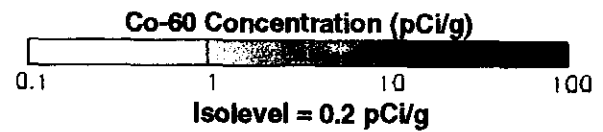
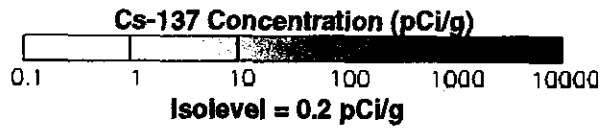
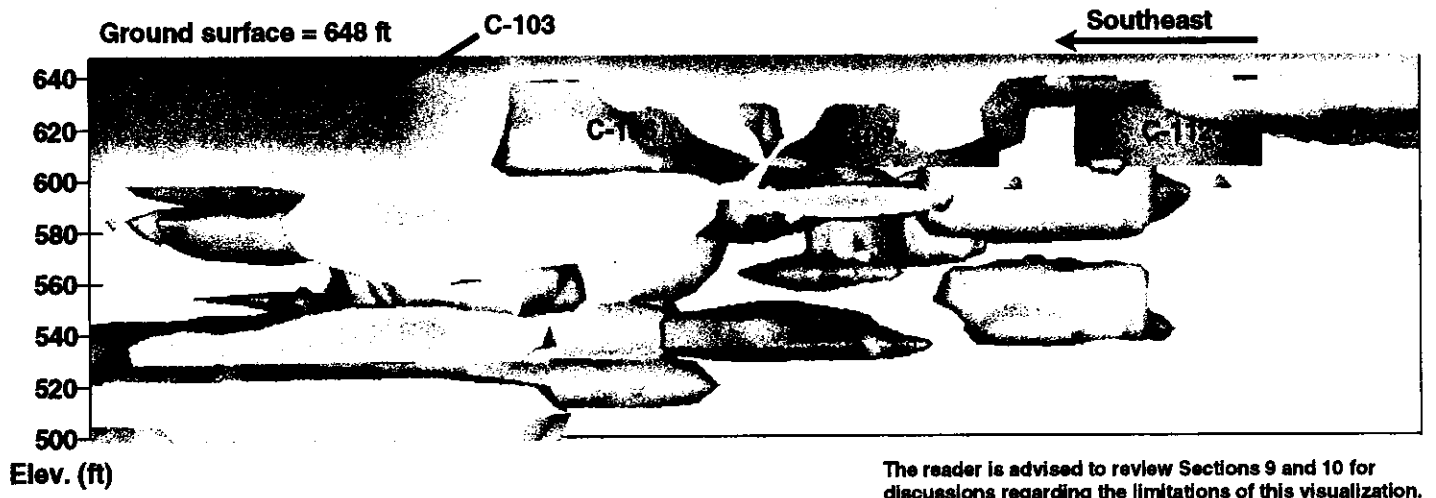


Figure 14-19. Visualization of the <sup>137</sup>Cs and <sup>60</sup>Co Plumes in the C Tank Farm Viewed From the East



The reader is advised to review Sections 9 and 10 for discussions regarding the limitations of this visualization.

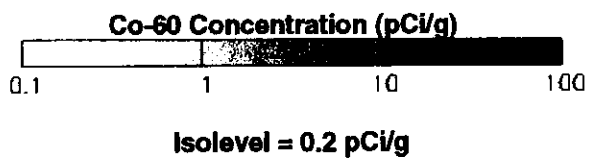
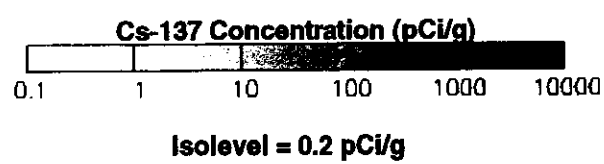


Figure 14-20. Visualization of the <sup>137</sup>Cs and <sup>60</sup>Co Plumes in the C Tank Farm Viewed From the Northeast

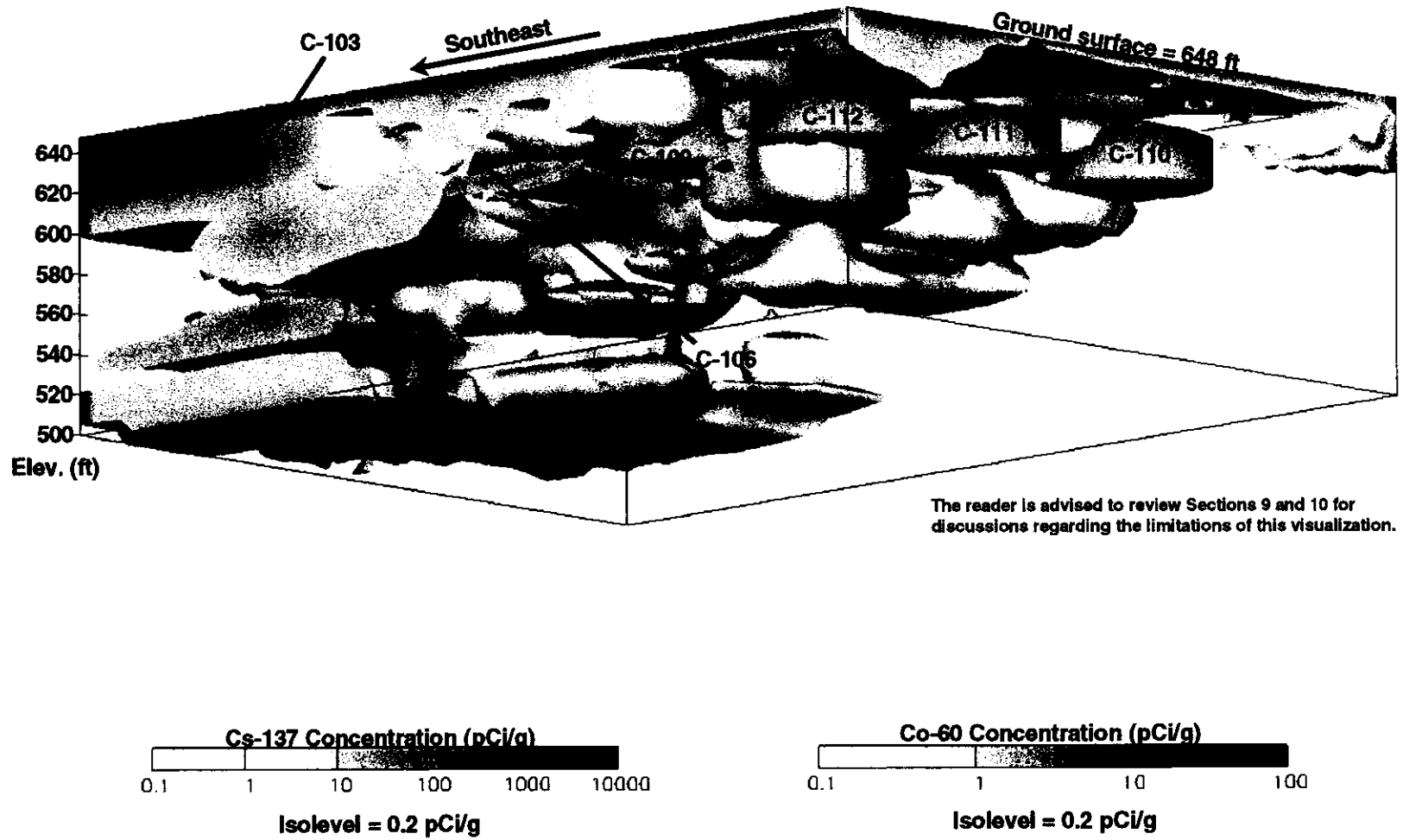
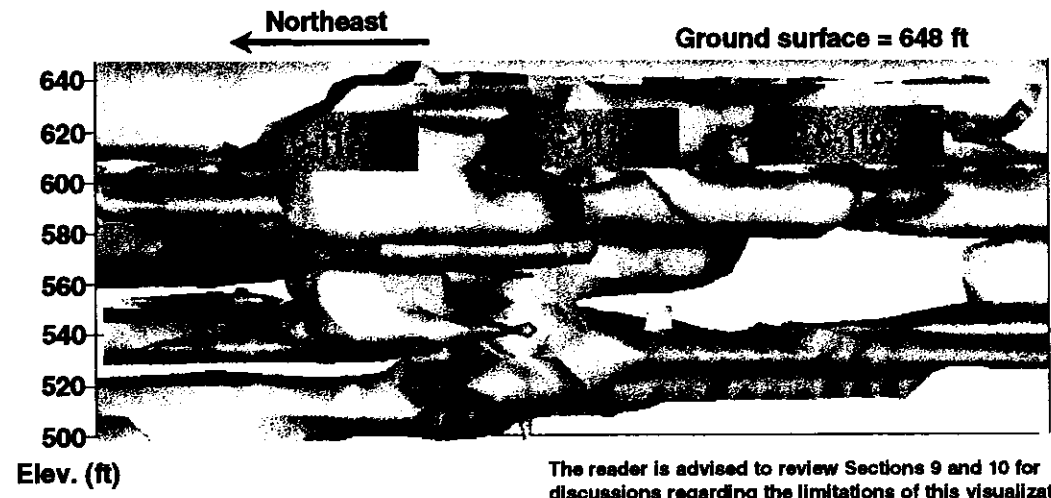


Figure 14-21. Visualization of the <sup>137</sup>Cs and <sup>60</sup>Co Plumes in the C Tank Farm Viewed From the North



The reader is advised to review Sections 9 and 10 for discussions regarding the limitations of this visualization.

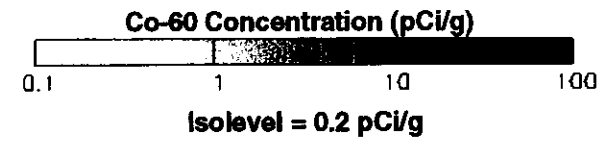
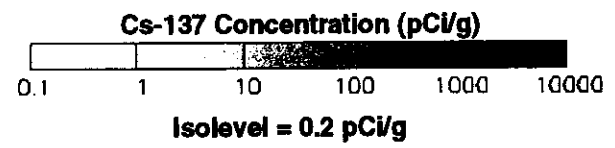


Figure 14-22. Visualization of the <sup>137</sup>Cs and <sup>60</sup>Co Plumes in the C Tank Farm Viewed From the Northwest

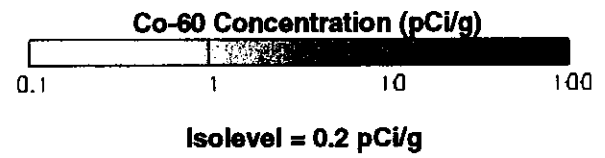
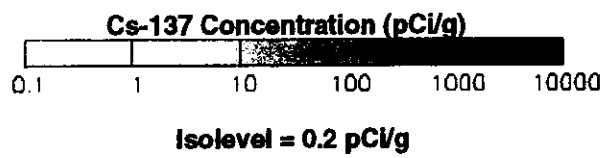
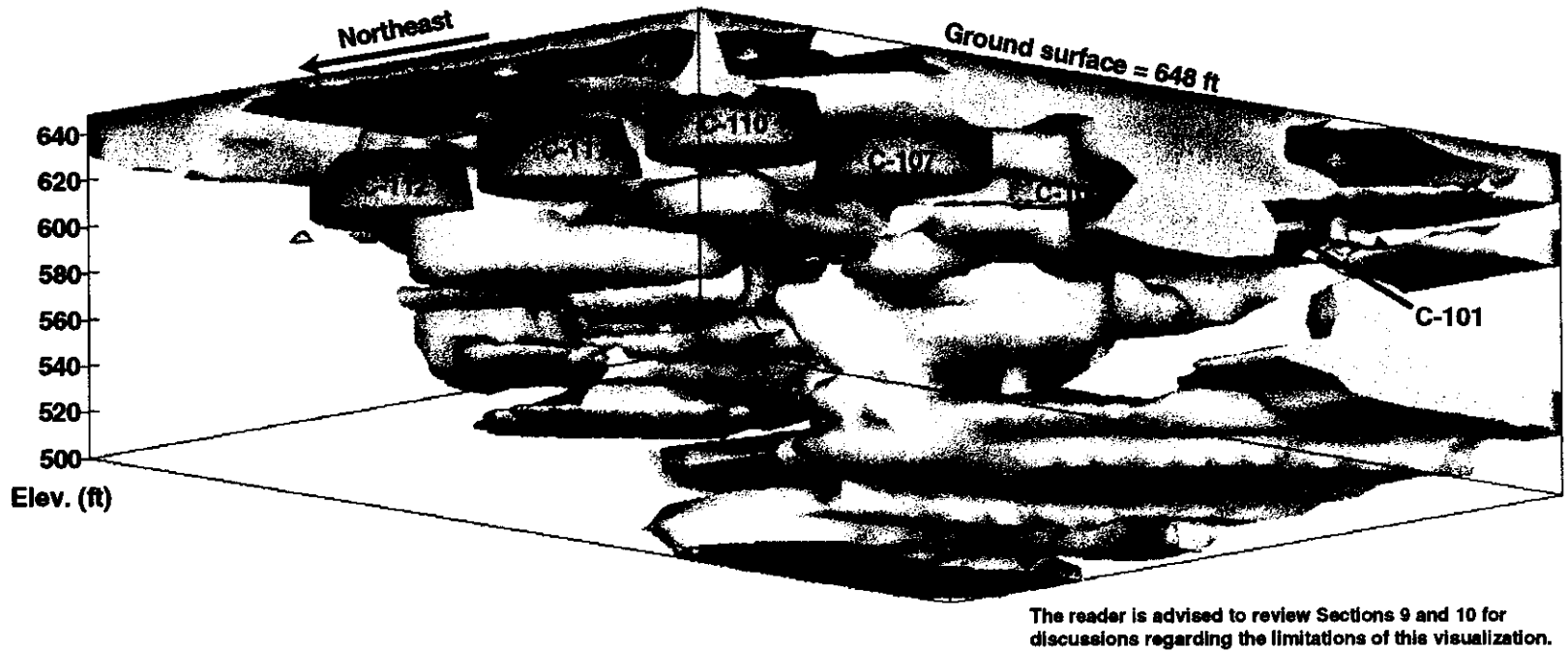


Figure 14-23. Visualization of the <sup>137</sup>Cs and <sup>60</sup>Co Plumes in the C Tank Farm Viewed From the West

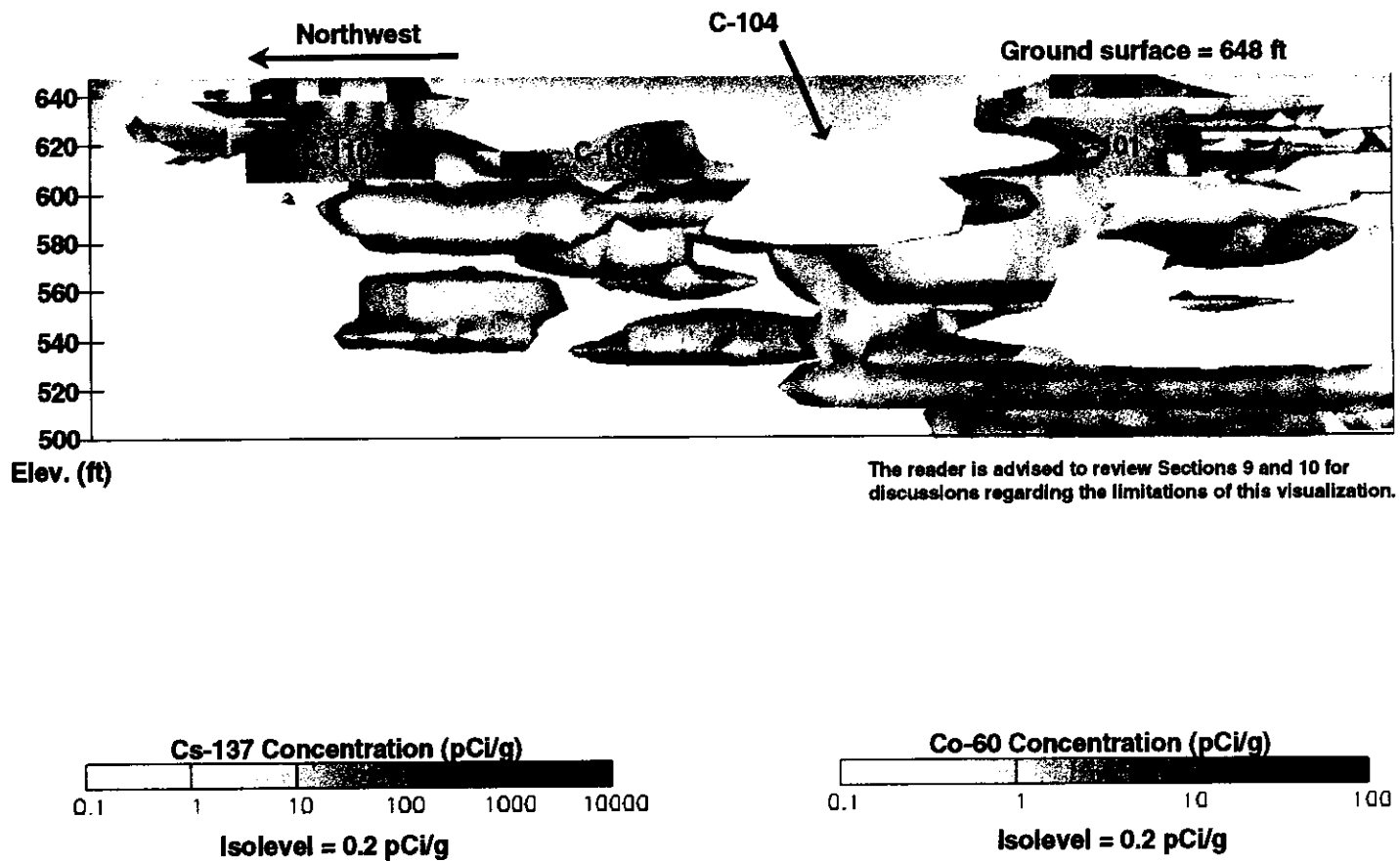


Figure 14-24. Visualization of the <sup>137</sup>Cs and <sup>60</sup>Co Plumes in the C Tank Farm Viewed From the Southwest

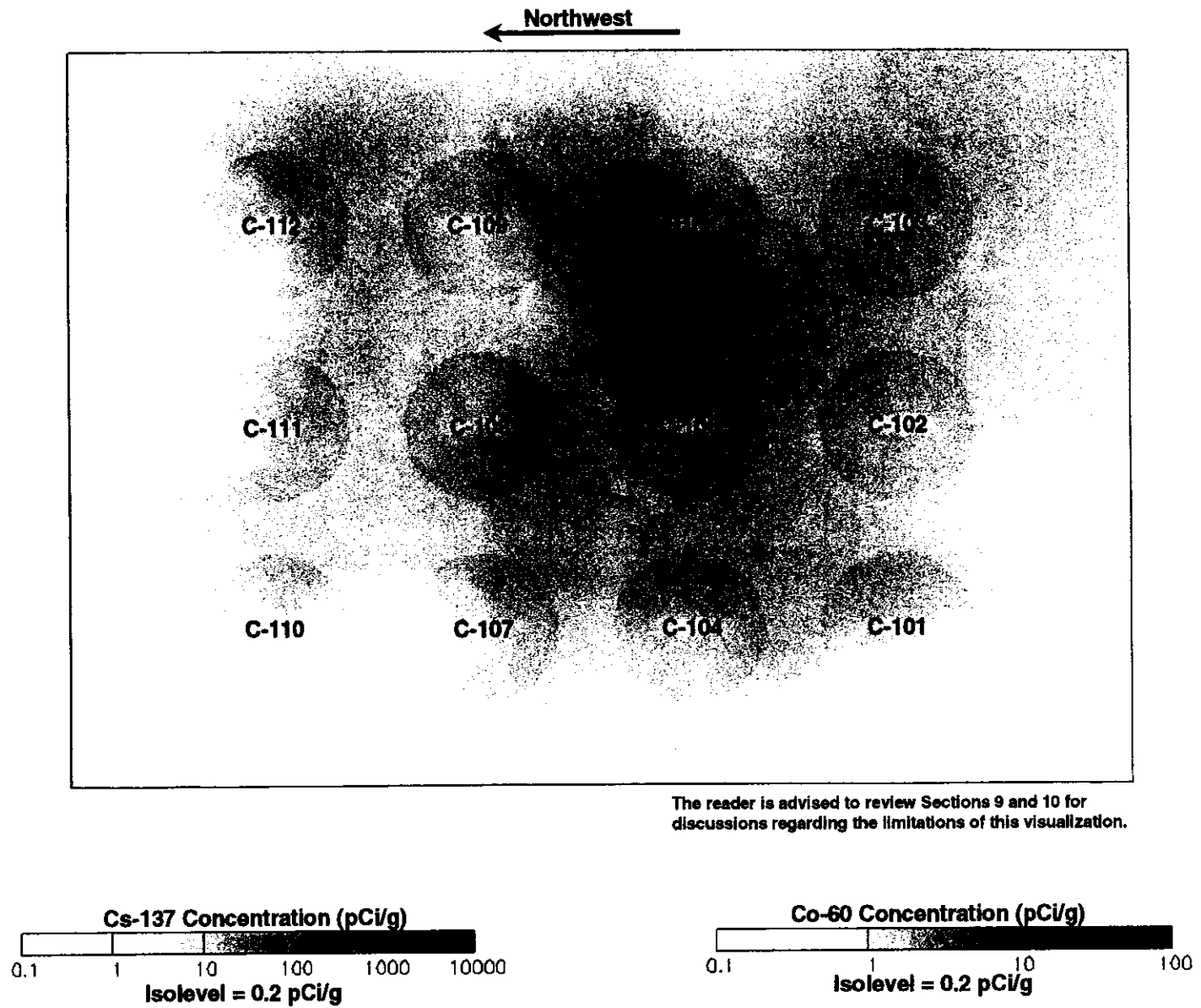
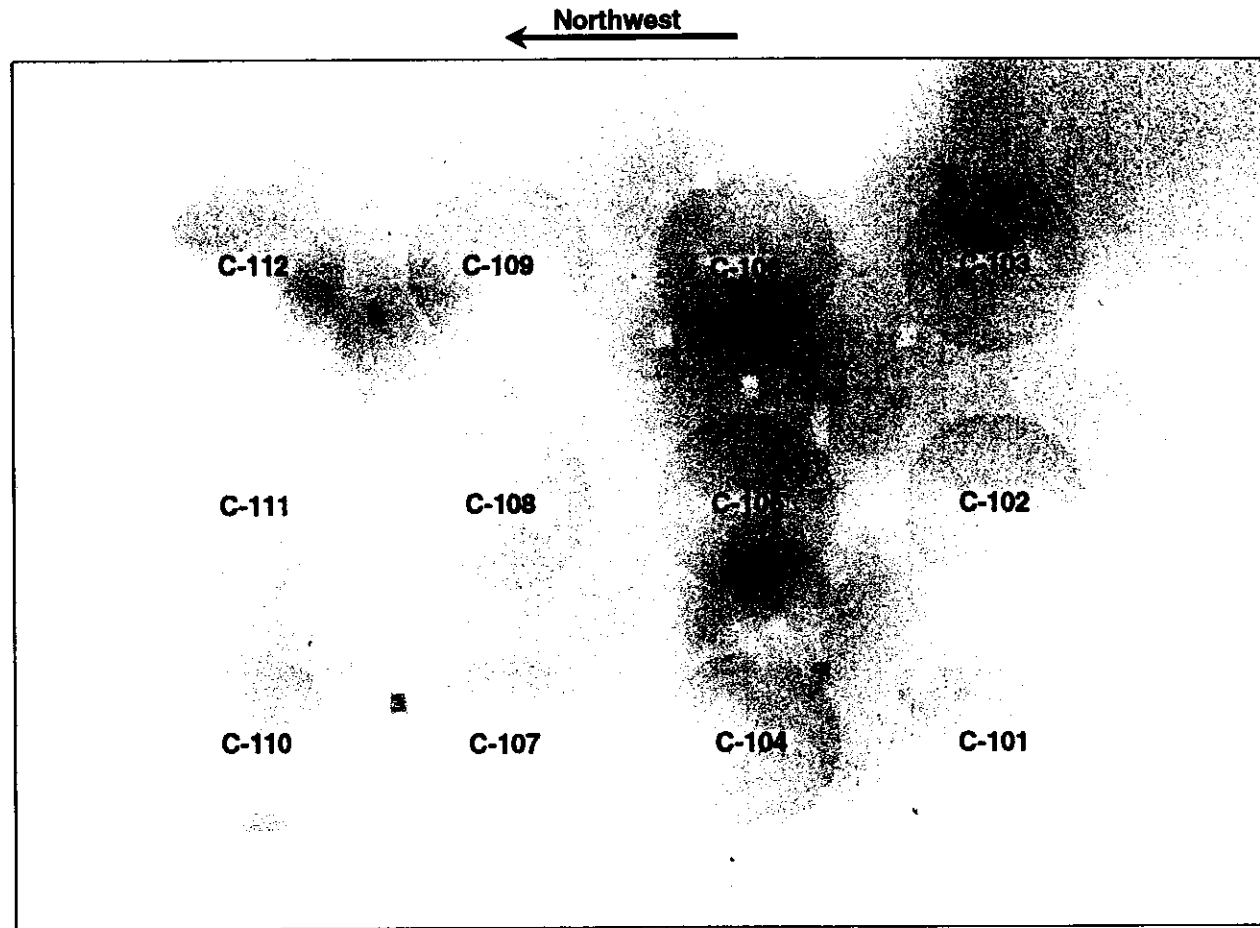


Figure 14-25. Visualization of the <sup>137</sup>Cs Contamination at the Ground Surface of the C Tank Farm



The reader is advised to review Sections 9 and 10 for discussions regarding the limitations of this visualization.

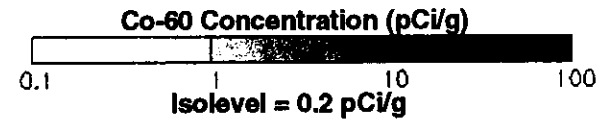
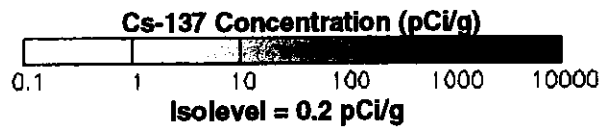


Figure 14-26. Visualization of the <sup>137</sup>Cs Contamination 5 ft Below the Surface of the C Tank Farm

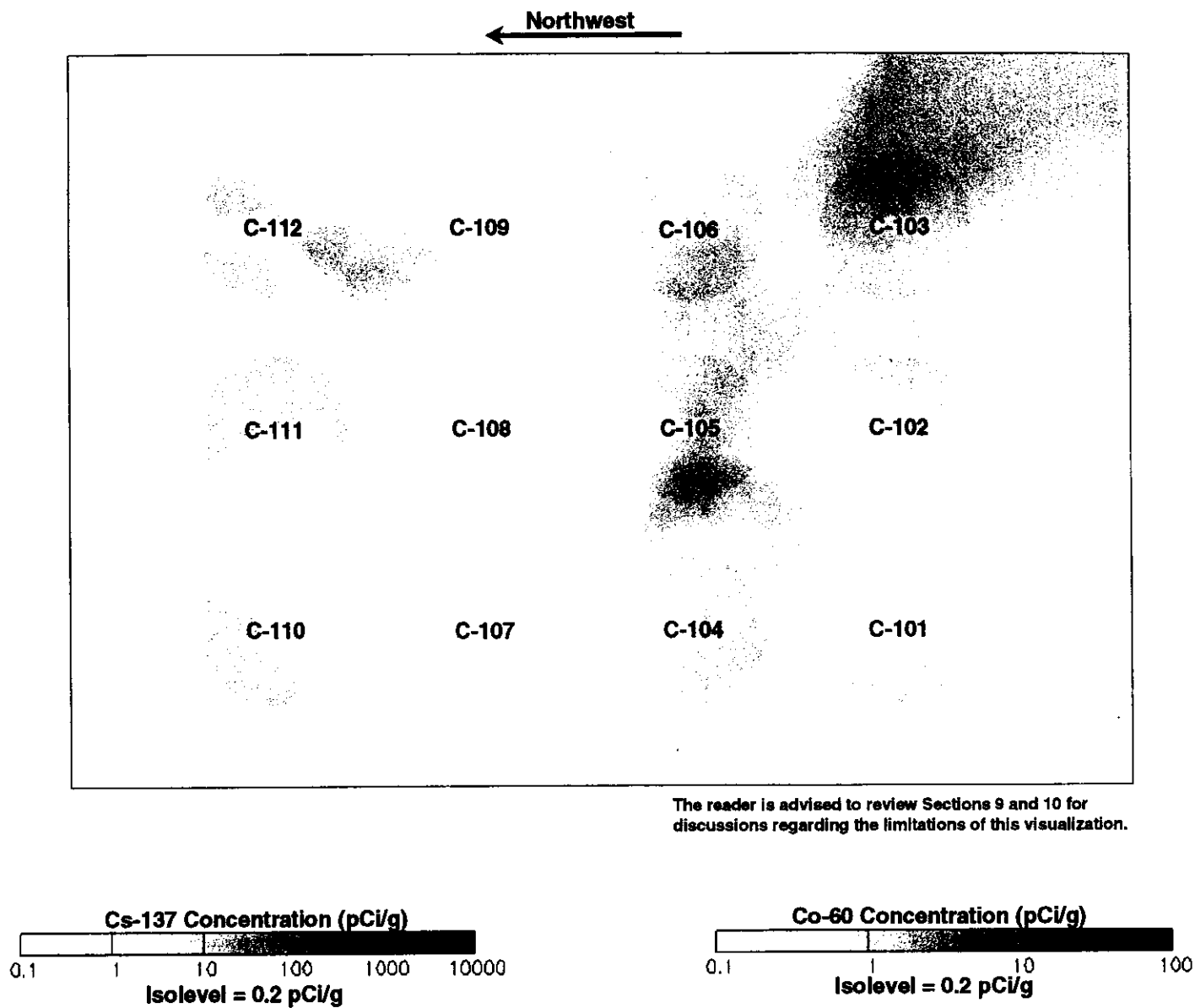
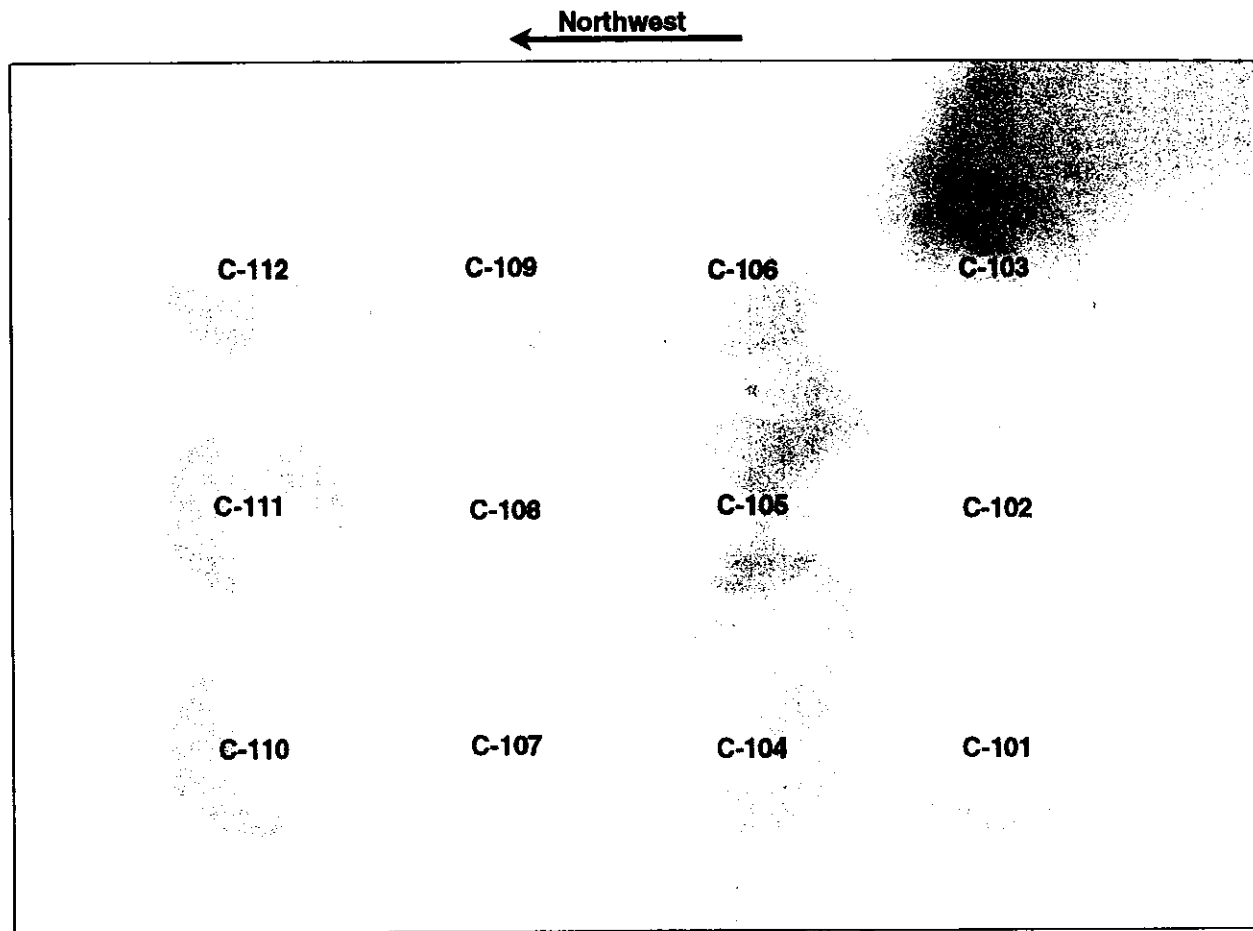


Figure 14-27. Visualization of the <sup>137</sup>Cs Contamination 10 ft Below the Surface of the C Tank Farm



The reader is advised to review Sections 9 and 10 for discussions regarding the limitations of this visualization.

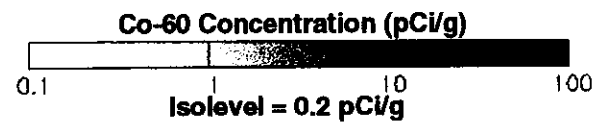
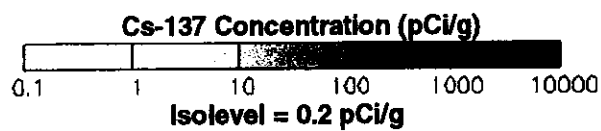
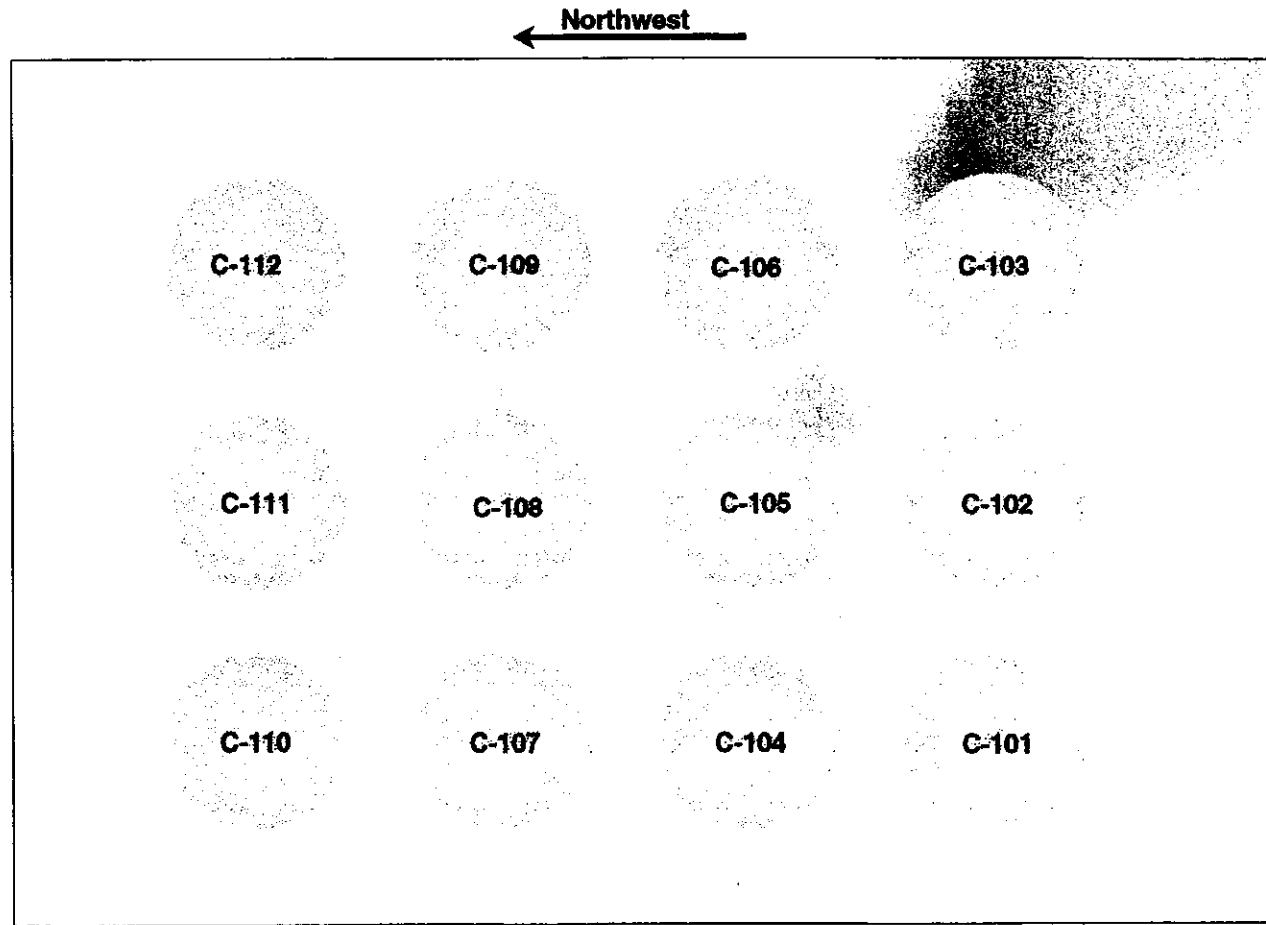


Figure 14-28. Visualization of the <sup>137</sup>Cs and <sup>60</sup>Co Contamination 15 ft Below the Surface of the C Tank Farm



The reader is advised to review Sections 9 and 10 for discussions regarding the limitations of this visualization.

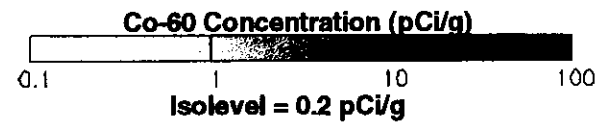
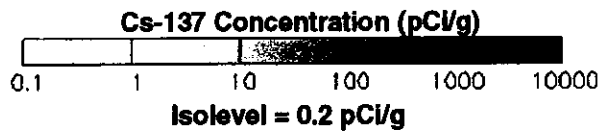


Figure 14-29. Visualization of the <sup>137</sup>Cs and <sup>60</sup>Co Contamination 20 ft Below the Surface of the C Tank Farm

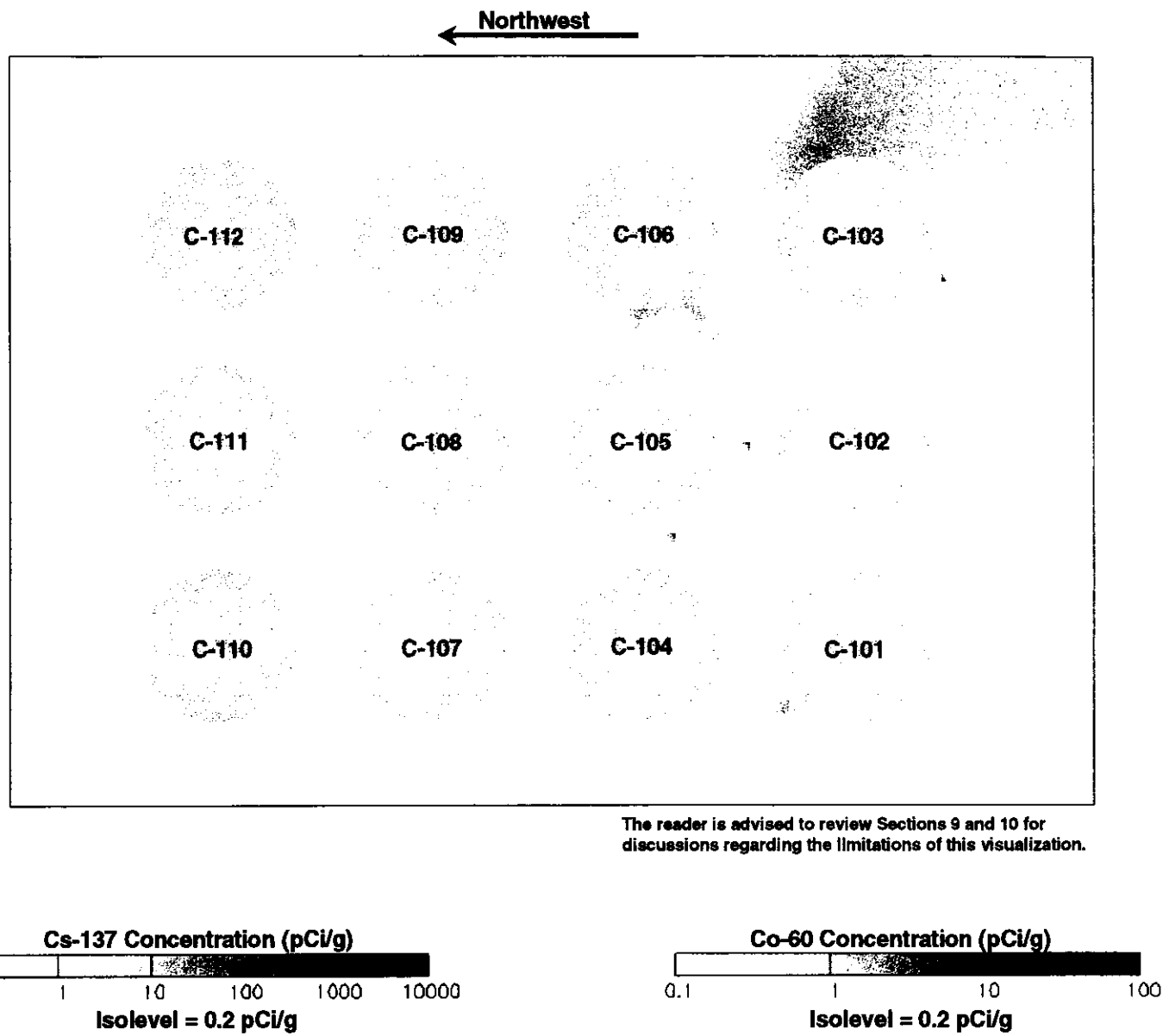


Figure 14-31. Visualization of the <sup>137</sup>Cs and <sup>60</sup>Co Contamination 30 ft Below the Surface of the C Tank Farm

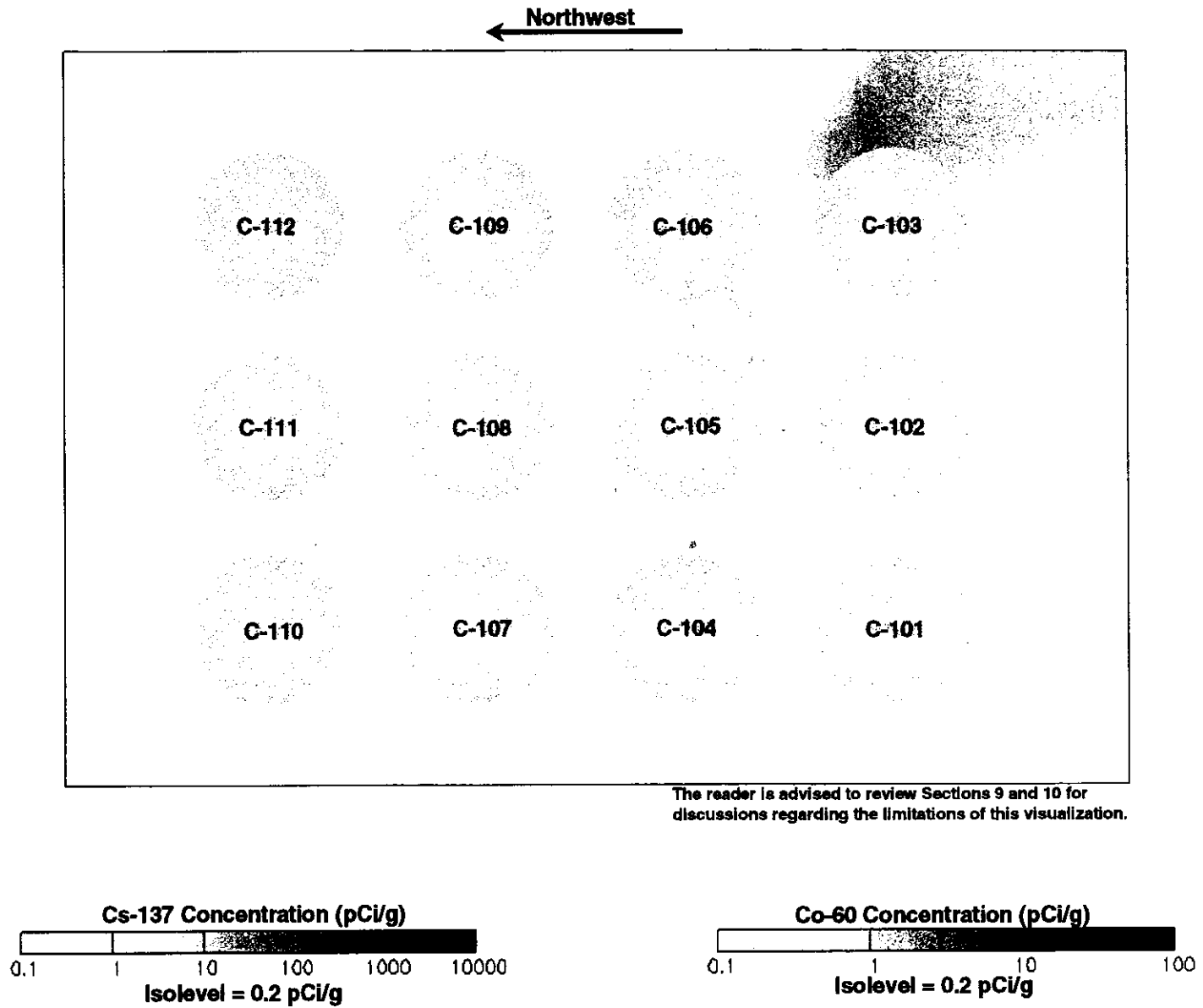
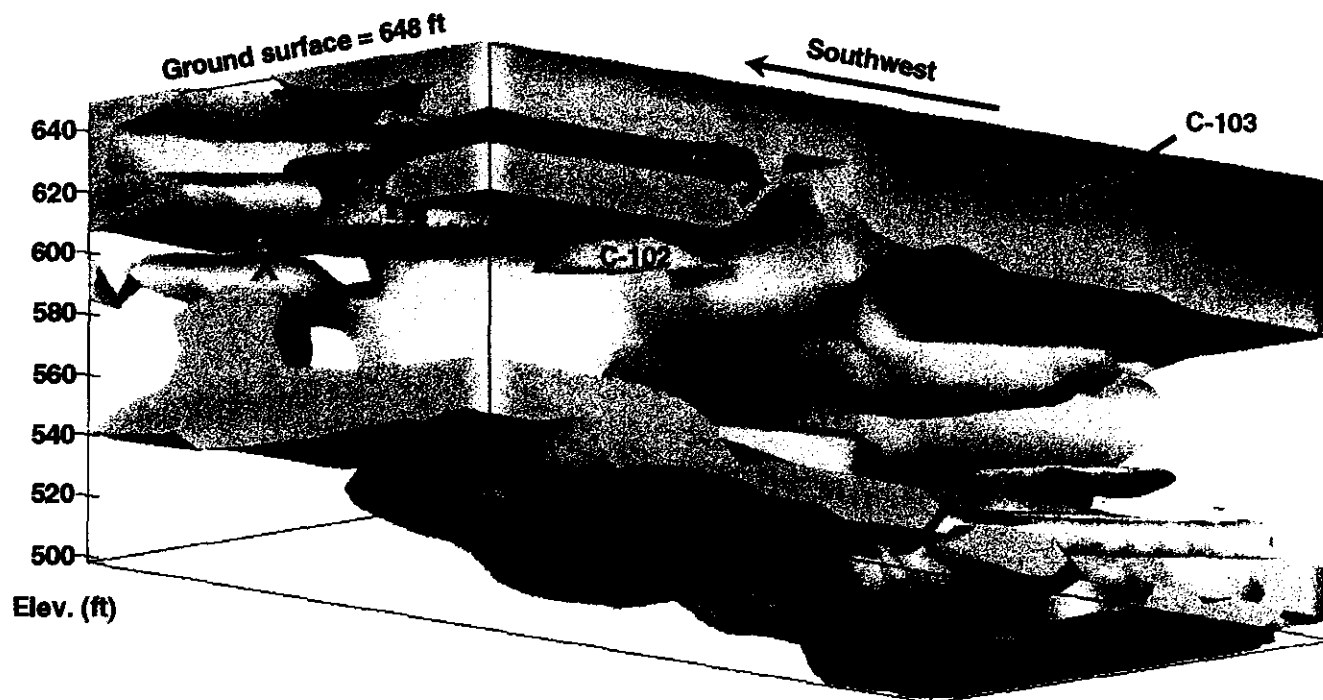


Figure 14-30. Visualization of the <sup>137</sup>Cs Contamination 25 ft Below the Surface of the C Tank Farm



The reader is advised to review Sections 9 and 10 for discussions regarding the limitations of this visualization.

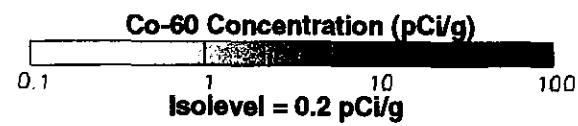
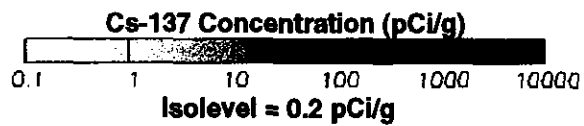


Figure 14-32. Visualization of the <sup>137</sup>Cs and <sup>60</sup>Co Contamination Around Tanks C-101, C-102, and C-103 Viewed From the South

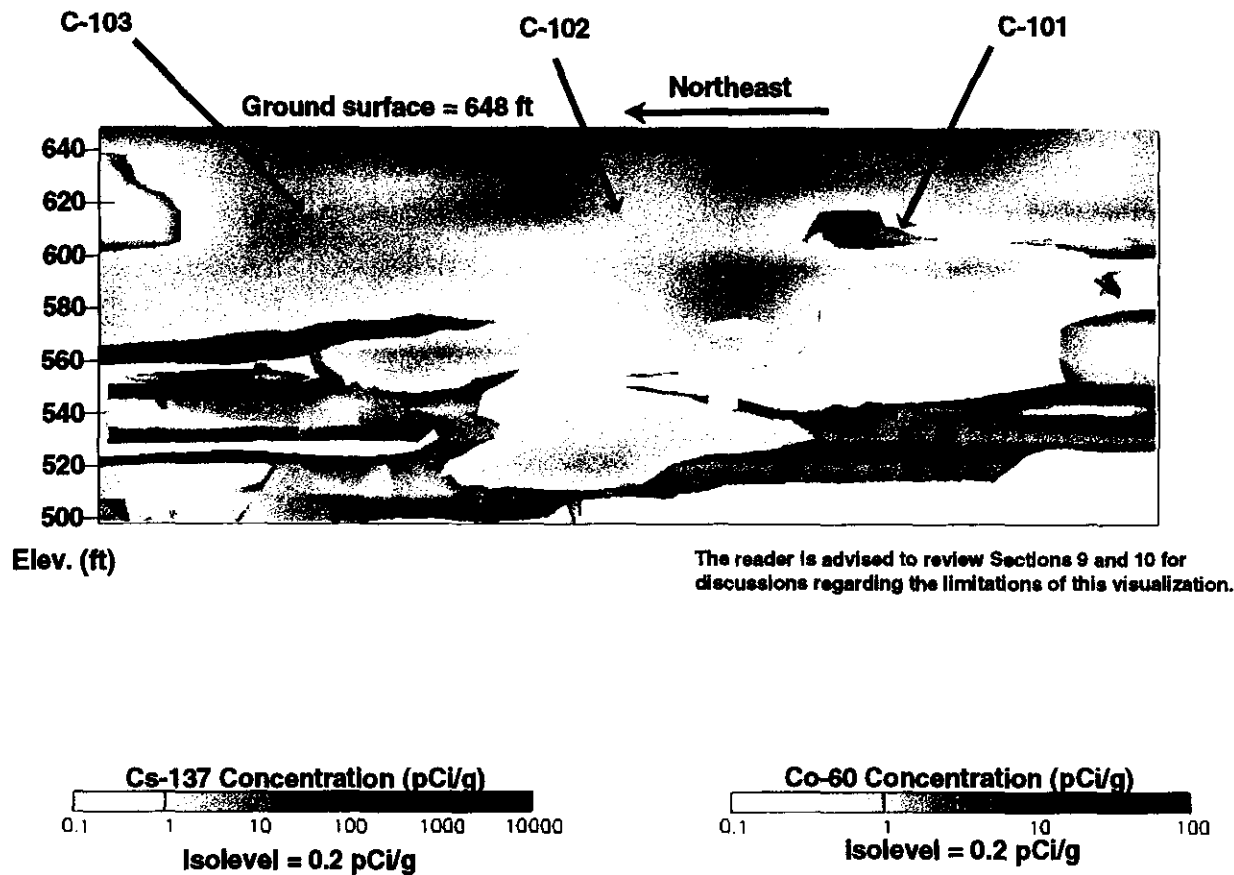


Figure 14-33. Visualization of the <sup>137</sup>Cs and <sup>60</sup>Co Contamination Around Tanks C-101, C-102, and C-103 Viewed From the Northwest

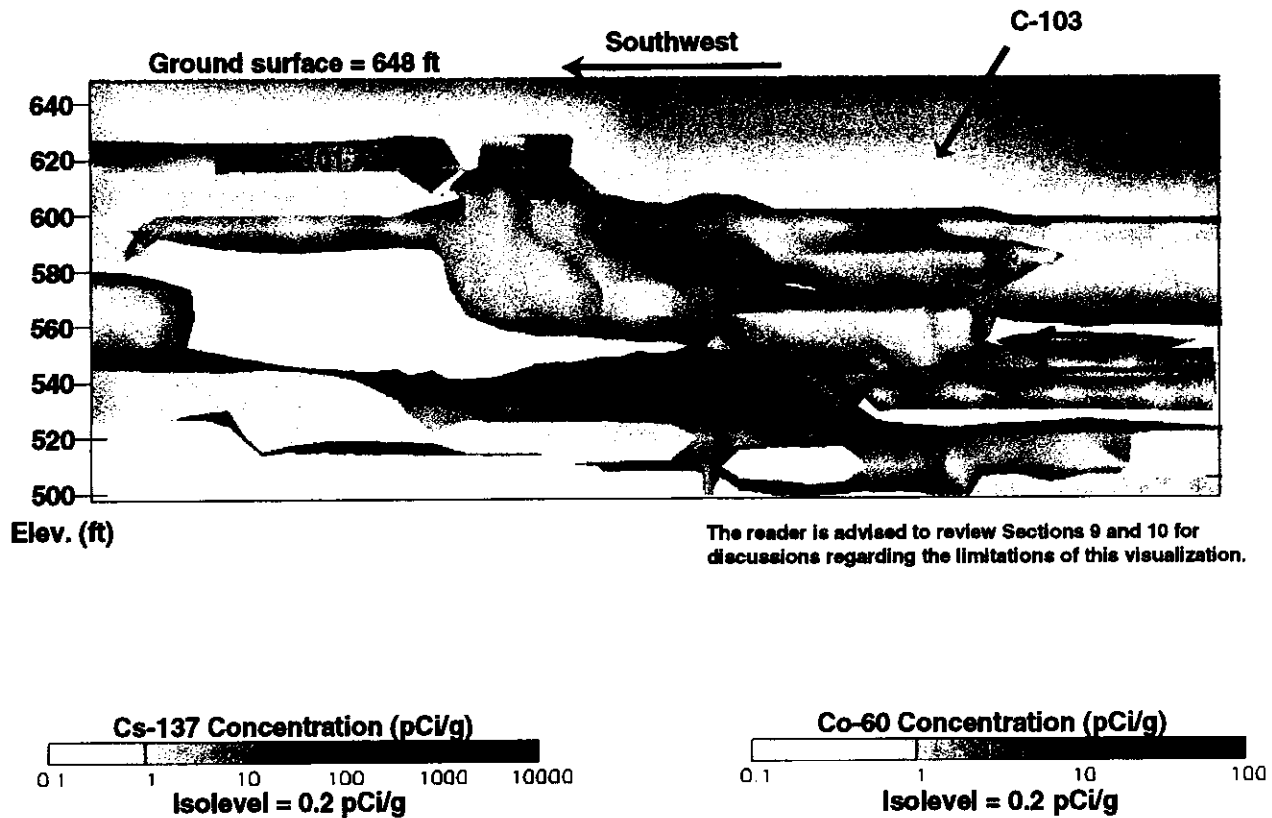
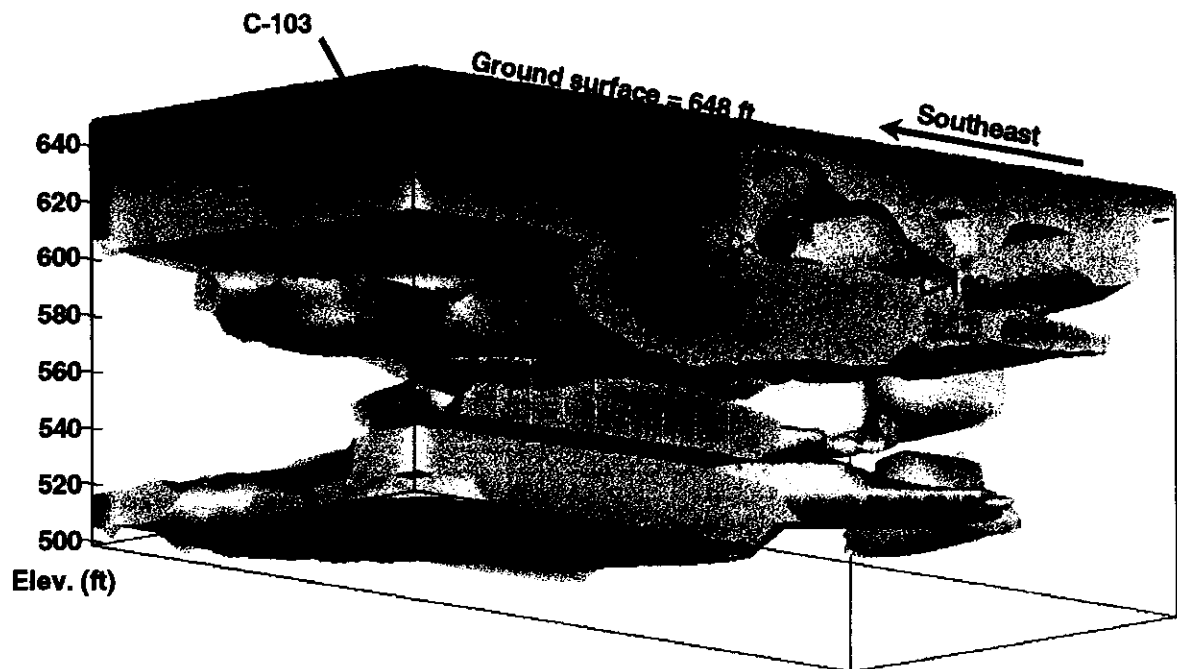


Figure 14-34. Visualization of the <sup>137</sup>Cs and <sup>60</sup>Co Contamination Around Tanks C-101, C-102, and C-103 Viewed From the Southeast



The reader is advised to review Sections 9 and 10 for discussions regarding the limitations of this visualization.

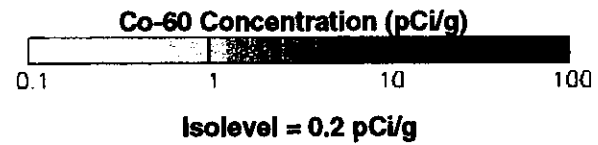
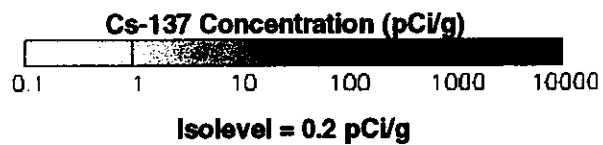
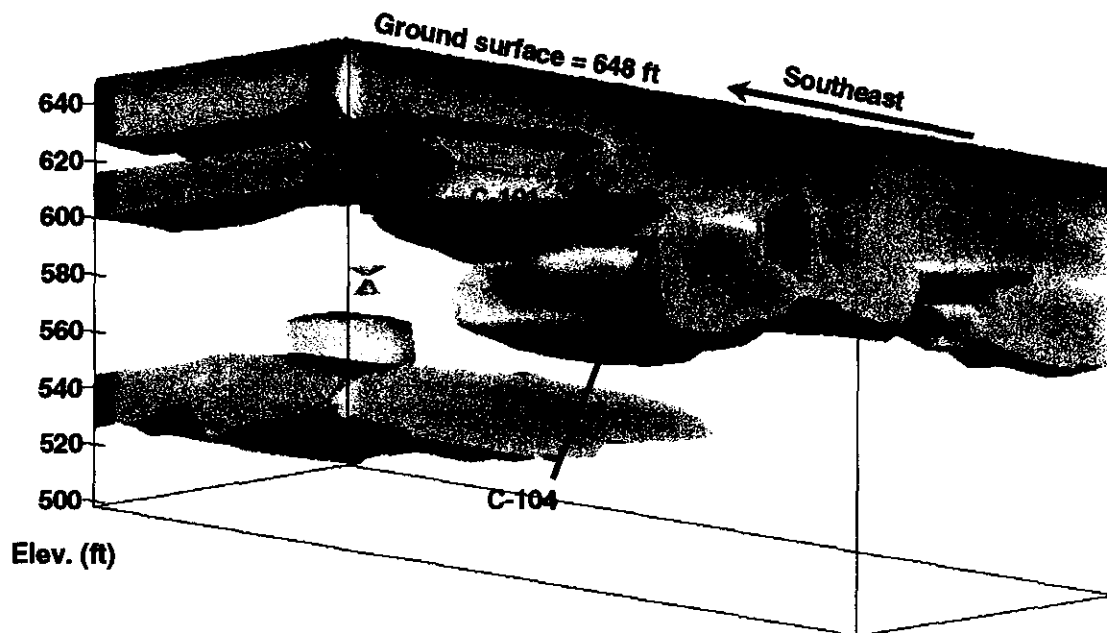


Figure 14-35. Visualization of the <sup>137</sup>Cs and <sup>60</sup>Co Contamination Around Tanks C-103, C-106, and C-109 Viewed From the South



The reader is advised to review Sections 9 and 10 for discussions regarding the limitations of this visualization.

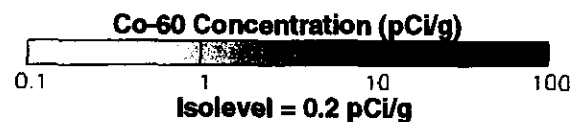
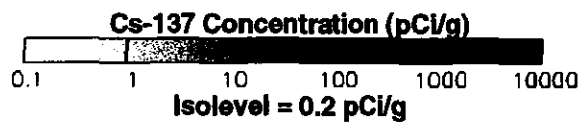
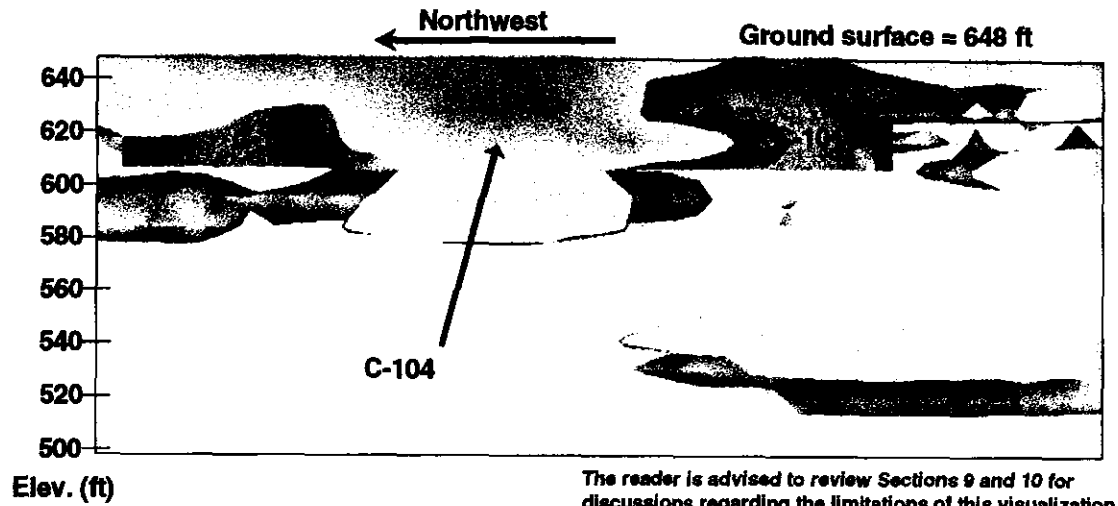


Figure 14-36. Visualization of the <sup>137</sup>Cs and <sup>60</sup>Co Contamination Around Tanks C-101, C-104, and C-107 Viewed From the East



The reader is advised to review Sections 9 and 10 for discussions regarding the limitations of this visualization.

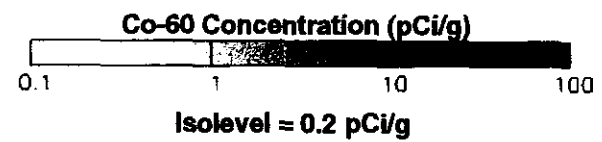
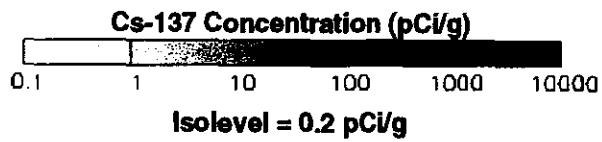


Figure 14-37. Visualization of the <sup>137</sup>Cs and <sup>60</sup>Co Contamination Around Tanks C-101, C-104, and C-107 Viewed From the Southwest

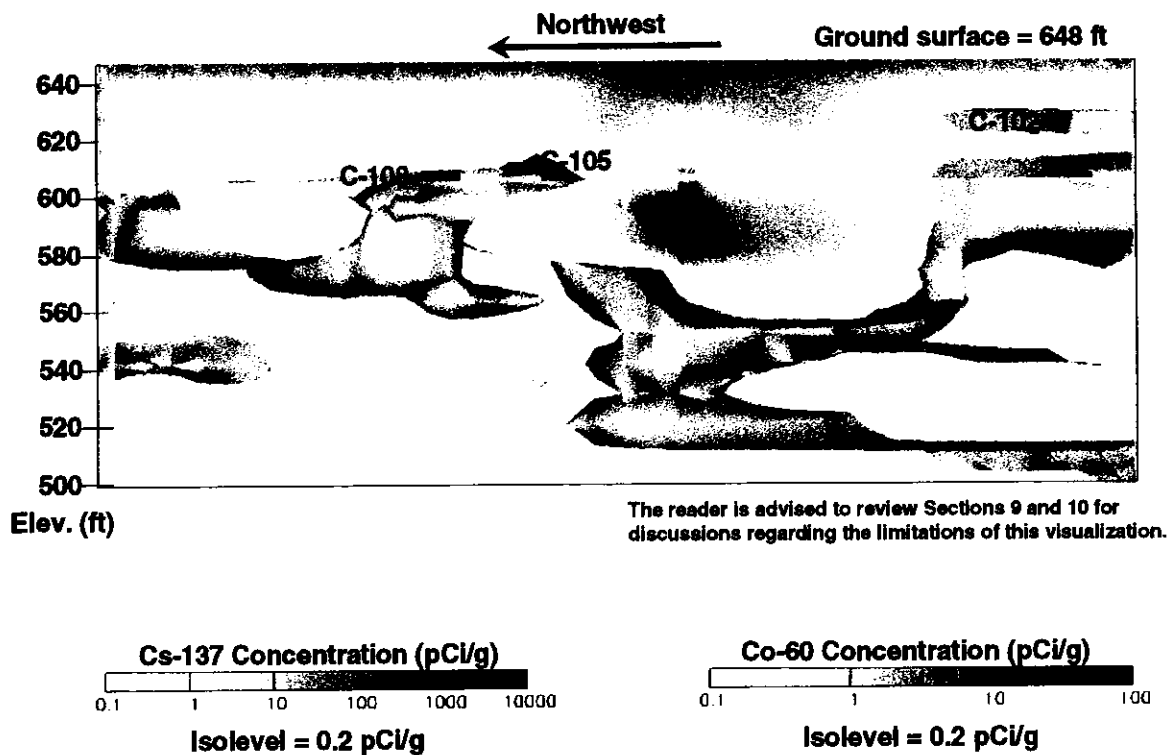
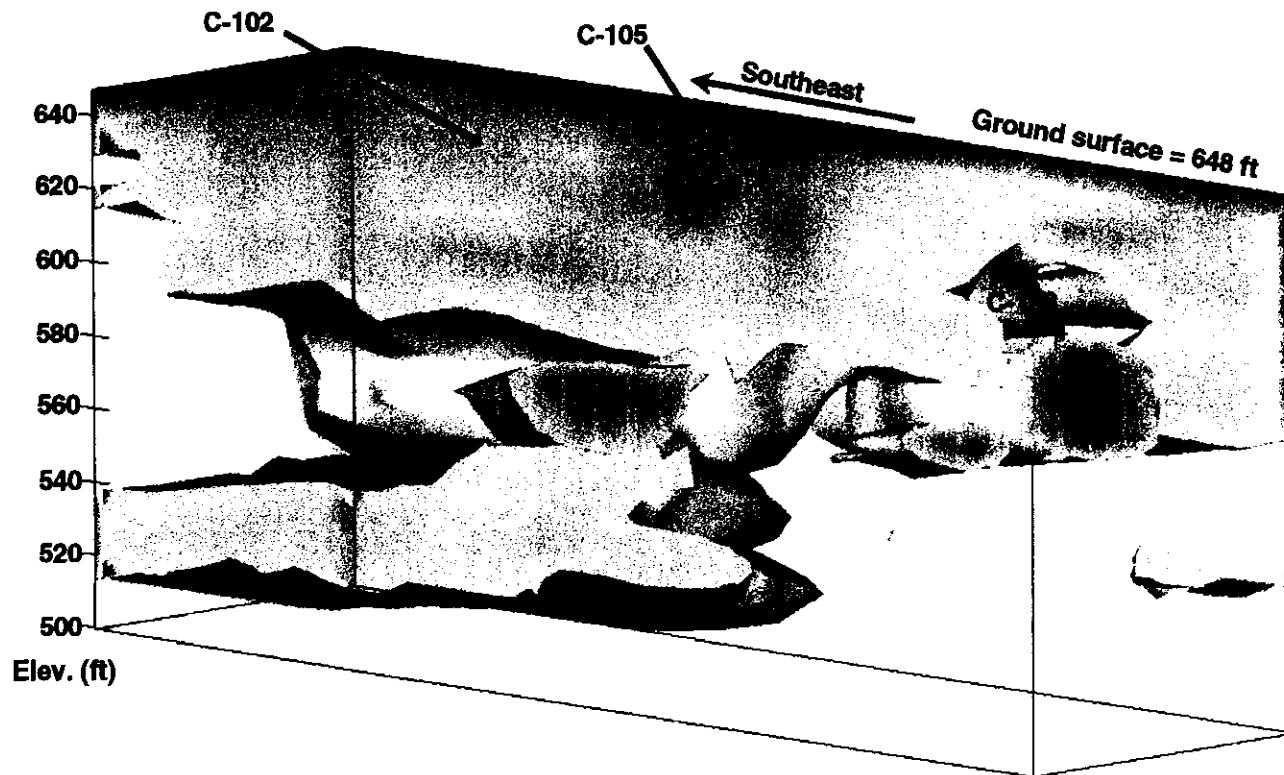


Figure 14-38. Visualization of the <sup>137</sup>Cs and <sup>60</sup>Co Contamination Around Tanks C-102, C-105, and C-108 Viewed From the Southwest



The reader is advised to review Sections 9 and 10 for discussions regarding the limitations of this visualization.

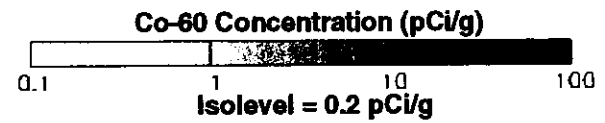
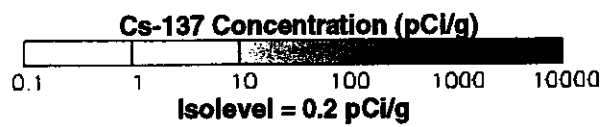


Figure 14-39. Visualization of the <sup>137</sup>Cs and <sup>60</sup>Co Contamination Around Tanks C-102, C-105, and C-108 Viewed From the East

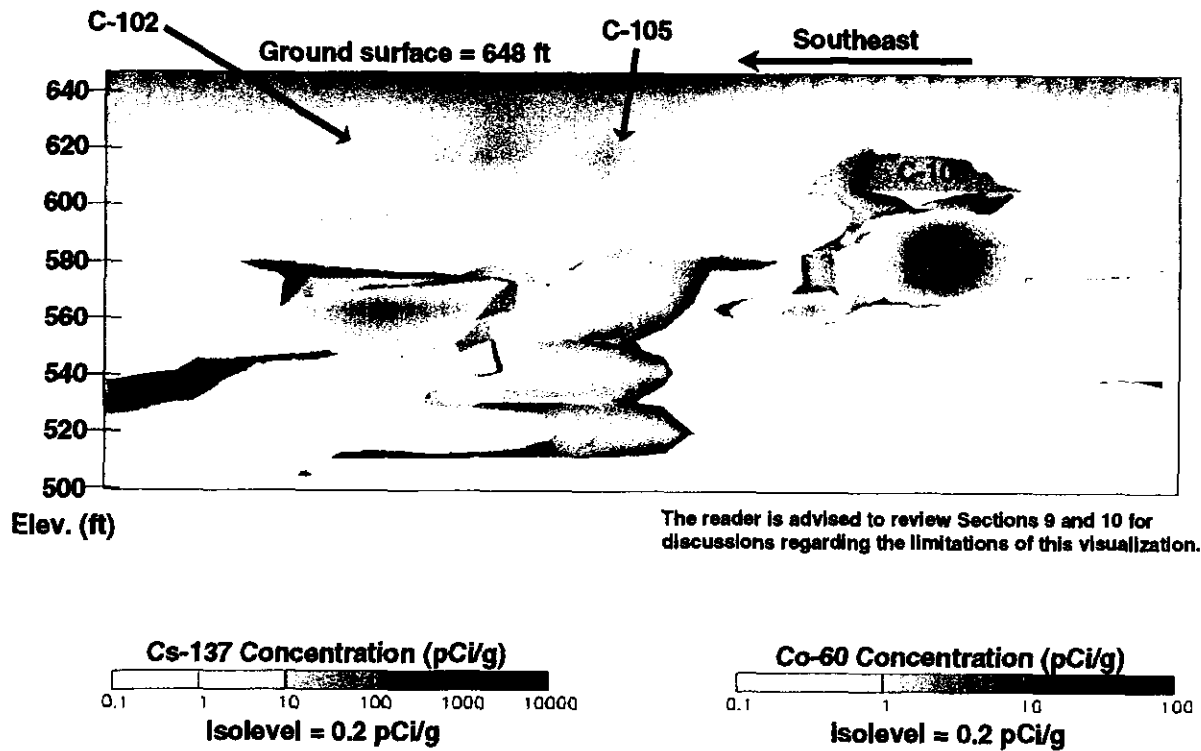


Figure 14-40. Visualization of the <sup>137</sup>Cs and <sup>60</sup>Co Contamination Around Tanks C-102, C-105, and C-108 Viewed From the Northeast

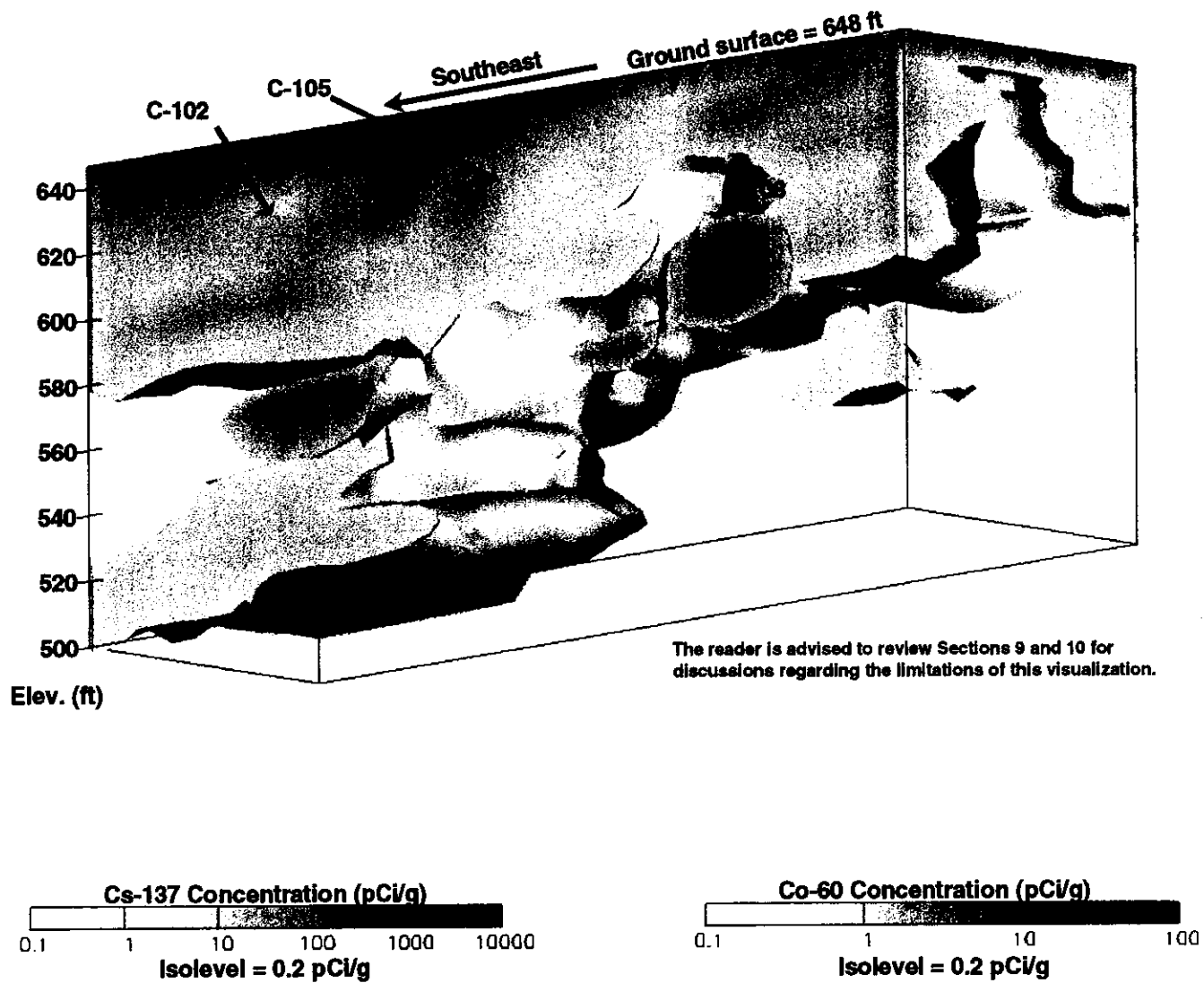
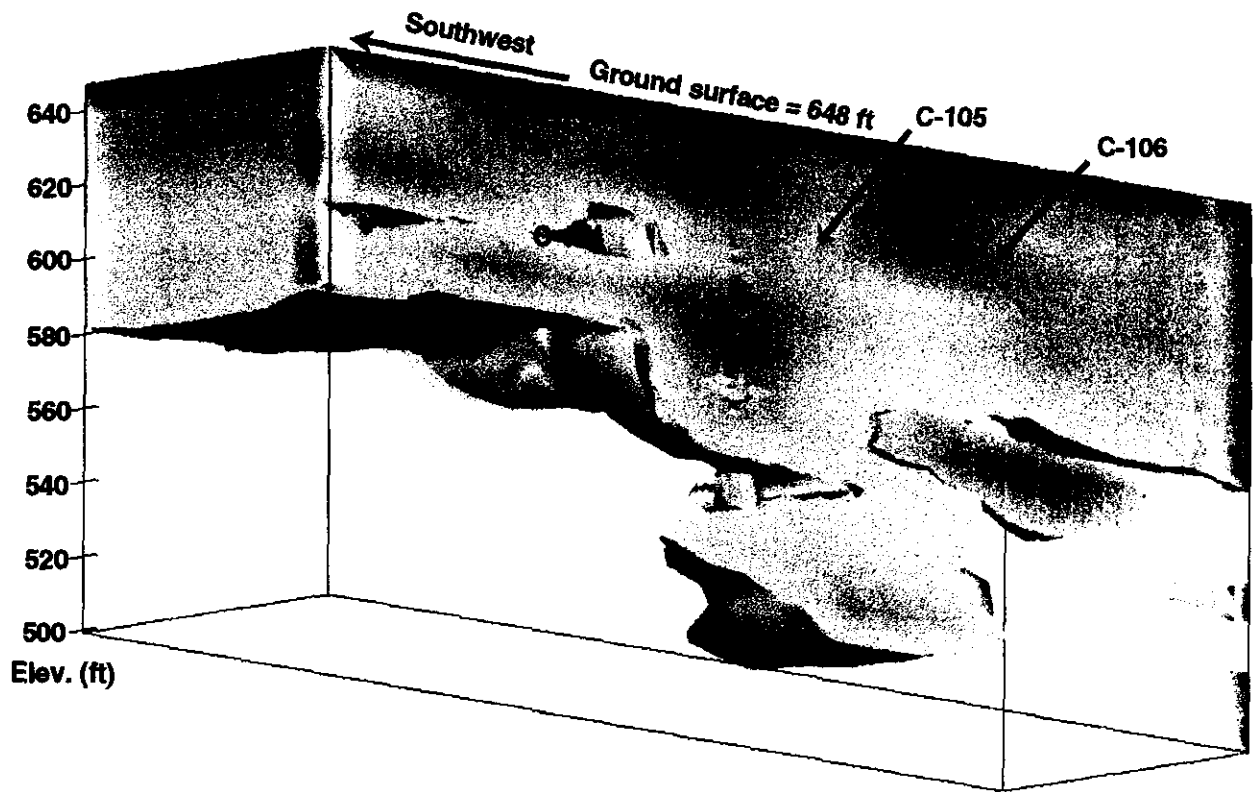


Figure 14-41. Visualization of the <sup>137</sup>Cs and <sup>60</sup>Co Contamination Around Tanks C-102, C-105, and C-108 Viewed From the North



The reader is advised to review Sections 9 and 10 for discussions regarding the limitations of this visualization.

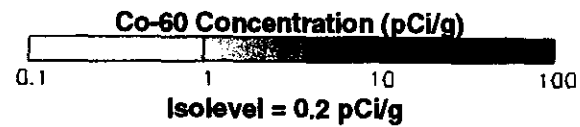
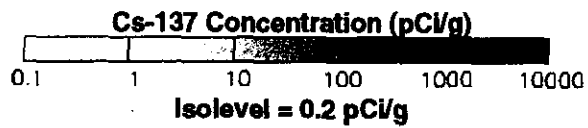
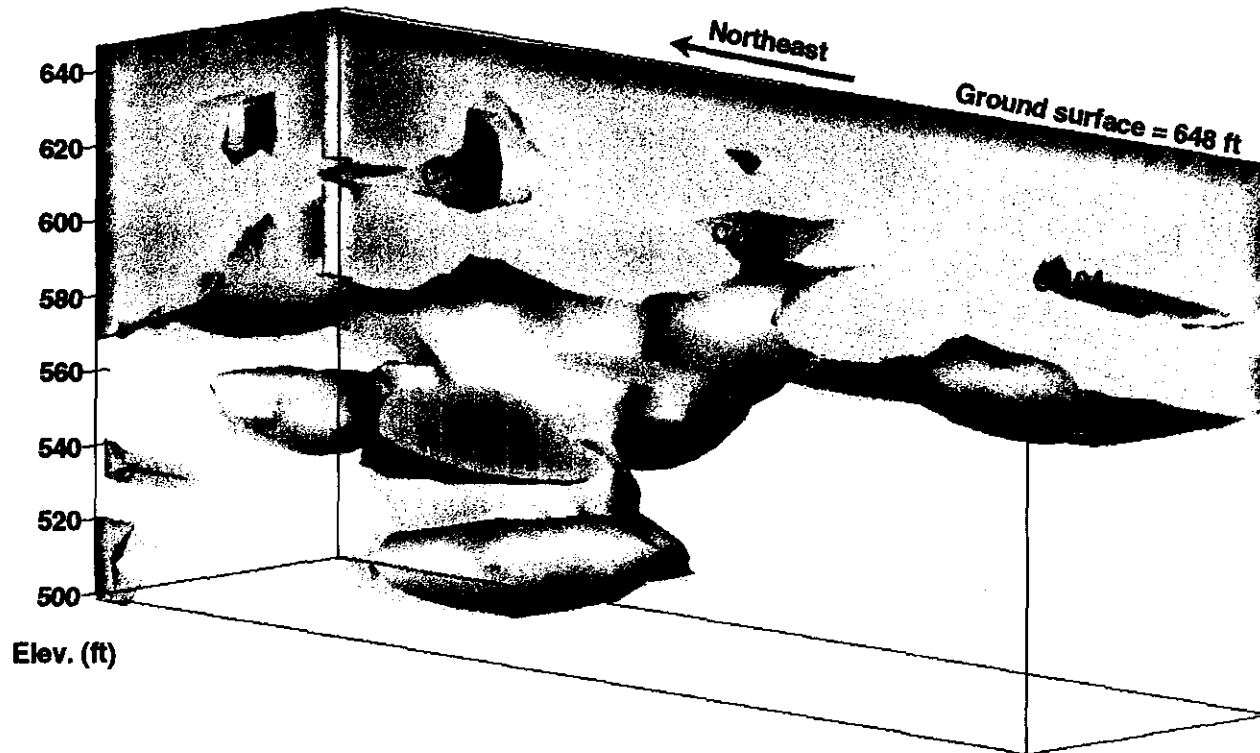


Figure 14-42. Visualization of the <sup>137</sup>Cs and <sup>60</sup>Co Contamination Around Tanks C-104, C-105, and C-106 Viewed From the South



The reader is advised to review Sections 9 and 10 for discussions regarding the limitations of this visualization.

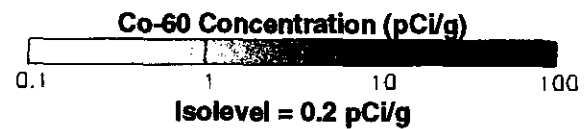
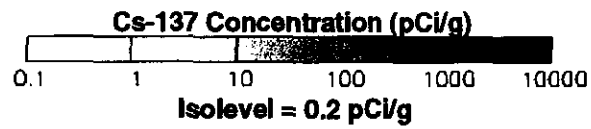
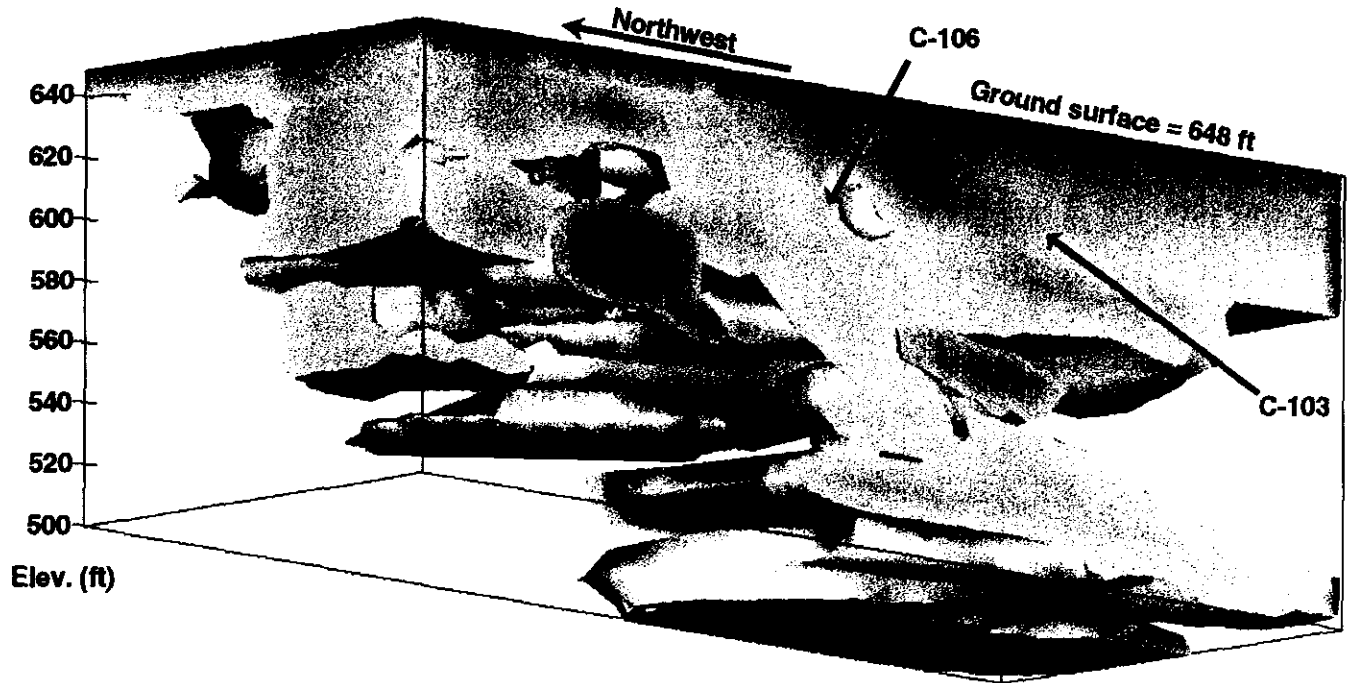


Figure 14-43. Visualization of the <sup>137</sup>Cs and <sup>60</sup>Co Contamination Around Tanks C-104, C-105, and C-106 Viewed From the North



The reader is advised to review Sections 9 and 10 for discussions regarding the limitations of this visualization.

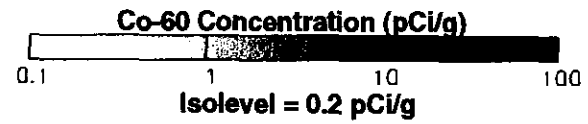
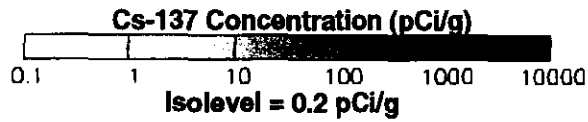


Figure 14-44. Visualization of the <sup>137</sup>Cs and <sup>60</sup>Co Contamination Around Tanks C-103, C-106, and C-109 Viewed From the West

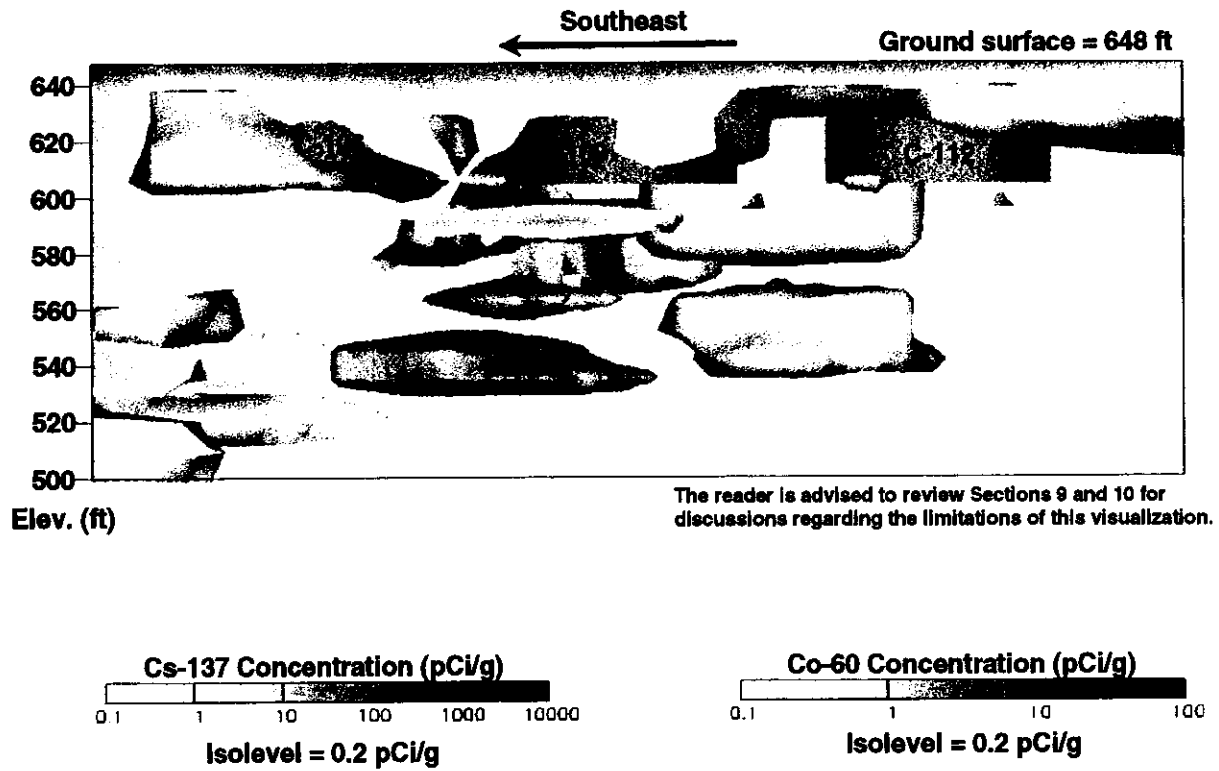


Figure 14-45. Visualization of the <sup>137</sup>Cs and <sup>60</sup>Co Contamination Around Tanks C-106, C-109, and C-112 Viewed From the Northeast

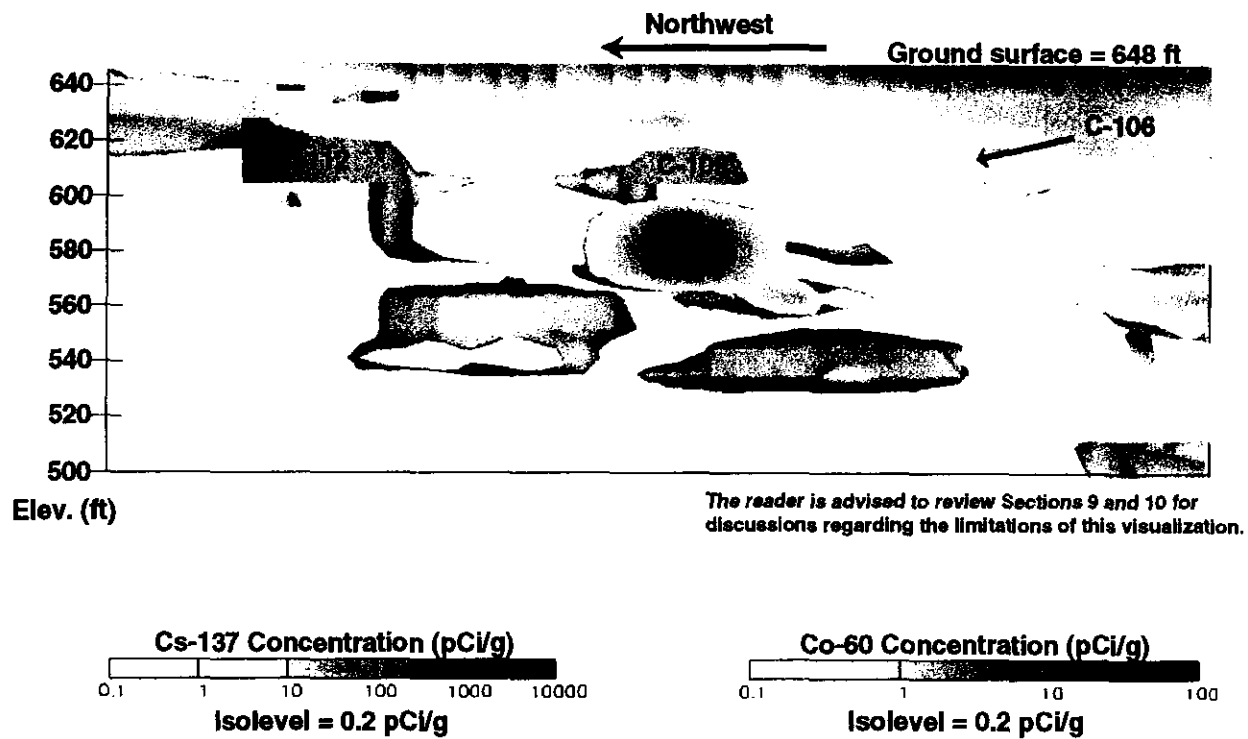


Figure 14-46. Visualization of the <sup>137</sup>Cs and <sup>60</sup>Co Contamination Around Tanks C-106, C-109, and C-112 Viewed From the Southwest

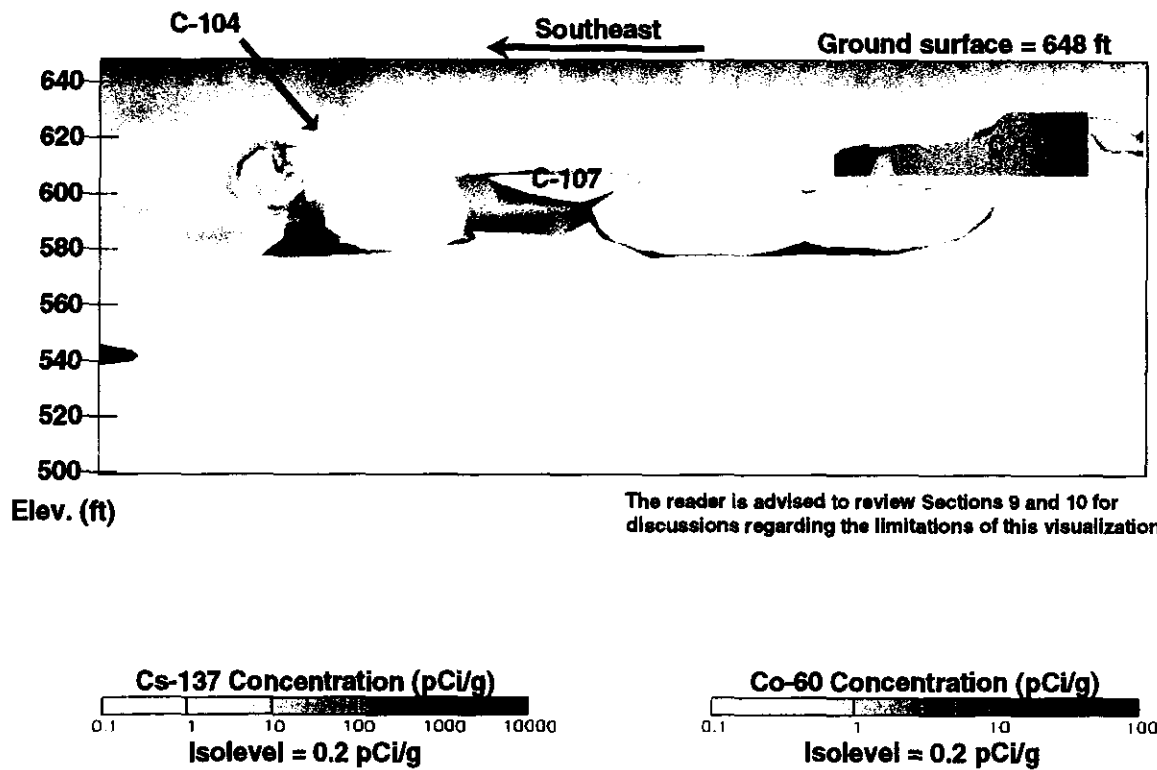


Figure 14-47. Visualization of the <sup>137</sup>Cs and <sup>60</sup>Co Contamination Around Tanks C-104, C-107, and C-110 Viewed From the Northeast

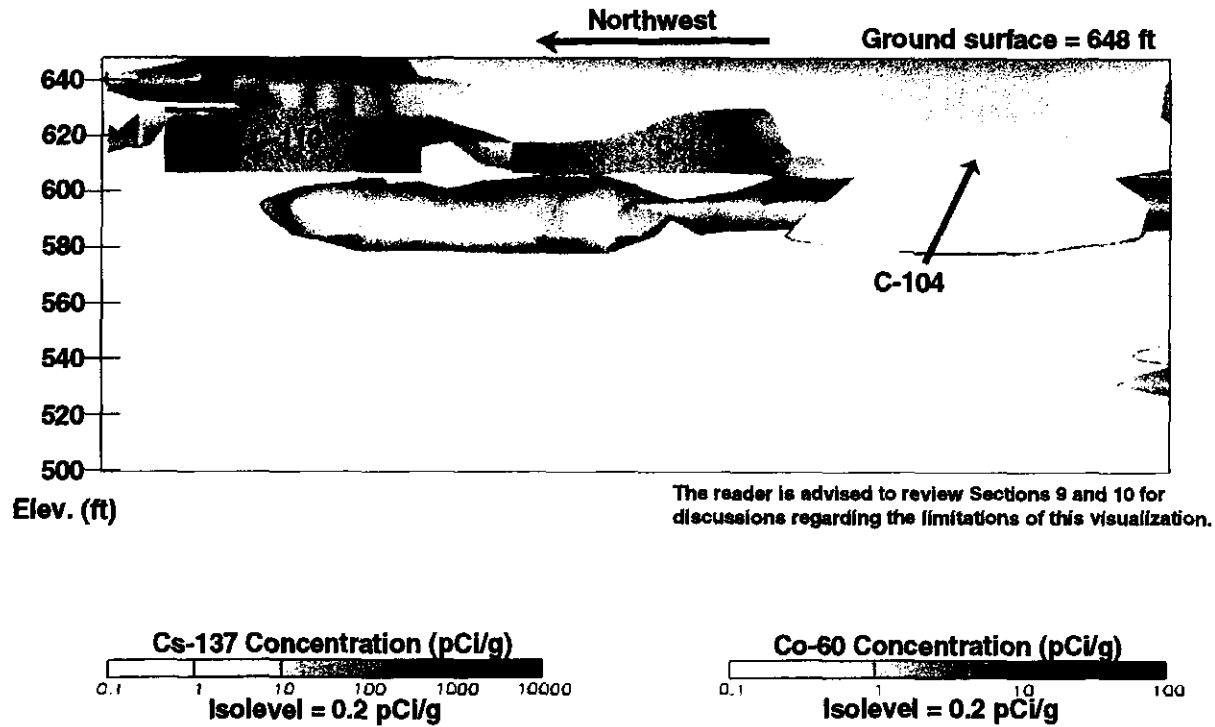


Figure 14-48. Visualization of the <sup>137</sup>Cs and <sup>60</sup>Co Contamination Around Tanks C-104, C-107, and C-110 Viewed From the Southwest

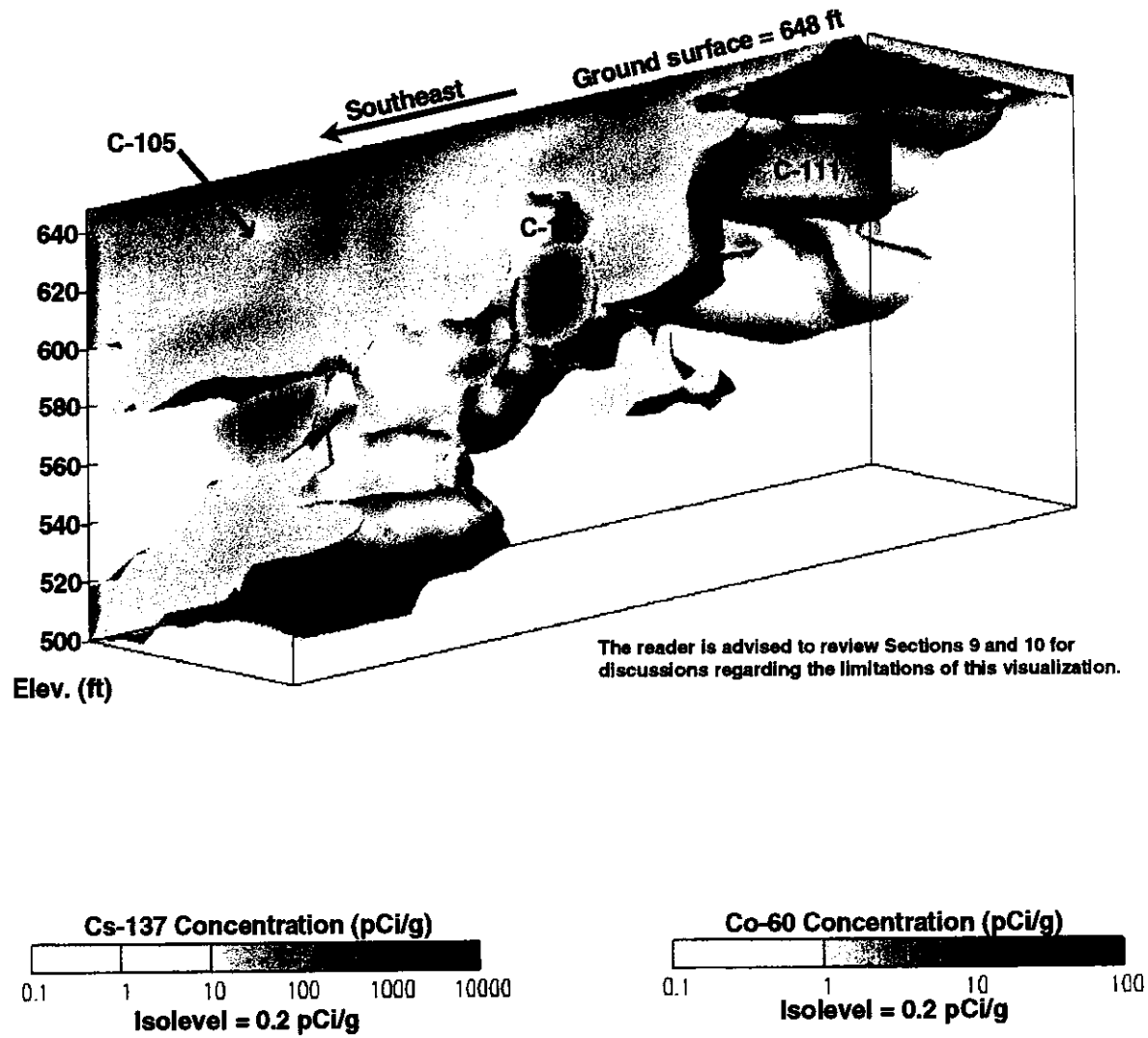
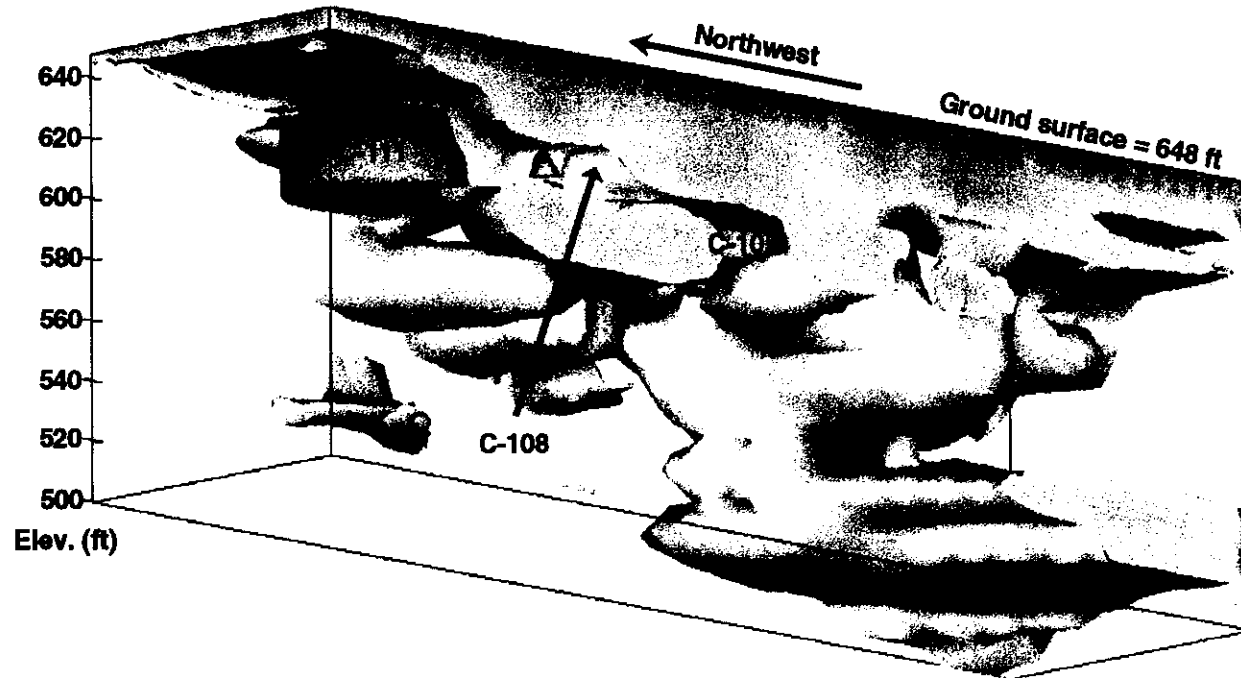


Figure 14-49. Visualization of the <sup>137</sup>Cs and <sup>60</sup>Co Contamination Around Tanks C-105, C-108, and C-111 Viewed From the North



The reader is advised to review Sections 9 and 10 for discussions regarding the limitations of this visualization.

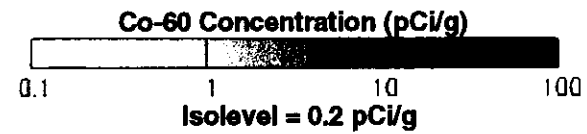
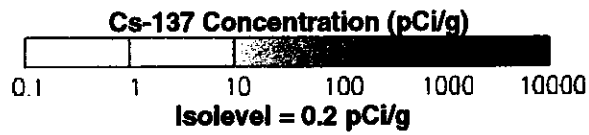


Figure 14-50. Visualization of the <sup>137</sup>Cs and <sup>60</sup>Co Contamination Around Tanks C-105, C-108, and C-111 Viewed From the West

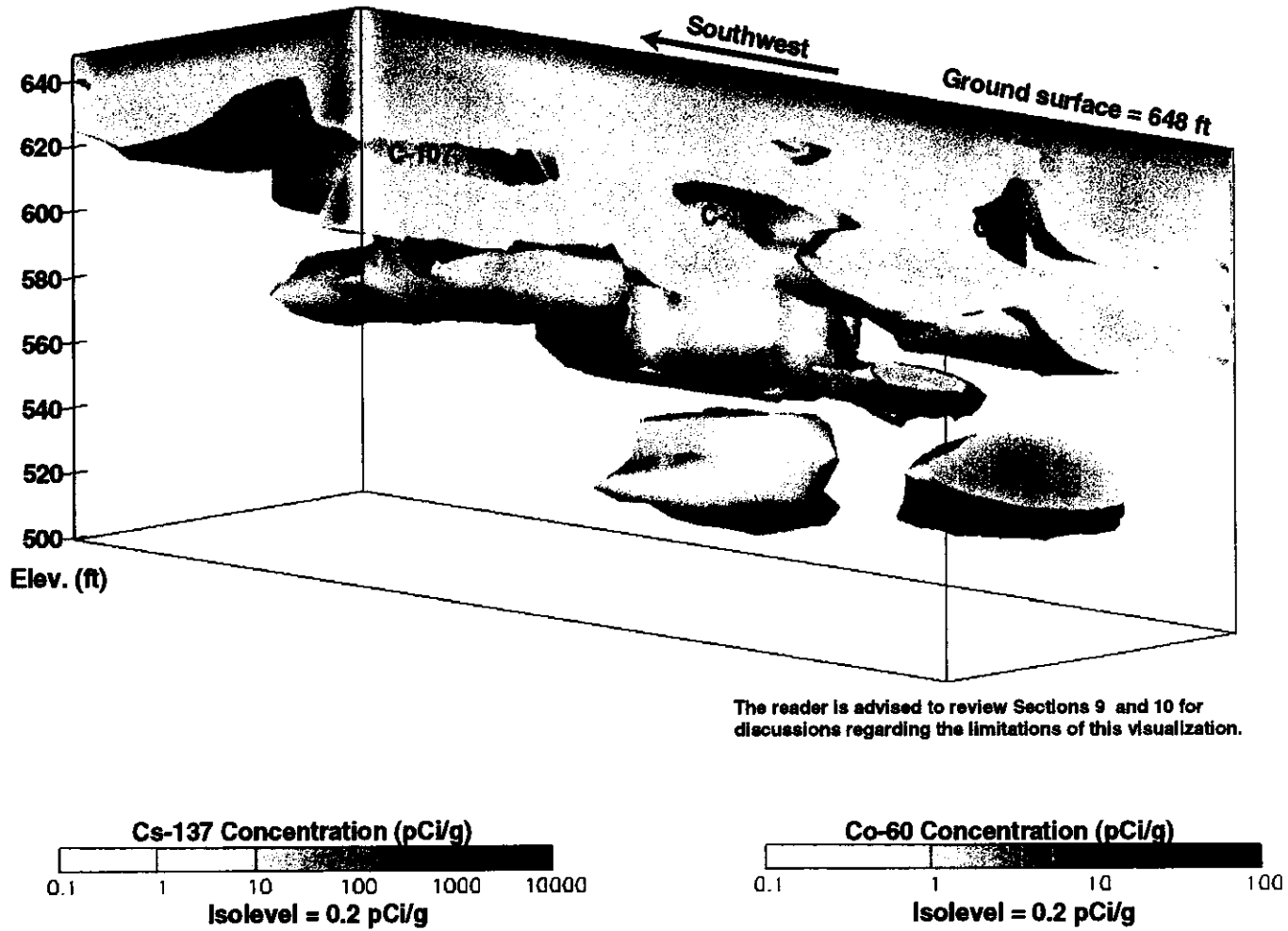


Figure 14-51. Visualization of the <sup>137</sup>Cs and <sup>60</sup>Co Contamination Around Tanks C-107, C-108, and C-109 Viewed From the South

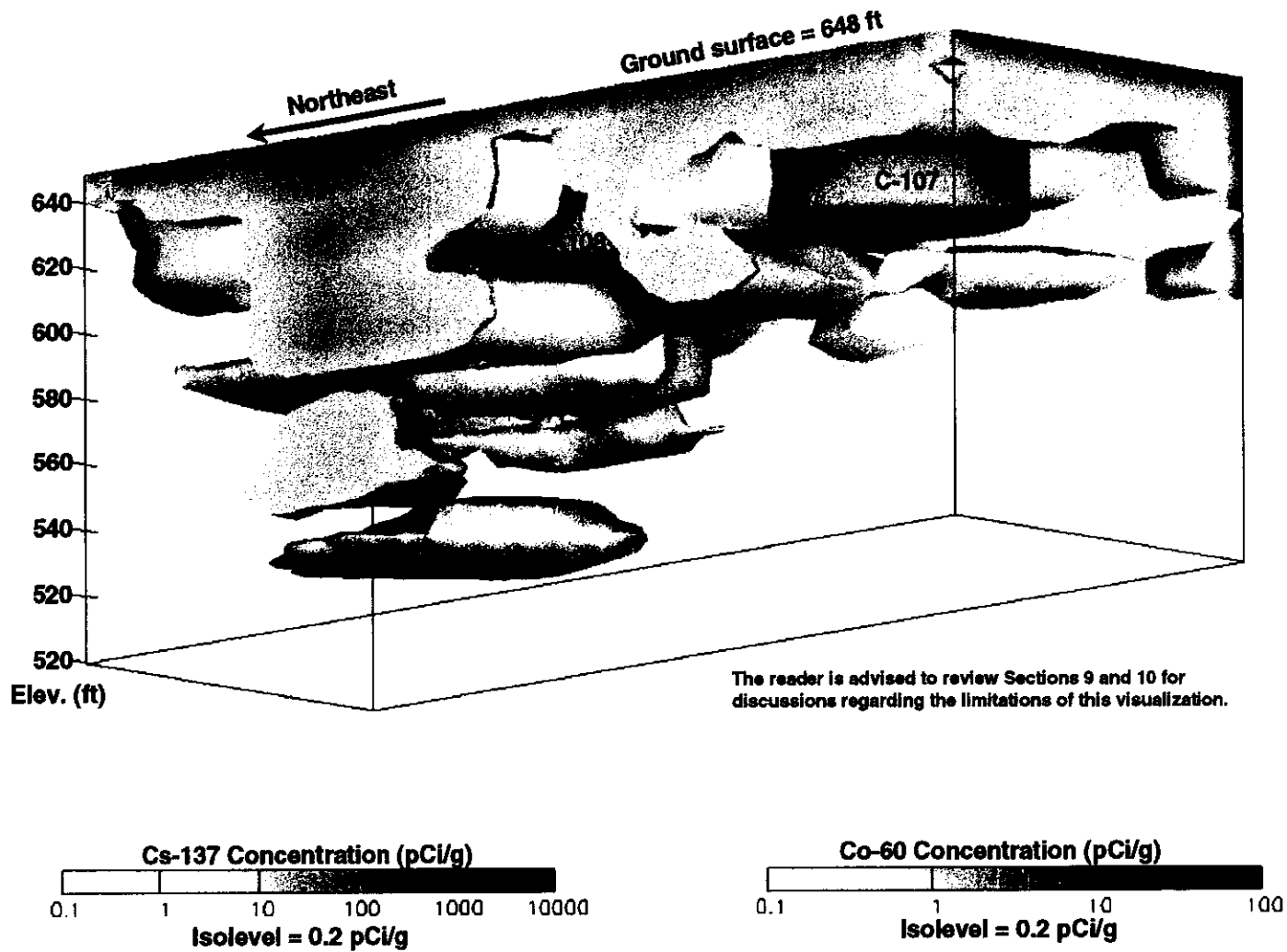
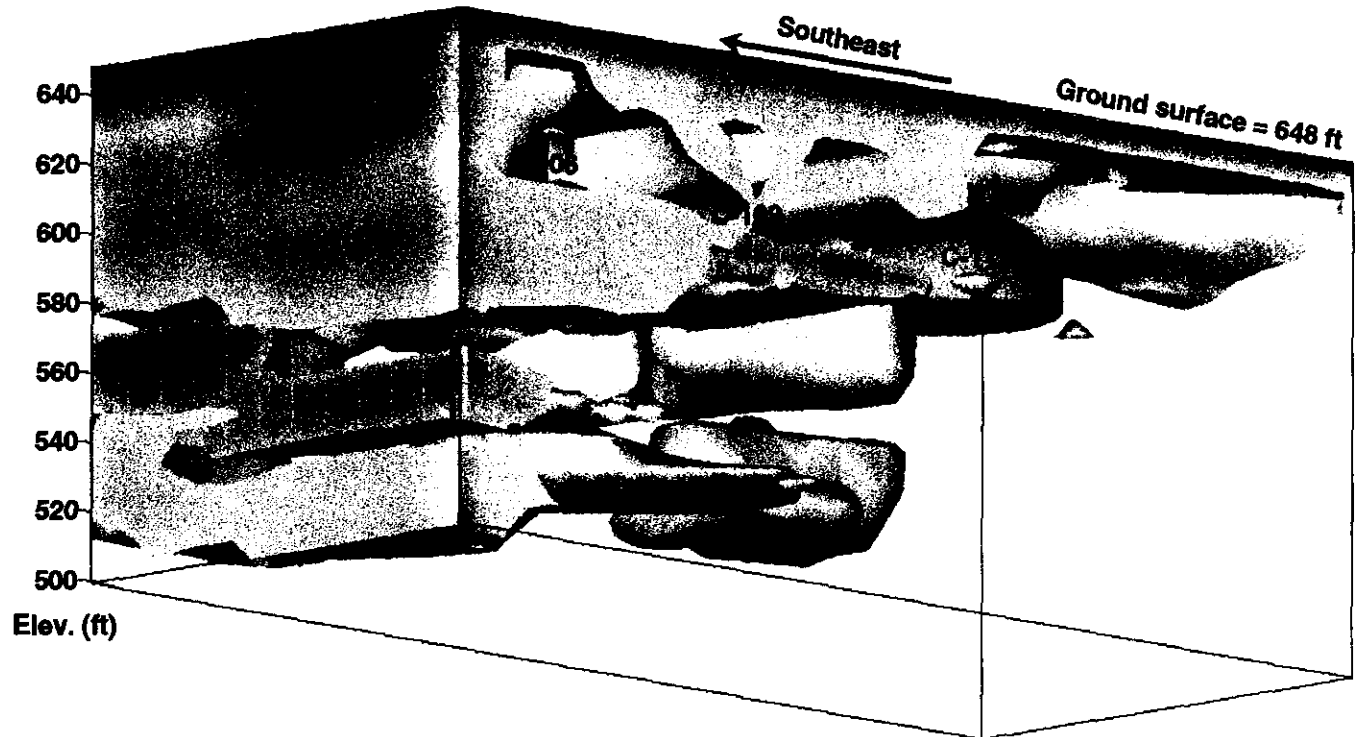


Figure 14-52. Visualization of the <sup>137</sup>Cs and <sup>60</sup>Co Contamination Around Tanks C-107, C-108, and C-109 Viewed From the West



The reader is advised to review Sections 9 and 10 for discussions regarding the limitations of this visualization.

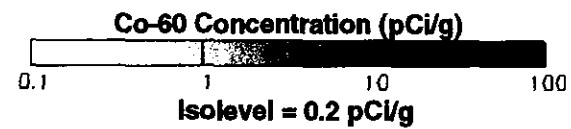
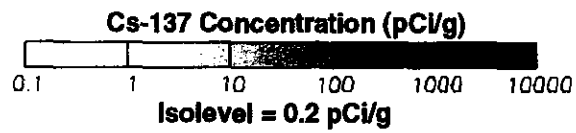
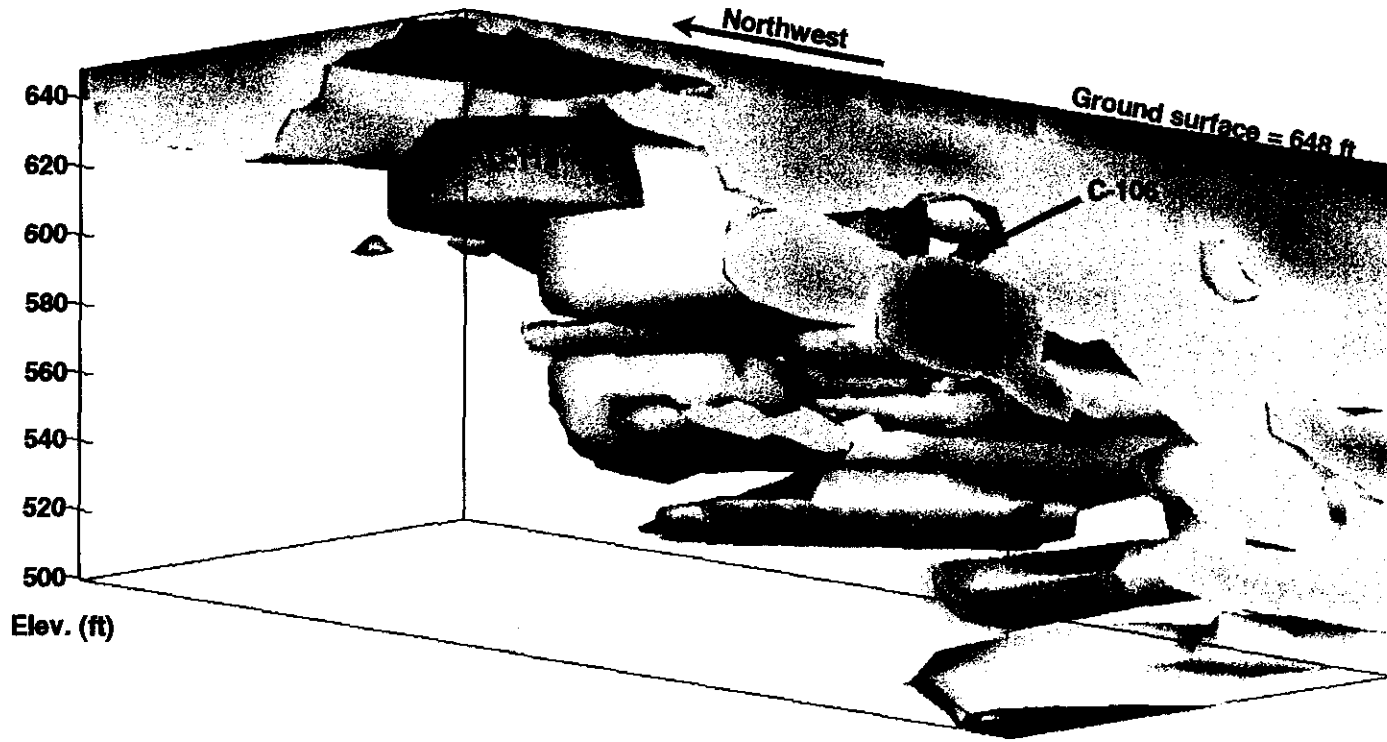


Figure 14-53. Visualization of the <sup>137</sup>Cs and <sup>60</sup>Co Contamination Around Tanks C-106, C-109, and C-112 Viewed From the East



The reader is advised to review Sections 9 and 10 for discussions regarding the limitations of this visualization.

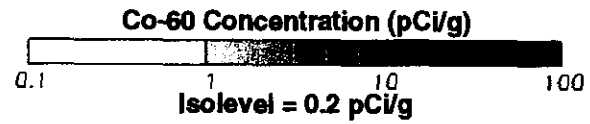
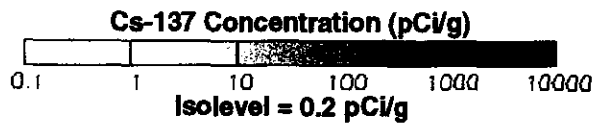


Figure 14-54. Visualization of the <sup>137</sup>Cs and <sup>60</sup>Co Contamination Around Tanks C-106, C-109, and C-112 Viewed From the West

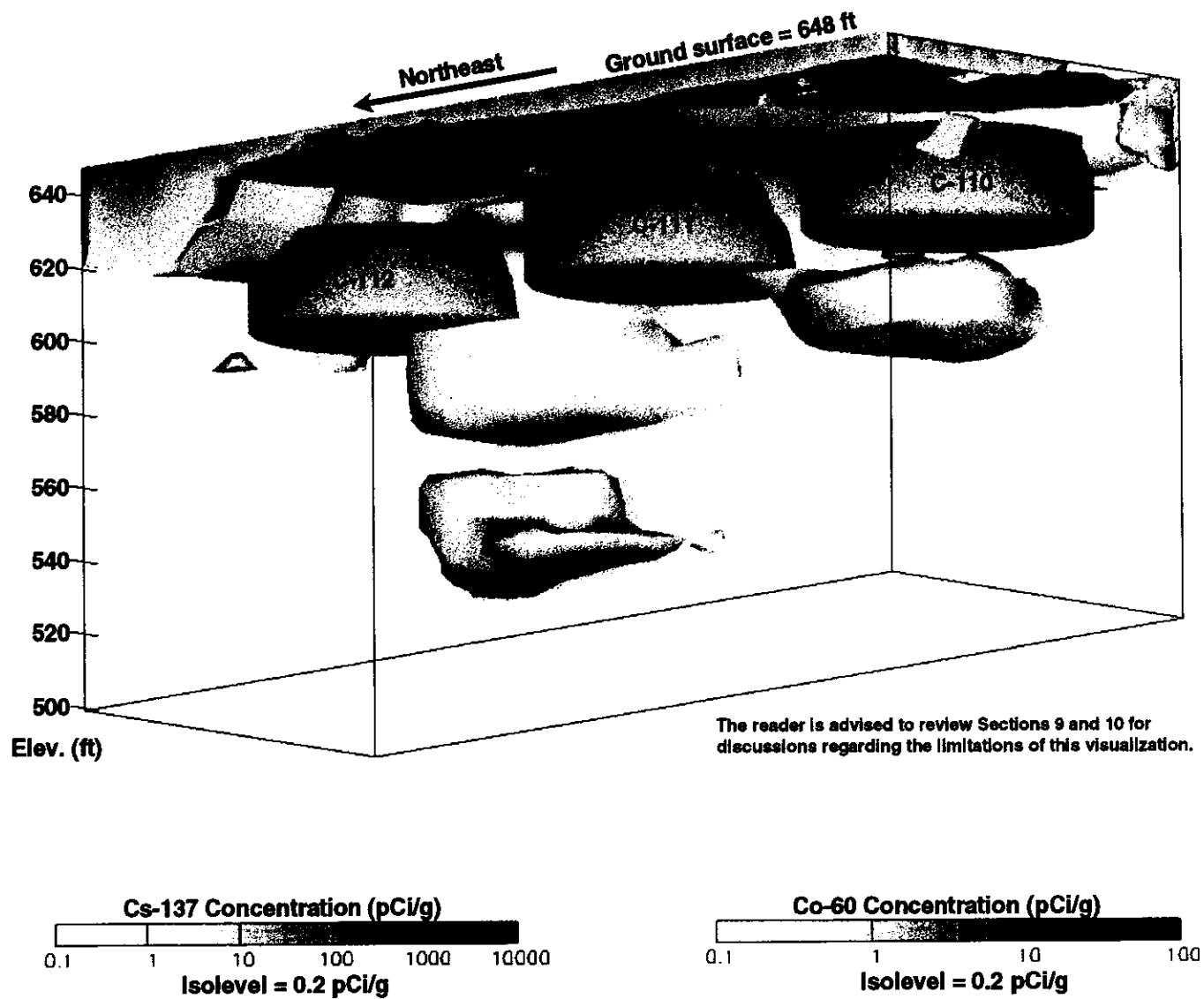
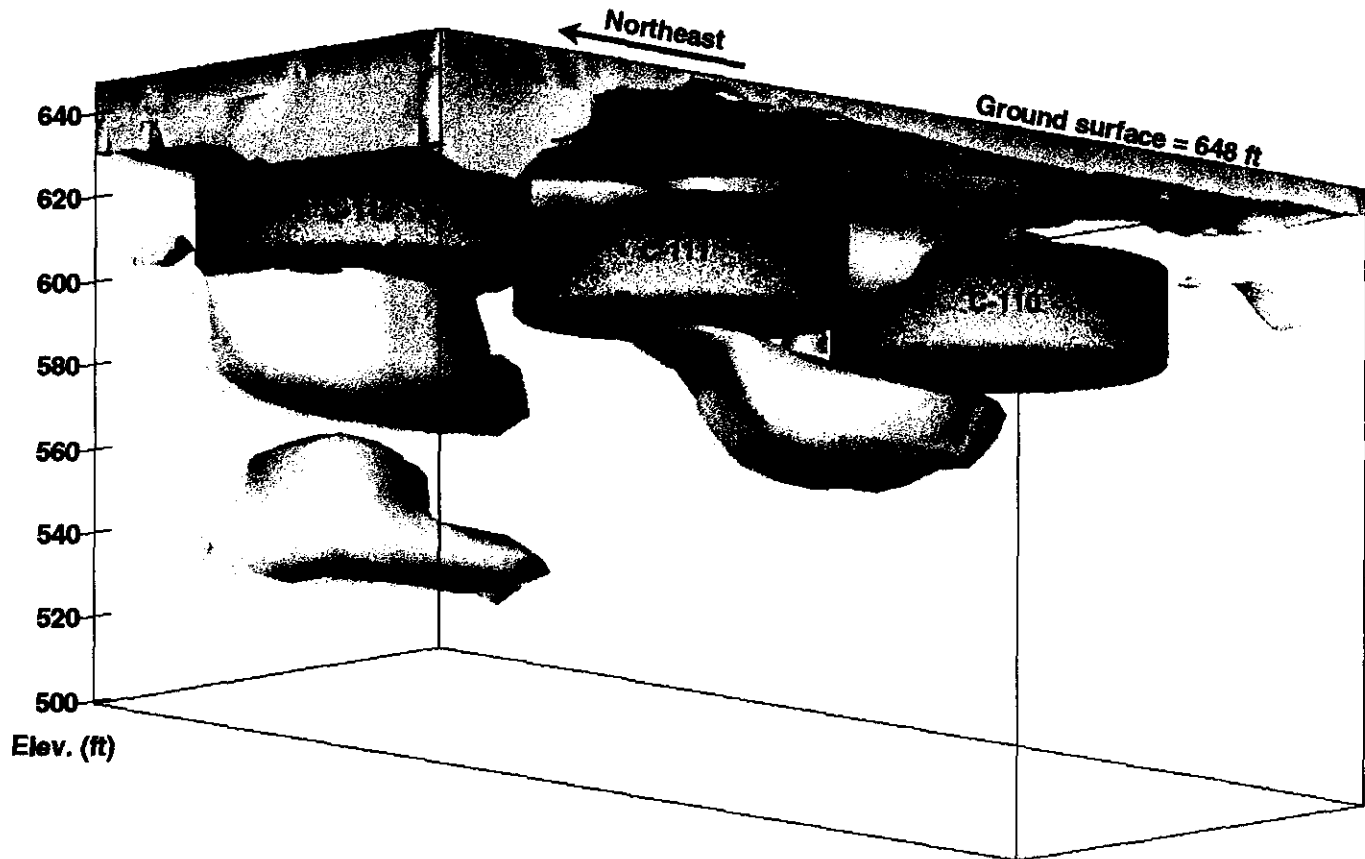


Figure 14-55. Visualization of the <sup>137</sup>Cs and <sup>60</sup>Co Contamination Around Tanks C-110, C-111, and C-112 Viewed From the West



The reader is advised to review Sections 9 and 10 for discussions regarding the limitations of this visualization.

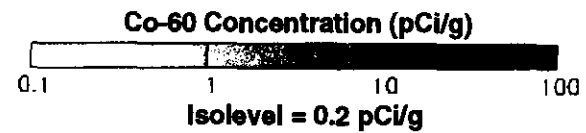
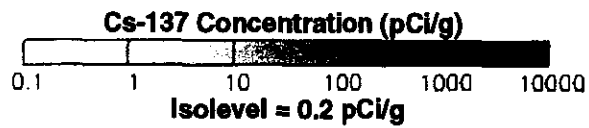


Figure 14-56. Visualization of the <sup>137</sup>Cs and <sup>60</sup>Co Contamination Around Tanks C-110, C-111, and C-112 Viewed From the North

## 15.0 References

Adams, J.P., 1995. *National Low-Level Waste Management Program Radionuclide Report Series*, Vol. 12, *Cobalt-60*, DOE/LLW-128, Idaho National Engineering Laboratory, Idaho Falls, Idaho.

Agnew, S.F., 1995. *Hanford Defined Wastes; Chemical and Radionuclide Compositions*, LAW-94-2657, Rev. 2, Los Alamos National Laboratory, Los Alamos, New Mexico.

\_\_\_\_\_, 1996. *Hanford Chemical and Radionuclide Inventories: HDW Model Rev. 3*, LAU-UR-96-858, Los Alamos National Laboratory, Los Alamos, New Mexico.

\_\_\_\_\_, 1997. *Hanford Tank Chemical and Radionuclide Inventories: HDW Model Rev. 4*, LA-UR-96-3860, Los Alamos National Laboratory, Los Alamos, New Mexico.

Anderson, J.D., 1990. *A History of the 200 Area Tank Farms*, WHC-MR-0132, Westinghouse Hanford Company, Richland, Washington.

Baker, U.R., B.N. Bjornstad, A.J. Busacca, K.R. Fecht, E.P. Kiver, U.L. Moody, J.G. Rigby, O.F. Stradling, and A.M. Tallman, 1991. "Quaternary Geology of the Columbia Plateau" in Morrison, R.B. (ed.), *Quaternary Non-Glacial Geology: Conterminous U.S. Boulder, Colorado*, GSA, *The Geology of North America*, Vol. K-2.

Black, R.F., 1980. *Clastic Dikes of the Pasco Basin, Southeastern Washington*, RHO-BWI-C-64, Rockwell Hanford Operations, Richland, Washington.

Boothe, G.F., 1996. *Predominant Radionuclides in Hanford Site Waste Tanks*, WHC-SD-WM-TI-731, Rev. 0, Westinghouse Hanford Company, Richland, Washington.

Brevick, C.H., L.A. Gaddis, and A.C. Walsh, 1994. *Supporting Document for the Historical Tank Content Estimate for C Tank Farm*, WHC-SD-WM-ER-313, Rev. 0, ICF Kaiser Hanford Company, Richland, Washington.

Brodeur, J.R., 1993. *Assessment of Unsaturated Zone Radionuclide Contamination Around Single-Shell Tanks 241-C-105 and 241-C-106*, WHC-SD-EN-TI-185, Rev. 0, Westinghouse Hanford Company, Richland, Washington.

Brodeur, J.R., C.J. Koizumi, W.H. Ulbricht, and R.K. Price, 1991. "Calibration of a High-Resolution Passive Gamma-Ray Logging System for Nuclear Waste Assessment" in *Proceedings of the 4th Annual International Symposium on Borehole Geophysics for Minerals, Geotechnical and Groundwater Applications*, sponsored by the Minerals and Geotechnical Logging Society of the Society of Professional Well Log Analysts, Houston, Texas.

- Caggiano, J.A., and S.M. Goodwin, 1991. *Interim Status Groundwater Monitoring Plan for the Single-Shell Tanks*, WHC-SD-EN-AP-012, Westinghouse Hanford Company, Richland, Washington.
- Carboneau, M.L., and R.S. Garcia, 1994. *National Low-Level Waste Management Program Radionuclide Report Series*, Vol. 9, *Plutonium-241*, DOE/LLW-125, Idaho National Engineering Laboratory, Idaho Falls, Idaho.
- Carboneau, M.L., J.P. Adams, and R.S. Garcia, 1994a. *National Low-Level Waste Management Program Radionuclide Report Series*, Vol. 7, *Strontium-90*, DOE/LLW-123, Idaho National Engineering Laboratory, Idaho Falls, Idaho.
- Carboneau, M.L., C.S. Olsen, and R.S. Garcia, 1994b. *National Low-Level Waste Management Program Radionuclide Report Series*, Vol. 6, *Cesium-137*, DOE/LLW-122, Idaho National Engineering Laboratory, Idaho Falls, Idaho.
- Catlin, R.J., 1980. *Assessment of the Surveillance Program of the High-Level Waste Storage Tanks at Hanford*, report to the U.S. Department of Energy Assistant Secretary for Environment, U.S. Department of Energy, Washington, D.C.
- Conaway, J.G., and P.G. Killeen, 1978. "Quantitative Uranium Determinations from Gamma-Ray Logs by Application of Digital Time Series Analysis," *Geophysics*, Vol. 43, No. 6.
- Connelly M.P., B.H. Ford, and J.V. Borghese, 1992. *Hydrogeologic Model for the 200 West Groundwater Aggregate Area*, WHC-SD-EN-TI-014, Rev. 0, Westinghouse Hanford Company, Richland, Washington.
- David, M., 1977. *Geostatistical Ore Reserve Estimation*, Elsevier, New York.
- Delaney, C.D., K.A. Lindsey, and S.P. Reidel, 1991. *Geology and Hydrology of the Hanford Site: A Standardized Text for Use in Westinghouse Hanford Company Documents and Reports*, WHC-SD-ER-TI-0003, Westinghouse Hanford Company, Richland, Washington.
- Dresel, P.E., P.D. Thome, S.P. Lutrell, B.M. Gillespie, W.D. Webber, J.K. Merz, J.T. Rieger, M.A. Chamness, S.K. Wurstner, and B.E. Opitz, 1995. *Hanford Site Ground-Water Monitoring for 1994*, PNL-10698, Pacific Northwest National Laboratory, Richland, Washington.
- Erdtmann, G., and W. Soyka, 1979. *The Gamma Rays of the Radionuclides: Tables for Applied Gamma Ray Spectrometry*, Verlag Chemie, Weinheim, New York.
- Fayer, M.J., and T.B. Walters, 1995. *Estimated Recharge Rates at the Hanford Site*, PNL-10285, Pacific Northwest Laboratory, Richland, Washington.
- General Electric Company (GE), 1989. *Nuclides and Isotopes, Fourteenth Edition, Chart of the Nuclides*, General Electric Company, San Jose, California.

- Hanlon, B.M., 1997. *Waste Tank Summary Report for Month Ending June 30, 1997*, HNF-EP-0182-111, Lockheed Martin Hanford Corporation, Richland, Washington.
- Isaacson, R.E., 1982. *Supporting Information for the Scientific Basis for Establishing Dry-Well Monitoring Frequencies*, RHO-RE-EV-4, Rockwell Hanford Operations, Richland, Washington.
- Johnson, V.G., 1993. *Westinghouse Hanford Company Operational Groundwater Status Report, 1990-1992*, WHC-EP-0595, Westinghouse Hanford Company, Richland, Washington.
- Journel, A.G., and Ch. J. Huijbregts, 1978. *Mining Geostatistics*, Academic Press, New York.
- Koizumi, C.J., 1993. *Calibration Standards for Passive Gamma-Ray Logging at the Hanford Site*, WHC-SD-EN-TI-192, Westinghouse Hanford Company, Richland, Washington.
- Koizumi, C.J., J.R. Brodeur, W.H. Ulbricht, and R.K. Price, 1991. *Calibration of the R.S. HPGc Spectral Gamma Ray Logging System*, WHC-EP-0464, Westinghouse Hanford Company, Richland, Washington.
- Koizumi, C.J., J.R. Brodeur, R.K. Price, J.E. Meisner, and D.C. Stromswold, 1994. *High-Resolution Gamma-Ray Spectrometry Logging for Contamination Assessment*, Nuclear Geophysics, Vol. 8, No. 2, pp. 149-164.
- Kos, S.E., 1995. *Assessment of Vadose Zone Radionuclide Contamination Around Single Shell Tank 241-C-103*, WHC-SD-EN-TI-299, Rev. 0, Westinghouse Hanford Company, Richland, Washington.
- Lederer, C.M., and V.S. Shirley (eds.), 1978. *Table of Isotopes 7th Edition*, John Wiley and Sons, Inc., New York.
- Lindsey, K.A., 1992. *Geologic Setting of the 200 East Area: An Update*, WHC-SD-EN-TI-012, Rev. 0, Westinghouse Hanford Company, Richland, Washington.
- \_\_\_\_\_, 1993. Westinghouse Hanford Company Internal Memo, Subject: "Geohydrologic Setting, Flow and Transport Parameters for the Single Shell Tank Farms," 81231-93-060, Westinghouse Hanford Company, Richland, Washington.
- \_\_\_\_\_, 1995. *Miocene- to Pliocene-Aged Suprabasalt Sediments of the Hanford Site, South-Central Washington*, BHI-00184, Bechtel Hanford, Inc., Richland, Washington.
- MACTEC-ERS, 1996. *General Administrative Procedures Manual*, MAC-1000, Grand Junction Office, Grand Junction Office, Grand Junction, Colorado.
- Maxfield, H.L., 1979. *Handbook of the 200 Areas Waste Sites*, RHO-CD-673, Rockwell Hanford Operations, Richland, Washington.

Pacific Northwest National Laboratory (PNNL), 1997a. *Hanford Site 1996 Environmental Report*, PNNL-11472, prepared by Pacific Northwest National Laboratory for the U.S. Department of Energy, Richland, Washington.

\_\_\_\_\_, 1997b. *Hanford Site Groundwater Monitoring for Fiscal Year 1996*, PNNL-11470, prepared by Pacific Northwest National Laboratory for the U.S. Department of Energy, Richland, Washington.

Price, W.H., and K.R. Fecht, 1976. *Geology of the 241-C Tank Farm*, ARH-LD-133, Atlantic Richfield Hanford Company, Richland, Washington.

Reidel, S.P., K.R. Fecht, M.C. Hagoood, and T.L. Tolan, 1989. "The Geologic Evolution of the Central Columbia Plateau," in *Volcanism and Tectonism in the Columbia River Flood-Basalt Province*, Special Paper 239, edited by S.P. Reidel and P.R. Hooper, Geological Society of America, Boulder, Colorado, pp. 247-264.

Rudin, M.J., and R.S. Garcia, 1992a. *National Low-Level Waste Management Program Radionuclide Report Series*, Vol. 1, *Introduction*, DOE/LLW-117, Idaho National Engineering Laboratory, Idaho Falls, Idaho.

\_\_\_\_\_, 1992b. *National Low-Level Waste Management Program Radionuclide Report Series*, Vol. 4, *Iodine-129*, DOE/LLW-120, Idaho National Engineering Laboratory, Idaho Falls, Idaho.

Rudin, M.J., C. Stanton, R.G. Patterson, and R.S. Garcia, 1992. *National Low-Level Waste Management Program Radionuclide Report Series*, Vol. 2, *Technetium-99*, DOE/LLW-118, Idaho National Engineering Laboratory, Idaho Falls, Idaho.

Scott, K.V., 1993. *Engineering Assessment of Hanford Single-Shell High-Level Waste Tank Leak Detection*, WHC-SD-WM-EX-264, Rev. 0, Westinghouse Hanford Company, Richland, Washington.

Tolan, T.L., and S.P. Reidel, 1989. "Structure Map of a Portion of the Columbia River Flood Basalt Province" in *Volcanism and Tectonism in the Columbia River Flood-Basalt Province*, Special Paper 239, edited by S.P. Reidel and P.R. Hooper, Geologic Society of America, Boulder, Colorado, Plate 1.

U.S. Department of Energy (DOE), 1993a. *200 East Groundwater Aggregate Area Management Study Report*, DOE/RL-92-19, Rev. 0, Westinghouse Hanford Company, Richland, Washington.

\_\_\_\_\_, 1993b. *PUREX Source Aggregate Area Management Study Report*, DOE/RL-92-04, Rev. 0, Westinghouse Hanford Company, Richland, Washington.

U.S. Department of Energy (DOE), 1995a. *Vadose Zone Characterization Project at the Hanford Tank Farms, Calibration of Two Spectral Gamma-Ray Logging Systems for Baseline Characterization Measurements in the Hanford Tank Farms*, GJPO-HAN-1, prepared by Rust Geotech for the Grand Junction Projects Office, Grand Junction, Colorado, August.

\_\_\_\_\_, 1995b. *Vadose Zone Characterization Project at the Hanford Tank Farms, Evaluation of In-Tank Leak Detection Methods and Recommendations for a Tank Leak-Verification and Monitoring System*, DOE/ID/12584-227, prepared by Rust Geotech for the Grand Junction Projects Office, Grand Junction, Colorado, August.

\_\_\_\_\_, 1995c. *Vadose Zone Characterization Project at the Hanford Tank Farms, Spectral Gamma-Ray Borehole Geophysical Logging Characterization and Baseline Monitoring Plan for the Hanford Single-Shell Tanks*, P-GJPO-1786, prepared by Rust Geotech for the Grand Junction Projects Office, Grand Junction, Colorado, July.

\_\_\_\_\_, 1996a. *Quarterly Report of RCRA Groundwater Monitoring Data for Period July 1, 1995 through September 30, 1995*, DOE/RL-95-69-3, U.S. Department of Energy, Richland Operations Office, Richland, Washington.

\_\_\_\_\_, 1996b. *Single-Shell Tank Closure Work Plan*, DOE/RL-89-16, Rev. 1, U.S. Department of Energy, Richland Operations Office, Richland, Washington.

\_\_\_\_\_, 1996c. *Vadose Zone Characterization Project at the Hanford Tank Farms, Biannual Recalibration of Two Spectral Gamma-Ray Logging Systems Used for Baseline Characterization Measurements in the Hanford Tank Farms*, GJPO-HAN-3, prepared by Rust Geotech for the Grand Junction Projects Office, Grand Junction, Colorado, May.

\_\_\_\_\_, 1996d. *Vadose Zone Characterization Project at the Hanford Tank Farms, Second Biannual Recalibration of Two Spectral Gamma-Ray Logging Systems Used for Baseline Characterization Measurements at the Hanford Tank Farms*, GJPO-HAN-5, prepared by Rust Geotech for the Grand Junction Projects Office, Grand Junction, Colorado, August.

\_\_\_\_\_, 1997a. *Hanford Tank Farms Vadose Zone, Calibration Plan for Spectral Gamma-Ray Logging Systems*, MAC-VZCP-1.7.3, Rev. 1, prepared by MACTEC-ERS for the Grand Junction Office, Grand Junction, Colorado.

\_\_\_\_\_, 1997b. *Hanford Tank Farms Vadose Zone, Data Analysis Manual*, MAC-VZCP 1.7.9, Rev. 1, prepared by MACTEC-ERS for the Grand Junction Office, Grand Junction, Colorado.

\_\_\_\_\_, 1997c. *Hanford Tank Farms Vadose Zone, Health and Safety Plan*, MAC-VZCP 1.7.4, Rev. 2, prepared by MACTEC-ERS for the Grand Junction Office, Grand Junction, Colorado.

U.S. Department of Energy (DOE), 1997d. *Hanford Tank Farms Vadose Zone, High-Resolution Passive Spectral Gamma-Ray Logging Procedures*, MAC-VZCP 1.7.10-1, Rev. 2, prepared by MACTEC-ERS for the Grand Junction Office, Grand Junction, Colorado.

\_\_\_\_\_, 1997e. *Hanford Tank Farms Vadose Zone, Preventive Maintenance Procedure for the Spectral Gamma Logging System*, MAC-VZCP 1.7.10-2, Rev. 1, prepared by MACTEC-ERS for the Grand Junction Office, Grand Junction, Colorado.

\_\_\_\_\_, 1997f. *Hanford Tank Farms Vadose Zone, Project Management Plan*, MAC-VZCP 1.7.2, Rev. 1, prepared by MACTEC-ERS for the Grand Junction Office, Grand Junction, Colorado.

\_\_\_\_\_, 1997g. *Hanford Tank Farms Vadose Zone, Third Biannual Recalibration of Two Spectral Gamma-Ray Logging Systems Used for Baseline Characterization Measurements in the Hanford Tank Farms*, GJO-HAN-13, prepared by MACTEC-ERS for the Grand Junction Office, Grand Junction, Colorado.

\_\_\_\_\_, 1997h. *TWRS Vadose Zone Contamination Issue Expert Panel Status Report*, DOE/RL-97-49, Rev. 0, Flour Daniel Hanford, Inc., Richland, Washington.

\_\_\_\_\_, 1997i. *Vadose Zone Characterization Project at the Hanford Tank Farms, Tank Summary Data Report for Tank C-101*, GJ-HAN-85, prepared by MACTEC-ERS for the Grand Junction Office, Grand Junction, Colorado.

\_\_\_\_\_, 1997j. *Vadose Zone Characterization Project at the Hanford Tank Farms, Tank Summary Data Report for Tank C-102*, GJ-HAN-86, prepared by MACTEC-ERS for the Grand Junction Office, Grand Junction, Colorado.

\_\_\_\_\_, 1997k. *Vadose Zone Characterization Project at the Hanford Tank Farms, Tank Summary Data Report for Tank C-103*, GJ-HAN-82, prepared by MACTEC-ERS for the Grand Junction Office, Grand Junction, Colorado.

\_\_\_\_\_, 1997l. *Vadose Zone Characterization Project at the Hanford Tank Farms, Tank Summary Data Report for Tank C-104*, GJ-HAN-87, prepared by MACTEC-ERS for the Grand Junction Office, Grand Junction, Colorado.

\_\_\_\_\_, 1997m. *Vadose Zone Characterization Project at the Hanford Tank Farms, Tank Summary Data Report for Tank C-105*, GJ-HAN-83, prepared by MACTEC-ERS for the Grand Junction Office, Grand Junction, Colorado.

\_\_\_\_\_, 1997n. *Vadose Zone Characterization Project at the Hanford Tank Farms, Tank Summary Data Report for Tank C-106*, GJ-HAN-84, prepared by MACTEC-ERS for the Grand Junction Office, Grand Junction, Colorado.

U.S. Department of Energy (DOE), 1997o. *Vadose Zone Characterization Project at the Hanford Tank Farms, Tank Summary Data Report for Tank C-107*, GJ-HAN-88, prepared by MACTEC-ERS for the Grand Junction Office, Grand Junction, Colorado.

\_\_\_\_\_, 1997p. *Vadose Zone Characterization Project at the Hanford Tank Farms, Tank Summary Data Report for Tank C-108*, GJ-HAN-90, prepared by MACTEC-ERS for the Grand Junction Office, Grand Junction, Colorado.

\_\_\_\_\_, 1997q. *Vadose Zone Characterization Project at the Hanford Tank Farms, Tank Summary Data Report for Tank C-109*, GJ-HAN-91, prepared by MACTEC-ERS for the Grand Junction Office, Grand Junction, Colorado.

\_\_\_\_\_, 1997r. *Vadose Zone Characterization Project at the Hanford Tank Farms, Tank Summary Data Report for Tank C-110*, GJ-HAN-92, prepared by MACTEC-ERS for the Grand Junction Office, Grand Junction, Colorado.

\_\_\_\_\_, 1998a. *Vadose Zone Characterization Project at the Hanford Tank Farms, Tank Summary Data Report for Tank C-111*, GJ-HAN-93, prepared by MACTEC-ERS for the Grand Junction Office, Grand Junction, Colorado.

\_\_\_\_\_, 1998b. *Vadose Zone Characterization Project at the Hanford Tank Farms, Tank Summary Data Report for Tank C-112*, GJ-HAN-94, prepared by MACTEC-ERS for the Grand Junction Office, Grand Junction, Colorado.

Washington State Department of Ecology (Ecology), 1994. *Dangerous Waste Portion of the Resource Conservation and Recovery Act Permit for the Treatment, Storage, and Disposal of Dangerous Waste*, Permit Number WA7890008967.

Washington State Department of Ecology (Ecology), United States Environmental Protection Agency, United States Department of Energy, 1996. *Hanford Federal Facility Agreement and Consent Order*, 89-10, Amendments 4, 5, and 6, Revision 4.

Welty, R.K., 1988. *Waste Storage Tank Status and Leak Detection Criteria*, SD-WM-TI-356, Vol. 1 and 2, Westinghouse Hanford Company, Richland, Washington.

Welty, R.K., and N.J. Vermeulen, 1989. *Waste Storage Tank Status and Leak Detection Criteria*, WHC-SD-WM-TI-357, Westinghouse Hanford Company, Richland, Washington.

Westinghouse Hanford Company (WHC), 1994. *Operating Specifications for Tank Farm Leak Detection*, WHC-OSD0151-00031, Westinghouse Hanford Company, Richland, Washington.

Wilson, R.D., 1997. *Spectrum Shape-Analysis Technique Applied to the Hanford Tank Farms Spectral Gamma Logs*, GJO-HAN-7, prepared by MACTEC-ERS for the Grand Junction Office, Grand Junction, Colorado.

Wilson, R.D., 1998. *Enhancements, Validations, and Applications of Spectrum Shape-Analysis Techniques Applied to Hanford Tank Farms Spectral Gamma Logs*, GJO-HAN-15, prepared by MACTEC-ERS for the Grand Junction Office, Grand Junction, Colorado.

Winberg, M.R., and R.S. Garcia, 1995. *National Low-Level Waste Management Program Radionuclide Report Series*, Vol. 14, *Americium-241*, DOE/LLW-130, Idaho National Engineering Laboratory, Idaho Falls, Idaho.

## **Appendix A**

### **C Tank Farm Correlation Plots**

The reader is advised to consult the appropriate Tank Summary Data Reports for explanations regarding what may appear to be discrepancies between total depth (TD) drilled (as indicated on the following correlation plots) and the maximum depth logged for several boreholes in the C Tank Farm.

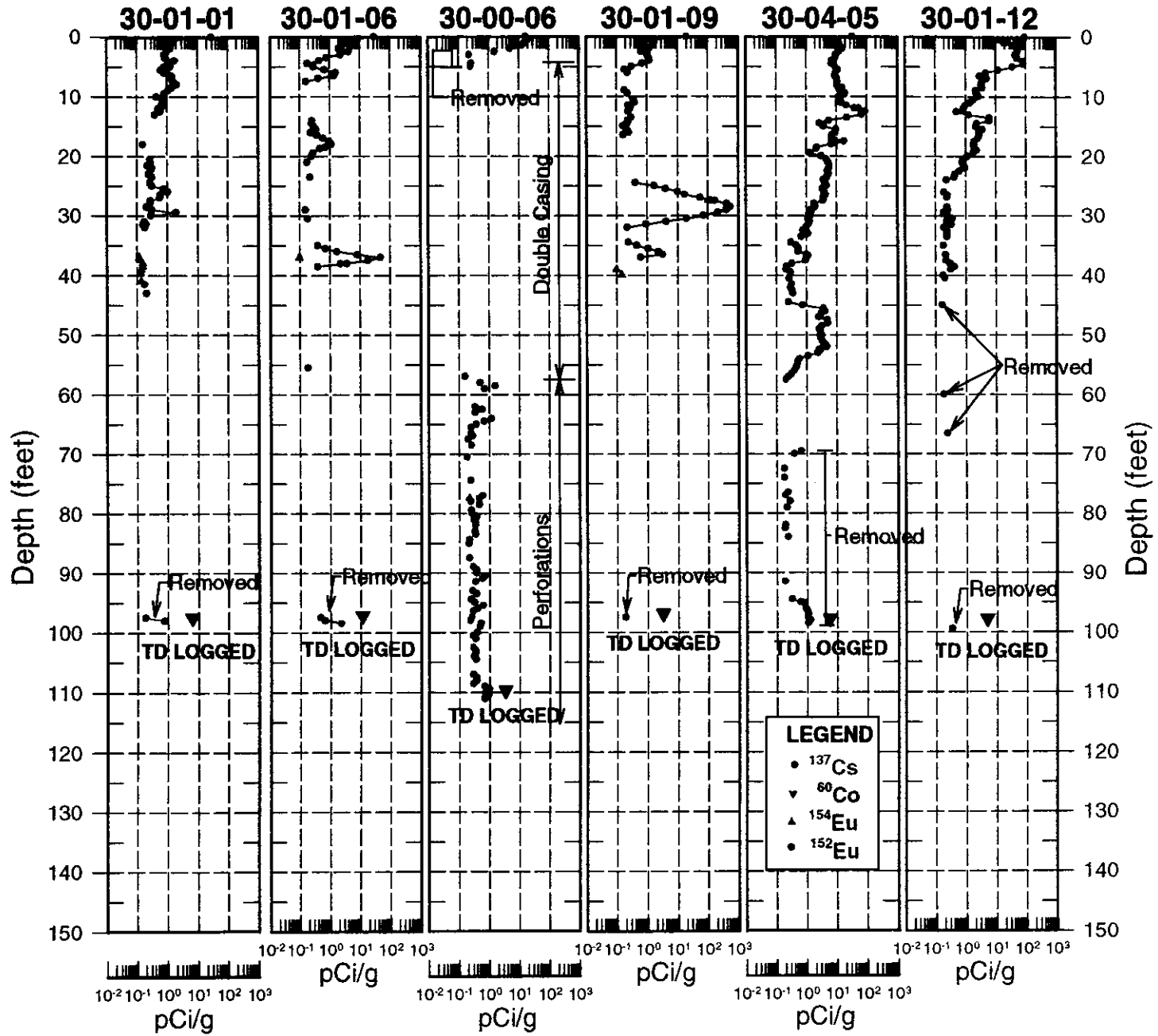


Figure A-1. Correlation Plot of  $^{137}\text{Cs}$ ,  $^{60}\text{Co}$ ,  $^{154}\text{Eu}$ , and  $^{152}\text{Eu}$  Concentrations in Boreholes Surrounding Tank C-101



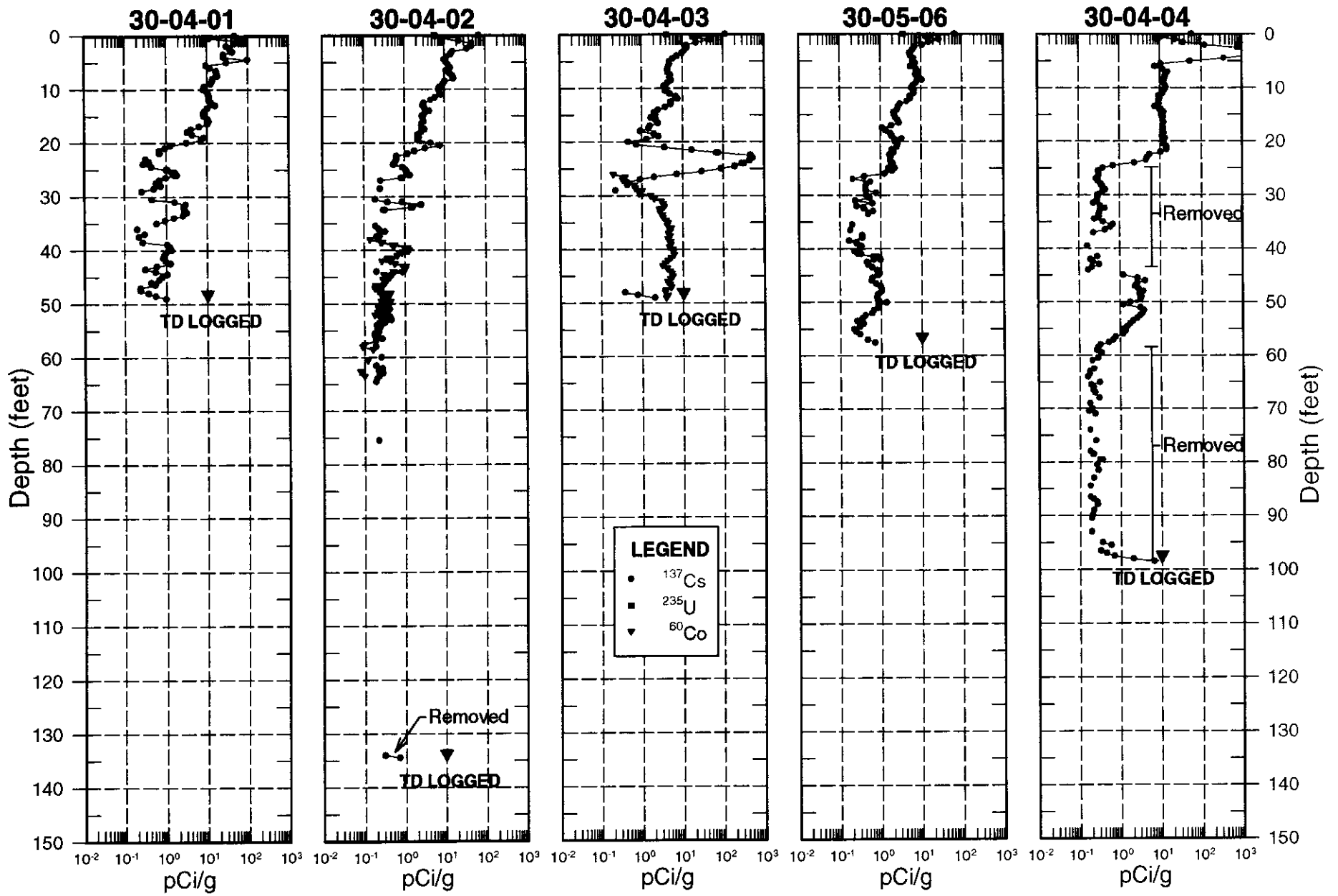


Figure A-3. Correlation Plot of <sup>137</sup>Cs, <sup>60</sup>Co, and <sup>235</sup>U Concentrations in Boreholes Surrounding Tank C-104

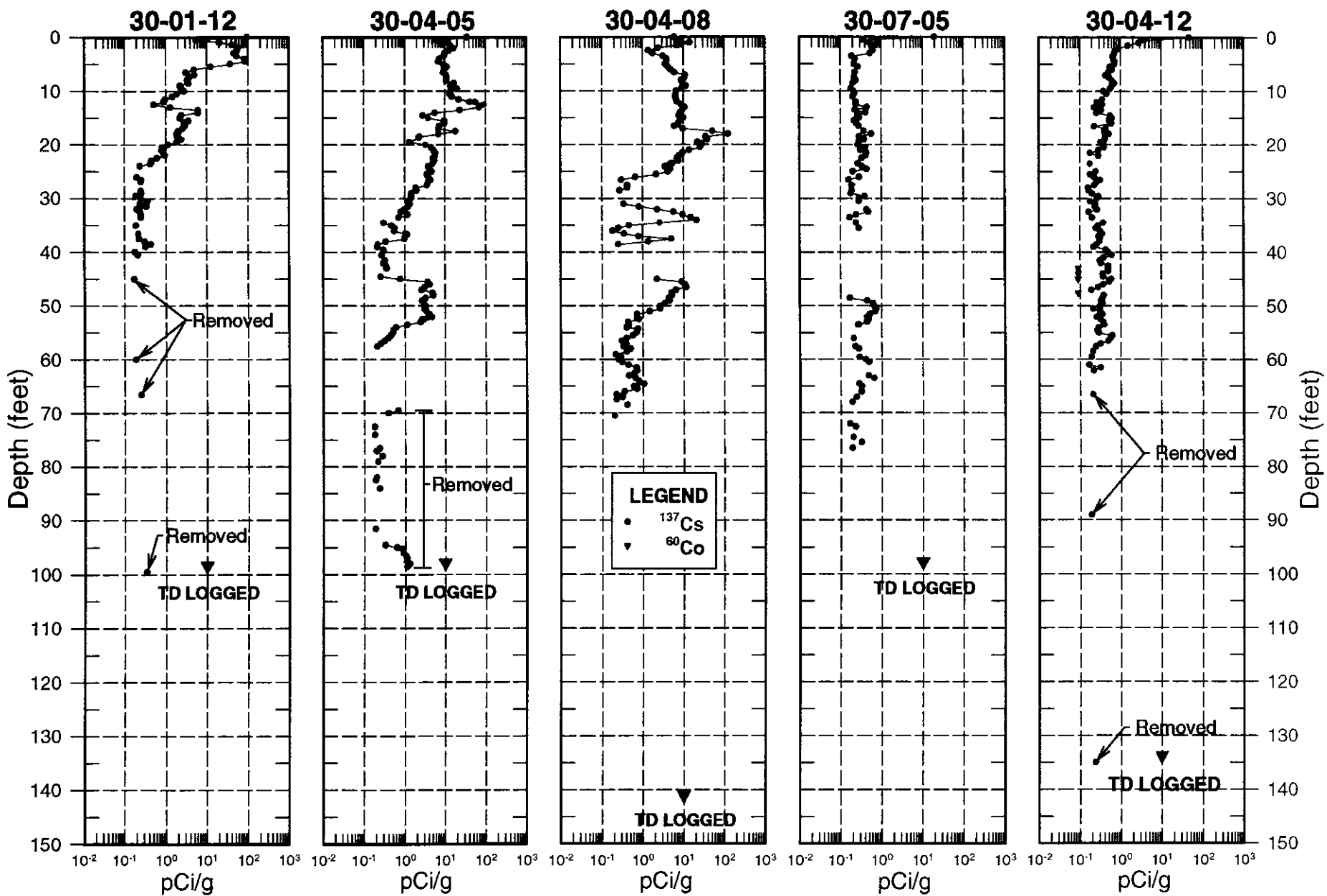


Figure A-3 (continued). Correlation Plot of <sup>137</sup>Cs and <sup>60</sup>Co Concentrations in Boreholes Surrounding Tank C-104

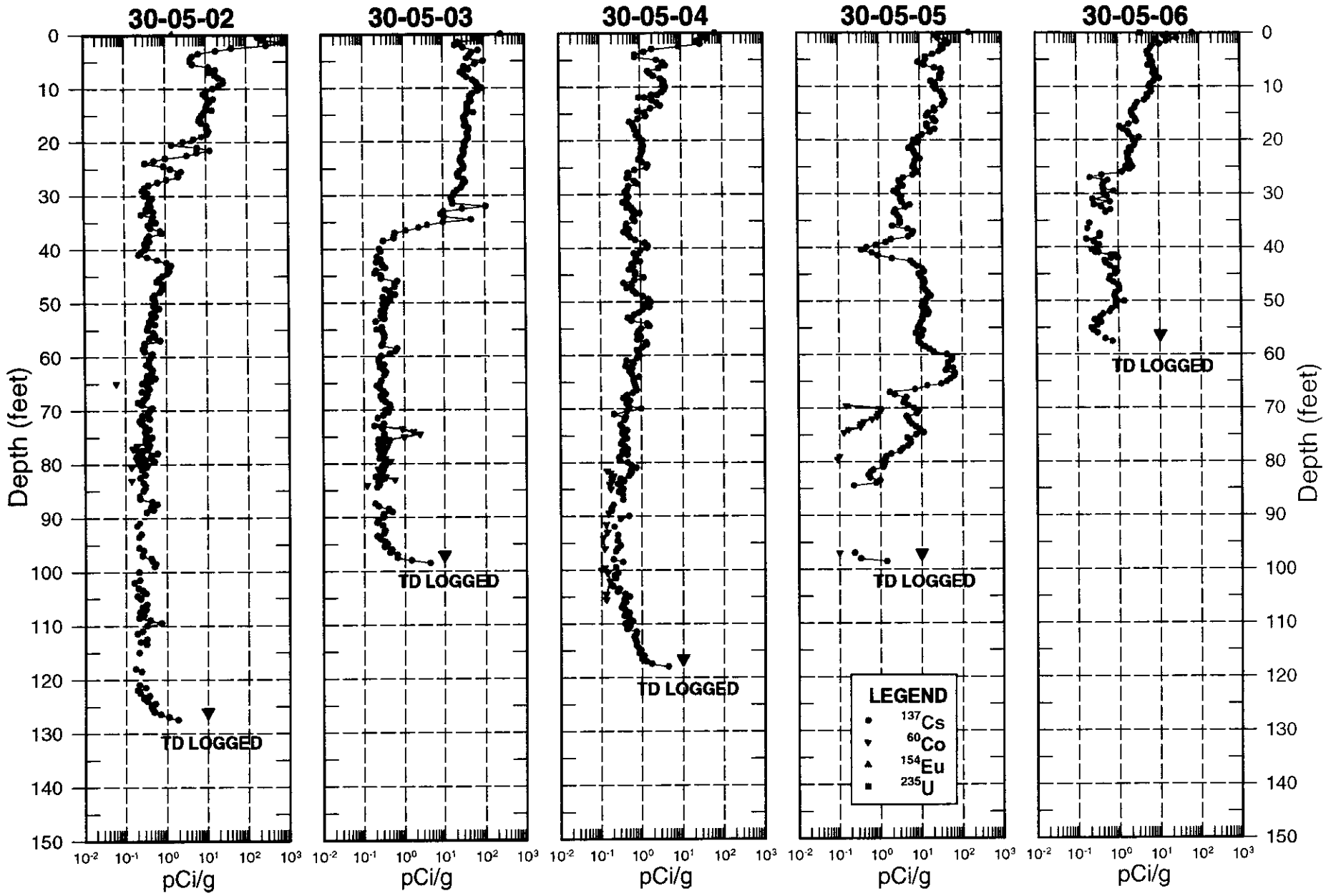


Figure A-4. Correlation Plot of <sup>137</sup>Cs, <sup>60</sup>Co, <sup>154</sup>Eu, and <sup>235</sup>U Concentrations in Boreholes Surrounding Tank C-105

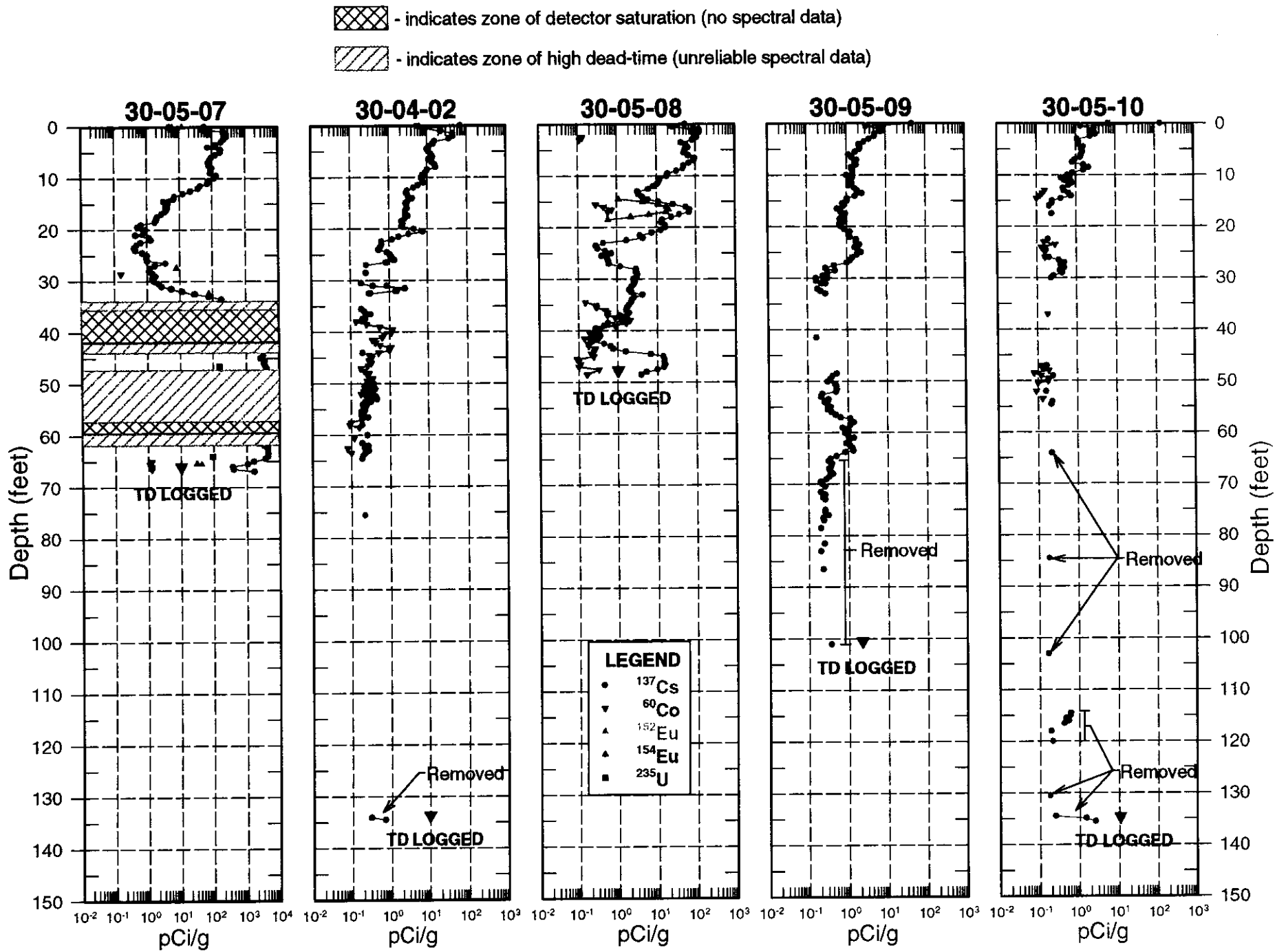


Figure A-4 (continued). Correlation Plot of  $^{137}\text{Cs}$ ,  $^{60}\text{Co}$ ,  $^{152}\text{Eu}$ ,  $^{154}\text{Eu}$ , and  $^{235}\text{U}$  Concentrations in Boreholes Surrounding Tank C-105

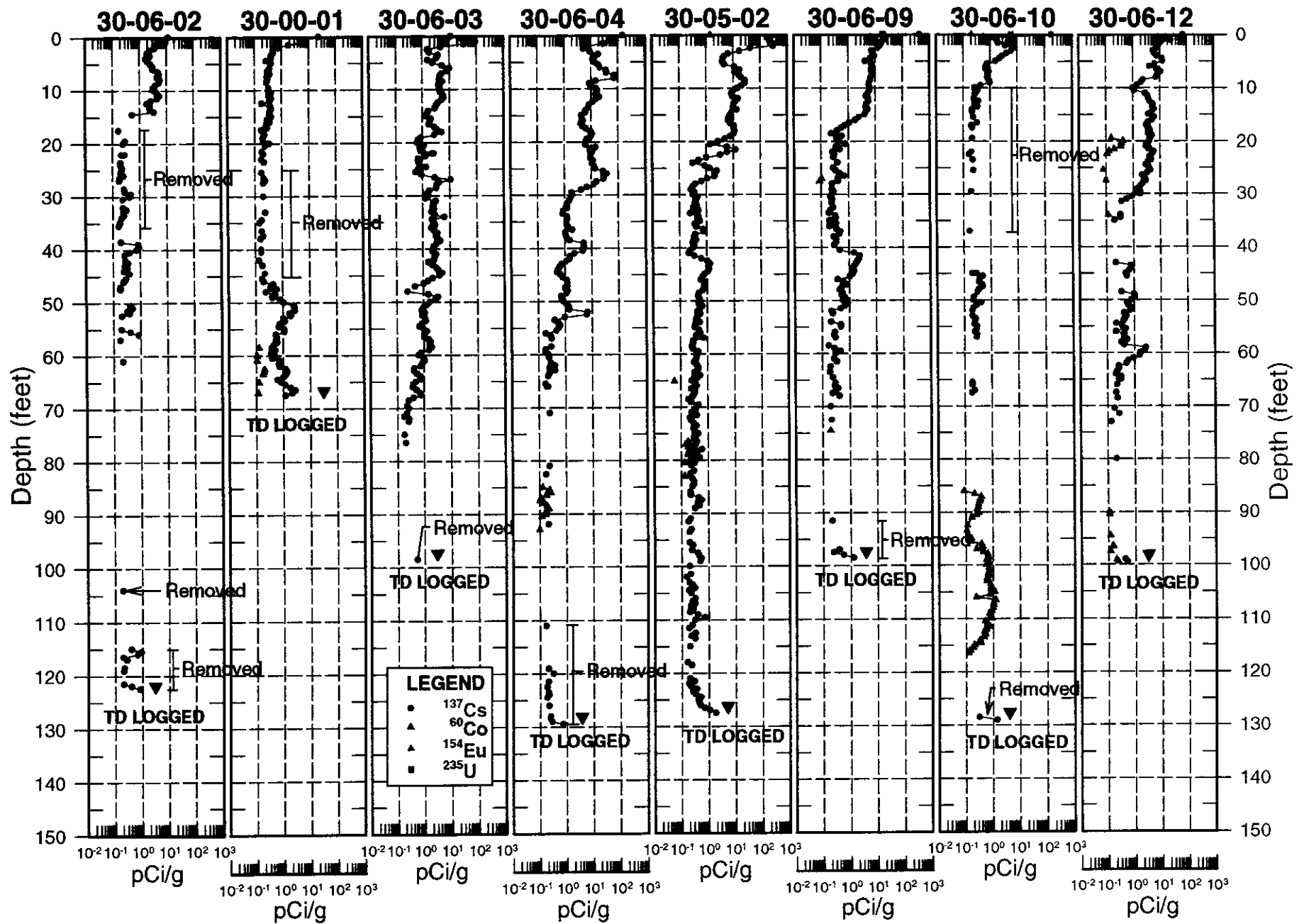


Figure A-5. Correlation Plot of  $^{137}\text{Cs}$ ,  $^{60}\text{Co}$ ,  $^{154}\text{Eu}$ , and  $^{235}\text{U}$  Concentrations in Boreholes Surrounding Tank C-106

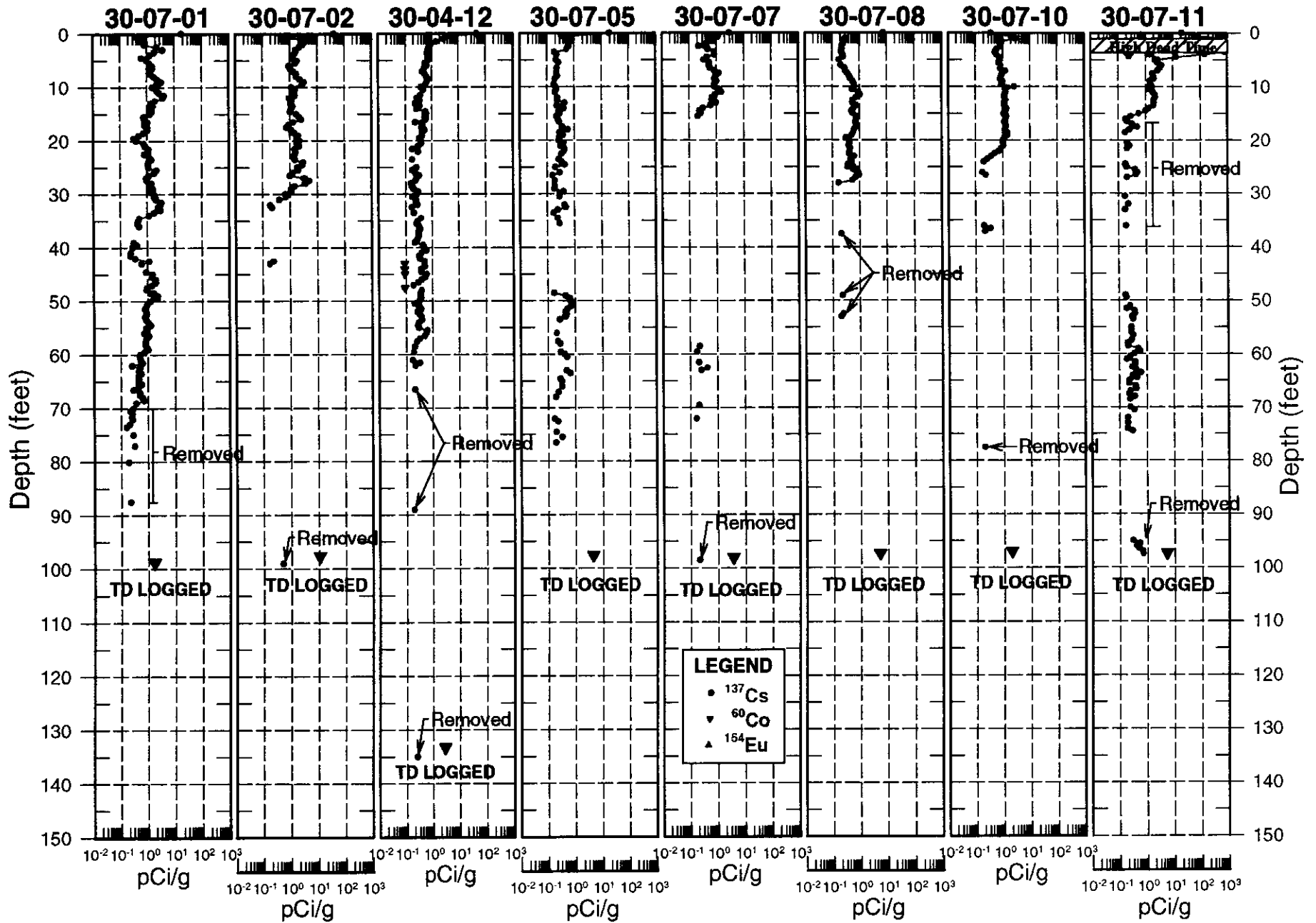


Figure A-6. Correlation Plot of  $^{137}\text{Cs}$ ,  $^{60}\text{Co}$ , and  $^{154}\text{Eu}$  Concentrations in Boreholes Surrounding Tank C-107

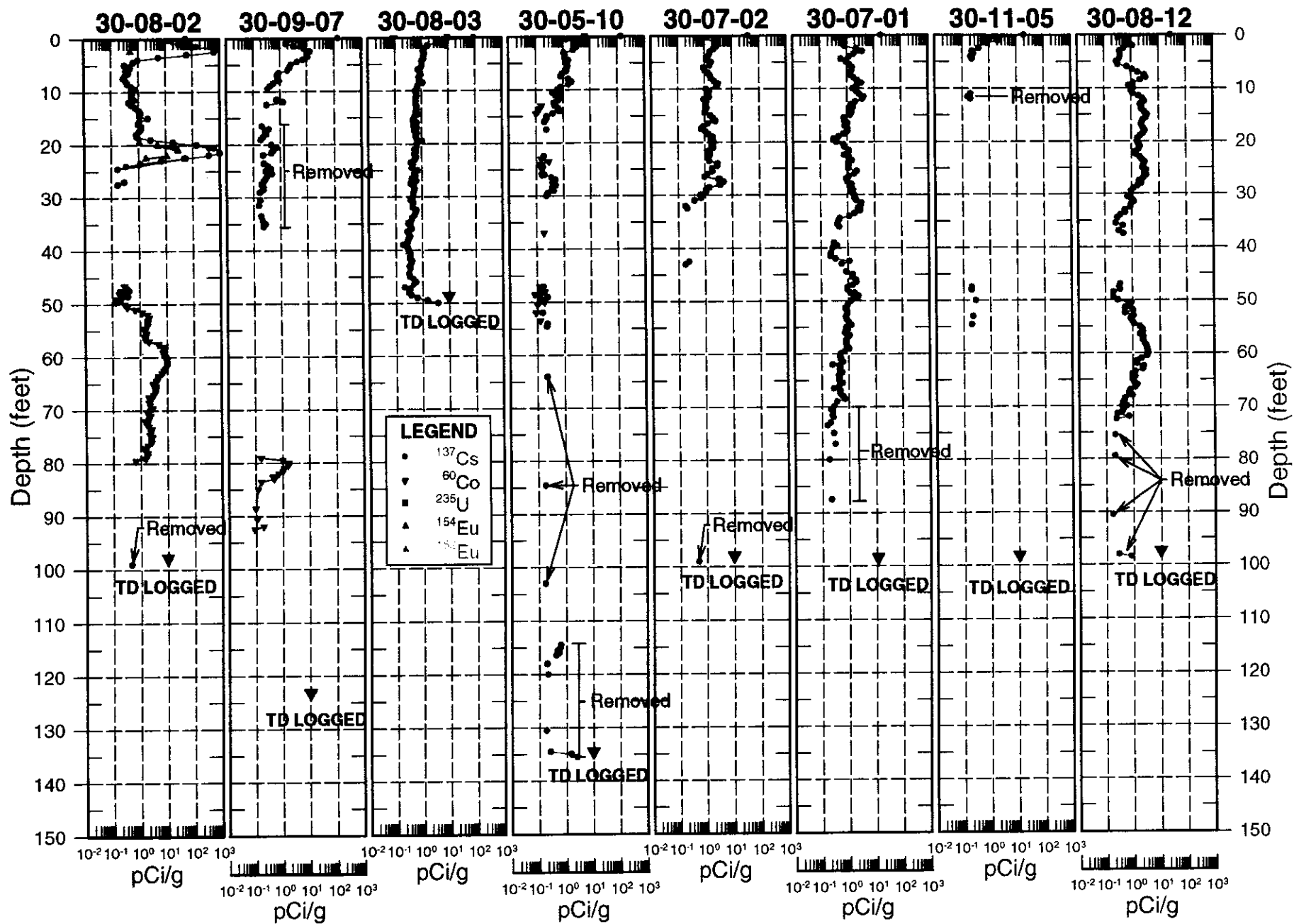


Figure A-7. Correlation Plot of  $^{137}\text{Cs}$ ,  $^{60}\text{Co}$ ,  $^{235}\text{U}$ ,  $^{154}\text{Eu}$ , and  $^{152}\text{Eu}$  Concentrations in Boreholes Surrounding Tank C-108

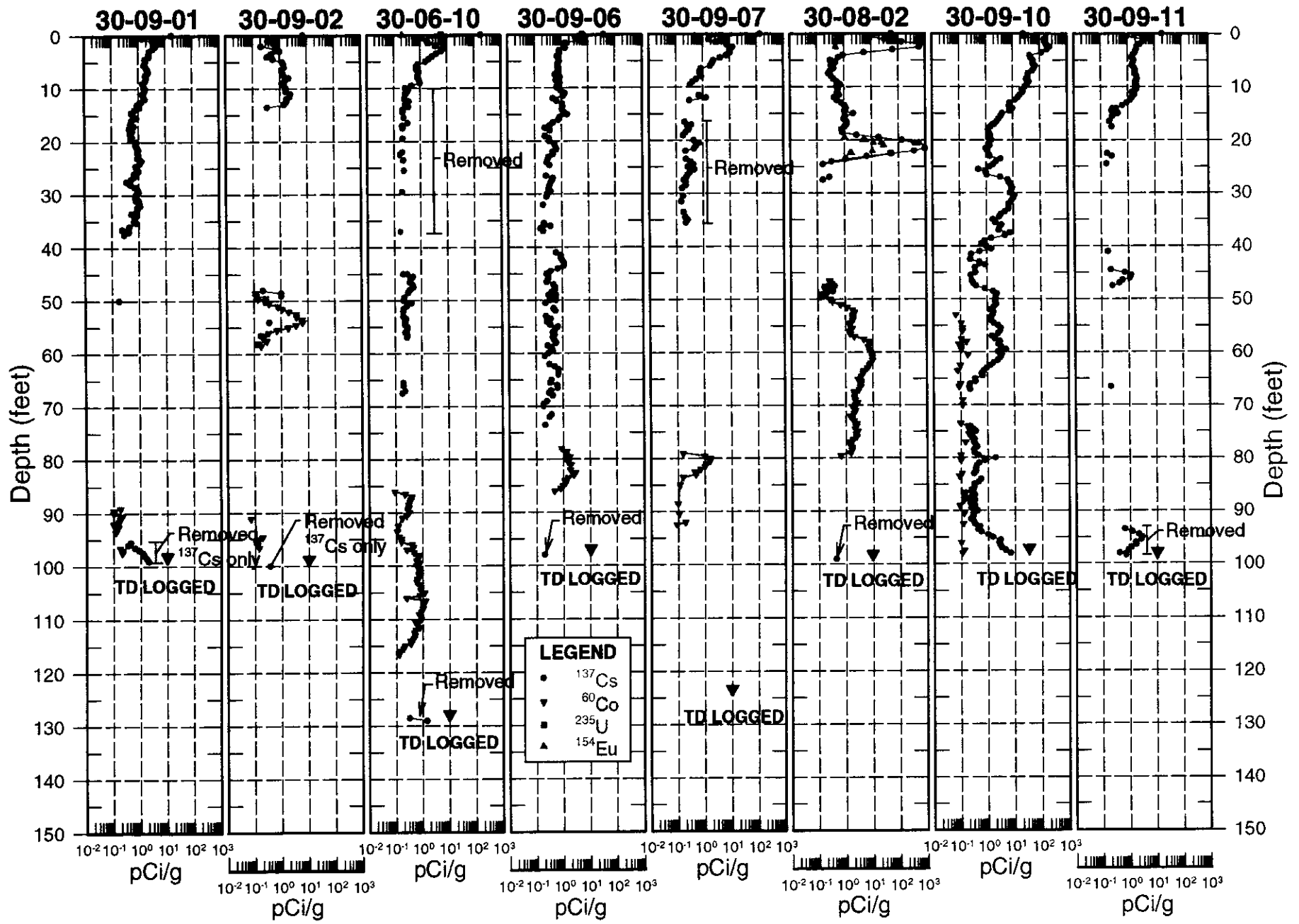


Figure A-8. Correlation Plot of  $^{137}\text{Cs}$ ,  $^{60}\text{Co}$ ,  $^{235}\text{U}$ , and  $^{154}\text{Eu}$  Concentrations in Boreholes Surrounding Tank C-109

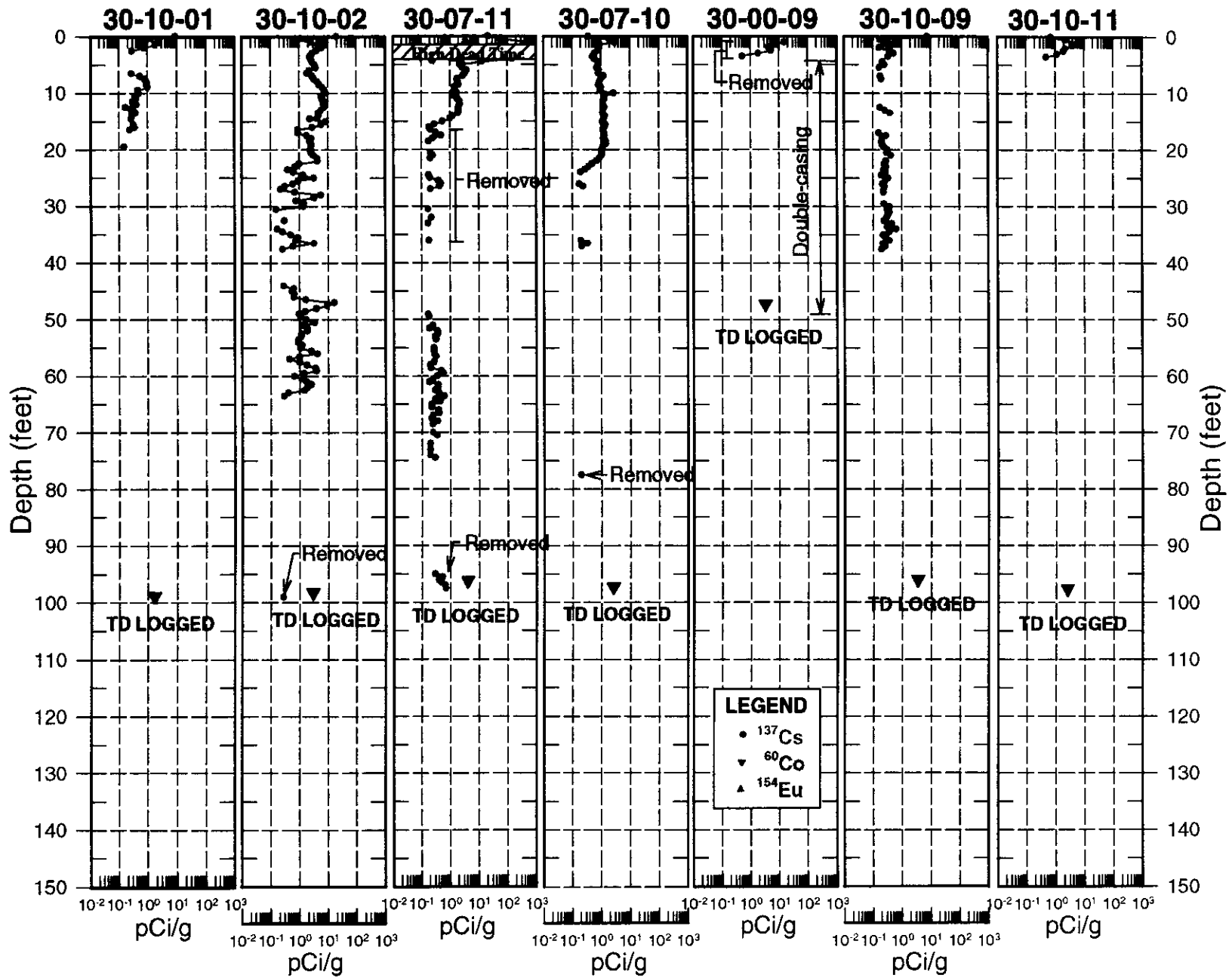


Figure A-9. Correlation Plot of  $^{137}\text{Cs}$ ,  $^{60}\text{Co}$ , and  $^{154}\text{Eu}$  Concentrations in Boreholes Surrounding Tank C-110

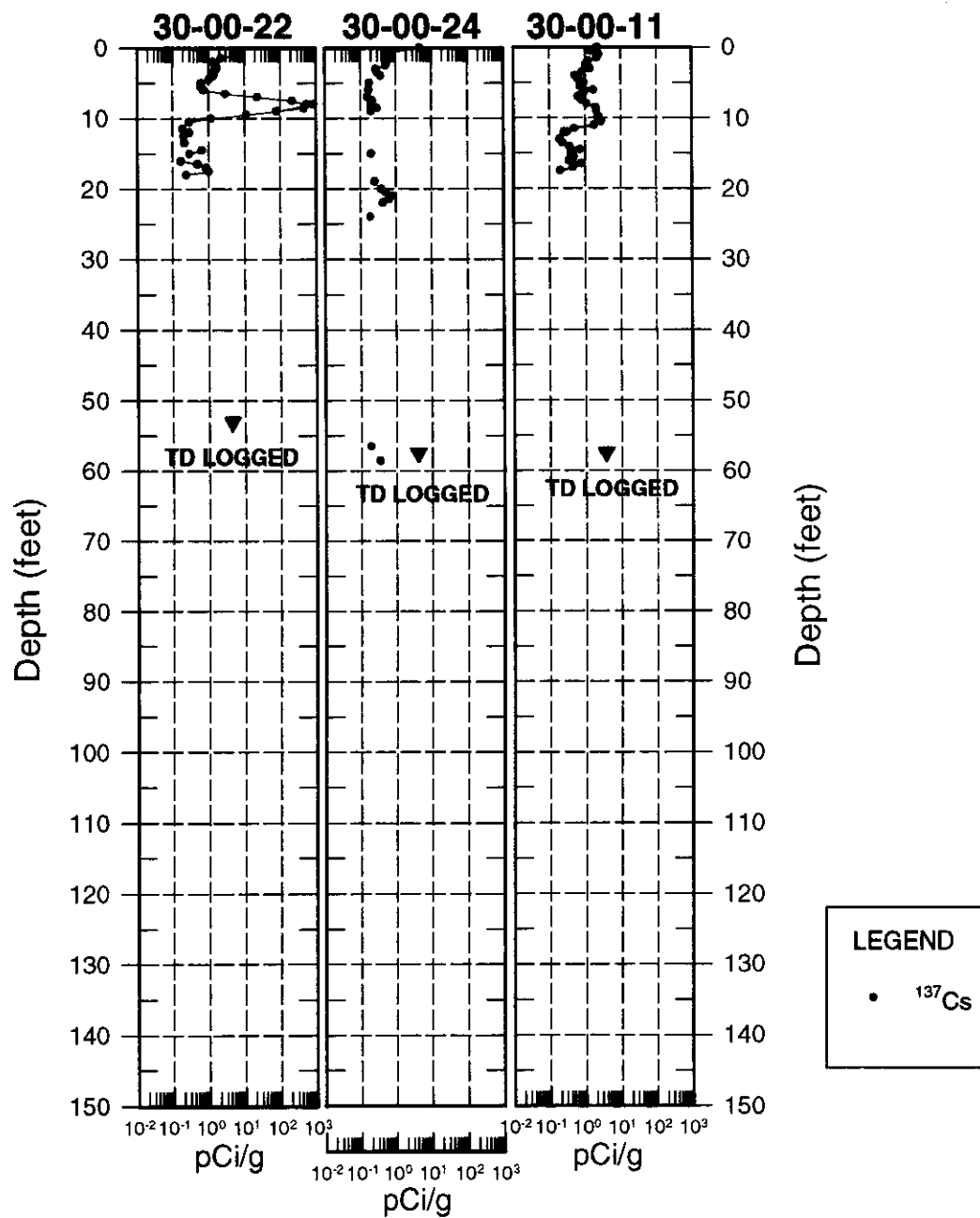


Figure A-9 (continued). Correlation Plot of <sup>137</sup>Cs, <sup>60</sup>Co, and <sup>154</sup>Eu Concentrations in Boreholes Surrounding Tank C-110

Depth (feet)

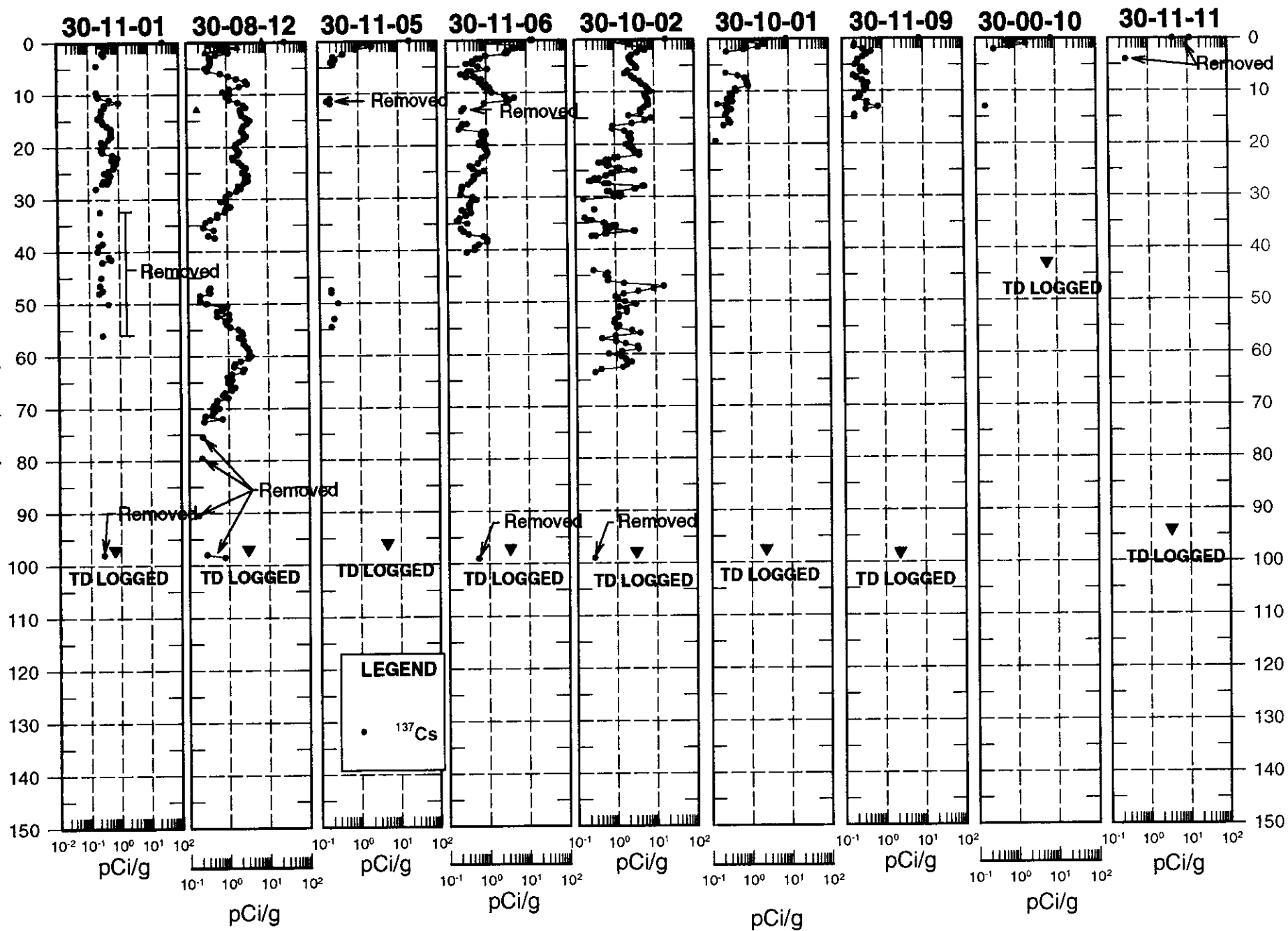


Figure A-10. Correlation Plot of <sup>137</sup>Cs Concentrations in Boreholes Surrounding Tank C-111

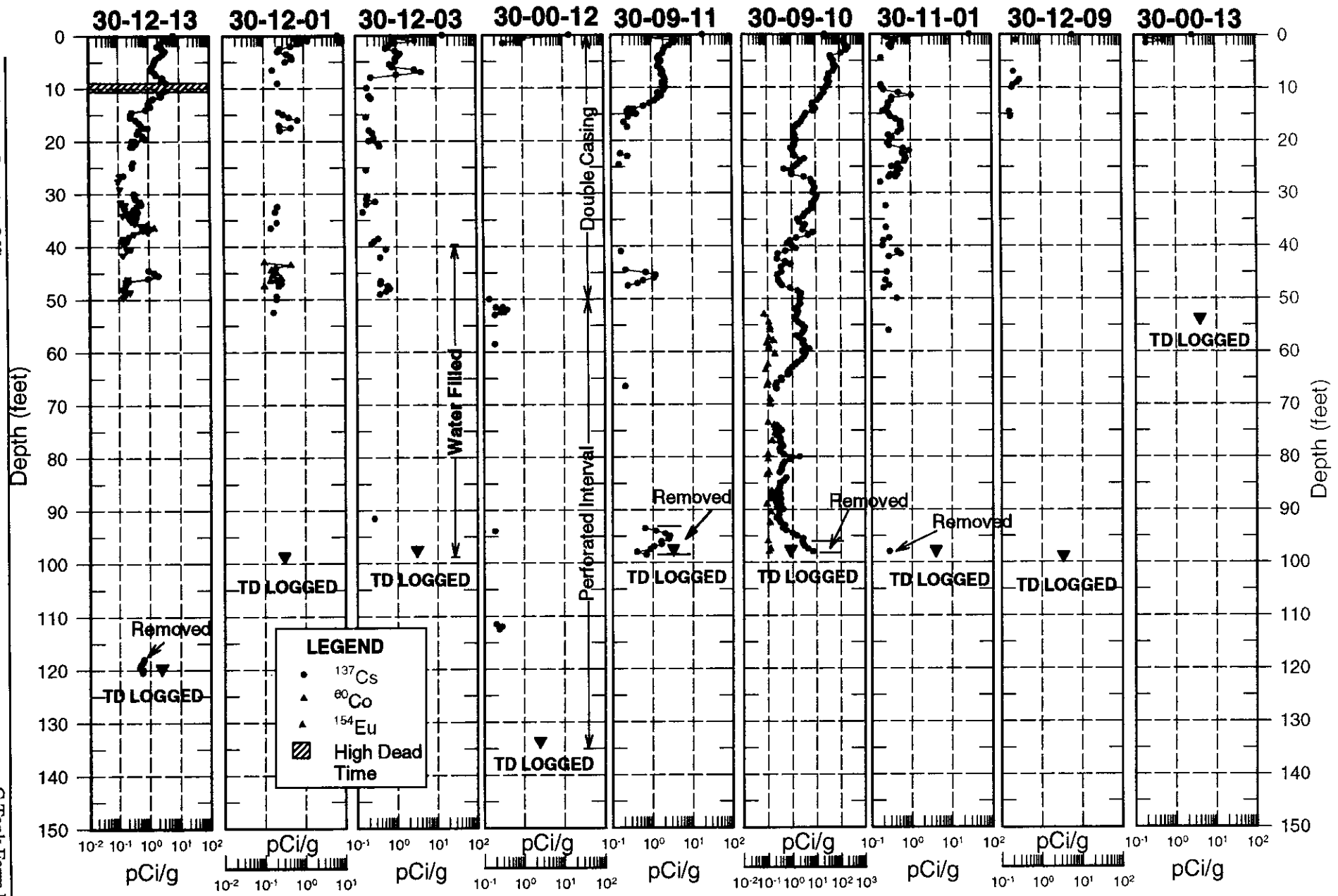


Figure A-11. Correlation Plot of  $^{137}\text{Cs}$ ,  $^{60}\text{Co}$ , and  $^{154}\text{Eu}$  Concentrations in Boreholes Surrounding Tank C-112

**Appendix B**  
**Shape Factor Analysis for Tanks**  
**C-101, C-103, C-104, C-105, and C-106**

This page intentionally left blank.

## B1.0 Introduction

The shape factor analysis method described in Section 8.5 of the C Tank Farm Report was not available for use on the SGLS log data prior to issuance of the individual Tank Summary Data Reports for tanks C-101, C-103, C-104, C-105, and C-106. Therefore, shape factor analysis of the log data was conducted during the preparation of the C Tank Farm Report and the results of the data analyses are presented in this appendix.

### B1.1 Shape Factor Analysis for Borehole 30-01-01

The Tank Summary Data Report for tank C-101 (DOE 1997i) presents the results of the data analysis for the boreholes surrounding tank C-101. Appendix A provides a log of the man-made contamination detected around borehole 30-01-01. SGLS data specific to borehole 30-01-01 are presented in Appendix A so the reader can compare the man-made radionuclide data to the shape factor analysis log presented in this appendix.

The man-made radionuclides  $^{137}\text{Cs}$  and  $^{60}\text{Co}$  were detected around this borehole.  $^{137}\text{Cs}$  was detected continuously from the ground surface to a depth of 13 ft, almost continuously from 20.5 to 32 ft, and at the bottom of the borehole.  $^{60}\text{Co}$  was measured almost continuously from 37 to 41 ft.

$^{137}\text{Cs}$  was present above the 1-cps (1.6 pCi/g) threshold for calculating shape factor CsSF1 from the ground surface to 12 ft, at 21 ft, at 29.5 ft, and at the bottom of the borehole.  $^{60}\text{Co}$  was not present above the 2-cps threshold for calculating shape factor CoSF1. The calculated results for the shape factor CsSF1 indicate the  $^{137}\text{Cs}$  between the ground surface and 12 ft varies in distribution from local to the borehole casing to uniformly distributed in the backfill sediments.

According to the Tank Summary Data Report for tank C-101, the contamination from the ground surface to 13 ft may be the result of a surface spill that migrated into the backfill sediments or down the outside of the borehole casing. The  $^{137}\text{Cs}$  from 20.5 to 32 ft may be from a subsurface pipeline leak. The Tank Summary Data Report for tank C-101 also concludes the  $^{60}\text{Co}$  from 37 to 41 ft is from a tank leak (DOE 1997i).

The interval from 5 to 6 ft was logged twice as a result of overlapping log runs. Within this interval, shape factor CsSF1 shows very poor repeatability. However, the  $^{238}\text{U}$  log plots show a decrease in concentration values with the second log run (DOE 1997i). According to the Tank Summary Data Report, the difference in  $^{238}\text{U}$  concentrations is the result of radon gas venting up the borehole. This variation in the background is the most likely cause of the poor repeatability of CsSF1.

The analysis of CsSF1 from just below the ground surface to 12 ft does support the conclusion that the  $^{137}\text{Cs}$  in this interval is the result of a surface spill that has migrated into the backfill sediments, and, to a limited extent, down the borehole casing (from 2 to 5 ft).

The individual occurrences of CsSF1 in the rest of the borehole did not provide meaningful results that could be used to determine the spatial distribution of the  $^{137}\text{Cs}$  to the borehole.

## **B1.2 Shape Factor Analysis for Borehole 30-01-06**

The Tank Summary Data Report for tank C-101 (DOE 1997i) presents the results of the data analysis for the boreholes surrounding tank C-101. Appendix A provides a log of the man-made contamination detected around borehole 30-01-06. SGLS data specific to borehole 30-01-06 are presented in Appendix A so the reader can compare the man-made radionuclide data to the shape factor analysis log presented in this appendix.

The man-made radionuclides  $^{137}\text{Cs}$  and  $^{60}\text{Co}$  were detected around this borehole.  $^{137}\text{Cs}$  was detected continuously from the ground surface to a depth of 7.5 ft, 14 to 20 ft, 35 to 38.5 ft, and at the bottom of the borehole.  $^{60}\text{Co}$  was measured only at 37 ft.

$^{137}\text{Cs}$  was present above the 1-cps (1.6 pCi/g) threshold for calculating shape factor CsSF1 from the ground surface to 4 ft, at 6 ft, at 17 ft, from 36 to 38 ft, and at the bottom of the borehole.  $^{60}\text{Co}$  was not present above the 2-cps threshold for calculating shape factor CoSF1.

According to the Tank Summary Data Report for tank C-101, the contamination from the ground surface to 20 ft may be the result of surface spills that have migrated into the backfill sediments or down the outside of the borehole casing. The Tank Summary Data Report for tank C-101 also concludes that the  $^{137}\text{Cs}$  from 35 to 38.5 ft is from a tank leak and has migrated along the base of the backfill material (DOE 1997i).

The analysis of CsSF1 from just below the ground surface to 17 ft indicates the  $^{137}\text{Cs}$  varies in distribution from uniformly distributed in the backfill sediments to on the borehole casing. The CsSF1 in this interval supports the conclusion that the  $^{137}\text{Cs}$  in this interval is the result of a surface spill that has migrated into the backfill sediments, and, to a some extent, down the borehole casing.

Analysis of CsSF1 from 36 to 38 ft indicates the  $^{137}\text{Cs}$  is deposited as a thin layer that is somewhat localized to the borehole region. The CsSF1 in this interval supports the conclusion that the  $^{137}\text{Cs}$  is from a tank leak that has migrated along the base of the backfill sediments.

CsSF1 in the bottom of the borehole cannot be analyzed by the shape factor method because the geometry of the source and detector in the borehole differs from the geometry used in the development model.

## **B1.3 Shape Factor Analysis for Borehole 30-01-09**

The Tank Summary Data Report for tank C-101 (DOE 1997i) presents the results of the data analysis for the boreholes surrounding tank C-101. Appendix A provides a log of the man-made contamination detected around borehole 30-01-09. SGLS data specific to borehole 30-01-09 are

presented in Appendix A so the reader can compare the man-made radionuclide data to the shape factor analysis log presented in this appendix.

The man-made radionuclides  $^{137}\text{Cs}$ ,  $^{60}\text{Co}$ ,  $^{154}\text{Eu}$ , and  $^{152}\text{Eu}$  were detected around this borehole.  $^{137}\text{Cs}$  was detected continuously from the ground surface to a depth of 6 ft, from 24.5 to 32 ft, from 34.5 to 37 ft, nearly continuously from 9 to 16.5 ft, and at the bottom of the borehole.  $^{60}\text{Co}$  was measured at 39.5 and 40 ft.  $^{152}\text{Eu}$  and  $^{154}\text{Eu}$  were both measured at 27.5 ft.

$^{137}\text{Cs}$  was present above the 1-cps (1.6 pCi/g) threshold for calculating shape factor CsSF1 from the ground surface to 4 ft, at 6 ft, from 25 to 31.5 ft, and from 35.5 to 36.5 ft.  $^{60}\text{Co}$  was not present above the 2-cps threshold for calculating shape factor CoSF1.

According to the Tank Summary Data Report for tank C-101, the contamination from the ground surface to 16.5 ft may be the result of surface spills that have migrated into the backfill sediments or down the outside of the borehole casing. The Tank Summary Data Report for tank C-101 also concludes the  $^{137}\text{Cs}$  from 24.5 to 32 ft and the  $^{152}\text{Eu}$  and  $^{154}\text{Eu}$  at 27.5 ft is from a tank leak (DOE 1997i). It was also concluded in the Tank Summary Data Report that the  $^{137}\text{Cs}$  from 34.5 to 37 ft and the  $^{60}\text{Co}$  at 39 and 40 ft is probably the result of contamination collecting at the base of the tank farm excavation.

The analysis of CsSF1 from the ground surface to 4 ft indicates the  $^{137}\text{Cs}$  varies in distribution from remote to uniformly distributed around the borehole. The CsSF1 in this interval supports the conclusion that the  $^{137}\text{Cs}$  is the result of a surface spill that has migrated into the backfill sediments.

Analysis of CsSF1 and SF2 from 25 to 31.5 ft provides contradictory results. However, throughout most of this interval the dead time exceeds 20 percent. It is recognized that the shape factor analysis method has significant uncertainty with dead times that exceed 20 percent. It is also recognized that the contribution of the radionuclides  $^{152}\text{Eu}$  and  $^{154}\text{Eu}$  at 27.5 ft may interfere with the shape factor results.

Shape factor analysis of the SGLS data between 25.5 to 36.5 ft indicates the majority of  $^{137}\text{Cs}$  between 34.5 to 37 ft is remote from this borehole location.

#### **B1.4 Shape Factor Analysis for Borehole 30-01-12**

The Tank Summary Data Report for tank C-101 (DOE 1997i) presents the results of the data analysis for the boreholes surrounding tank C-101. Appendix A provides a log of the man-made contamination detected around borehole 30-01-12. SGLS data specific to borehole 30-01-12 are presented in Appendix A so the reader can compare the man-made radionuclide data to the shape factor analysis log presented in this appendix.

The only man-made radionuclide detected around this borehole was  $^{137}\text{Cs}$ .  $^{137}\text{Cs}$  was detected almost continuously from the ground surface to a depth of 40.5 ft. Isolated occurrences of  $^{137}\text{Cs}$  were identified at 45 ft, 60 ft, 66.5 ft, and at the bottom of the borehole.  $^{137}\text{Cs}$  was present above

the 1-cps (1.6 pCi/g) threshold for calculating shape factor CsSF1 from the ground surface to 22 ft.

According to the Tank Summary Data Report for tank C-101 (DOE 1997i), the contamination from the ground surface to 22.5 ft is the result of surface spills that have migrated into the backfill sediments or down the outside of the borehole casing and leaks from subsurface pipelines.

The analysis of CsSF1 from just below the ground surface to 22 ft indicates the  $^{137}\text{Cs}$  varies in distribution from uniformly distributed in the backfill sediments to somewhat localized to the borehole casing. The CsSF1 in this interval supports the conclusion that the  $^{137}\text{Cs}$  is the result of a surface spill that has migrated into the backfill sediments and leaks from subsurface pipelines. However, some of the  $^{137}\text{Cs}$  appears to have migrated down the borehole casing.

### **B1.5 Shape Factor Analysis for Borehole 30-03-01**

The Tank Summary Data Report for tank C-103 (DOE 1997k) presents the results of the data analysis for the boreholes surrounding tank C-103. Appendix A provides a log of the man-made contamination detected around borehole 30-03-01. SGLS data specific to borehole 30-03-01 are presented in Appendix A so the reader can compare the man-made radionuclide data to the shape factor analysis log presented in this appendix.

The man-made radionuclides  $^{137}\text{Cs}$  and  $^{60}\text{Co}$  were detected around this borehole.  $^{137}\text{Cs}$  was detected continuously from the ground surface to a depth of 82 ft, intermittently from 85 to 88 ft, and continuously from 100 to 102 ft.  $^{60}\text{Co}$  was measured continuously from 95 to 112.5 ft, intermittently from 113.5 to 120.5 ft, and continuously from 121.5 to 124.5 ft.

$^{137}\text{Cs}$  was present above the 1-cps (1.6 pCi/g) threshold for calculating shape factor CsSF1 from the ground surface to 79 ft and at 101 ft.  $^{60}\text{Co}$  was not present above the 2-cps threshold for calculating shape factor CoSF1. The calculated results for shape factor CsSF1 indicate the  $^{137}\text{Cs}$  is non-uniformly distributed around the borehole and may be somewhat local to the borehole casing.

According to the Tank Summary Data Report for tank C-103, the contamination from the ground surface to 51 ft may be the result of surface spills that have migrated into the backfill sediments and/or leaks from subsurface sources. The Tank Summary Data Report for tank C-103 also concludes the  $^{137}\text{Cs}$  from 51 to 82 ft was dragged deeper into the vadose zone when this borehole was deepened in 1983 (DOE 1997k).

The results for CsSF1 indicate the  $^{137}\text{Cs}$  in the upper 51 ft may be more localized to the borehole region than originally believed. However, the  $^{137}\text{Cs}$  does correlate with contamination identified in other nearby boreholes, indicating at least some of the  $^{137}\text{Cs}$  is in the backfill sediments.

## **B1.6 Shape Factor Analysis for Borehole 30-03-05**

The Tank Summary Data Report for tank C-103 (DOE 1997k) presents the results of the data analysis for the boreholes surrounding tank C-103. Appendix A provides a log of the man-made contamination detected around borehole 30-03-05. SGLS data specific to borehole 30-03-05 are presented in Appendix A so the reader can compare the man-made radionuclide data to the shape factor analysis log presented in this appendix.

The only man-made radionuclide detected around this borehole was  $^{137}\text{Cs}$ .  $^{137}\text{Cs}$  was detected almost continuously from the ground surface to a depth of 43 ft, continuously from 54.5 to 76 ft, and at the bottom of the borehole.  $^{137}\text{Cs}$  was present above the 1-cps (1.6 pCi/g) threshold for calculating shape factor CsSF1 from the ground surface to 27.5 ft, from 36 to 40.5 ft, from 56.5 to 65.5 ft, and at the bottom of the borehole.

According to the Tank Summary Data Report for tank C-103, the contamination from the ground surface to 43.5 ft is probably the result of surface spills and leaks from subsurface pipelines that have migrated through the backfill material. The Tank Summary Data Report for tank C-103 also concludes that the  $^{137}\text{Cs}$  from 54.5 to 76 ft is from a tank leak that has migrated into the Hanford formation sediments below the base of the tank farm excavation (DOE 1997k).

The analysis of CsSF1 from just below the ground surface to 27.5 ft indicates the  $^{137}\text{Cs}$  varies in distribution from uniformly distributed in the backfill sediments to somewhat localized to the borehole casing. The CsSF1 in this interval supports the conclusion that the  $^{137}\text{Cs}$  is the result of a surface spill that has migrated into the backfill sediments, and, to some extent, down the borehole casing.

Analysis of CsSF1 from 36 to 40.5 ft appears to indicate the  $^{137}\text{Cs}$  is deposited as a thin layer at the base of the backfill sediments. Therefore, CsSF1 in this interval appears to support the conclusion that the  $^{137}\text{Cs}$  is from a tank leak that has migrated along the base of the backfill sediments.

The shape factor CsSF1 between 56.5 and 65.5 ft indicates the  $^{137}\text{Cs}$  is generally distributed in the Hanford formation sediments. This supports the conclusion that the  $^{137}\text{Cs}$  from 54.5 to 76 ft is from a tank leak that has migrated into the Hanford formation sediments below the base of the tank farm excavation.

CsSF1 in the bottom of the borehole cannot be analyzed by the shape factor method because the geometry of the source and detector in the borehole differs from the geometry used in the development model.

## **B1.7 Shape Factor Analysis for Borehole 30-03-07**

The Tank Summary Data Report for tank C-103 (DOE 1997k) presents the results of the data analysis for the boreholes surrounding tank C-103. Appendix A provides a log of the man-made contamination detected around borehole 30-03-07. SGLS data specific to borehole 30-03-07 are

presented in Appendix A so the reader can compare the man-made radionuclide data to the shape factor analysis log presented in this appendix.

The only man-made radionuclide detected around this borehole is  $^{137}\text{Cs}$ .  $^{137}\text{Cs}$  was detected continuously from the ground surface to a depth of 40 ft, almost continuously from 42.5 to 62.5 ft, and at the bottom of the borehole.  $^{137}\text{Cs}$  was present above the 1-cps (1.6 pCi/g) threshold for calculating shape factor CsSF1 from the ground surface to 37 ft, from 43 to 58 ft, and at the bottom of the borehole.

According to the Tank Summary Data Report for tank C-103, the contamination from the ground surface to 40 ft is probably the result of surface spills and leaks from subsurface pipelines that have migrated through the backfill material or along the borehole casing. The Tank Summary Data Report for tank C-103 also concludes the  $^{137}\text{Cs}$  from 42.5 to 62.5 ft is from a leak in a tank or nearby subsurface pipeline that has migrated into the Hanford formation sediments below the base of the tank farm excavation (DOE 1997k).

The analysis of shape factor CsSF1 from the ground surface to 11 ft indicates the  $^{137}\text{Cs}$  varies in distribution from remote to uniformly distributed in the backfill sediments. The CsSF1 in this interval supports the conclusion that the  $^{137}\text{Cs}$  between the ground surface and 10 ft is the result of a surface spill that has migrated into the backfill sediments.

Results of the shape factor CsSF1 for the interval from 11 to 27 ft vary from near uniformly distributed in the backfill sediments to localized to the borehole casing. The Tank Summary Data Report for Tank C-103 (DOE 1997k) concludes the  $^{137}\text{Cs}$  in this interval is deposited in the formation. However, shape factor analysis indicates the contamination is somewhat more localized to the borehole than originally believed.

The shape factor analysis results in the interval between 27.5 and 37 ft indicate the  $^{137}\text{Cs}$  is generally deposited uniformly around the borehole in the backfill sediments. This supports the interpretation promulgated in the Tank Summary Data Report that the  $^{137}\text{Cs}$  is deposited in the formation.

In the interval from 42.5 to 62.5 ft, CsSF1 indicates the  $^{137}\text{Cs}$  is generally deposited around the borehole uniformly in the Hanford formation sediments. This supports the conclusion in the Tank Summary Data Report for tank C-103 that the  $^{137}\text{Cs}$  is from a leak in a tank or subsurface pipeline that has migrated into the Hanford formation sediments below the base of the tank farm excavation.

CsSF1 in the bottom of the borehole did not provide meaningful results that could be used to assess the spatial relationship of the  $^{137}\text{Cs}$  to the borehole.

## **B1.8 Shape Factor Analysis for Borehole 30-03-09**

The Tank Summary Data Report for tank C-103 (DOE 1997k) presents the results of the data analysis for the boreholes surrounding tank C-103. Appendix A provides a log of the man-made

contamination detected around borehole 30-03-09. SGLS data specific to borehole 30-03-09 are presented in Appendix A so the reader can compare the man-made radionuclide data to the shape factor analysis log presented in this appendix.

The anthropogenic radionuclides  $^{137}\text{Cs}$ ,  $^{60}\text{Co}$ ,  $^{152}\text{Eu}$ , and  $^{154}\text{Eu}$  were detected around this borehole.  $^{137}\text{Cs}$  was detected almost continuously from the ground surface to a depth of 61.5 ft and intermittently from 62.5 ft to the bottom of the borehole.  $^{60}\text{Co}$  was detected continuously from 78 ft to the bottom of the logged interval. The  $^{152}\text{Eu}$  and  $^{154}\text{Eu}$  were detected only at the ground surface.

$^{137}\text{Cs}$  was present above the 1-cps (1.6 pCi/g) threshold for calculating shape factor CsSF1 from the ground surface to 15 ft, from 20 to 40.5 ft, from 45 to 55.5 ft, and from 58.5 to 61 ft.  $^{60}\text{Co}$  was present above the 2-cps threshold for calculating shape factor CoSF1 from 78.5 to 81.5 ft, at 84 ft, and at 88 ft.

According to the Tank Summary Data Report for tank C-103, the contamination from the ground surface to 41.5 ft is probably the result of surface spills and leaks from subsurface pipelines that have migrated through the backfill material or along the borehole casing. The Tank Summary Data Report for tank C-103 also concludes the  $^{137}\text{Cs}$  from 44.5 to 61.5 ft is from a leak in a tank or subsurface pipeline that has migrated into the Hanford formation sediments below the base of the tank farm excavation. The  $^{60}\text{Co}$  contamination from 78 ft to the bottom of the logged interval is probably the result of a tank or pipeline leak that migrated into the Hanford formation sediments (DOE 1997k).

The analysis of CsSF1 from just below the ground surface to 10 ft indicates the  $^{137}\text{Cs}$  is uniformly distributed in the backfill sediments. The CsSF1 in this interval supports the conclusion that the  $^{137}\text{Cs}$  between the ground surface and 10 ft is the result of a surface spill that has migrated into the backfill sediments.

The results of the shape factor CsSF1 for the intervals from 10 to 15 ft and from 20 to 25 ft appear to indicate the contaminant distribution varies from near uniformly distributed in the backfill sediments to localized to the borehole casing. The Tank Summary Data Report for Tank C-103 concludes the  $^{137}\text{Cs}$  in this interval is deposited in the formation. However, shape factor analysis indicates the contamination is somewhat more localized to the borehole.

The shape factor analysis results in the interval between 45 to 50.5 ft and between 58.5 to 61 ft indicate the  $^{137}\text{Cs}$  is generally deposited uniformly around the borehole in the Hanford formation sediments. This supports the conclusion in the Tank Summary Data Report that the  $^{137}\text{Cs}$  is from a leak in a tank or subsurface pipeline that has migrated into the Hanford formation sediments below the base of the tank farm excavation.

The analysis of CoSF1 indicates the  $^{60}\text{Co}$  is distributed uniformly in the Hanford formation sediments. This supports the Tank Summary Data Report interpretation that the  $^{60}\text{Co}$  is the result of a tank or pipeline leak that has migrated into the Hanford formation sediments.

## **B1.9 Shape Factor Analysis for Borehole 30-04-01**

The Tank Summary Data Report for tank C-104 (DOE 1997) presents the results of the data analysis for the boreholes surrounding tank C-104. Appendix A provides a log of the man-made contamination detected around borehole 30-04-01. SGLS data specific to borehole 30-04-01 are presented in Appendix A so the reader can compare the man-made radionuclide data to the shape factor analysis log presented in this appendix.

The only man-made radionuclide detected around this borehole was  $^{137}\text{Cs}$ .  $^{137}\text{Cs}$  was detected nearly continuously from the ground surface to the bottom of the logged interval at 49 ft.  $^{137}\text{Cs}$  was present above the 1-cps (1.6 pCi/g) threshold for calculating shape factor CsSF1 from the ground surface to 21 ft, from 25 to 26.5 ft, from 31 to 34.5 ft, from 39 to 45 ft, and at 49 ft.

According to the Tank Summary Data Report for tank C-104, most of the contamination appears to have originated from surface spills and leaks from subsurface pipelines that have migrated through the backfill material or along the borehole casing.

The analysis of CsSF1 from just below the ground surface to 5 ft indicates the  $^{137}\text{Cs}$  is uniformly distributed in the backfill sediments. The CsSF1 in this interval supports the conclusion that the  $^{137}\text{Cs}$  between the ground surface and 5 ft is the result of a surface spill that has migrated into the backfill sediments.

Shape factor CsSF1 for the intervals from 5 to 20 ft indicates the  $^{137}\text{Cs}$  is not distributed uniformly around the borehole, and, in fact, some small intervals may be localized to the borehole casing. The Tank Summary Data Report concludes the  $^{137}\text{Cs}$  in this interval is deposited in the formation. However, shape factor analysis indicates the contamination is not uniformly distributed in the backfill sediments.

The shape factor analysis results in the rest of the borehole indicate the  $^{137}\text{Cs}$  is generally deposited uniformly around the borehole in the backfill sediments. This supports the conclusion in the Tank Summary Data Report for tank C-104 that the  $^{137}\text{Cs}$  is from a leak in a subsurface pipeline or surface spills that have migrated through the backfill sediments.

## **B1.10 Shape Factor Analysis for Borehole 30-04-02**

The Tank Summary Data Report for tank C-104 (DOE 1997) presents the results of the data analysis for the boreholes surrounding tank C-104. Appendix A provides a log of the man-made contamination detected around borehole 30-04-02. SGLS data specific to borehole 30-04-02 are presented in Appendix A so the reader can compare the man-made radionuclide data to the shape factor analysis log presented in this appendix.

The man-made radionuclides  $^{137}\text{Cs}$ ,  $^{60}\text{Co}$ , and  $^{235}\text{U}$  were detected around this borehole.  $^{137}\text{Cs}$  was detected nearly continuously from the ground surface to 27 ft, 31 to 32.5 ft, 35.5 to 37 ft, 50 to

56.5 ft, and 61.5 to 64.5 ft.  $^{60}\text{Co}$  was detected nearly continuously from 38 to 63.5 ft. The  $^{235}\text{U}$  was detected only at the ground surface.

$^{137}\text{Cs}$  was present above the 1-cps (1.6 pCi/g) threshold for calculating shape factor CsSF1 from the ground surface to 22 ft, from 24.5 to 26.5 ft, and from 31 to 32 ft.  $^{60}\text{Co}$  was not present above the 2-cps threshold for calculating shape factor CoSF1.

According to the Tank Summary Data Report for tank C-104, the contamination between the ground surface and 8 ft as well as the  $^{137}\text{Cs}$  peaks at 20.5, 26, 31.5, and 53 ft appear to have originated from surface spills and leaks from subsurface pipelines that have migrated through the backfill sediments. The rest of the  $^{137}\text{Cs}$  apparently was carried down during borehole construction or migrated down the outside of the casing.

The analysis of CsSF1 indicates the  $^{137}\text{Cs}$  from just below the ground surface indicates the contamination is uniformly distributed in the backfill sediments. At some locations of the borehole, the  $^{137}\text{Cs}$  appears to be localized to the borehole casing. The CsSF1 generally supports the conclusions that are discussed in the Tank Summary Data Report for this tank.

### **B1.11 Shape Factor Analysis for Borehole 30-04-03**

The Tank Summary Data Report for tank C-104 (DOE 1997i) presents the results of the data analysis for the boreholes surrounding tank C-104. Appendix A provides a log of the man-made contamination detected around borehole 30-04-03. SGLS data specific to borehole 30-04-03 are presented in Appendix A so the reader can compare the man-made radionuclide data to the shape factor analysis log presented in this appendix.

The man-made radionuclides  $^{137}\text{Cs}$ ,  $^{60}\text{Co}$ , and  $^{235}\text{U}$  were detected around this borehole.  $^{137}\text{Cs}$  was detected continuously from the ground surface to 28 ft and at the bottom of the logged interval.  $^{60}\text{Co}$  was detected continuously from 26 ft to the bottom of the logged interval at 49 ft. The  $^{235}\text{U}$  was detected only at the ground surface.

$^{137}\text{Cs}$  was present above the 1-cps (1.6 pCi/g) and below the 20-percent dead time limits for calculating shape factor CsSF1 from the ground surface to 19.5 ft.  $^{60}\text{Co}$  was present above the 2-cps threshold for calculating shape factor CoSF1 from 29.5 ft to the bottom of the logged interval and the  $^{137}\text{Cs}$  is sufficiently low in concentration that it does not interfere with the  $^{60}\text{Co}$  shape factor analysis.

According to the Tank Summary Data Report for tank C-104, the contamination between the ground surface and 26 ft appears to have originated from surface spills and leaks from subsurface pipelines that have migrated through the backfill material. The  $^{60}\text{Co}$  contamination is also thought to have been the result of a leak from a subsurface pipeline (DOE 1997i).

The analysis of CsSF1 and CoSF1 indicates the  $^{137}\text{Cs}$  and  $^{60}\text{Co}$  varies in distribution from remote to uniformly distributed around the borehole casing. The shape factors CsSF1 and CoSF1 generally support the conclusion that the contamination is distributed in the backfill sediments.

## **B1.12 Shape Factor Analysis for Borehole 30-04-04**

The Tank Summary Data Report for tank C-104 (DOE 1997i) presents the results of the data analysis for the boreholes surrounding tank C-104. Appendix A provides a log of the man-made contamination detected around borehole 30-04-04. SGLS data specific to borehole 30-04-04 are presented in Appendix A so the reader can compare the man-made radionuclide data to the shape factor analysis log presented in this appendix.

The only man-made radionuclide detected around this borehole was  $^{137}\text{Cs}$ .  $^{137}\text{Cs}$  was measured continuously from the ground surface to 37 ft, nearly continuously from 41.5 to 59.5 ft, and intermittently from 60 ft to the bottom of the borehole.  $^{137}\text{Cs}$  was present above the 1-cps (1.6 pCi/g) threshold for calculating shape factor CsSF1 from the ground surface to 24 ft, 45 to 56.5 ft, and at the bottom of the borehole.

According to the Tank Summary Data Report for tank C-104, the contamination between the ground surface and 22 ft as well as the  $^{137}\text{Cs}$  between 45 and 56 ft appears to have originated from surface spills and leaks from subsurface pipelines that have migrated through the backfill material. The rest of the  $^{137}\text{Cs}$  apparently was carried down during borehole construction or migrated down the outside of the casing (DOE 1997i).

The analysis of CsSF1 in the interval from just below the ground surface and 24 ft indicates the  $^{137}\text{Cs}$  varies in distribution from remote to uniformly distributed in the backfill sediments to non-uniformly distributed in the backfill material. The shape factor results are consistent with the conclusion the  $^{137}\text{Cs}$  from the ground surface to 22 ft is generally deposited in the backfill sediments.

The shape factor CsSF1 for the interval from 45 to 56.5 ft indicates the  $^{137}\text{Cs}$  is distributed in the Hanford formation uniformly around the borehole. The shape factor analysis results for this interval are consistent with the conclusion the  $^{137}\text{Cs}$  originated from a subsurface source that has migrated below the base of the tank farm excavation into the Hanford formation sediments.

CsSF1 in the bottom of the borehole cannot be analyzed by the shape factor method because the geometry of the source and detector in the borehole differs from the geometry used in the development model.

## **B1.13 Shape Factor Analysis for Borehole 30-04-05**

The Tank Summary Data Report for tank C-104 (DOE 1997i) presents the results of the data analysis for the boreholes surrounding tank C-104. Appendix A provides a log of the man-made contamination detected around borehole 30-04-05. SGLS data specific to borehole 30-04-05 are presented in Appendix A so the reader can compare the man-made radionuclide data to the shape factor analysis log presented in this appendix.

The only man-made radionuclide detected around this borehole was  $^{137}\text{Cs}$ .  $^{137}\text{Cs}$  was detected nearly continuously from the ground surface to 57.5 ft, intermittently from 69.5 to 91.5 ft, and continuously from 94.5 to 98.5 ft (the bottom of the logged interval).  $^{137}\text{Cs}$  was present above the 1-cps (1.6 pCi/g) threshold for calculating shape factor CsSF1 from the ground surface to 33 ft, from 36.5 to 37.5 ft, from 45 to 53.5 ft, and at the bottom of the borehole.

According to the Tank Summary Data Report for tank C-104, the  $^{137}\text{Cs}$  between the ground surface and 18 ft originated from surface spills and leaks from subsurface pipelines that have migrated through the backfill material. The  $^{137}\text{Cs}$  between 45 and 57 ft may have resulted from a leak in a nearby cascade line. The rest of the  $^{137}\text{Cs}$  apparently was carried down during borehole construction or later migrated down the outside of the casing (DOE 1997).

The analysis of CsSF1 in the interval from just below the ground surface to 15 ft indicates the  $^{137}\text{Cs}$  is uniformly distributed in the backfill sediments. The shape factor results are consistent with the conclusion the  $^{137}\text{Cs}$  from the ground surface to 15 ft is generally deposited in the backfill sediments. However, the Tank Summary Data Report concluded the contamination had migrated through the backfill sediments to a depth of 18 ft.

The shape factor CsSF1 indicates that the  $^{137}\text{Cs}$  from 15.5 to 33 ft varies in distribution from localized to the borehole to distributed somewhat uniformly in the backfill sediments. This supports the interpretation contained in the Tank Summary Data Report that the contamination is somewhat localized to the borehole in this interval but is not entirely the result of carry down during drilling activities.

The shape factor CsSF1 for the interval from 45 to 56.5 ft indicates the  $^{137}\text{Cs}$  is distributed in the Hanford formation uniformly around the borehole. The shape factor analysis results for this interval are consistent with the conclusion the  $^{137}\text{Cs}$  originated from a subsurface pipeline leak that has migrated below the base of the tank farm excavation into the Hanford formation sediments.

CsSF1 in the bottom of the borehole cannot be analyzed by the shape factor method because the geometry of the source and detector in the borehole differs from the geometry used in the development model.

### **B1.14 Shape Factor Analysis for Borehole 30-04-08**

The Tank Summary Data Report for tank C-104 (DOE 1997) presents the results of the data analysis for the boreholes surrounding tank C-104. Appendix A provides a log of the man-made contamination detected around borehole 30-04-08. SGLS data specific to borehole 30-04-08 are presented in Appendix A so the reader can compare the man-made radionuclide data to the shape factor analysis log presented in this appendix.

The only man-made radionuclide detected around this borehole was  $^{137}\text{Cs}$ .  $^{137}\text{Cs}$  was detected nearly continuously from the ground surface to 38.5 ft and from 40 to 70.5 ft.  $^{137}\text{Cs}$  was present

above the 1-cps (1.6 pCi/g) threshold for calculating shape factor CsSF1 from the ground surface to 25.5 ft, 31.5 to 34.5 ft, 37 to 38 ft, 45 to 51 ft, and at 52.5, 54.5, 46, and 64.5 ft.

According to the Tank Summary Data Report for tank C-104, the  $^{137}\text{Cs}$  between the ground surface and 17 ft originated from surface spills that have migrated through the backfill material and along the borehole casing. The  $^{137}\text{Cs}$  between 17 and 21 ft may have resulted from a leak in a nearby subsurface pipeline. The  $^{137}\text{Cs}$  between 45 and 51 ft may be from a leak in a nearby cascade line or from a tank. The contamination below 51 ft was apparently carried down during borehole construction or migrated down the outside of the casing (DOE 1997).

The analysis of CsSF1 in the interval between the ground surface and 15 ft indicates the  $^{137}\text{Cs}$  non-uniformly distributed in the backfill sediments and may be somewhat localized to the borehole. The shape factor results are consistent with the conclusion the  $^{137}\text{Cs}$  from the ground surface to 15 ft is the result of surface spills.

The shape factor CsSF1 indicates that the  $^{137}\text{Cs}$  from 15.5 to 25 ft varies in distribution from localized to the borehole to distributed non-uniformly in the backfill sediments. This supports the interpretation presented in the Tank Summary Data Report that the contamination is from a nearby subsurface pipeline.

The shape factor CsSF1 for the interval from 45 to 51 ft indicates the  $^{137}\text{Cs}$  is distributed non-uniformly in the Hanford formation. The shape factor analysis results for this interval are consistent with the conclusion the  $^{137}\text{Cs}$  originated from a subsurface pipeline leak or possibly a tank leak.

### **B1.15 Shape Factor Analysis for Borehole 30-05-02**

The Tank Summary Data Report for tank C-105 (DOE 1997m) presents the results of the data analysis for the boreholes surrounding tank C-105. Appendix A provides a log of the man-made contamination detected around borehole 30-05-02. SGLS data specific to borehole 30-05-02 are presented in Appendix A so the reader can compare the man-made radionuclide data to the shape factor analysis log presented in this appendix.

The man-made radionuclides  $^{137}\text{Cs}$ ,  $^{60}\text{Co}$ , and  $^{154}\text{Eu}$  were detected around this borehole.  $^{137}\text{Cs}$  was detected continuously from the ground surface to 81 ft and intermittently from 82 ft to the bottom of the logged interval at 127 ft. Alternating zones of intermittent and continuous  $^{137}\text{Cs}$  contamination were detected from 82 to 127.5 ft (the bottom of the logged interval). Continuous  $^{60}\text{Co}$  contamination was detected from 75 to 80.5 ft and intermittently from 65 to 83 ft.  $^{154}\text{Eu}$  was detected only at the ground surface.

$^{137}\text{Cs}$  was present above the 1-cps (1.6 pCi/g) threshold for calculating shape factor CsSF1 from the ground surface to 27 ft and from 42.5 to 47.5 ft.  $^{60}\text{Co}$  was not present above the 2-cps threshold for calculating shape factor CoSF1.

According to the Tank Summary Data Report for tank C-105, the  $^{137}\text{Cs}$  between the ground surface and 27 ft originated from surface spills and leaks from subsurface pipelines that have migrated through the backfill material. The elevated  $^{137}\text{Cs}$  at 41 ft may be contamination that has accumulated at the base of the tank farm excavation. The rest of the  $^{137}\text{Cs}$  was apparently carried down during borehole construction or migrated down the outside of the casing (DOE 1997m).

The analysis of CsSF1 in the interval from just below the ground surface to 7 ft indicates the  $^{137}\text{Cs}$  varies in distribution from remote to uniformly distributed in the backfill sediments. However, the shape factor results for this interval are more likely due to the high concentration gradient and do not represent the actual  $^{137}\text{Cs}$  distribution.

The  $^{137}\text{Cs}$  between 7 and 19 ft is non-uniformly distributed around the borehole casing. The shape factor results from 20 to 27 ft indicate the contamination is nearly uniformly distributed in the backfill sediments. The shape factor results are consistent with the conclusion the  $^{137}\text{Cs}$  from the ground surface to 27 ft is generally deposited in the backfill sediments.

The shape factor CsSF1 indicates that the  $^{137}\text{Cs}$  from 42.5 and 47.5 ft is distributed somewhat uniformly in the backfill sediments. This supports the interpretation contained in the Tank Summary Data Report that the contamination has accumulated at the base of the tank farm excavation.

### **B1.16 Shape Factor Analysis for Borehole 30-05-03**

The Tank Summary Data Report for tank C-105 (DOE 1997m) presents the results of the data analysis for the boreholes surrounding tank C-105. Appendix A provides a log of the man-made contamination detected around borehole 30-05-03. SGLS data specific to borehole 30-05-03 are presented in Appendix A so the reader can compare the man-made radionuclide data to the shape factor analysis log presented in this appendix.

The man-made radionuclides  $^{137}\text{Cs}$  and  $^{60}\text{Co}$  were detected around this borehole.  $^{137}\text{Cs}$  was detected continuously from the ground surface to 38.5 ft and semi-continuously from 40 to 98.5 ft (the bottom of the logged interval). Continuous  $^{60}\text{Co}$  contamination was detected from 73 to 83 ft.

$^{137}\text{Cs}$  was present above the 1-cps (1.6 pCi/g) threshold for calculating shape factor CsSF1 from the ground surface to 32 ft and at the bottom of the borehole.  $^{60}\text{Co}$  was present above the 2-cps threshold for calculating shape factor CoSF1 at 74 ft.

According to the Tank Summary Data Report for tank C-105, the  $^{137}\text{Cs}$  between the ground surface and 40 ft originated from surface spills and leaks from subsurface pipelines that have migrated through the backfill material. The  $^{137}\text{Cs}$  below 40 ft was carried down during borehole construction or migrated down the outside of the casing. The  $^{60}\text{Co}$  contamination is probably the remnant of a subsurface plume (DOE 1997m).

The analysis of CsSF1 in the interval from just below the ground surface to 6 ft indicates the  $^{137}\text{Cs}$  is uniformly distributed in the backfill sediments. However, below 6 ft the  $^{137}\text{Cs}$  appears to be non-uniformly distributed in the backfill sediments and may be somewhat localized to the borehole region. The shape factor results are consistent with the conclusion the  $^{137}\text{Cs}$  from the ground surface to about 40 ft is generally deposited in the backfill sediments.

The shape factor CoSF1 indicates that the  $^{60}\text{Co}$  is probably distributed uniformly in the Hanford formation sediments. This supports the interpretation presented in the Tank Summary Data Report that the contamination is the remnant of a subsurface plume.

### **B1.17 Shape Factor Analysis for Borehole 30-05-04**

The Tank Summary Data Report for tank C-105 (DOE 1997m) presents the results of the data analysis for the boreholes surrounding tank C-105. Appendix A provides a log of the man-made contamination detected around borehole 30-05-04. SGLS data specific to borehole 30-05-04 are presented in Appendix A so the reader can compare the man-made radionuclide data to the shape factor analysis log presented in this appendix.

The man-made radionuclides  $^{137}\text{Cs}$  and  $^{60}\text{Co}$  were detected around this borehole.  $^{137}\text{Cs}$  was detected nearly continuously from the ground surface to the bottom of the logged interval. Continuous  $^{60}\text{Co}$  contamination was detected from 81.5 to 84 ft and intermittently from 85 to 105.5 ft.

$^{137}\text{Cs}$  was present above the 1-cps (1.6 pCi/g) threshold for calculating shape factor CsSF1 at numerous intervals from the ground surface to 70 ft and at the bottom of the borehole.  $^{60}\text{Co}$  was not present above the 2-cps threshold for calculating shape factor CoSF1.

The shape factor CsSF1 is highly variable over short intervals of the borehole. This pattern is repeated from the ground surface to 70 ft. Throughout most of this interval, the  $^{137}\text{Cs}$  activity is just above the 1-cps threshold. It is possible the  $^{137}\text{Cs}$  distribution is highly variable, or the shape factor method at 1 cps is not reliable. Regardless, the results of the shape factor analysis for this borehole are inconclusive.

### **B1.18 Shape Factor Analysis for Borehole 30-05-05**

The Tank Summary Data Report for tank C-105 (DOE 1997m) presents the results of the data analysis for the boreholes surrounding tank C-105. Appendix A provides a log of the man-made contamination detected around borehole 30-05-05. SGLS data specific to borehole 30-05-05 are presented in Appendix A so the reader can compare the man-made radionuclide data to the shape factor analysis log presented in this appendix.

The man-made radionuclides  $^{137}\text{Cs}$  and  $^{60}\text{Co}$  were detected around this borehole.  $^{137}\text{Cs}$  was detected continuously from the ground surface to 84.5 ft. Continuous  $^{60}\text{Co}$  contamination was detected from 69.5 to 74.5 ft and at 79, 79.5, and 97 ft.

<sup>137</sup>Cs was present above the 1-cps (1.6 pCi/g) threshold for calculating shape factor CsSF1 from the ground surface to 82 ft, at 84 ft, and at the bottom of the borehole. <sup>60</sup>Co was not present above the 2-cps threshold for calculating shape factor CoSF1.

According to the Tank Summary Data Report for tank C-105, the <sup>137</sup>Cs between the ground surface and 75 ft originated from surface spills and leaks from subsurface pipelines that have migrated through the backfill material. The <sup>60</sup>Co from 69.5 to 74.5 ft is most likely related to the <sup>137</sup>Cs contamination. The <sup>137</sup>Cs below about 75 ft was apparently carried down during borehole construction or migrated down the outside of the casing (DOE 1997m).

The analysis of CsSF1 in the interval from just below the ground surface to 7 ft indicates the <sup>137</sup>Cs varies in distribution from remote to uniformly distributed in the backfill sediments. However, the shape factor analysis results for the <sup>137</sup>Cs between 7 and 80 ft indicates the contamination is non-uniformly distributed in the backfill and Hanford formation sediments and may be somewhat localized to the borehole region.

The shape factor results generally support the origins of the contamination described in the Tank Summary Data Report, but the <sup>137</sup>Cs contamination may be more localized to the borehole casing region than originally believed. However, the <sup>137</sup>Cs does correlate with contamination in other boreholes, indicating at least some of the contamination migrated through the backfill and Hanford formation sediments.

### **B1.19 Shape Factor Analysis for Borehole 30-05-06**

The Tank Summary Data Report for tank C-105 (DOE 1997m) presents the results of the data analysis for the boreholes surrounding tank C-105. Appendix A provides a log of the man-made contamination detected around borehole 30-05-06. SGLS data specific to borehole 30-05-06 are presented in Appendix A so the reader can compare the man-made radionuclide data to the shape factor analysis log presented in this appendix.

The man-made radionuclides <sup>137</sup>Cs and <sup>235</sup>U were detected around this borehole. <sup>137</sup>Cs was detected continuously from the ground surface to 33.5 ft and from 37.5 to 57.5 ft (the bottom of the logged interval). <sup>235</sup>U was detected only at the ground surface. <sup>137</sup>Cs was present above the 1-cps (1.6 pCi/g) threshold for calculating shape factor CsSF1 from the ground surface to 26 ft and from 41.5 to 51 ft.

According to the Tank Summary Data Report for tank C-105, the <sup>137</sup>Cs between the ground surface and 57.5 ft originated from surface spills and leaks from subsurface pipelines that have migrated through the backfill material. The <sup>137</sup>Cs from 41 to 52 ft is most likely the result of a subsurface pipeline leak. The <sup>137</sup>Cs between 26 and 52 ft was apparently carried down during borehole construction or migrated down the outside of the casing (DOE 1997m).

The analysis of CsSF1 in the interval between the ground surface and 18 ft indicates the <sup>137</sup>Cs is uniformly distributed in the backfill sediments. Between about 18.5 and 26 ft, the shape factor CsSF1 indicates the <sup>137</sup>Cs distribution varies from somewhat localized to the borehole region to

uniformly distributed in the backfill sediments. The shape factor results from 41 to 52 ft indicate the contamination is somewhat remote from the borehole.

The shape factor results generally support the conclusions presented in the Tank Summary Data Report. However, the contamination from 18.5 to 26 ft may be more localized to the borehole region than originally believed.

### **B1.20 Shape Factor Analysis for Borehole 30-05-07**

The Tank Summary Data Report for tank C-105 (DOE 1997m) presents the results of the data analysis for the boreholes surrounding tank C-105. Appendix A provides a log of the man-made contamination detected around borehole 30-05-07. SGLS data specific to borehole 30-05-07 are presented in Appendix A so the reader can compare the man-made radionuclide data to the shape factor analysis log presented in this appendix.

The man-made radionuclides  $^{137}\text{Cs}$ ,  $^{60}\text{Co}$ ,  $^{152}\text{Eu}$ ,  $^{154}\text{Eu}$ , and  $^{235}\text{U}$  were detected around this borehole.  $^{137}\text{Cs}$  was detected continuously from the ground surface to 33.5 ft, from 44.5 to 47 ft, and from 61.5 to 67 ft (the bottom of the logged interval). Continuous  $^{60}\text{Co}$  contamination was detected at 28.5 ft and continuously from 65 to 66.5 ft.  $^{152}\text{Eu}$  was detected at the ground surface and at 65.5 ft.  $^{154}\text{Eu}$  contamination was detected at 27.5, 32.5, and 65.5 ft.  $^{235}\text{U}$  was detected only at the ground surface.

$^{137}\text{Cs}$  was present above the 1-cps (1.6 pCi/g) and below the 20-percent dead time limits for calculating shape factor CsSF1 from the ground surface to 31 ft and at the bottom of the borehole.  $^{60}\text{Co}$  was not present above the 2-cps threshold for calculating shape factor CoSF1,

According to the Tank Summary Data Report for tank C-105, the  $^{137}\text{Cs}$  between the ground surface and 10 ft originated from surface spills and leaks from subsurface pipelines that have migrated through the backfill material. The  $^{137}\text{Cs}$  below 20 ft is interpreted to have originated from a nearby cascade line (DOE 1997m).

The results of the shape factor analysis between the ground surface and 13 ft indicate the contamination is distributed somewhat uniformly in the backfill sediments. The shape factor CsSF1 below 13 ft becomes highly influenced by the regions of high dead time and does not provide interpretable results.

### **B1.21 Shape Factor Analysis for Borehole 30-05-08**

The Tank Summary Data Report for tank C-105 (DOE 1997m) presents the results of the data analysis for the boreholes surrounding tank C-105. Appendix A provides a log of the man-made contamination detected around borehole 30-05-08. SGLS data specific to borehole 30-05-08 are presented in Appendix A so the reader can compare the man-made radionuclide data to the shape factor analysis log presented in this appendix.

The man-made radionuclides  $^{137}\text{Cs}$ ,  $^{60}\text{Co}$ , and  $^{154}\text{Eu}$  were detected around this borehole.  $^{137}\text{Cs}$  was detected continuously from the ground surface to 49 ft (the bottom of the logged interval).  $^{60}\text{Co}$  was detected from 2.5 to 3 ft, 15.5 to 17 ft, and 34.5 to 48.5 ft. Continuous  $^{154}\text{Eu}$  contamination was detected from 14.5 to 18.5 ft.

$^{137}\text{Cs}$  was present above the 1-cps (1.6 pCi/g) threshold for calculating shape factor CsSF1 from the ground surface to 22.5 ft, from 27.5 to 38 ft, and from 43.5 to 48.5 ft.  $^{60}\text{Co}$  was above the 2-cps threshold for calculating shape factor CoSF1 from 38 to 38.5 ft.

According to the Tank Summary Data Report for tank C-105, the  $^{137}\text{Cs}$  and  $^{60}\text{Co}$  between the ground surface and 49 ft originated from surface spills and leaks from subsurface pipelines that have migrated through the backfill material (DOE 1997m).

The analysis of CsSF1 in the interval from just below the ground surface to 44.5 ft indicates the  $^{137}\text{Cs}$  is distributed around the borehole casing in the backfill sediments. The indicated remote sources from 14 to 30 ft and from 35 to 45 ft are most likely due to the uncorrected influence of the  $^{60}\text{Co}$  and  $^{154}\text{Eu}$  in these intervals.

Between about 45 and 49 ft, the shape factor CsSF1 indicates the  $^{137}\text{Cs}$  is localized to the borehole casing. The shape factor results for the  $^{60}\text{Co}$  contamination from 41 to 52 ft indicate the contamination is somewhat remote from the borehole.

The shape factor results generally support the conclusion presented in the Tank Summary Data Report that the  $^{137}\text{Cs}$  and  $^{60}\text{Co}$  contamination is generally distributed in the formation sediments. However, the contamination from 45 to 49 ft may be more localized to the borehole region than originally believed.

## **B1.22 Shape Factor Analysis for Borehole 30-05-09**

The Tank Summary Data Report for tank C-105 (DOE 1997m) presents the results of the data analysis for the boreholes surrounding tank C-105. Appendix A provides a log of the man-made contamination detected around borehole 30-05-09. SGLS data specific to borehole 30-05-09 are presented in Appendix A so the reader can compare the man-made radionuclide data to the shape factor analysis log presented in this appendix.

The only man-made radionuclide detected around this borehole was  $^{137}\text{Cs}$ .  $^{137}\text{Cs}$  was detected nearly continuously from the ground surface to 32.5 ft and from 48.5 to 77 ft. Scattered occurrences of  $^{137}\text{Cs}$  were detected at 41.5 ft, from 78.5 to 86.5 ft, and at the bottom of the borehole.  $^{235}\text{U}$  was detected only at the ground surface.  $^{137}\text{Cs}$  was present above the 1-cps (1.6 pCi/g) threshold for calculating shape factor CsSF1 from the ground surface to 27 ft and from 57.5 to 63.5 ft.

According to the Tank Summary Data Report for tank C-105, the  $^{137}\text{Cs}$  between the ground surface and 27 ft originated from surface spills and leaks from subsurface pipelines that have migrated through the backfill material. The  $^{137}\text{Cs}$  from 58 to 63 ft is most likely the result of a

subsurface source such as a pipeline leak. The  $^{137}\text{Cs}$  between 27 and 58 ft was apparently carried down during borehole construction or migrated down the outside of the casing (DOE 1997m).

The analysis of CsSF1 in the interval between the ground surface and 27 ft indicates the  $^{137}\text{Cs}$  is uniformly distributed in the backfill sediments. Between about 57.5 to 63.5 ft, the shape factor CsSF1 indicates the  $^{137}\text{Cs}$  distribution varies from somewhat localized to the borehole region to uniformly distributed in the Hanford formation sediments.

The shape factor results from the ground surface to 27 ft supports the interpretation that the  $^{137}\text{Cs}$  is distributed in the backfill sediments. The shape factor results from 57.5 to 63.5 ft generally support the conclusion that the  $^{137}\text{Cs}$  is distributed in the Hanford formation sediments; however, some contamination is localized to the borehole casing.

### **B1.23 Shape Factor Analysis for Borehole 30-06-02**

The Tank Summary Data Report for tank C-106 (DOE 1997n) presents the results of the data analysis for the boreholes surrounding tank C-106. Appendix A provides a log of the man-made contamination detected around borehole 30-06-02. SGLS data specific to borehole 30-06-02 are presented in Appendix A so the reader can compare the man-made radionuclide data to the shape factor analysis log presented in this appendix.

The only man-made radionuclide detected around this borehole was  $^{137}\text{Cs}$ .  $^{137}\text{Cs}$  was detected nearly continuously from the ground surface to 14.5 ft, from 23.5 to 56 ft, from 115 to 117 ft, and from 121.5 to 122.5 ft (the bottom of the logged interval).  $^{137}\text{Cs}$  was present above the 1-cps (1.6 pCi/g) threshold for calculating shape factor CsSF1 from the ground surface to 14 ft, from 39 to 40 ft, at 56 ft, from 115.5 to 116 ft, and at the bottom of the borehole.

According to the Tank Summary Data Report for tank C-106, the  $^{137}\text{Cs}$  between the ground surface and 14 ft originated from surface spills and leaks from subsurface pipelines that have migrated through the backfill material. The  $^{137}\text{Cs}$  from 39 to 40 ft is most likely the result of a subsurface source such as a pipeline leak. The rest of the  $^{137}\text{Cs}$  was apparently carried down during borehole construction or migrated down the outside of the casing (DOE 1997n).

The analysis of CsSF1 in the interval from just below the ground surface to 14 ft indicates the  $^{137}\text{Cs}$  is distributed in the backfill sediments and somewhat localized to the borehole. Between about 39 and 40 ft, the shape factor CsSF1 indicates the  $^{137}\text{Cs}$  distribution uniformly distributed in the backfill sediments.

The discrete CsSF1 values below 40 ft are not sufficient for interpreting the  $^{137}\text{Cs}$  distributions at these locations. However, the results do seem to indicate the contamination may be distributed in the Hanford formation.

## **B1.24 Shape Factor Analysis for Borehole 30-06-03**

The Tank Summary Data Report for tank C-106 (DOE 1997n) presents the results of the data analysis for the boreholes surrounding tank C-106. Appendix A provides a log of the man-made contamination detected around borehole 30-06-03. SGLS data specific to borehole 30-06-03 are presented in Appendix A so the reader can compare the man-made radionuclide data to the shape factor analysis log presented in this appendix.

The only man-made radionuclide detected around this borehole was  $^{137}\text{Cs}$ .  $^{137}\text{Cs}$  was detected nearly continuously from the ground surface to 76.5 ft and at the bottom of the borehole.  $^{137}\text{Cs}$  was present above the 1-cps (1.6 pCi/g) threshold for calculating shape factor CsSF1 from the ground surface to 67.5 ft.

According to the Tank Summary Data Report for tank C-106, the near-surface zone of contamination resulted from surface spills and leaks from subsurface pipelines that have migrated through the backfill material. The  $^{137}\text{Cs}$  at about 27 ft is most likely the result of a subsurface source such as a pipeline leak. The rest of the  $^{137}\text{Cs}$  was apparently carried down during borehole construction or migrated down the outside of the casing (DOE 1997n).

The analysis of CsSF1 indicates the  $^{137}\text{Cs}$  varies in distribution from deposited in the backfill sediments to somewhat localized to the borehole. Interpretations presented in the Tank Summary Data Report concluded most of the  $^{137}\text{Cs}$  was localized to the borehole casing. However, the shape factor analysis indicates at least some of the  $^{137}\text{Cs}$  is distributed in the backfill and Hanford formation sediments.

## **B1.25 Shape Factor Analysis for Borehole 30-06-04**

The Tank Summary Data Report for tank C-106 (DOE 1997n) presents the results of the data analysis for the boreholes surrounding tank C-106. Appendix A provides a log of the man-made contamination detected around borehole 30-06-04. SGLS data specific to borehole 30-06-04 are presented in Appendix A so the reader can compare the man-made radionuclide data to the shape factor analysis log presented in this appendix.

The man-made radionuclides  $^{137}\text{Cs}$  and  $^{60}\text{Co}$  were detected around this borehole.  $^{137}\text{Cs}$  was detected continuously from the ground surface to 57 ft, from 23.5 to 56 ft, and intermittently from 58.5 to 66 ft and 119 to 129.5 ft.  $^{60}\text{Co}$  was detected continuously from 85 to 90.5 ft and at 93 ft.  $^{137}\text{Cs}$  was present above the 1-cps (1.6 pCi/g) threshold for calculating shape factor CsSF1 from the ground surface to 53 ft and at the bottom of the borehole.  $^{60}\text{Co}$  was not present above the 2-cps threshold for calculating shape factor CoSF1.

According to the Tank Summary Data Report for tank C-106, the  $^{137}\text{Cs}$  between the ground surface and 56 ft originated from surface spills and leaks from subsurface pipelines that have migrated through the backfill material. The  $^{137}\text{Cs}$  below 56 ft was apparently carried down during borehole construction or migrated down the outside of the casing (DOE 1997n).

The analysis of CsSF1 in the interval between the ground surface and 53 ft indicates the  $^{137}\text{Cs}$  is generally distributed in the backfill and Hanford formation sediments, but somewhat localized to the borehole.

### **B1.26 Shape Factor Analysis for Borehole 30-06-09**

The Tank Summary Data Report for tank C-106 (DOE 1997n) presents the results of the data analysis for the boreholes surrounding tank C-106. Appendix A provides a log of the man-made contamination detected around borehole 30-06-09. SGLS data specific to borehole 30-06-09 are presented in Appendix A so the reader can compare the man-made radionuclide data to the shape factor analysis log presented in this appendix.

The man-made radionuclides  $^{137}\text{Cs}$ ,  $^{60}\text{Co}$ , and  $^{235}\text{U}$  were detected around this borehole.  $^{137}\text{Cs}$  was detected continuously from the ground surface to 52.5 ft, intermittently from 54 to 72.5 ft, at 91.5 ft, and at the bottom of the borehole.  $^{60}\text{Co}$  was detected from 22 to 22.5 ft and at 74.5 ft.  $^{235}\text{U}$  was detected only at the ground surface.  $^{137}\text{Cs}$  was present above the 1-cps (1.6 pCi/g) threshold for calculating shape factor CsSF1 from the ground surface to 17 ft, at 20.5 ft, at 26.5 ft, from 41 to 45.5 ft, at 47 ft, from 49.5 to 51 ft, and at the bottom of the borehole.  $^{60}\text{Co}$  was not present above the 2-cps threshold for calculating shape factor CoSF1.

According to the Tank Summary Data Report for tank C-106, the  $^{137}\text{Cs}$  between the ground surface and 17 ft originated from surface spills and leaks from subsurface pipelines that have migrated through the backfill material. The  $^{137}\text{Cs}$  between 26 and 27.5 ft may be related to a leak from a nearby subsurface pipeline. The interpretation presented in the Tank Summary Data Report concludes the  $^{137}\text{Cs}$  between 41 and 46 ft accumulated at the base of the tank farm excavation. The rest of the contamination was apparently carried down during borehole construction or migrated down the outside of the casing (DOE 1997n).

The analysis of CsSF1 in the interval between the ground surface and 17 ft indicates the  $^{137}\text{Cs}$  is generally distributed in the backfill sediments, but somewhat localized to the borehole. Shape factor CsSF1 indicates the  $^{137}\text{Cs}$  from 41 to 45 ft and from 49.5 to 51 ft is distributed uniformly in the Hanford formation sediments. The shape factor analysis appears to support the interpretations presented in the Tank Summary Data Report.

### **B1.27 Shape Factor Analysis for Borehole 30-06-10**

The Tank Summary Data Report for tank C-106 (DOE 1997n) presents the results of the data analysis for the boreholes surrounding tank C-106. Appendix A provides a log of the man-made contamination detected around borehole 30-06-10. SGLS data specific to borehole 30-06-10 are presented in Appendix A so the reader can compare the man-made radionuclide data to the shape factor analysis log presented in this appendix.

The man-made radionuclides  $^{137}\text{Cs}$ ,  $^{60}\text{Co}$ ,  $^{154}\text{Eu}$ , and  $^{235}\text{U}$  were detected around this borehole.  $^{137}\text{Cs}$  was detected continuously from the ground surface to 11 ft, from 12 to 17 ft, from 45 to 57 ft, from 65.5 to 67.5 ft, and at the bottom of the borehole.  $^{60}\text{Co}$  was detected continuously

from 86 to 116.5 ft.  $^{154}\text{Eu}$  and  $^{235}\text{U}$  were detected only at the ground surface.  $^{137}\text{Cs}$  was present above the 1-cps (1.6 pCi/g) threshold for calculating shape factor CsSF1 from the ground surface to 9 ft and at the bottom of the borehole.  $^{60}\text{Co}$  was present above the 2-cps threshold for calculating shape factor CoSF1 only at 106.5 ft.

According to the Tank Summary Data Report for tank C-106, the near-surface  $^{137}\text{Cs}$  originated from surface spills and leaks from subsurface pipelines that have migrated through the backfill material. Shape factor CsSF1 from the ground surface to 9 ft indicates the contamination is deposited in the backfill sediments (DOE 1997n).

Although it is not possible to accurately describe the contaminant distribution based on one shape factor data point, the single occurrence of shape factor CoSF1 indicates the  $^{60}\text{Co}$  may be deposited in the Hanford formation sediments.

## **B1.28 Shape Factor Analysis for Borehole 30-06-12**

The Tank Summary Data Report for tank C-106 (DOE 1997n) presents the results of the data analysis for the boreholes surrounding tank C-106. Appendix A provides a log of the man-made contamination detected around borehole 30-06-12. SGLS data specific to borehole 30-06-12 are presented in Appendix A so the reader can compare the man-made radionuclide data to the shape factor analysis log presented in this appendix.

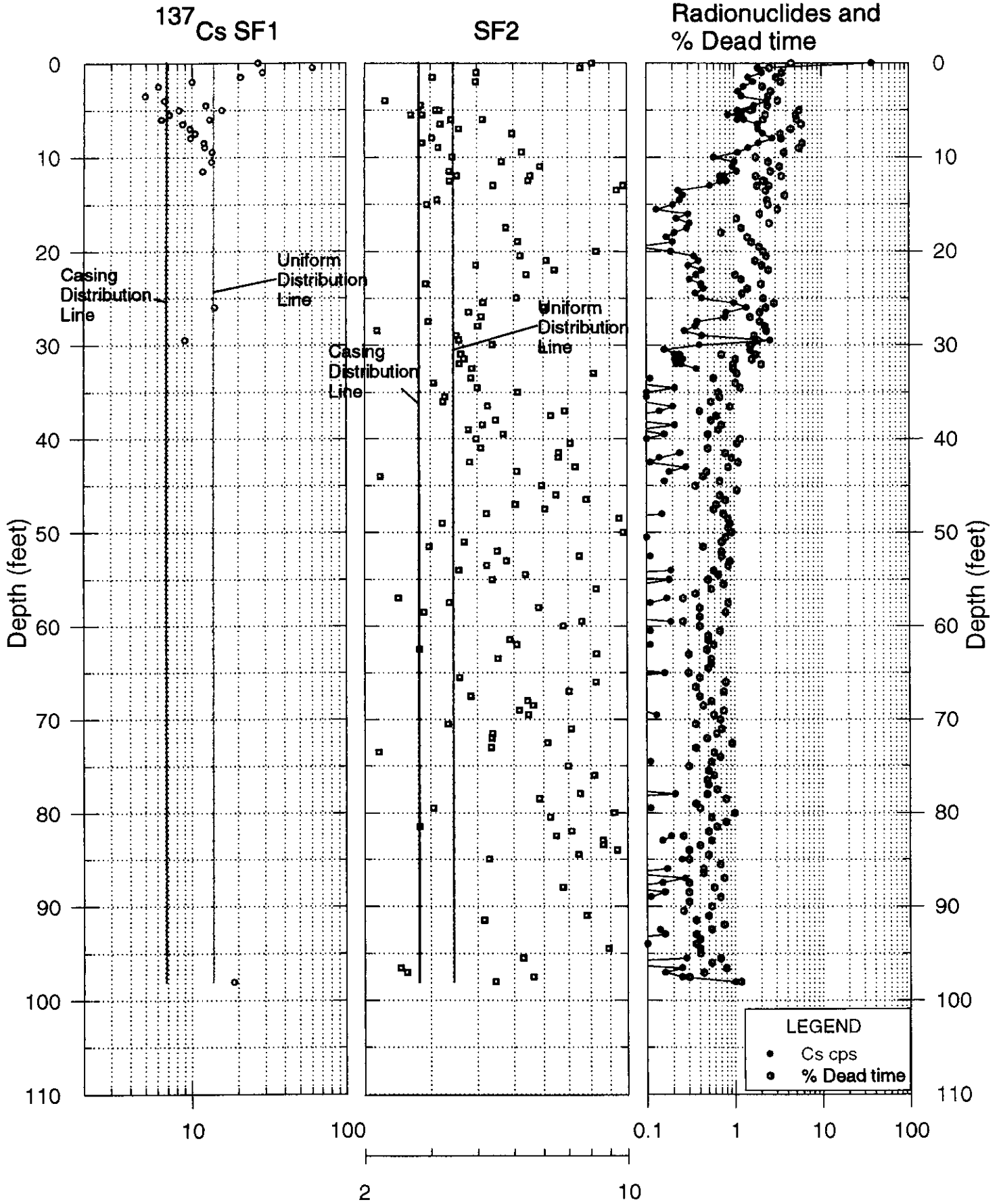
The man-made radionuclides  $^{137}\text{Cs}$  and  $^{60}\text{Co}$  were detected around this borehole.  $^{137}\text{Cs}$  was detected continuously from the ground surface to 31.5 ft and from 48.5 to 65 ft. Small zones of continuous  $^{137}\text{Cs}$  were also detected from 34 to 35 ft, 43 to 45.5 ft, and at the bottom of the borehole. Isolated occurrences of  $^{137}\text{Cs}$  were detected between 66 and 80 ft.  $^{60}\text{Co}$  was detected continuously from 19.5 to 22.5 ft and intermittently from 90 ft to the bottom of the borehole.  $^{137}\text{Cs}$  was present above the 1-cps (1.6 pCi/g) threshold for calculating shape factor CsSF1 from the ground surface to 30.5 ft, from 43.5 to 44 ft, from 49 to 50 ft, from 51.5 to 52 ft, and from 59 to 61 ft.  $^{60}\text{Co}$  was not present above the 2-cps threshold for calculating shape factor CoSF1.

According to the Tank Summary Data Report for tank C-106, the  $^{137}\text{Cs}$  between the ground surface and 30 ft originated from surface spills and leaks from subsurface pipelines that have migrated through the backfill material. The  $^{137}\text{Cs}$  from 43 to 62 ft may have resulted from tank dome runoff that accumulated below the tank farm excavation. The  $^{137}\text{Cs}$  below 62 ft was apparently carried down during borehole construction or migrated down the outside of the casing (DOE 1997n).

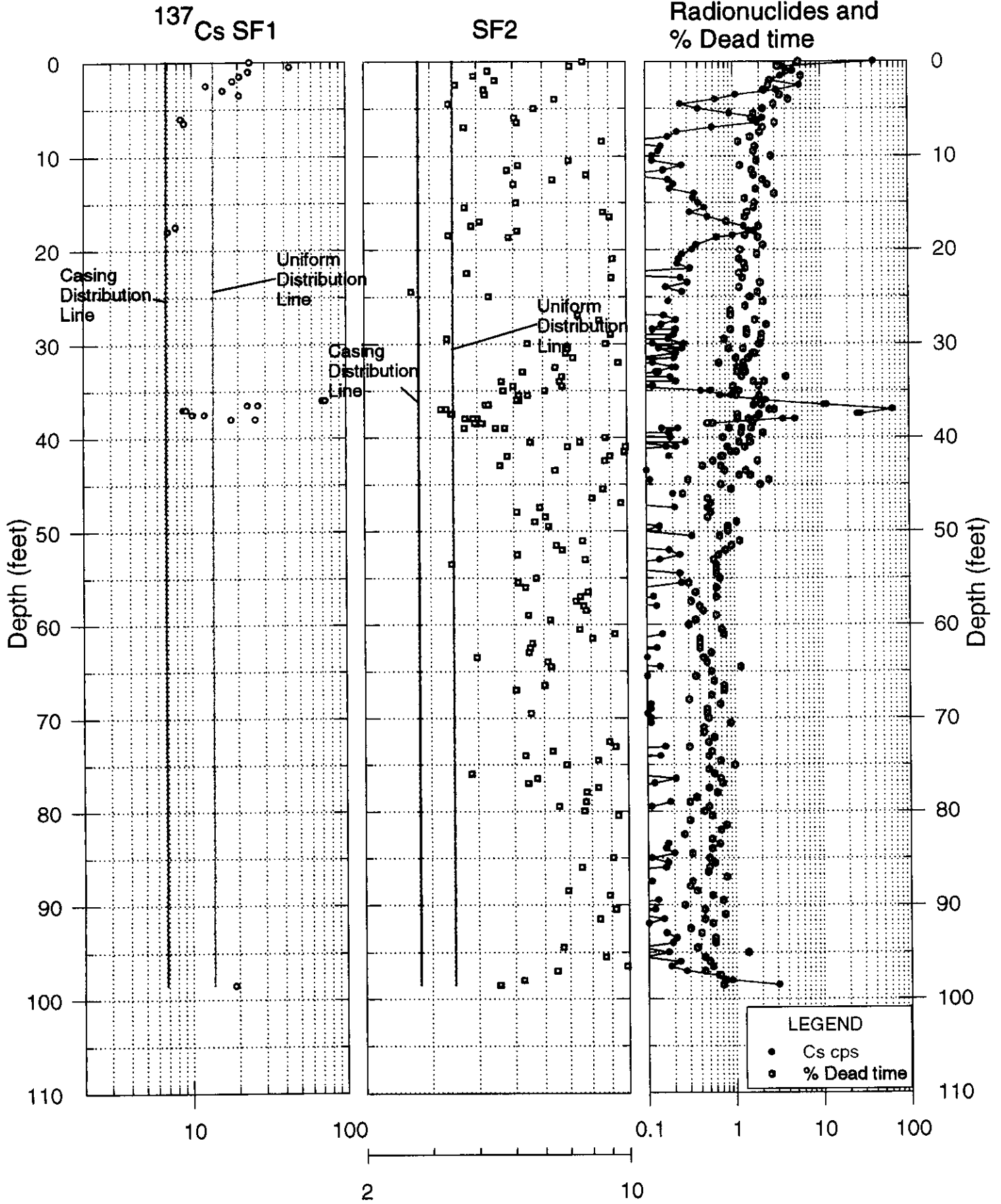
The analysis of CsSF1 in the interval between the ground surface and 30 ft indicates the  $^{137}\text{Cs}$  is generally distributed in the backfill sediments, but somewhat localized to the borehole. The shape factor analysis for this interval supports the interpretation that the  $^{137}\text{Cs}$  is generally deposited in the backfill sediments.

The isolated occurrences of shape factor CsSF1 between 43.5 and 61 ft generally support the conclusion the contamination is distributed in the Hanford formation sediments.

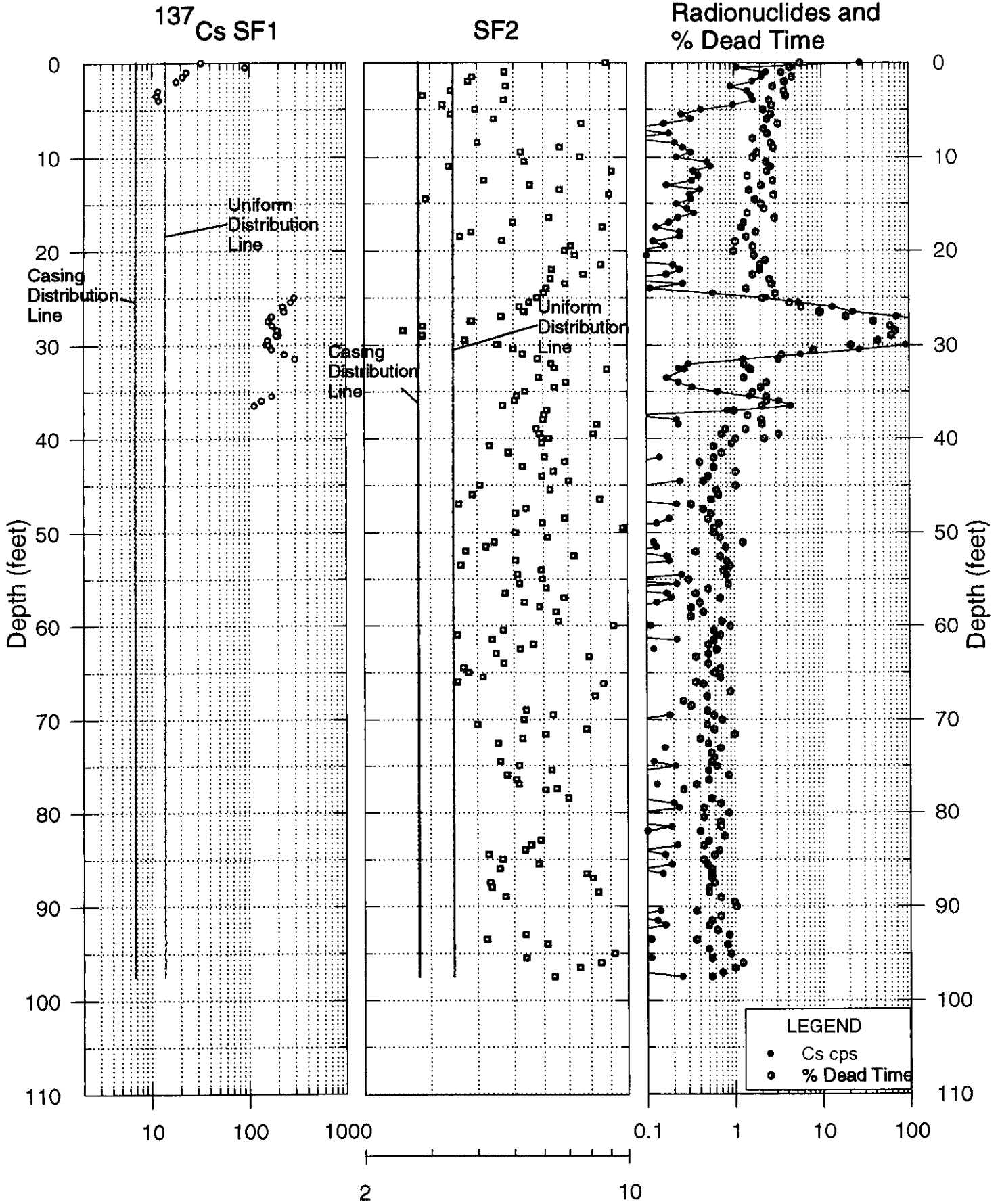
# 30-01-01 Shape Factor Analysis Logs



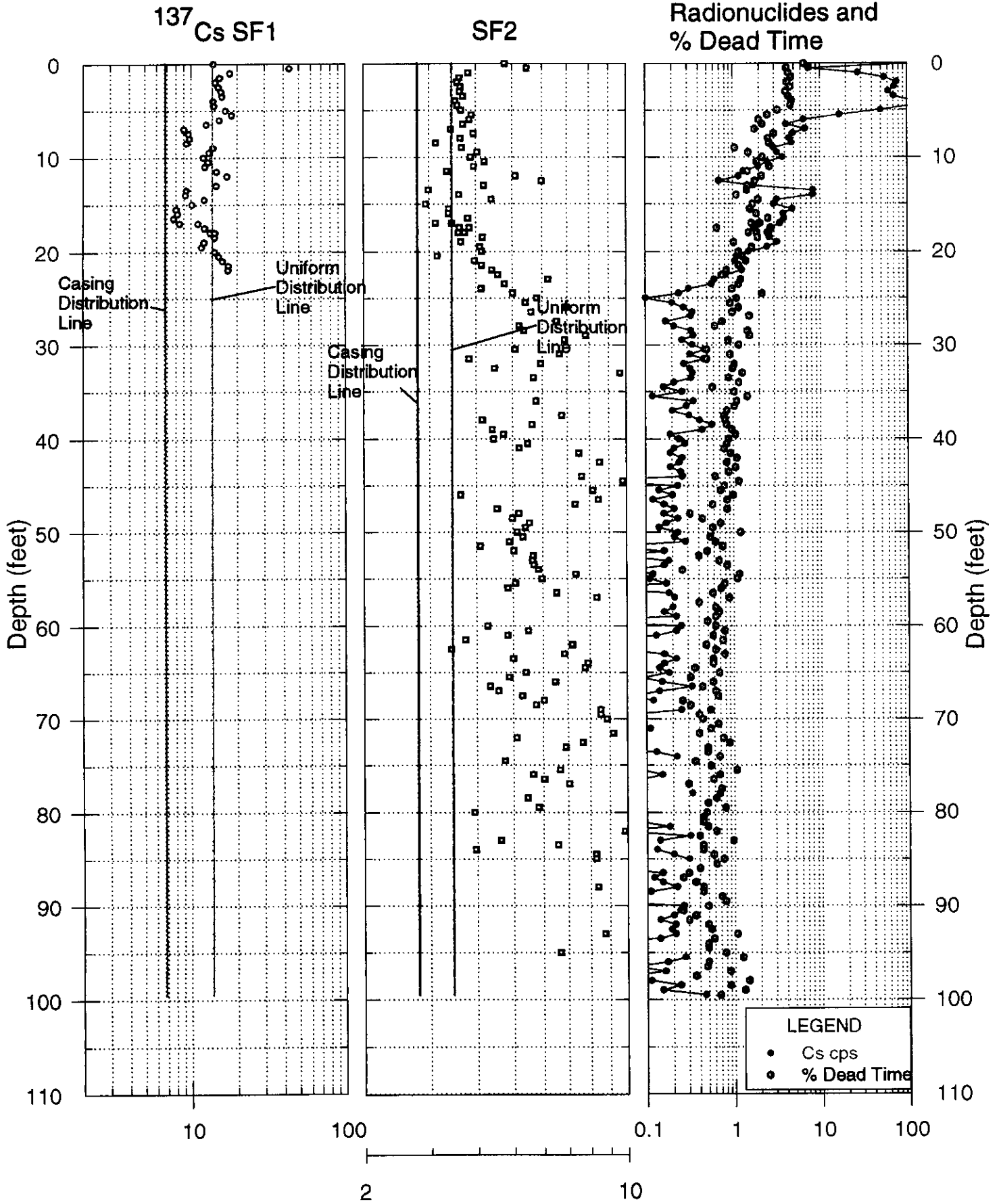
30-01-06  
Shape Factor Analysis Logs



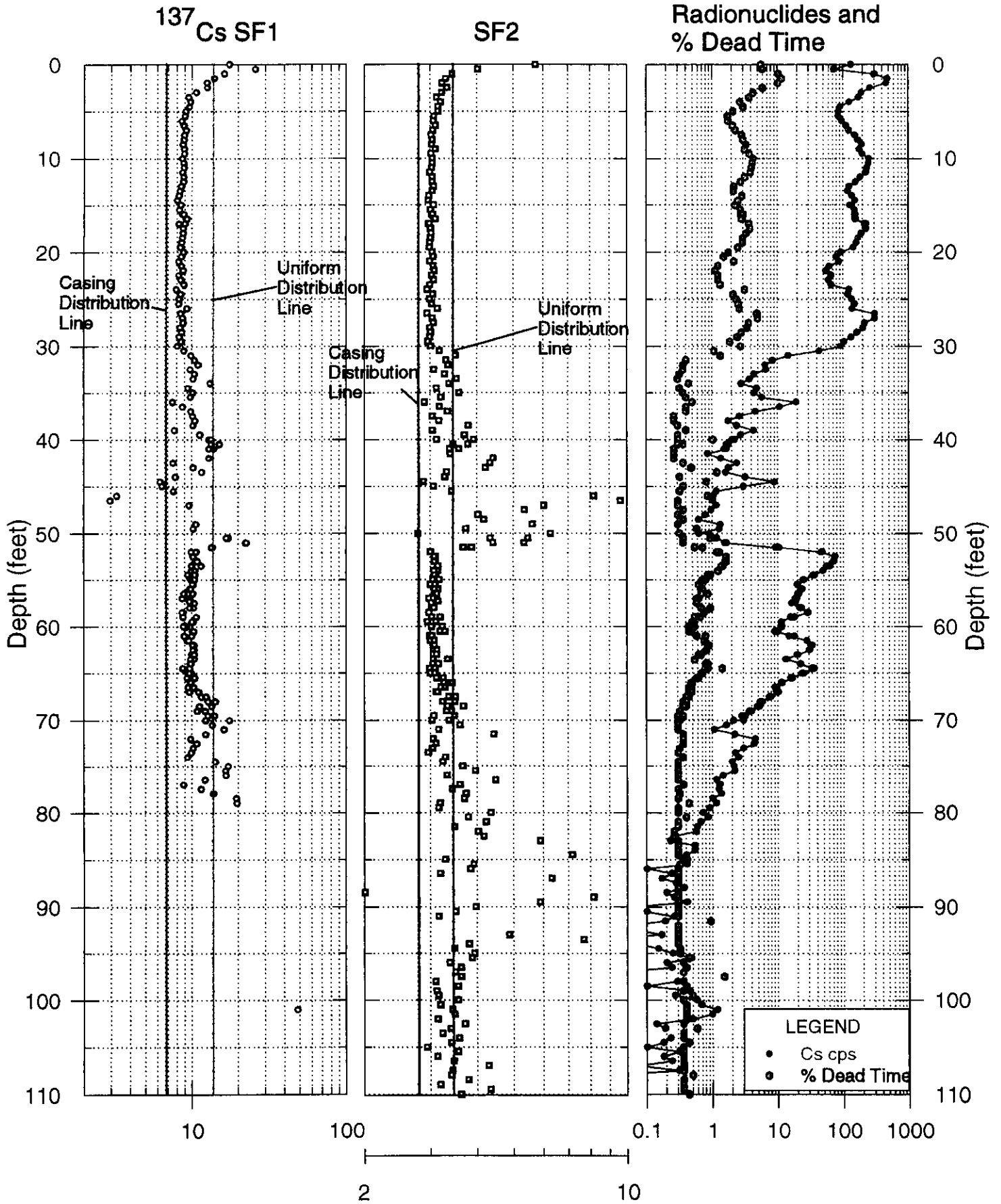
30-01-09  
Shape Factor Analysis Logs



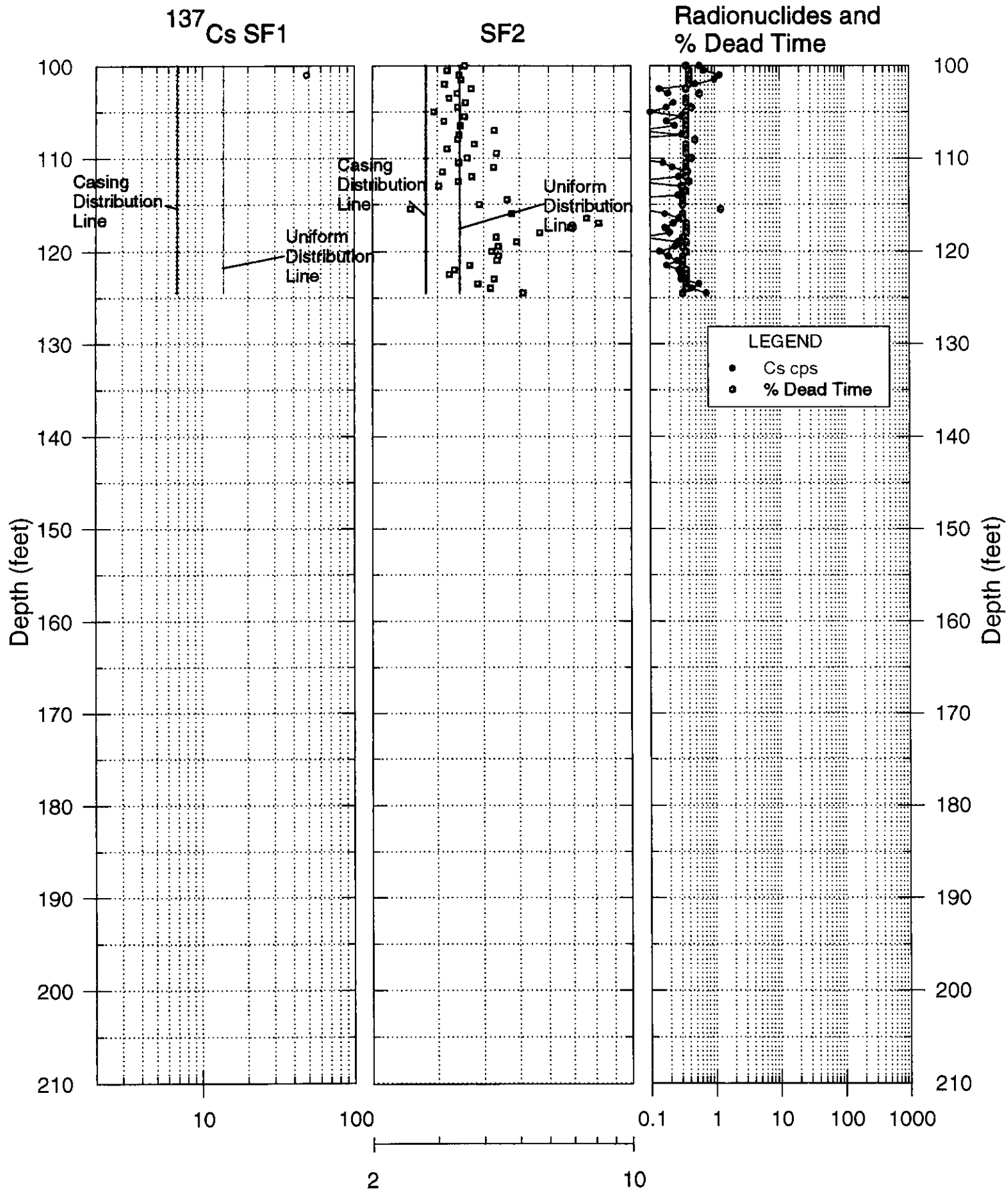
# 30-01-12 Shape Factor Analysis Logs



30-03-01  
Shape Factor Analysis Logs

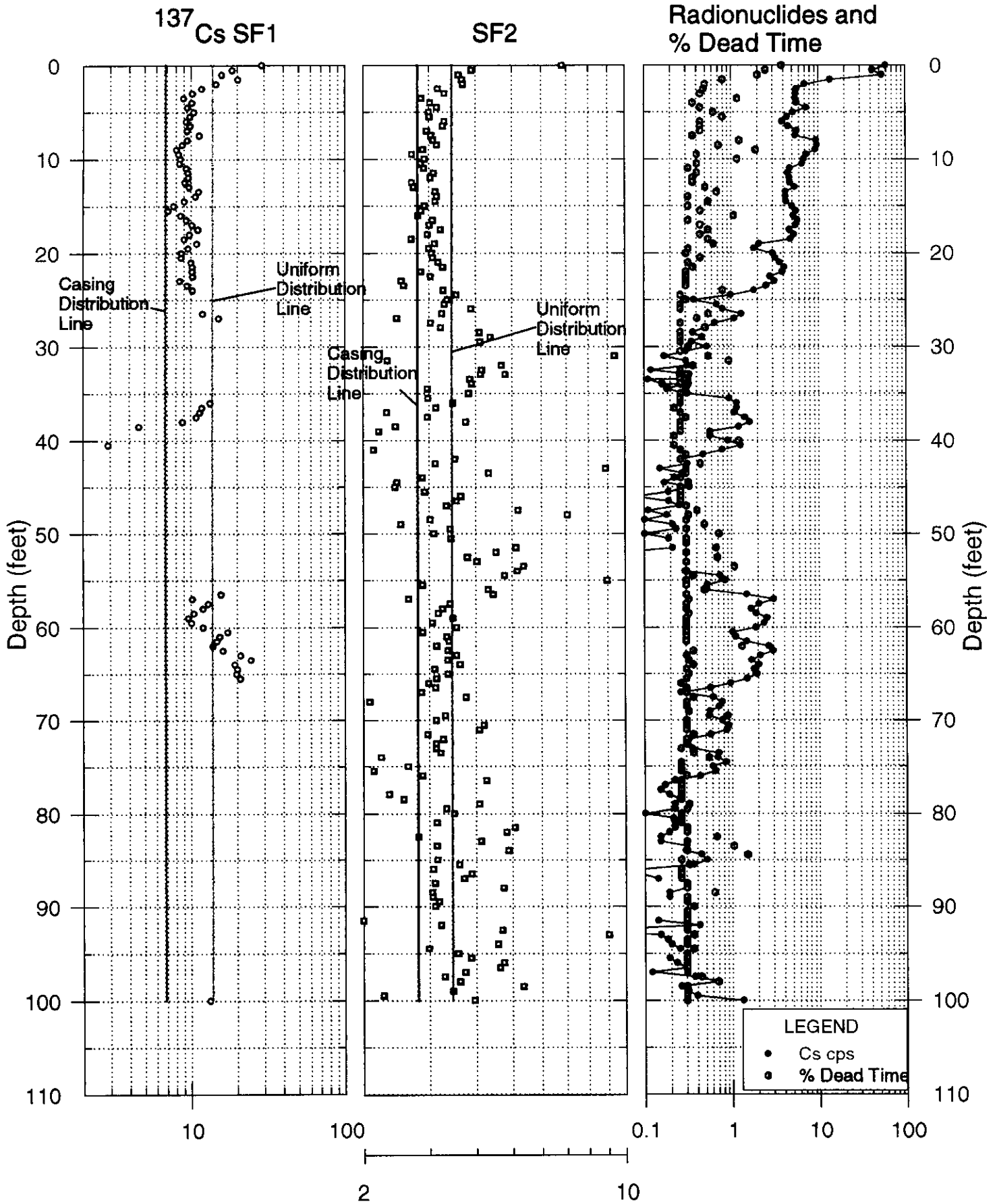


# 30-03-01 Shape Factor Analysis Logs



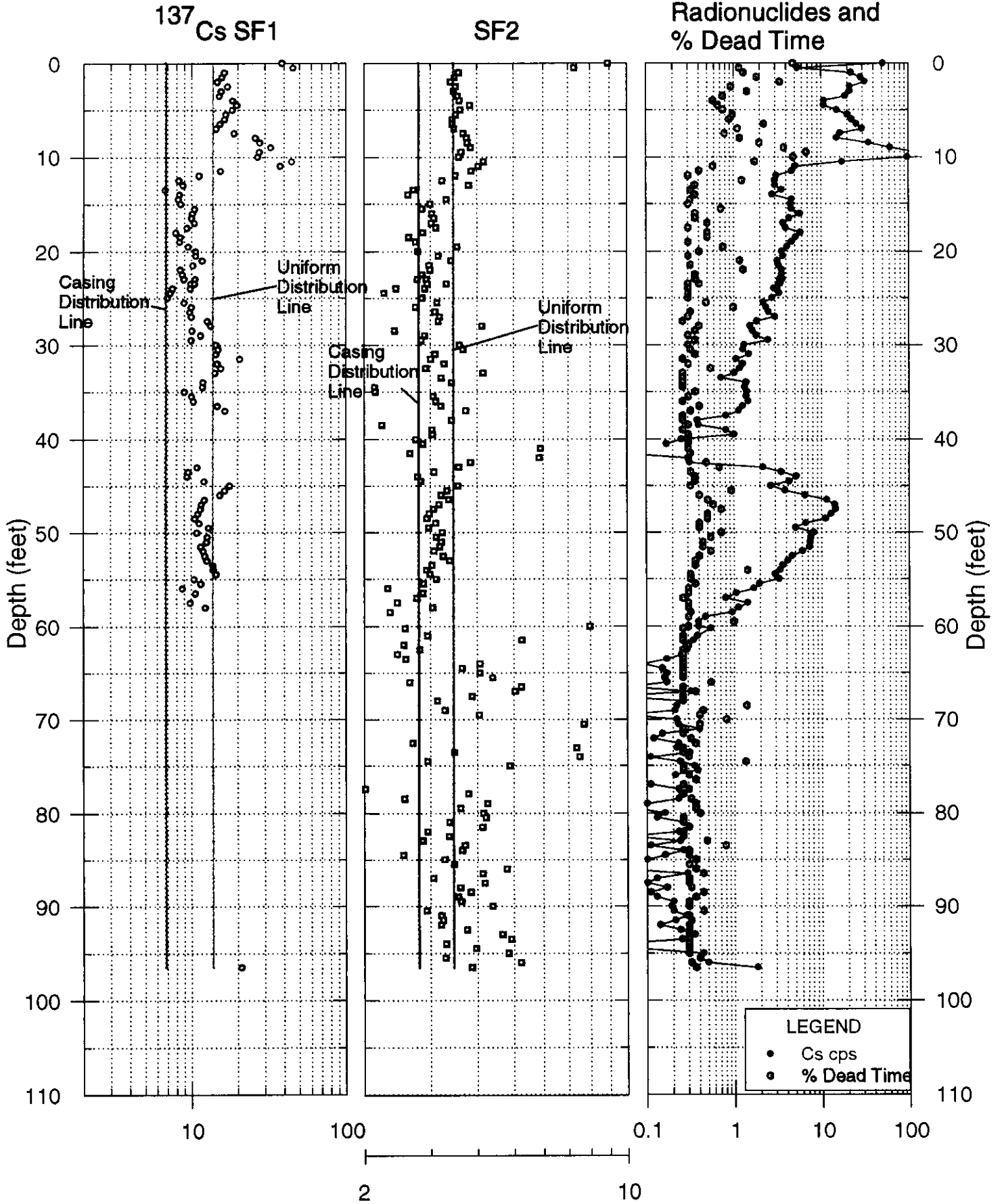
30-03-05

# Shape Factor Analysis Logs



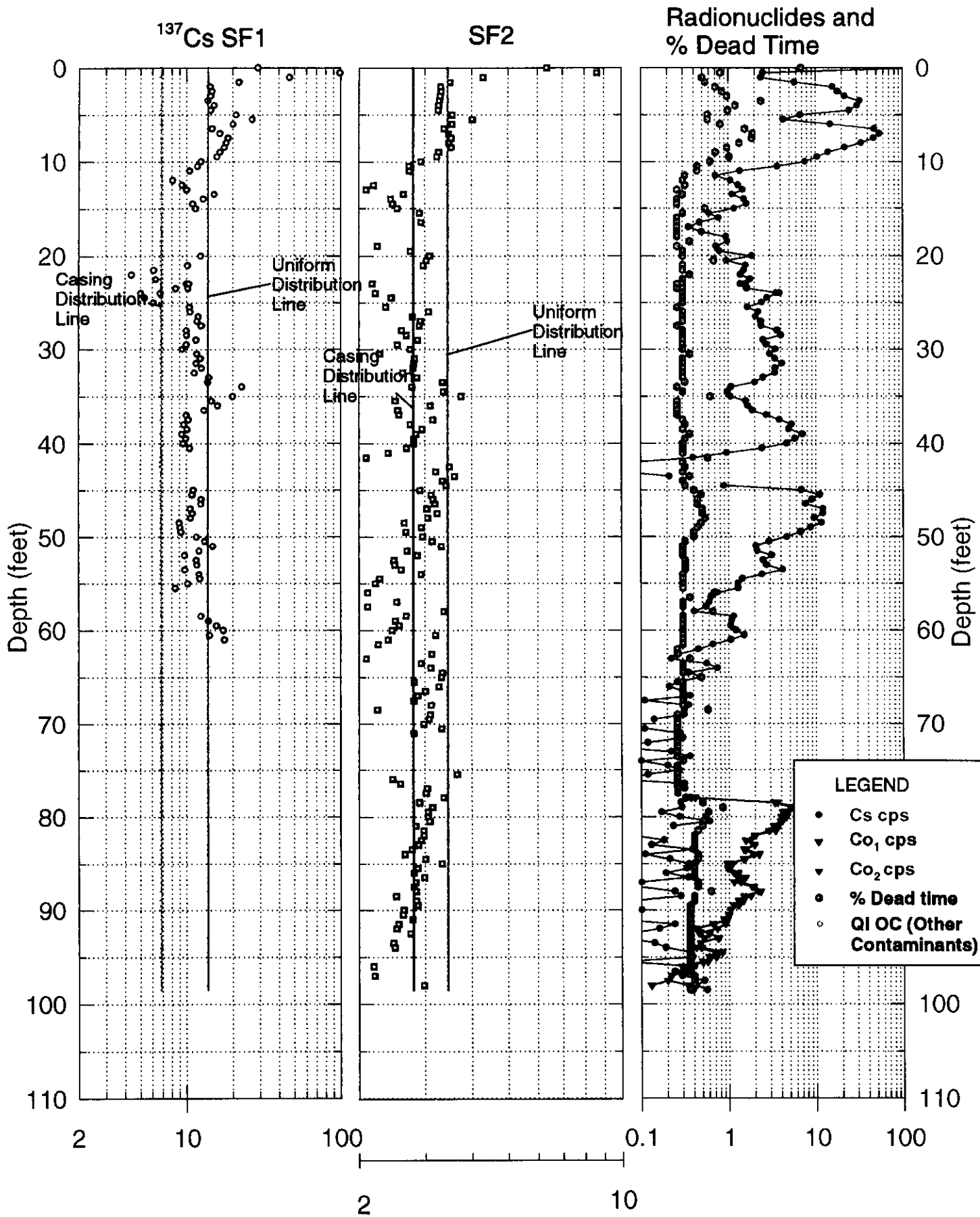
30-03-07

# Shape Factor Analysis Logs



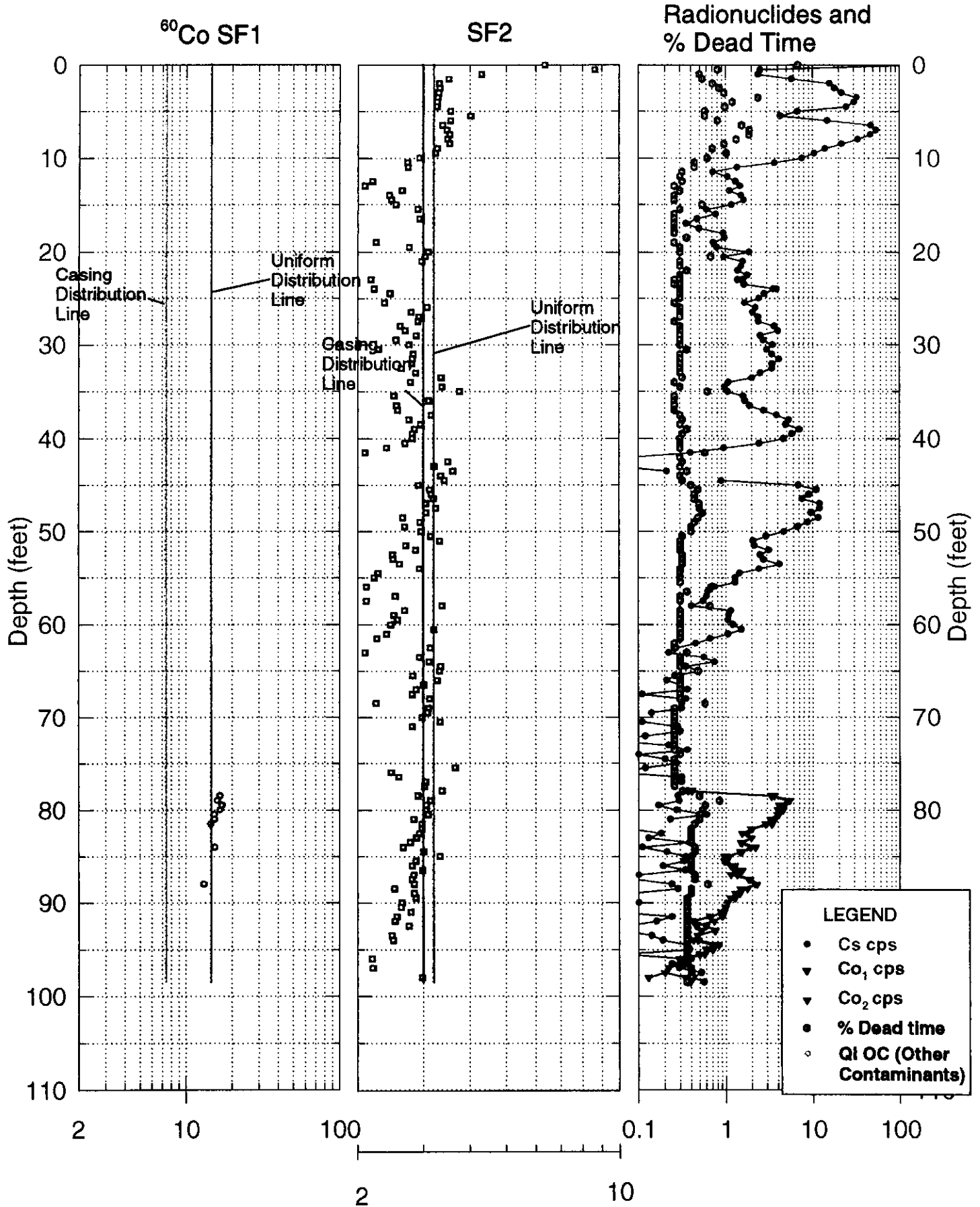
30-03-09

# Shape Factor Analysis Logs

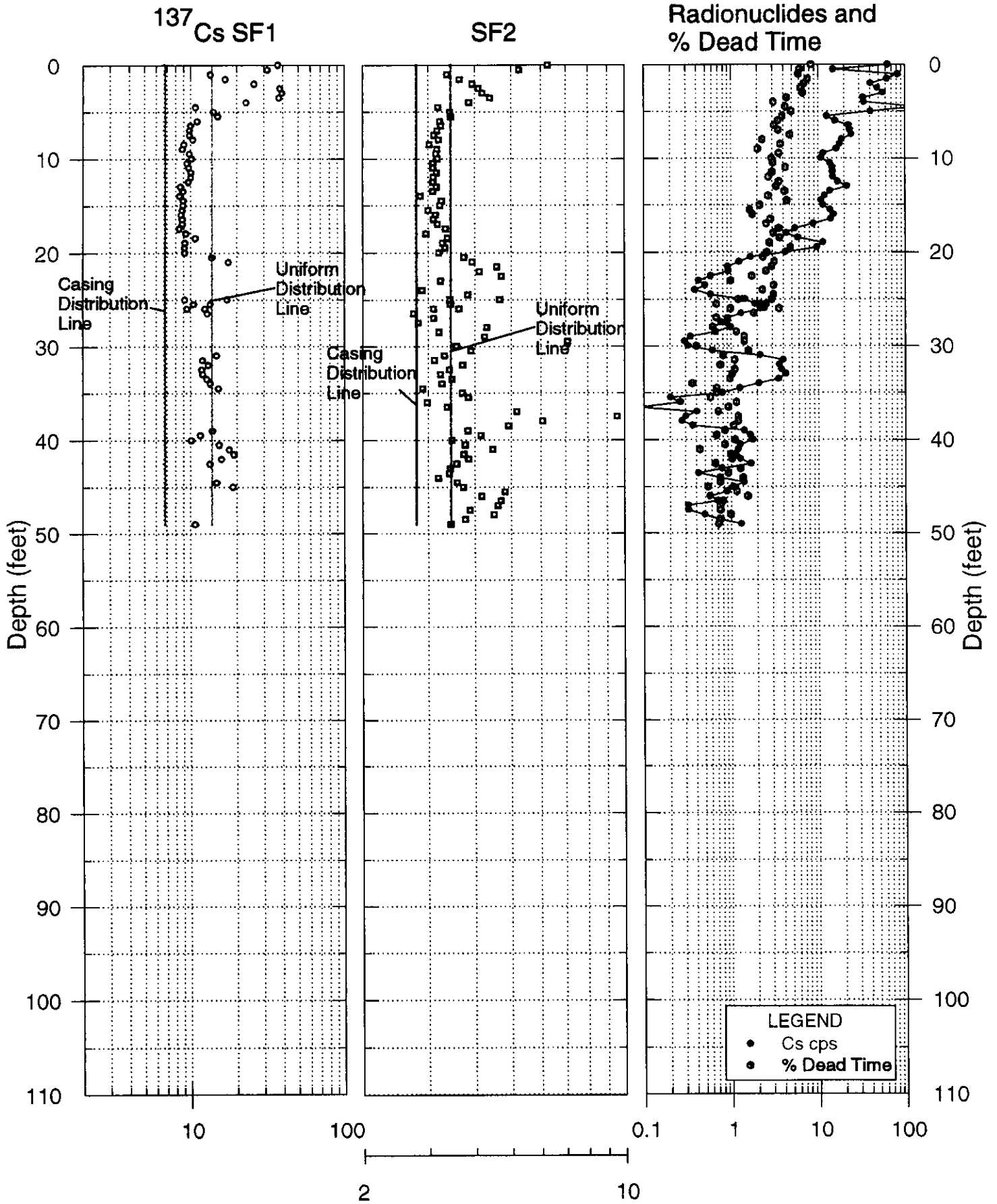


30-03-09

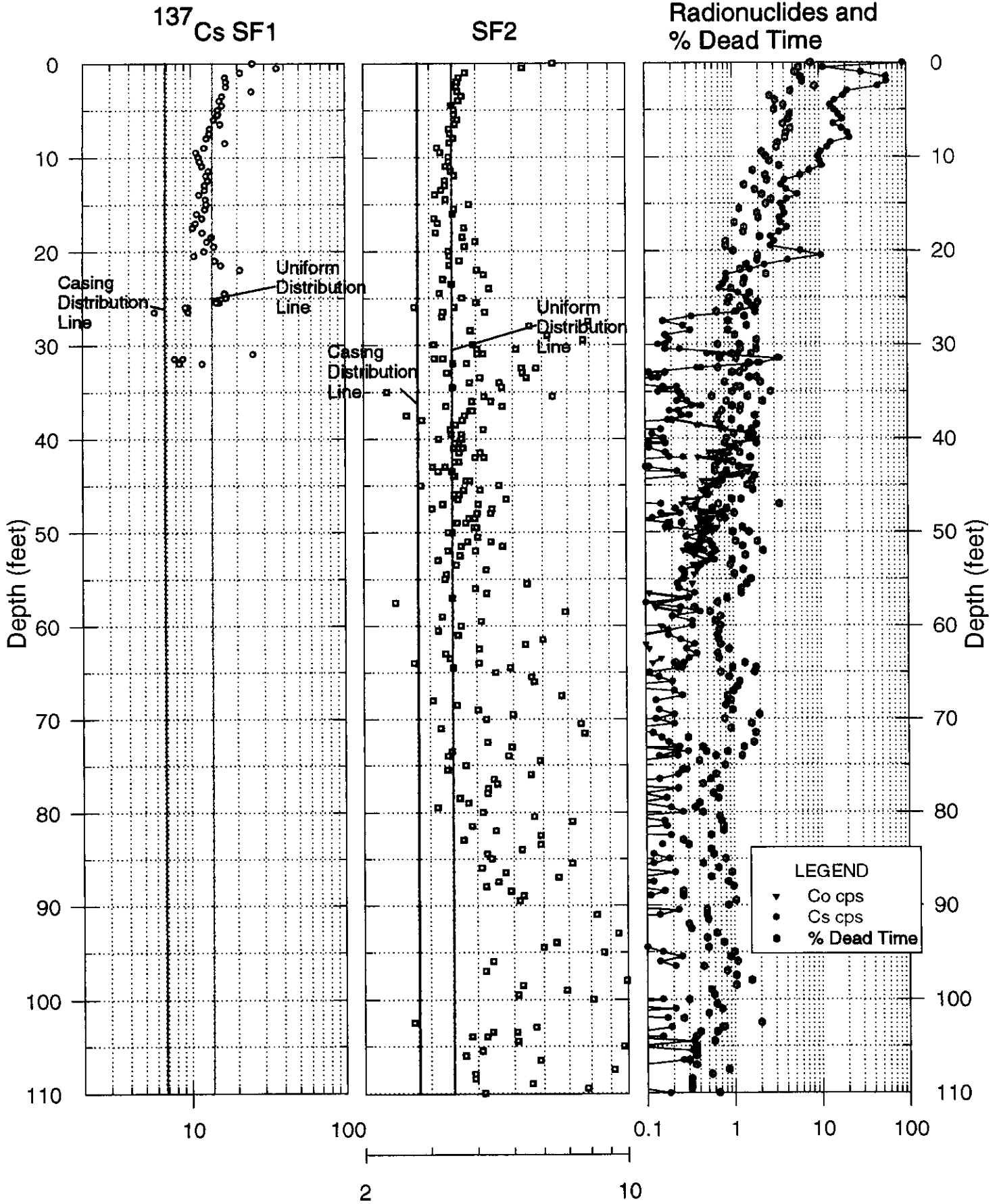
# Shape Factor Analysis Logs



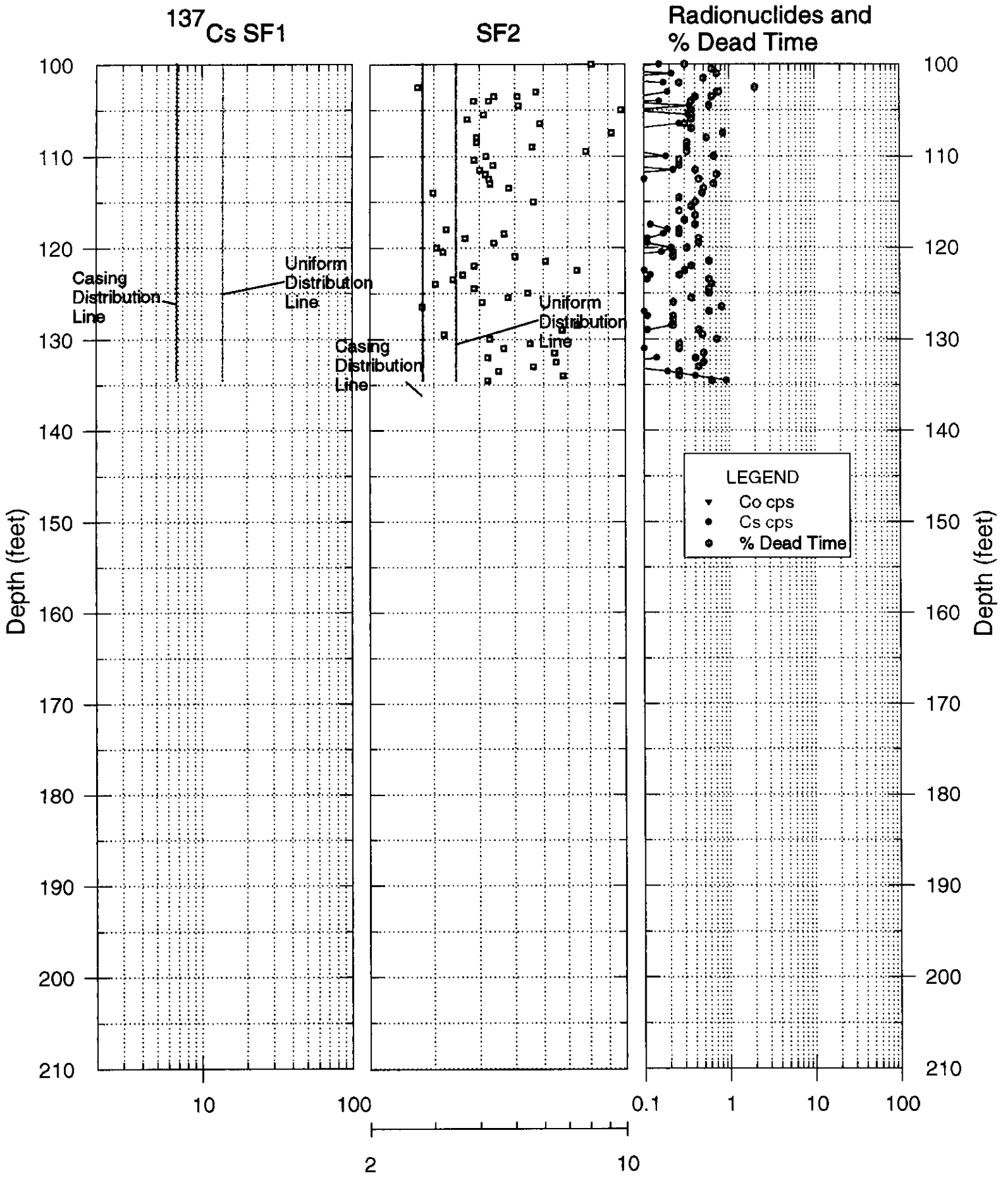
# 30-04-01 Shape Factor Analysis Logs



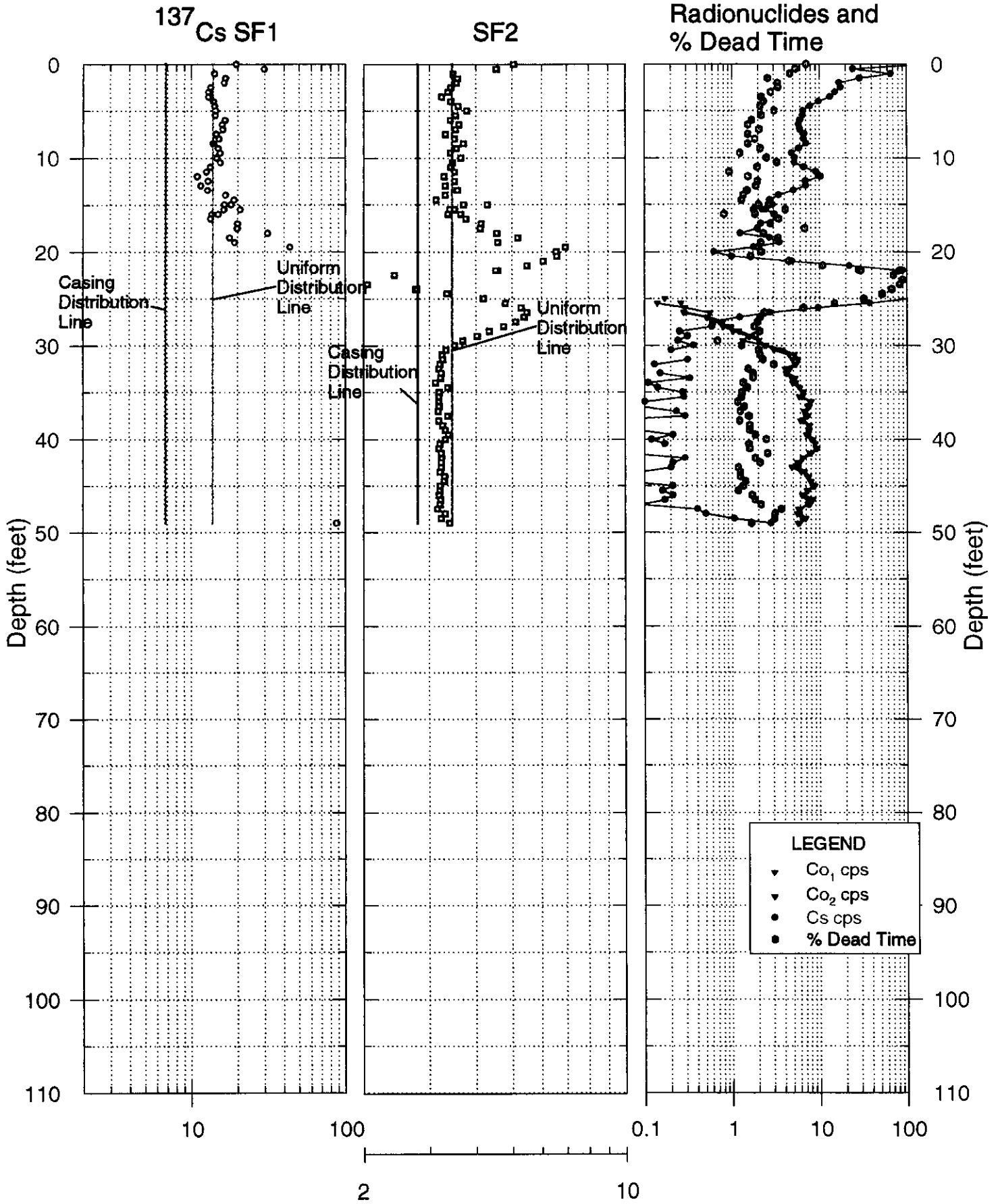
30-04-02  
Shape Factor Analysis Logs



# 30-04-02 Shape Factor Analysis Logs

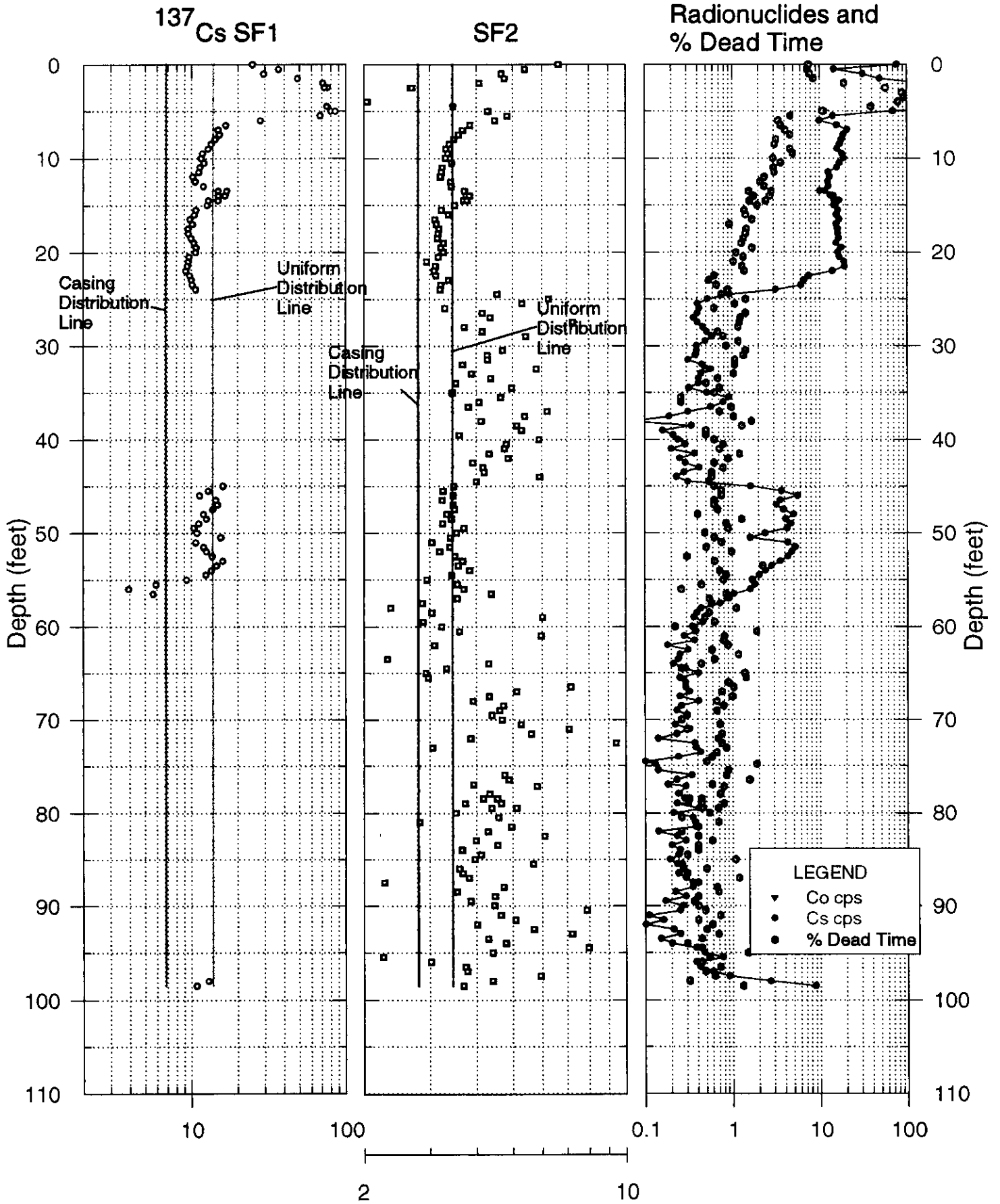


# 30-04-03 Shape Factor Analysis Logs

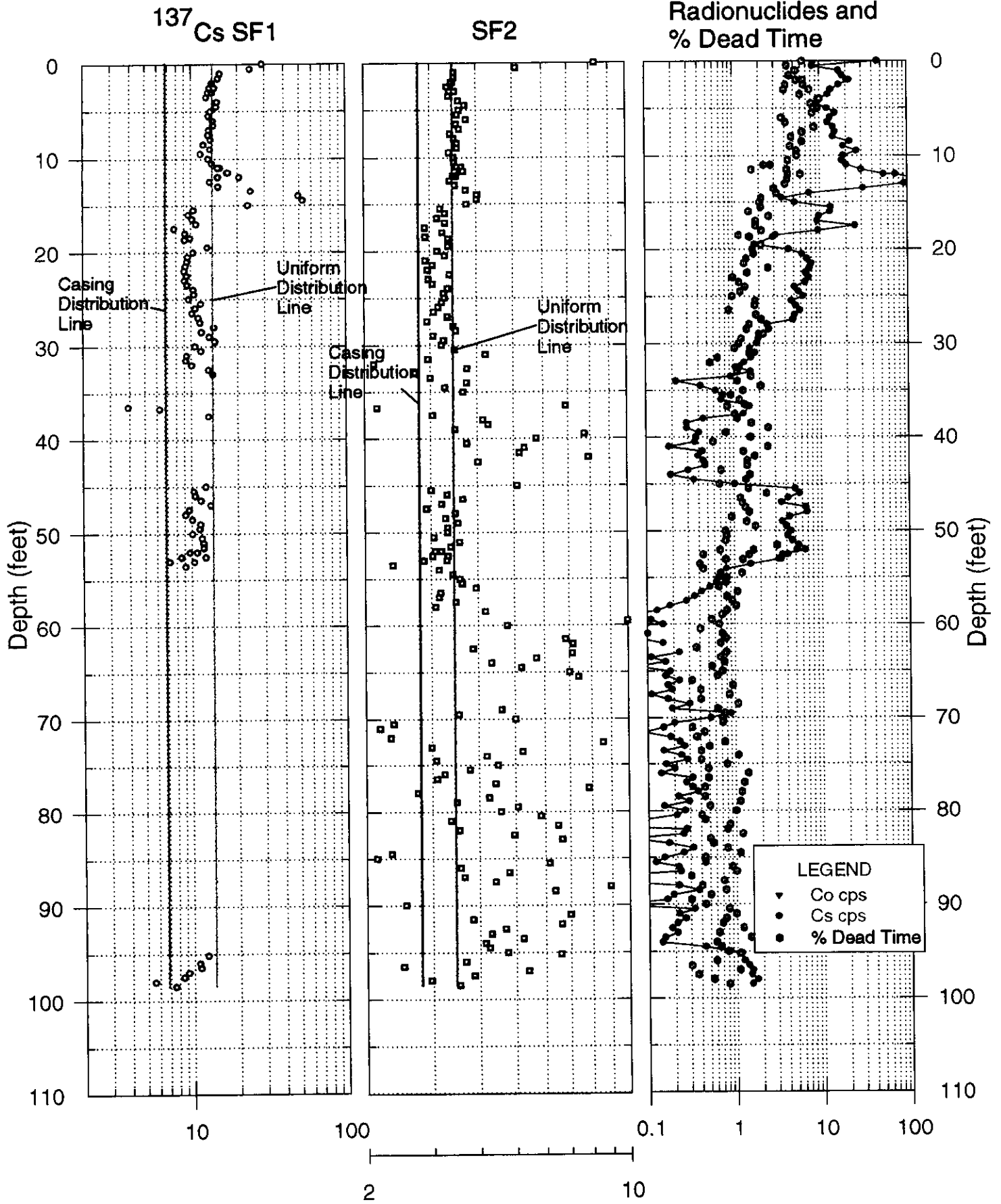




30-04-04  
Shape Factor Analysis Logs

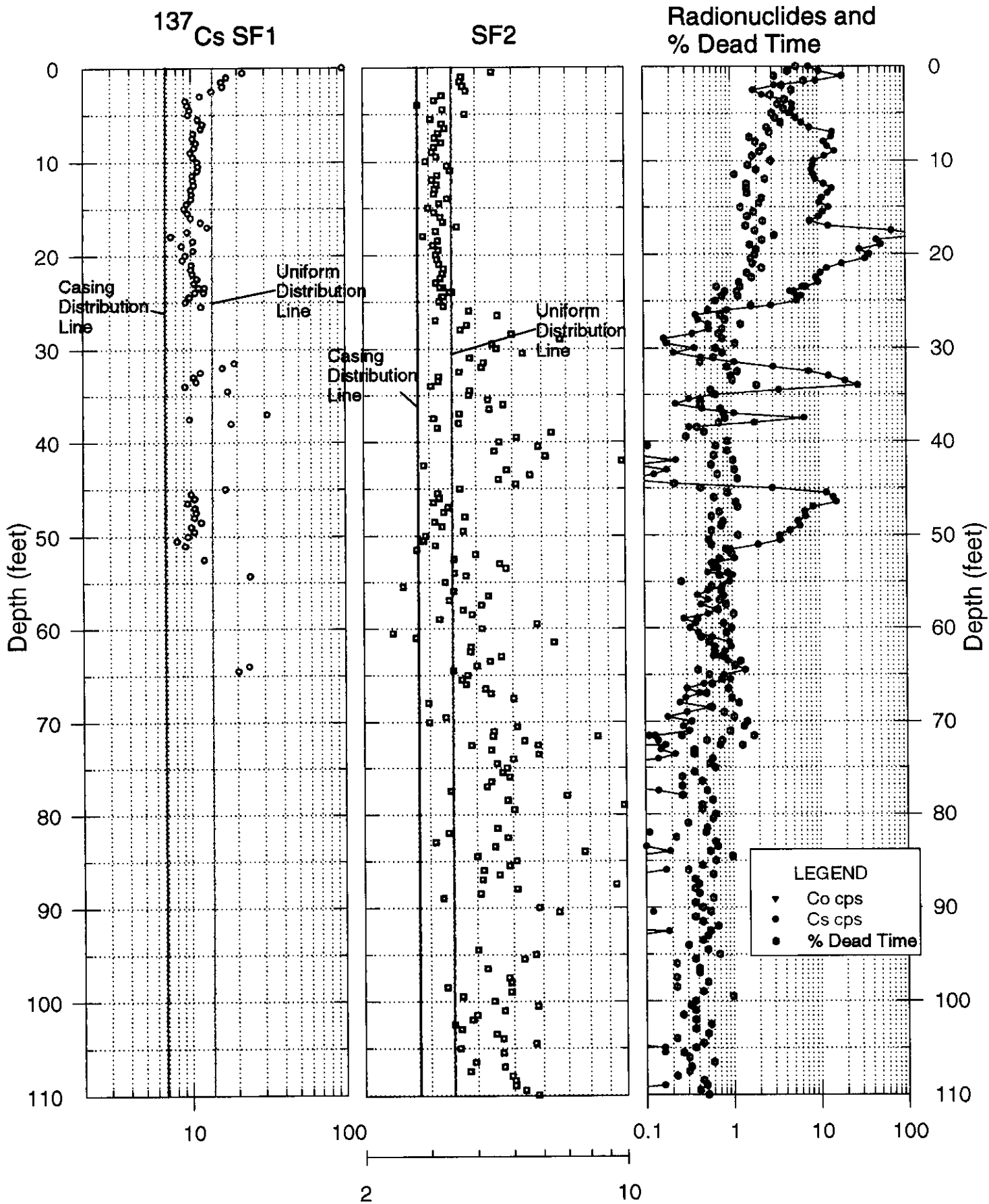


30-04-05  
Shape Factor Analysis Logs

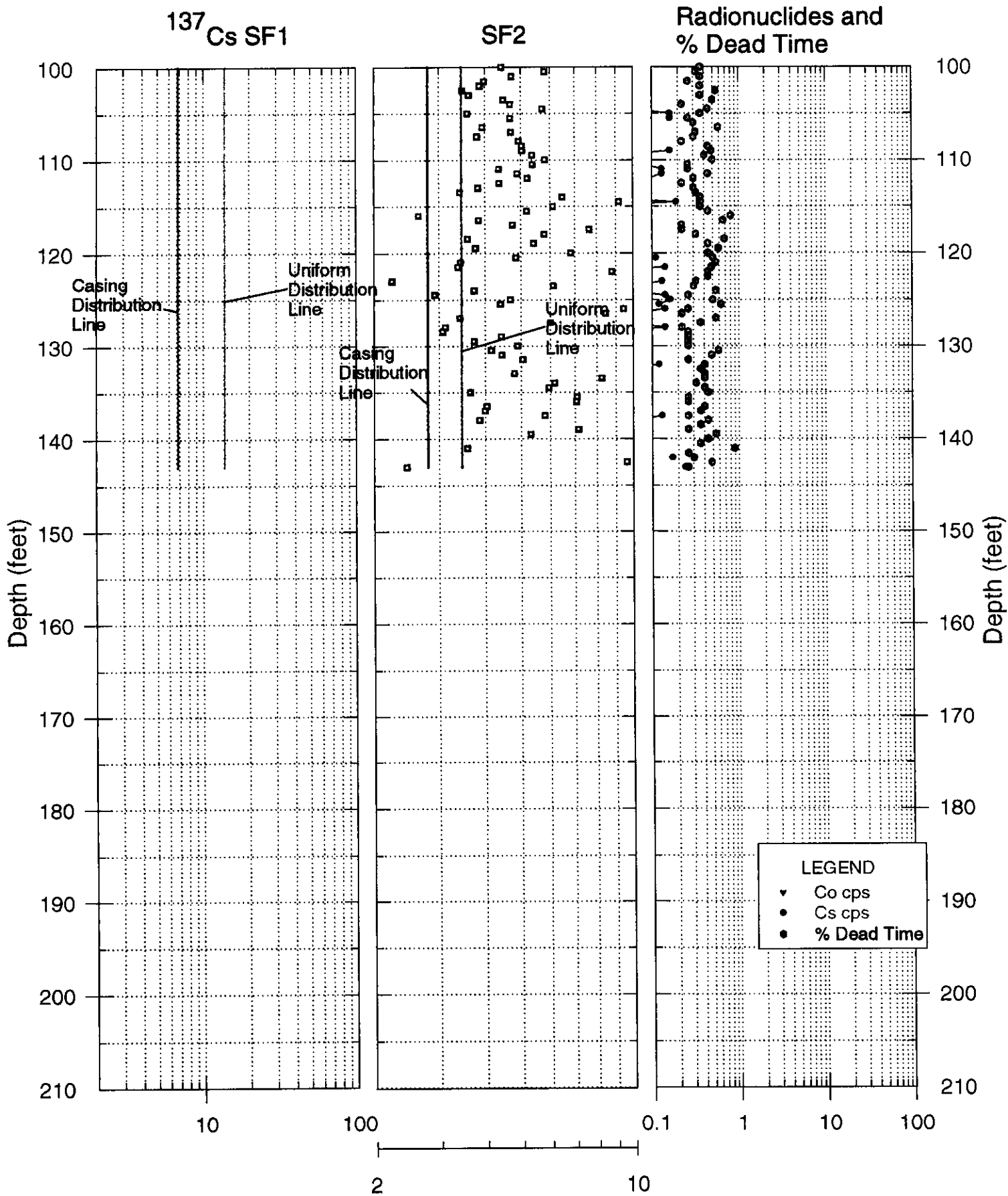


30-04-08

# Shape Factor Analysis Logs

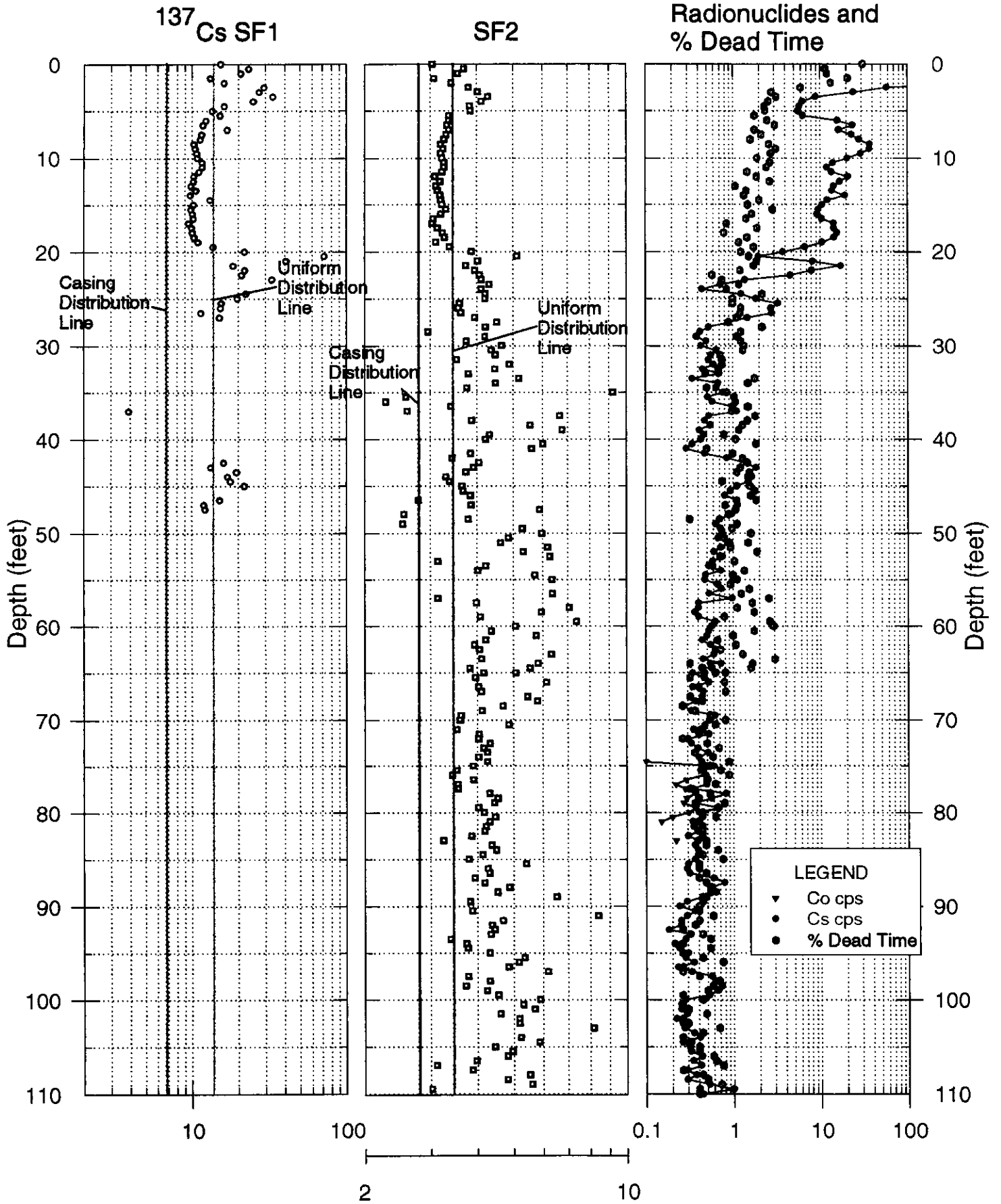


# 30-04-08 Shape Factor Analysis Logs

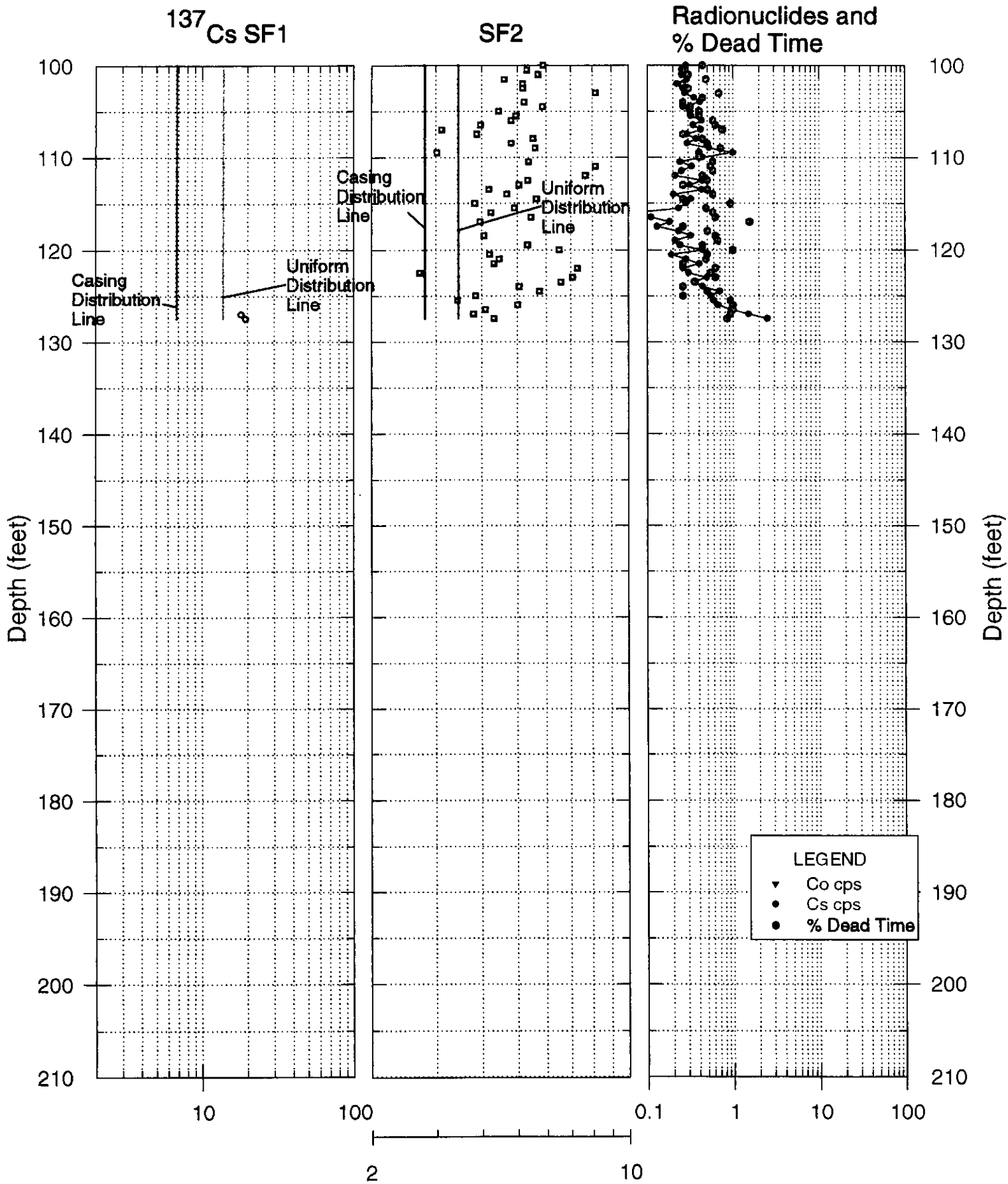


30-05-02

# Shape Factor Analysis Logs

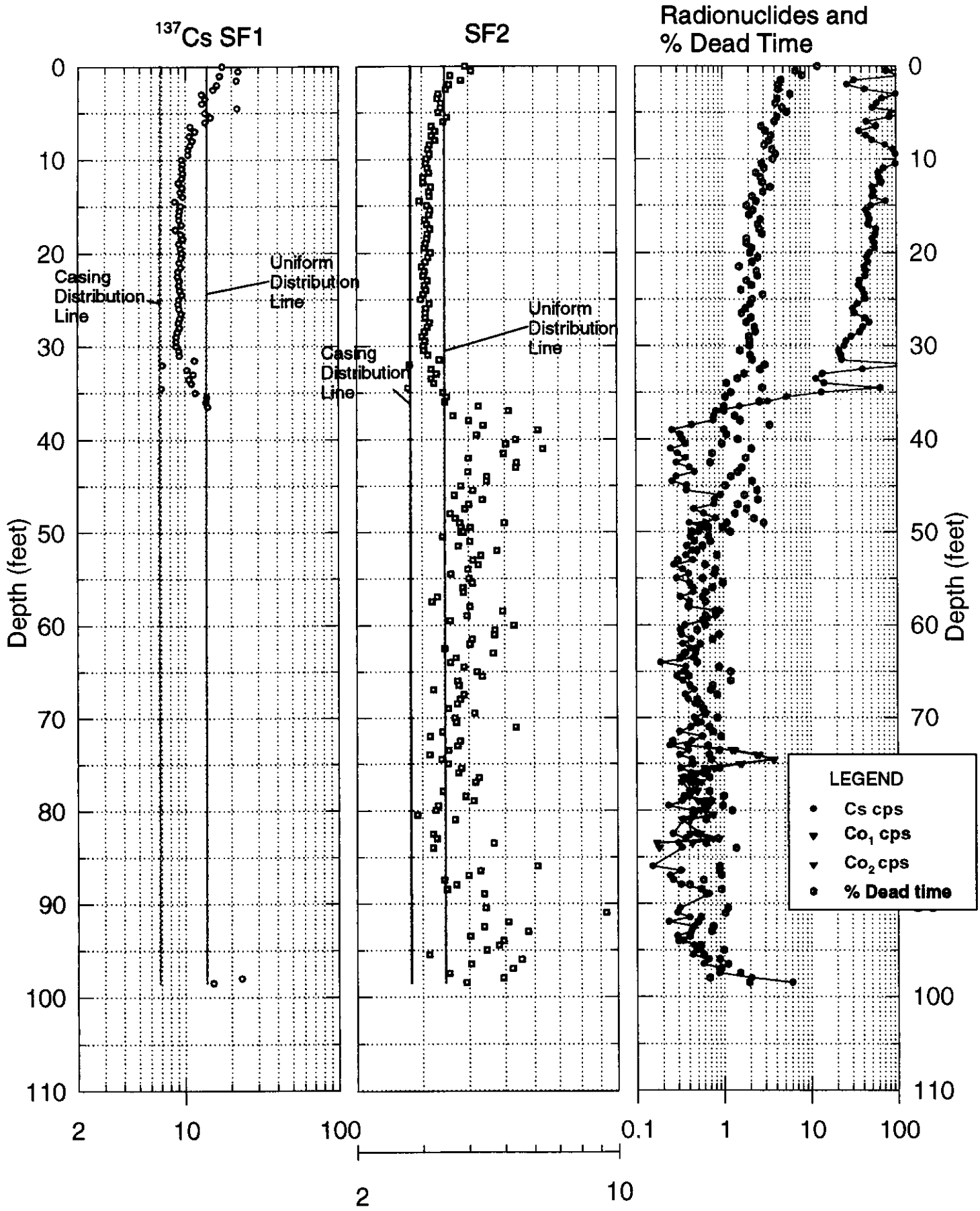


# 30-05-02 Shape Factor Analysis Logs

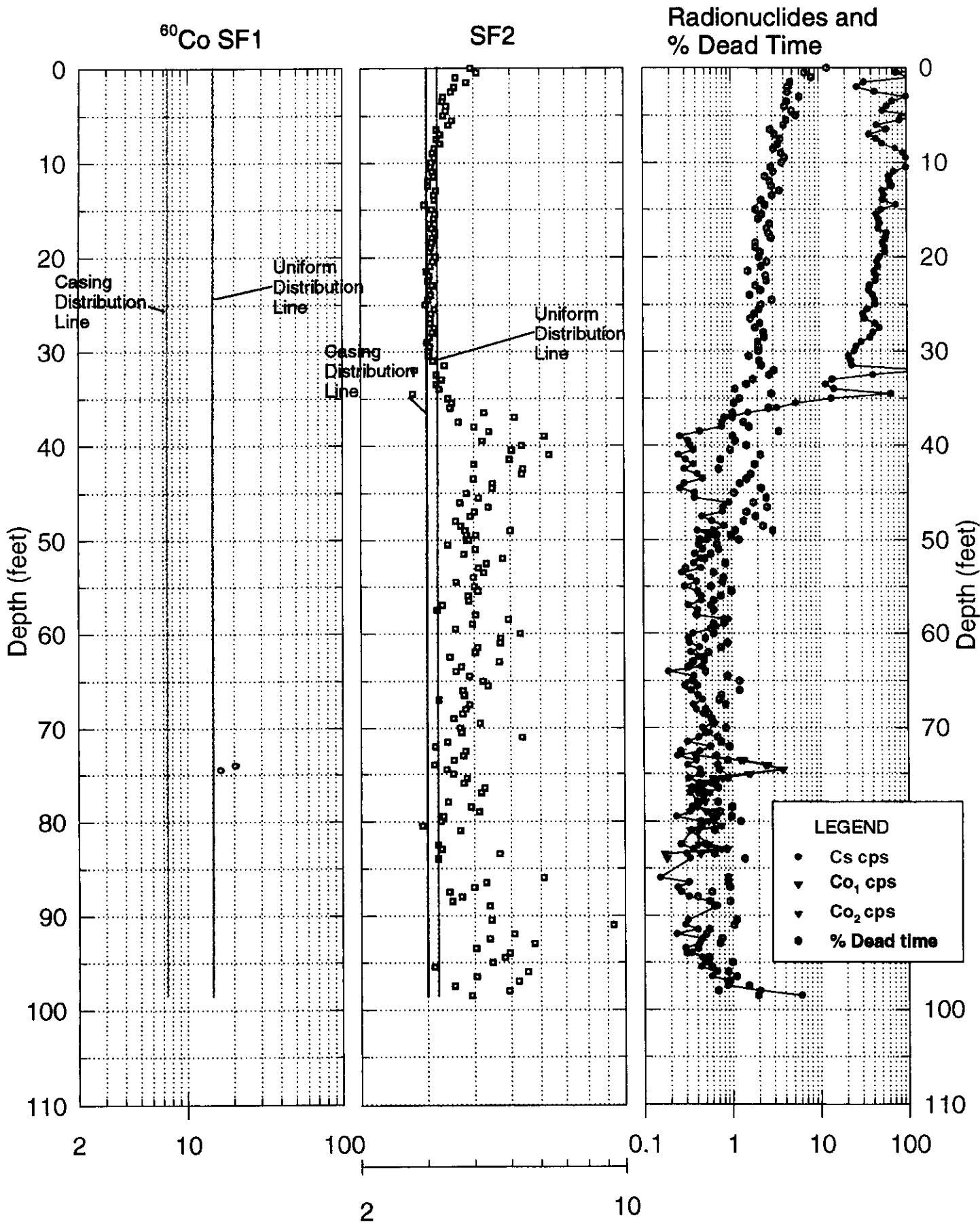


30-05-03

# Shape Factor Analysis Logs

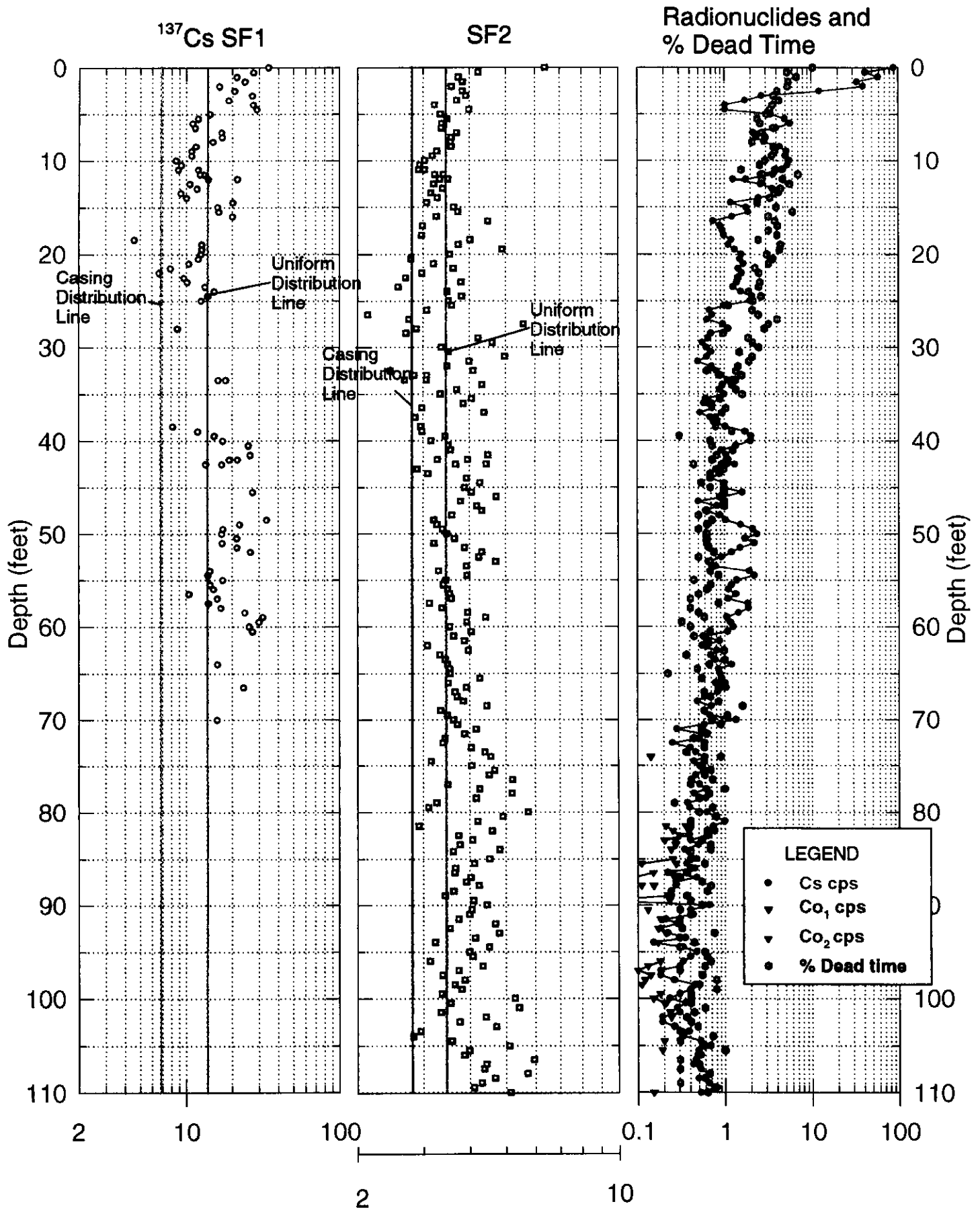


# 30-05-03 Shape Factor Analysis Logs



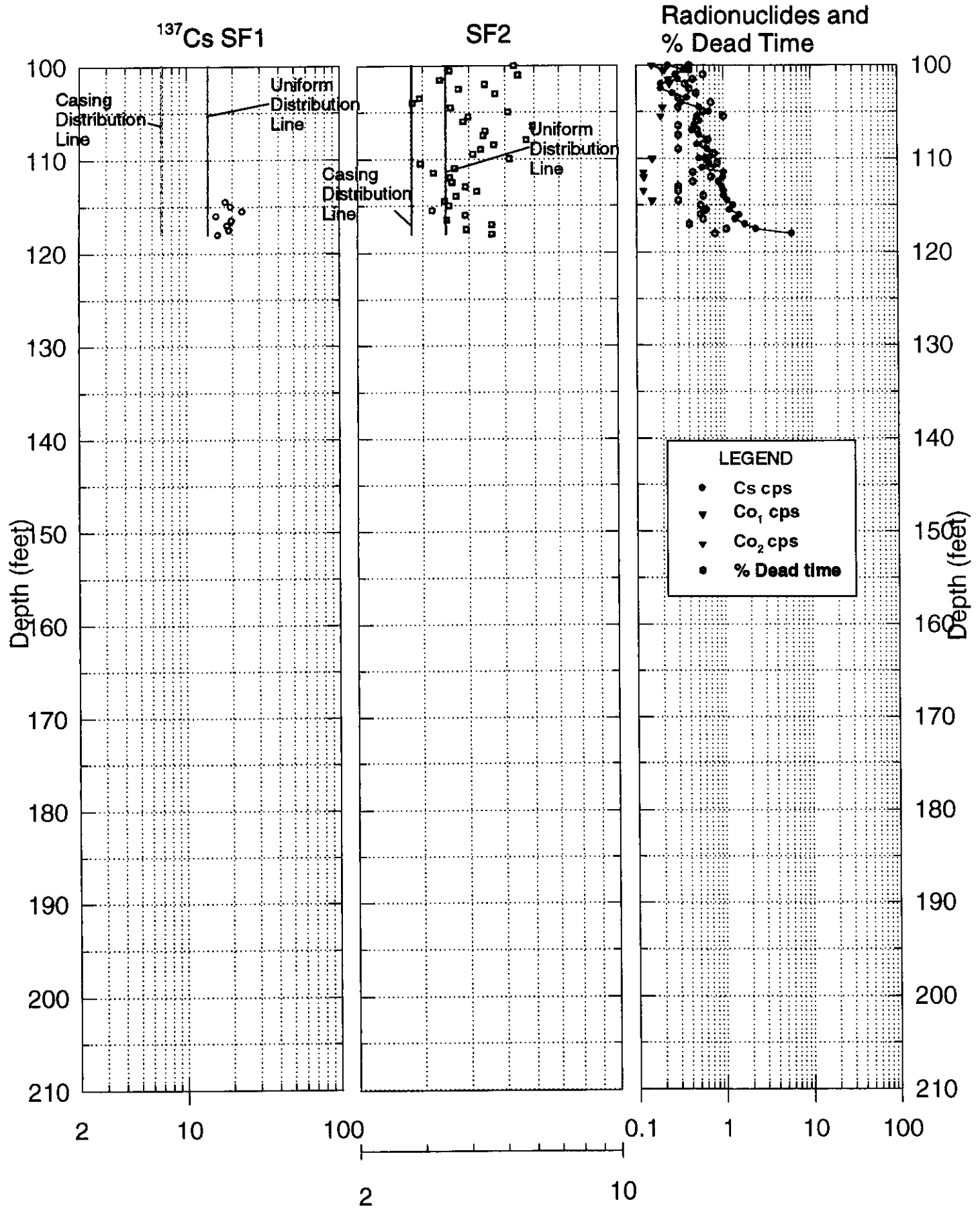
30-05-04

# Shape Factor Analysis Logs

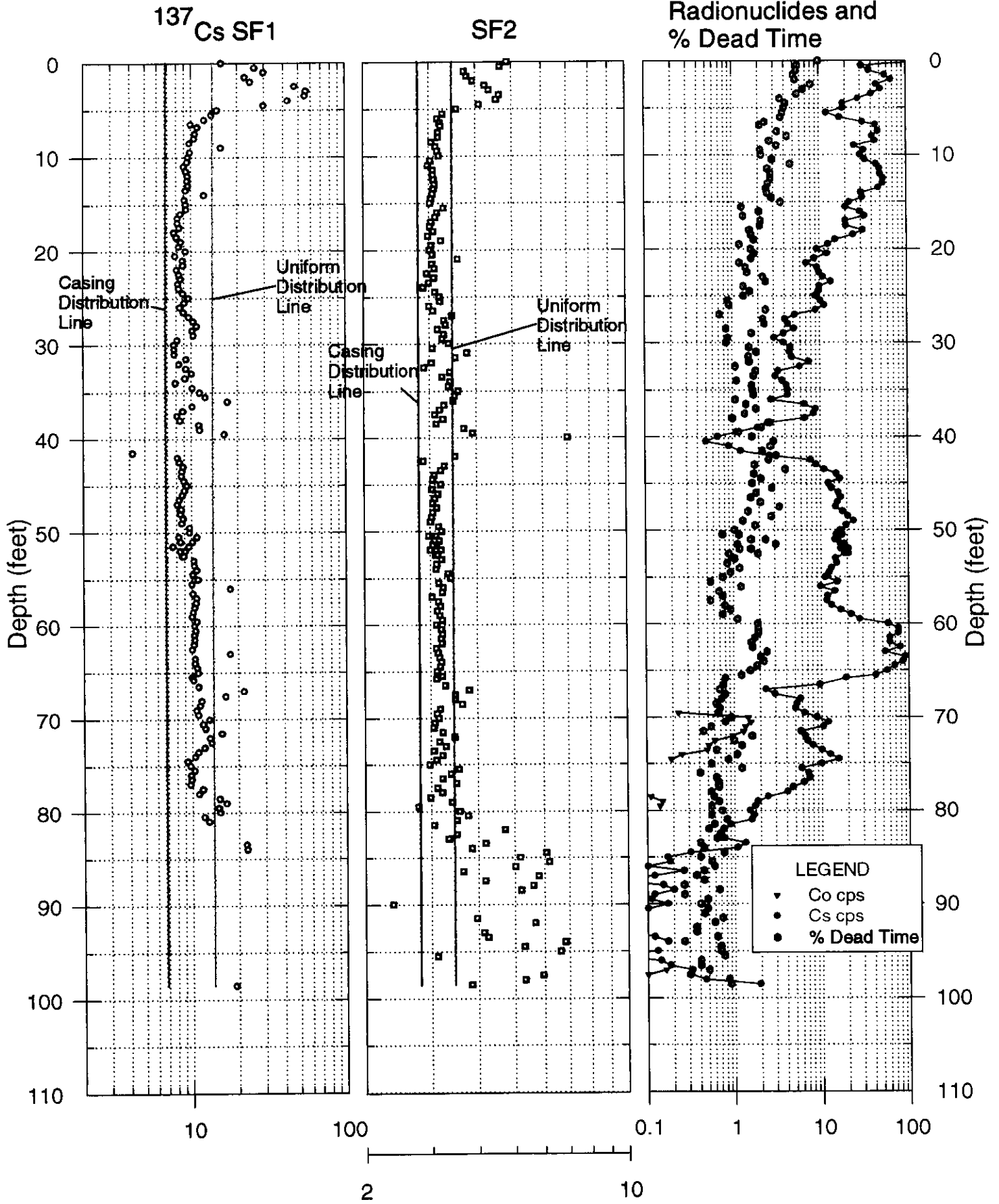


30-05-04

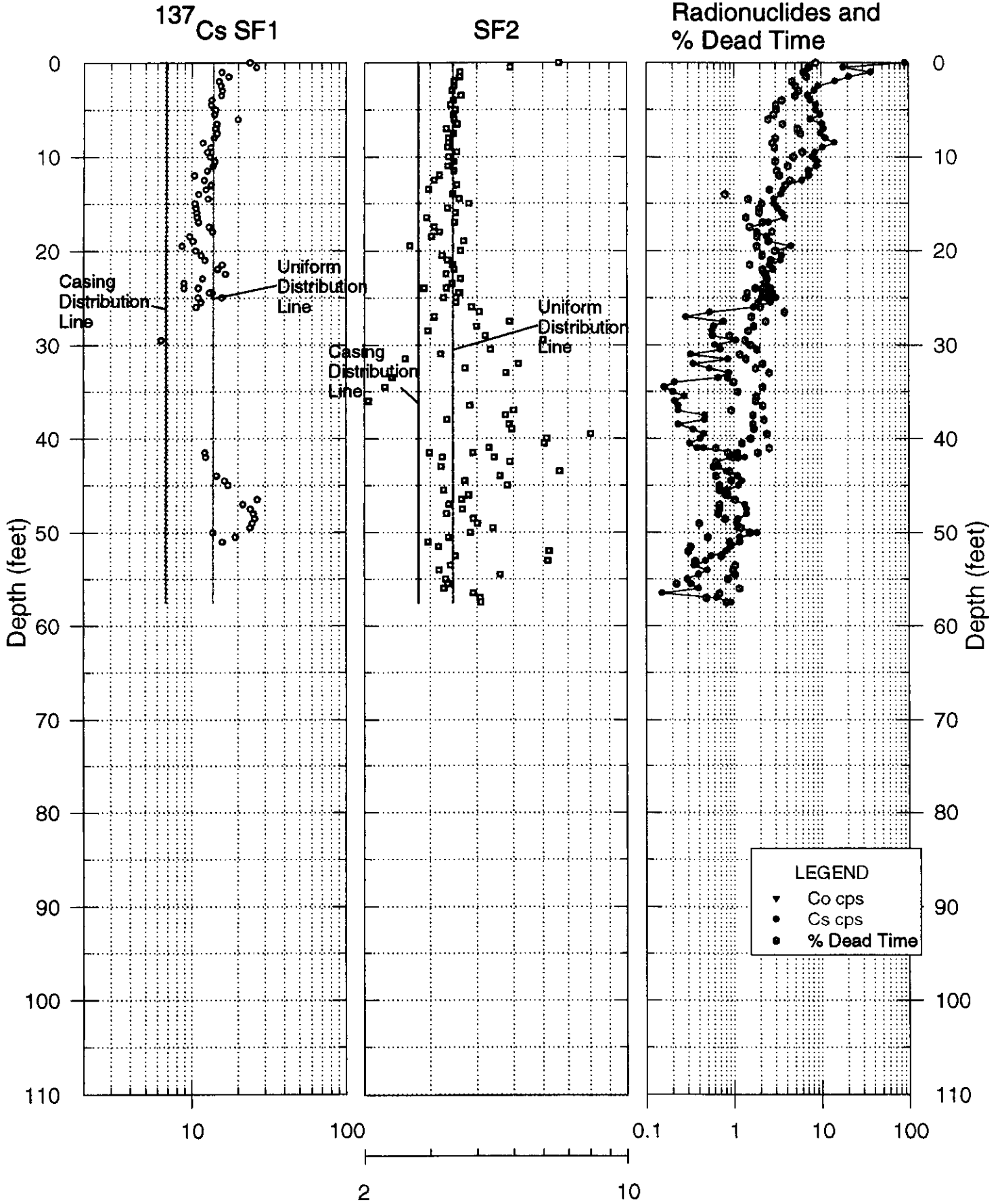
# Shape Factor Analysis Logs



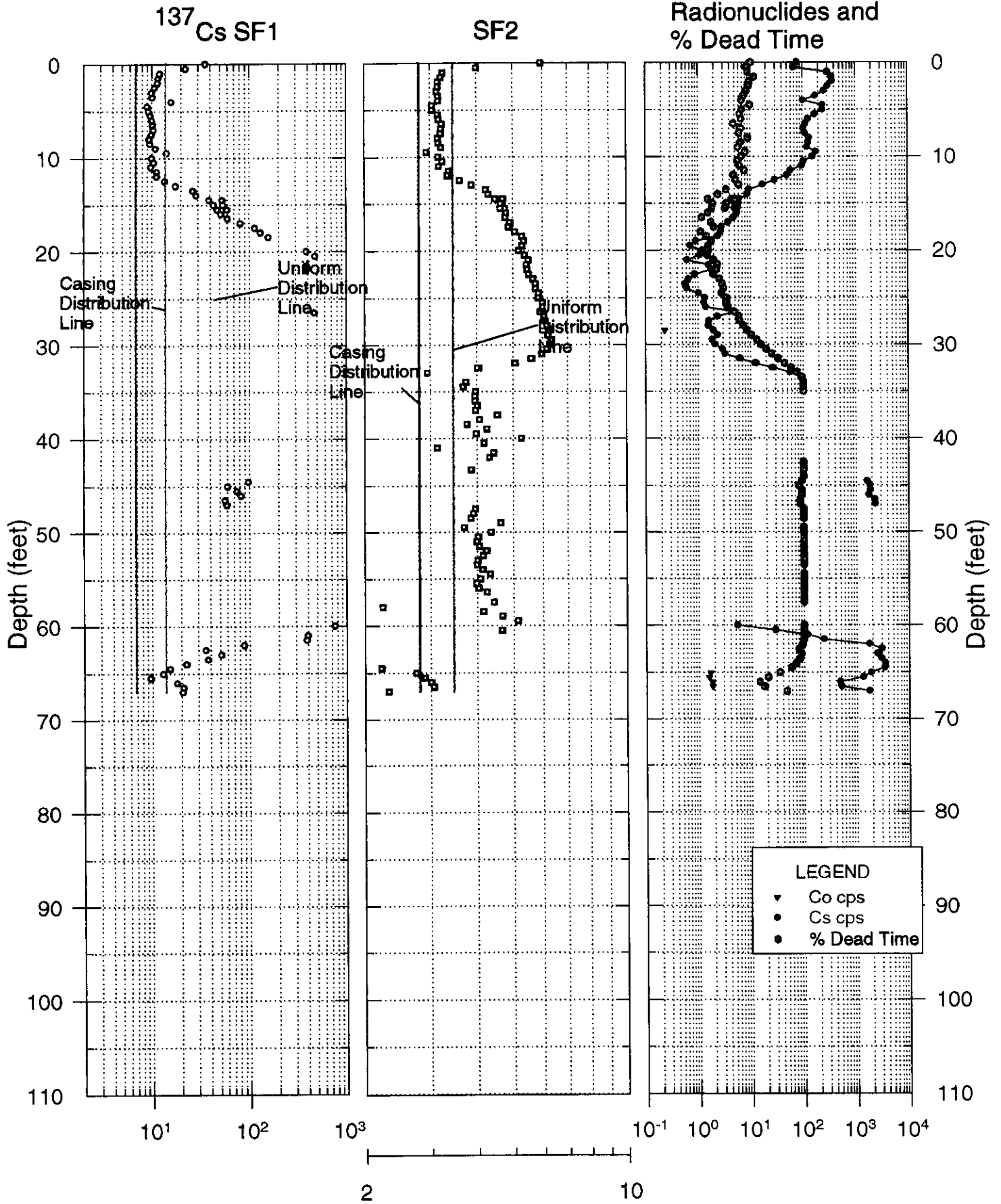
30-05-05  
Shape Factor Analysis Logs



# 30-05-06 Shape Factor Analysis Logs

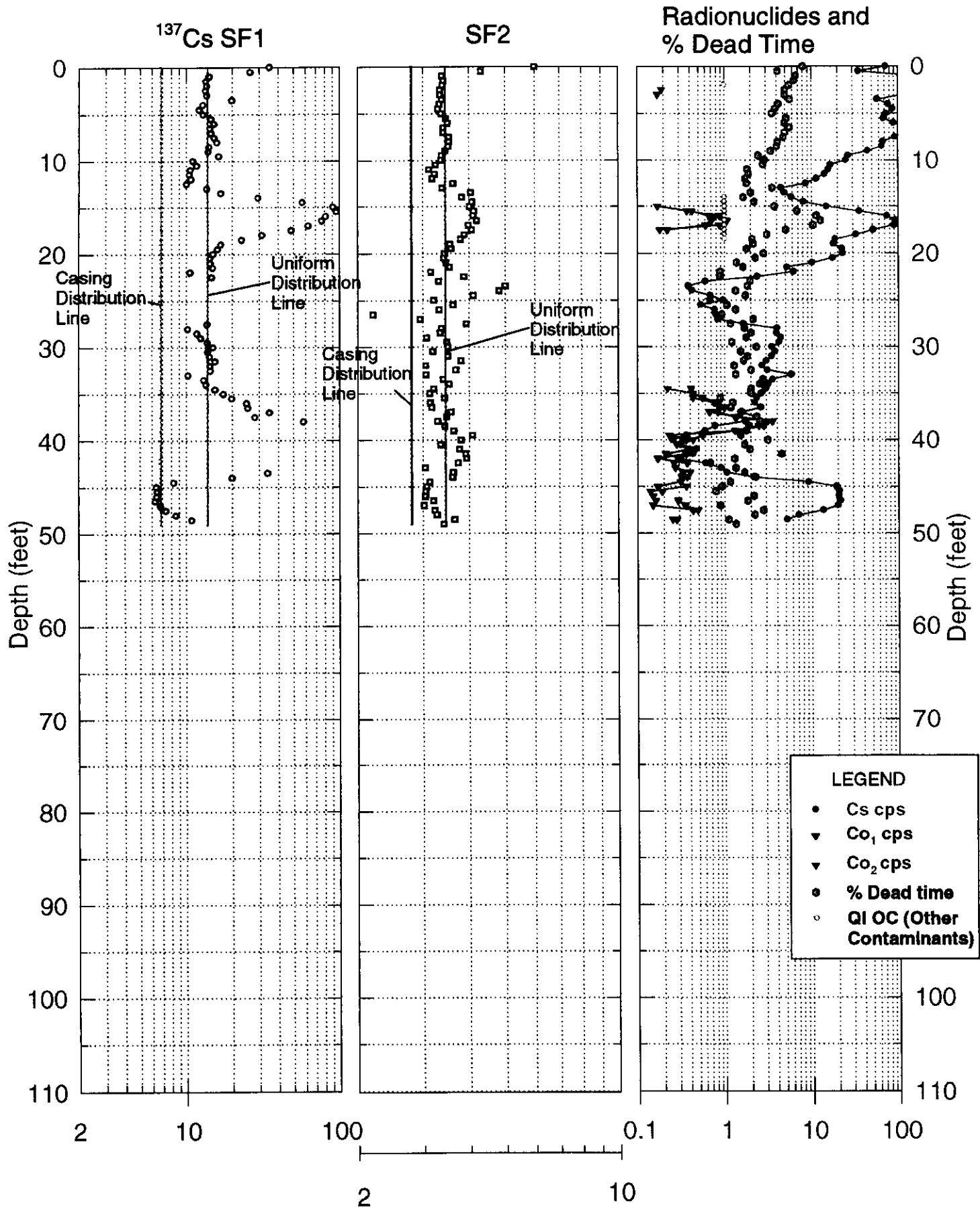


# 30-05-07 Shape Factor Analysis Logs



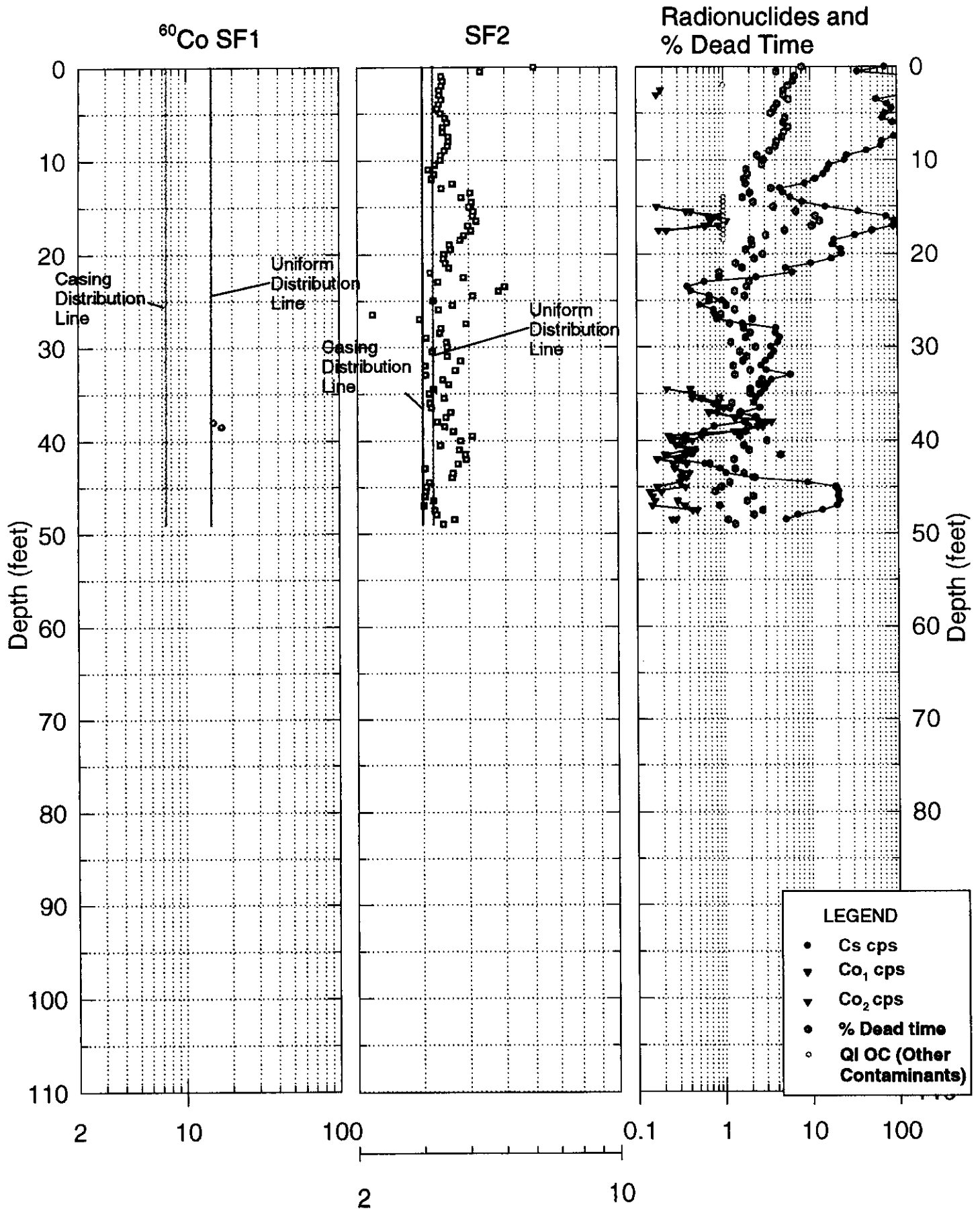
30-05-08

# Shape Factor Analysis Logs

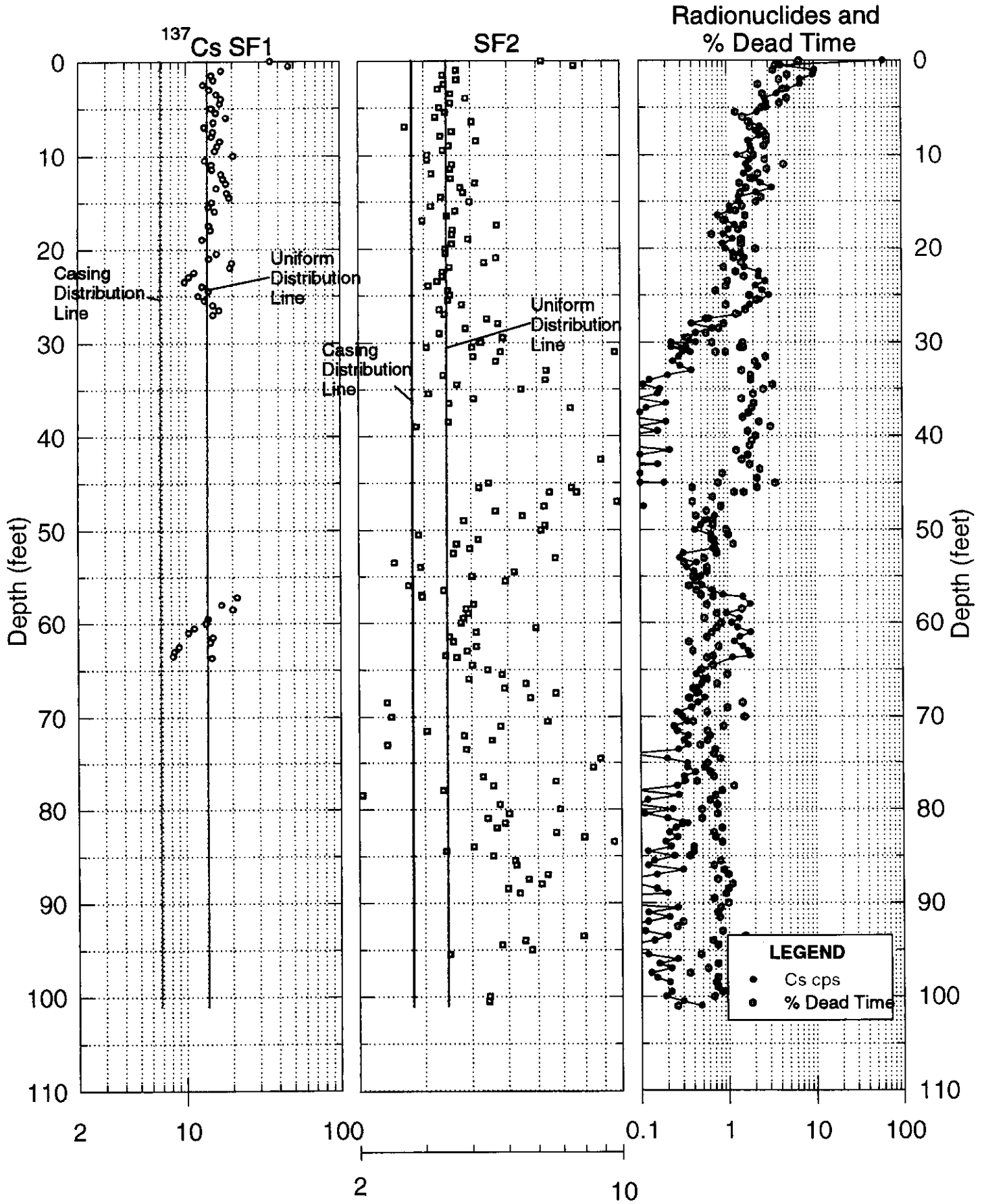


30-05-08

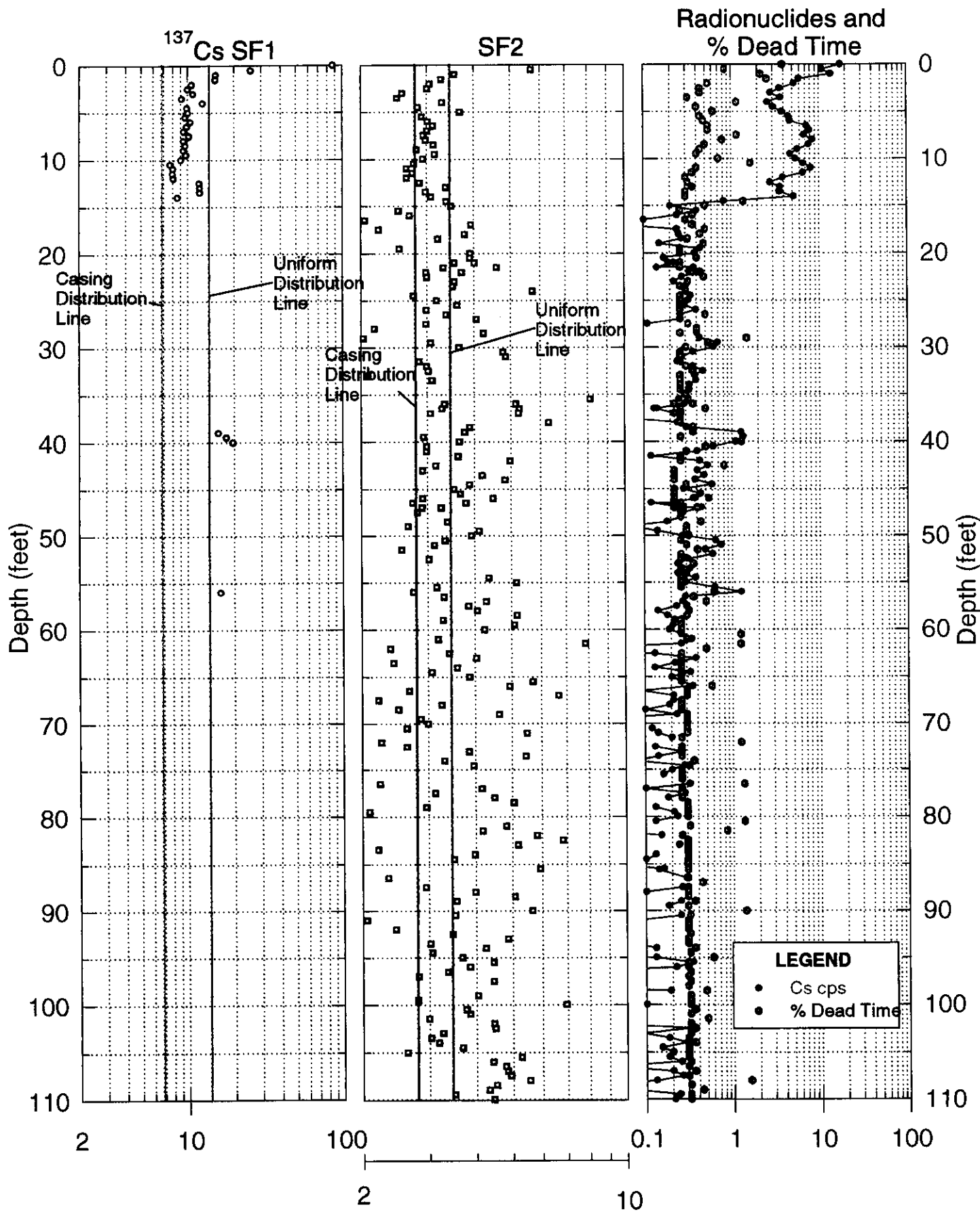
# Shape Factor Analysis Logs



30-05-09  
Shape Factor Analysis Logs

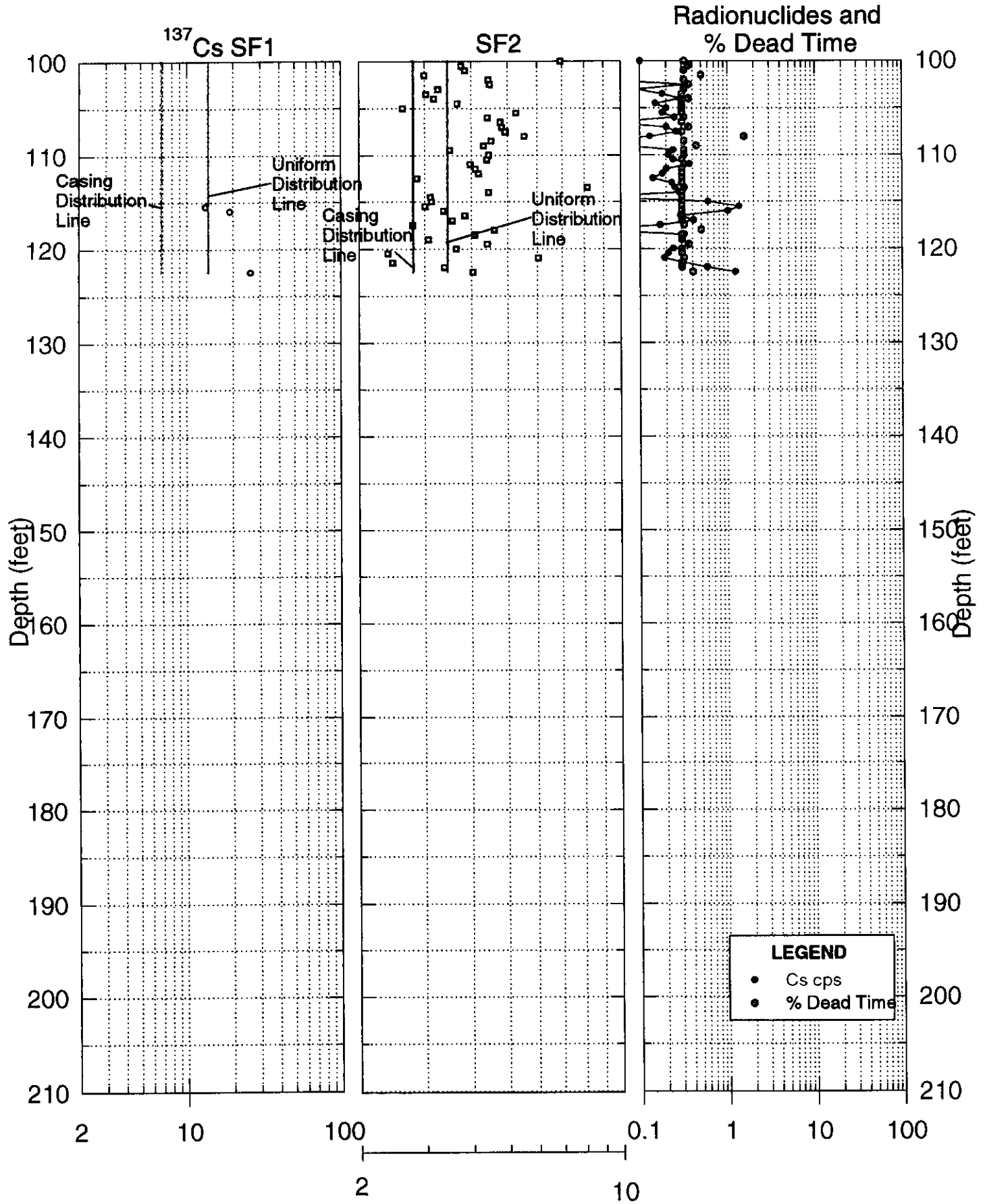


30-06-02  
Shape Factor Analysis Logs



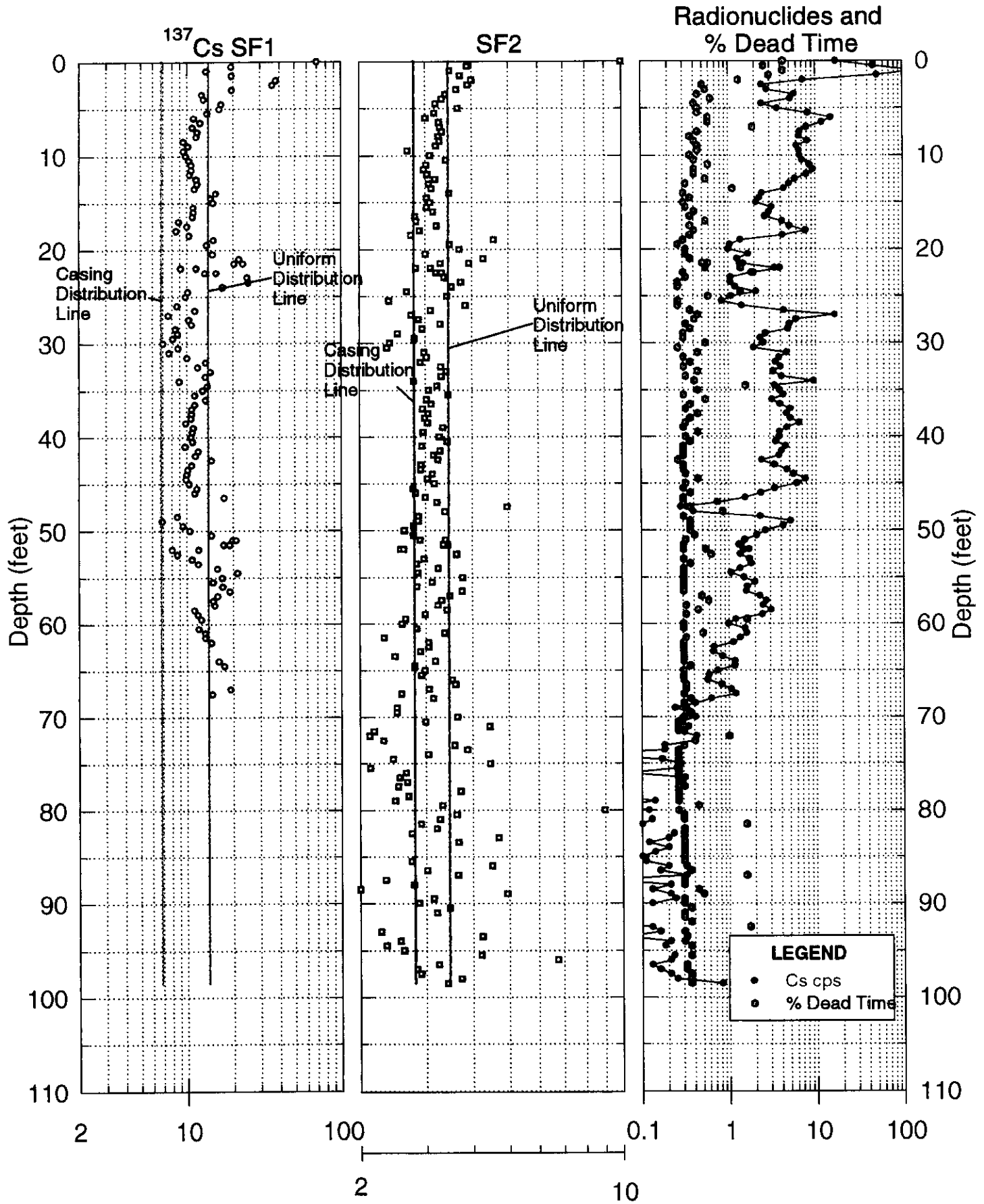
30-06-02

# Shape Factor Analysis Logs



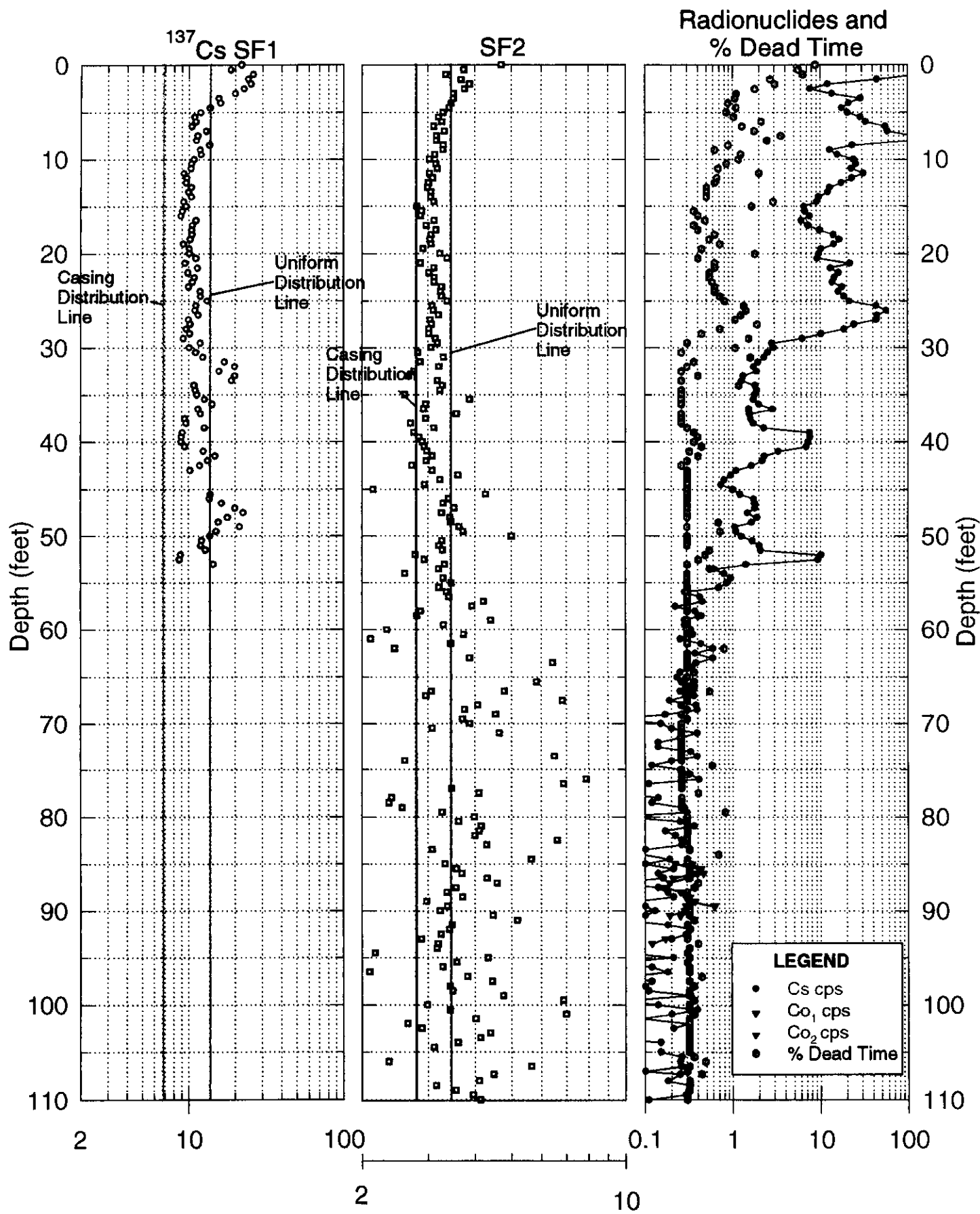
30-06-03

# Shape Factor Analysis Logs

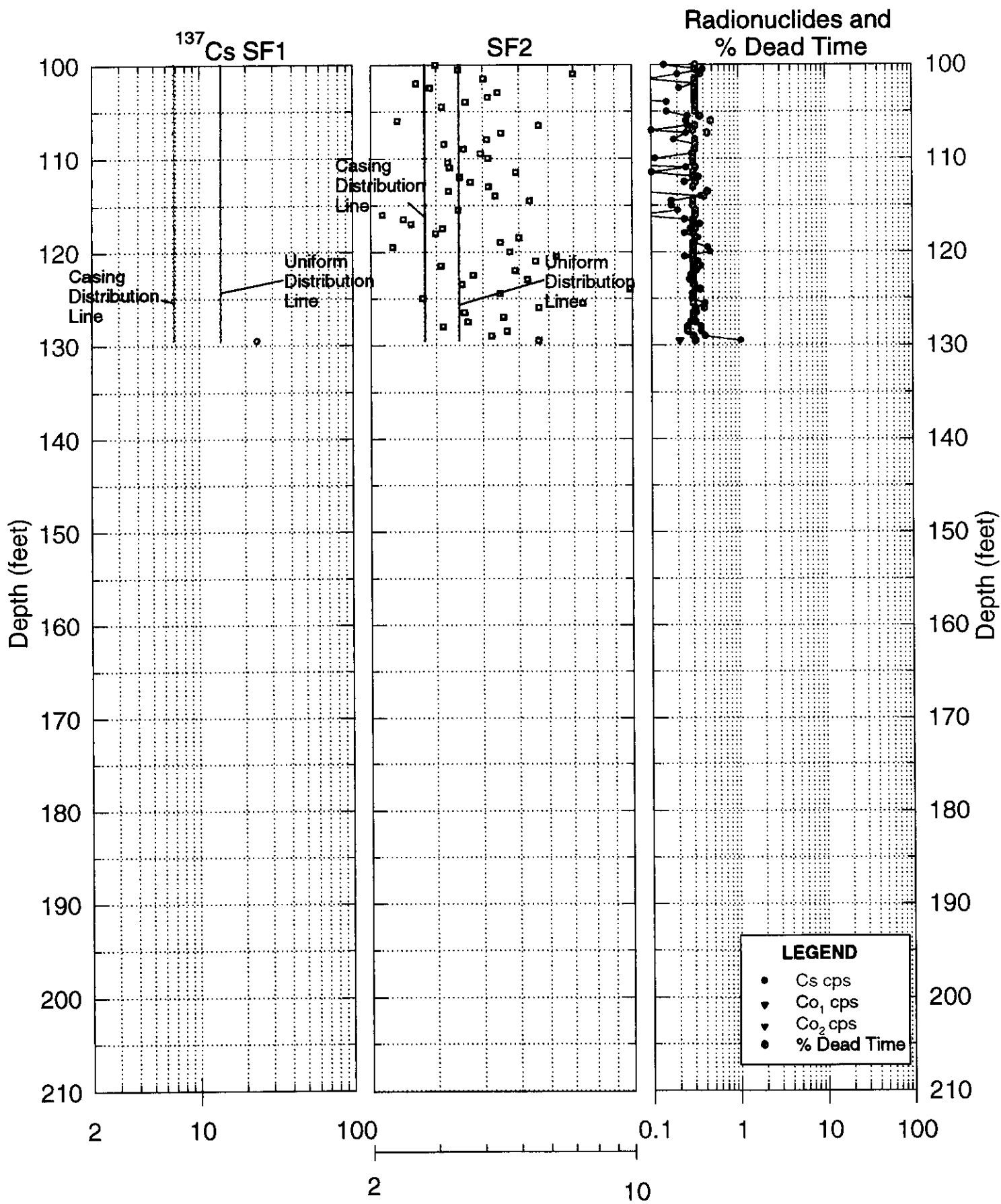


30-06-04

# Shape Factor Analysis Logs

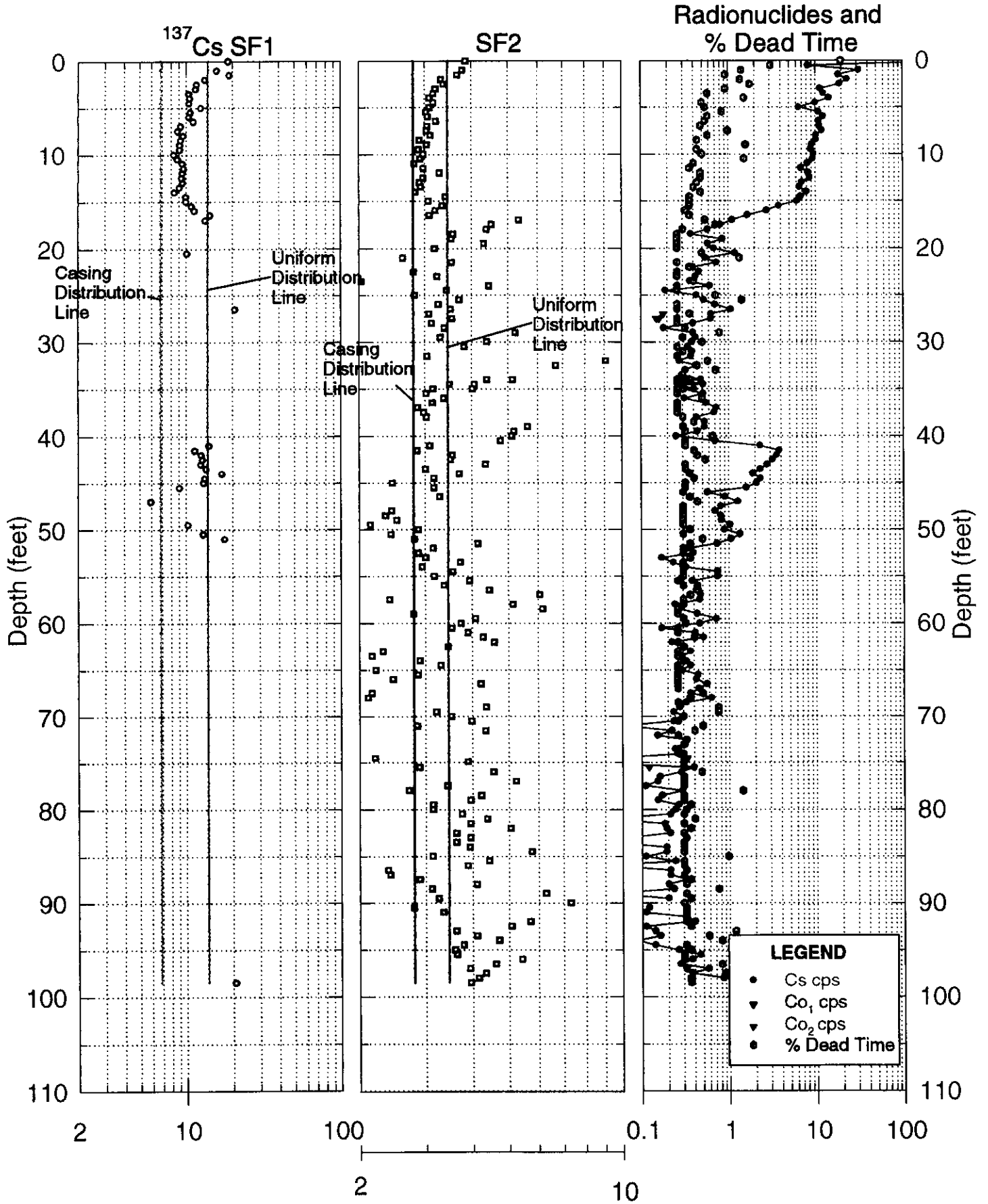


# 30-06-04 Shape Factor Analysis Logs

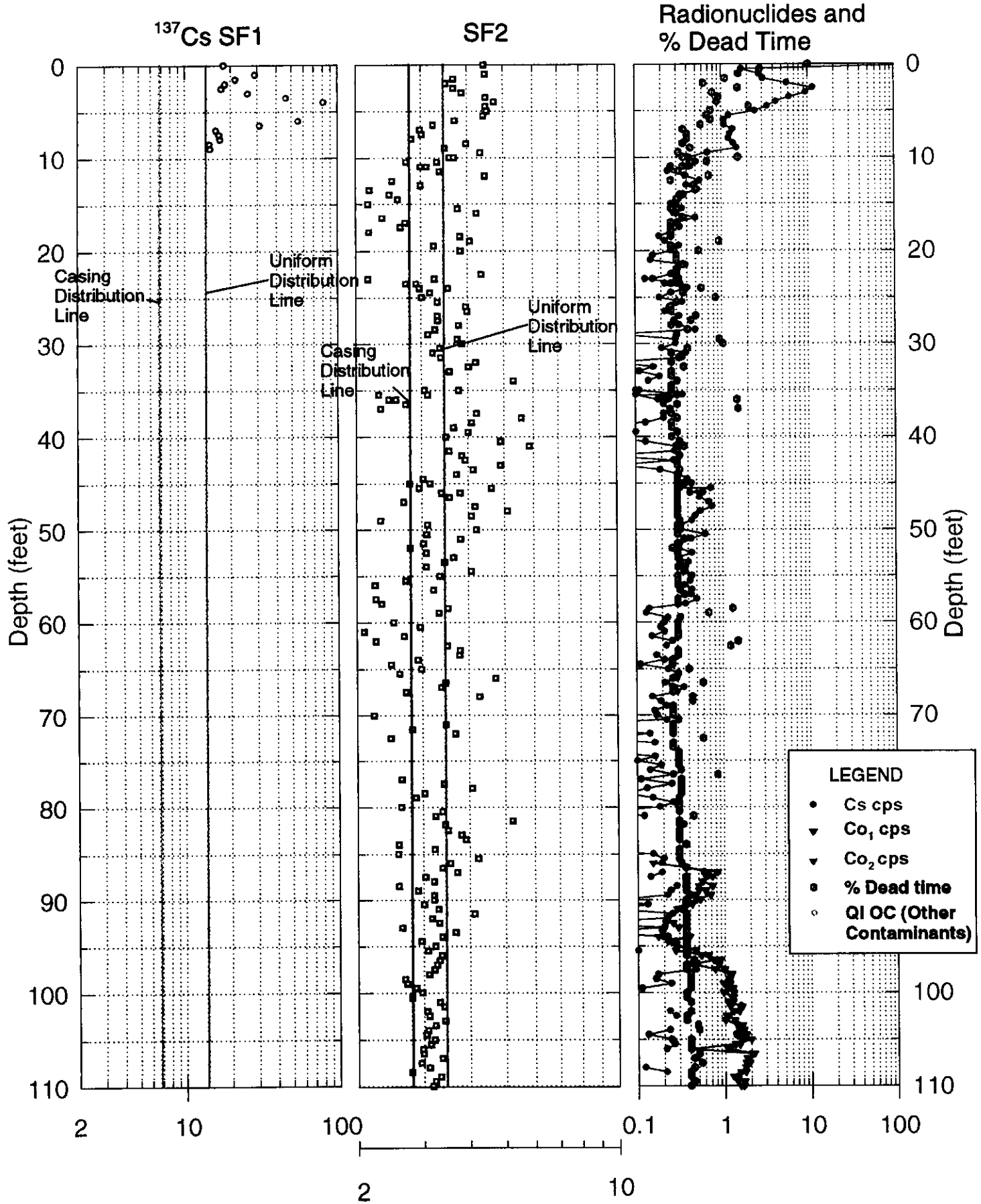


30-06-09

# Shape Factor Analysis Logs

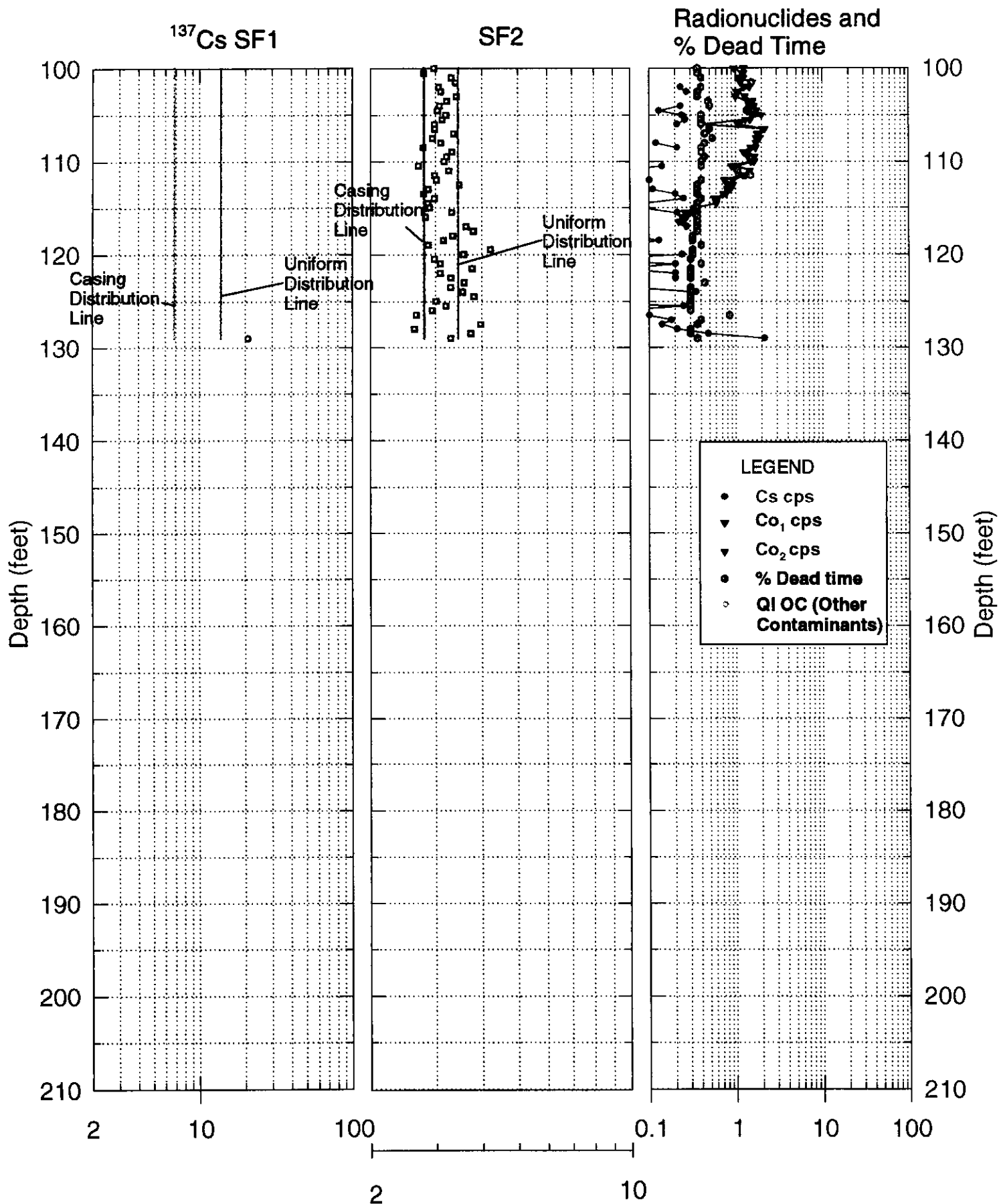


# 30-06-10 Shape Factor Analysis Logs

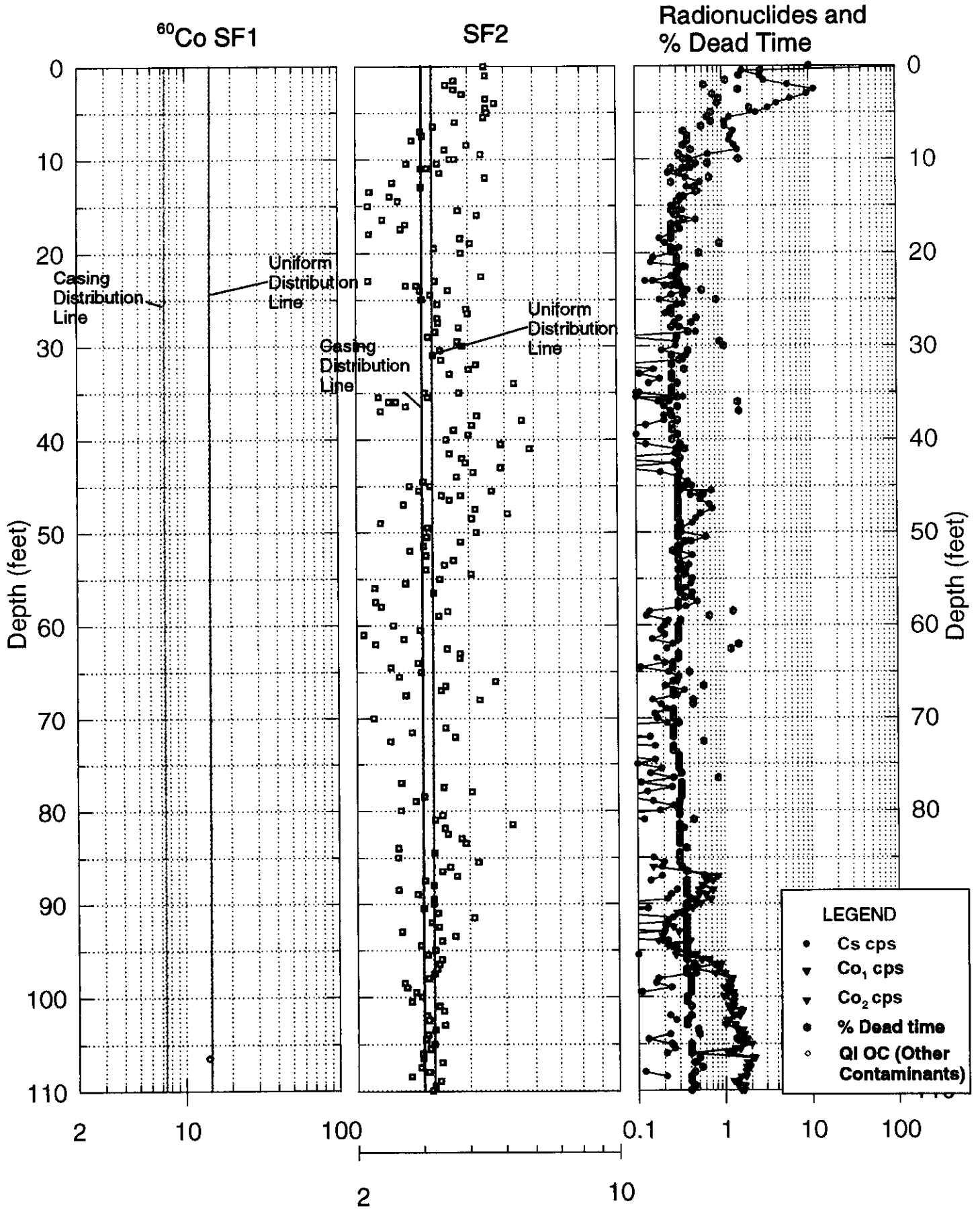


30-06-10

# Shape Factor Analysis Logs

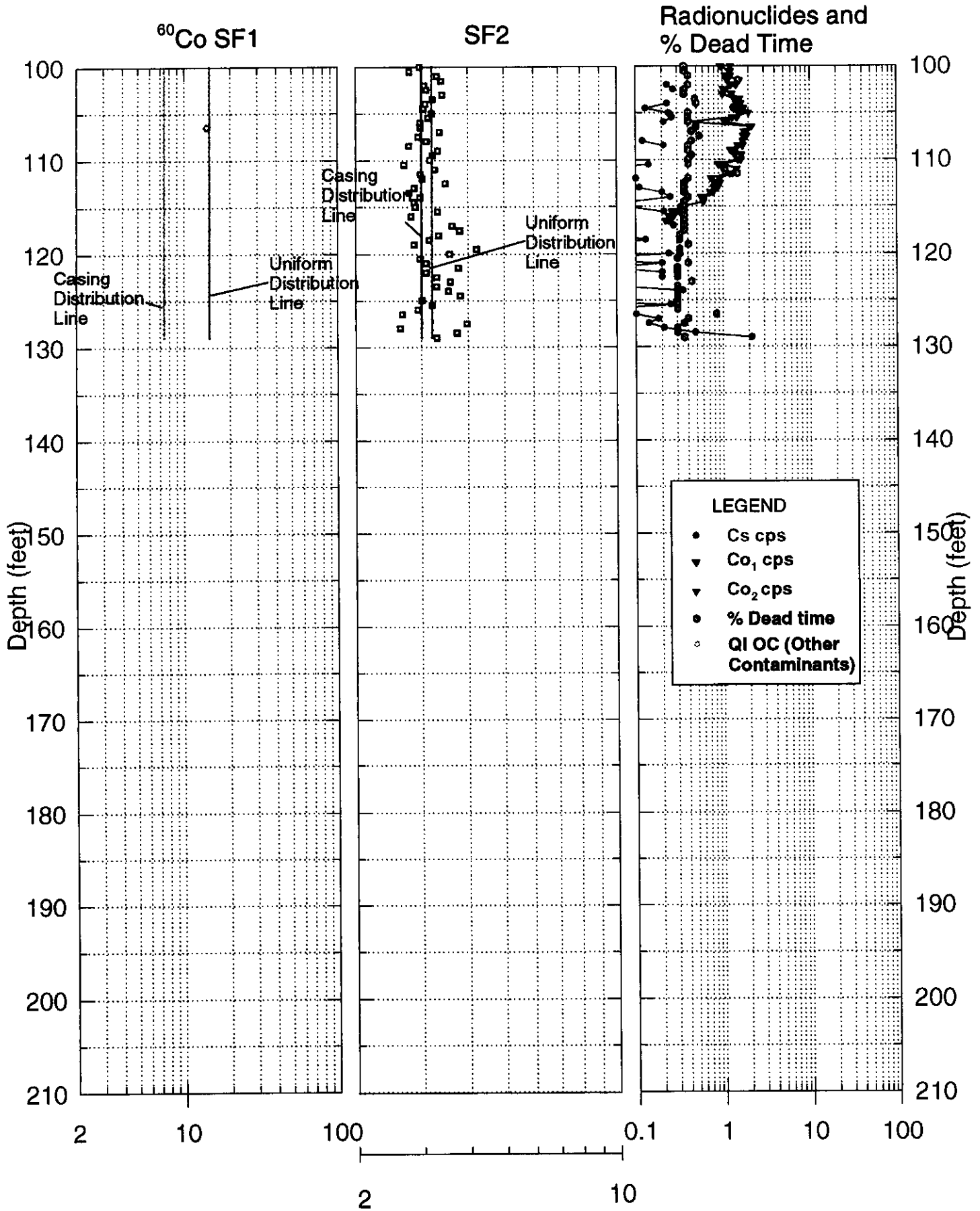


# 30-06-10 Shape Factor Analysis Logs



30-06-10

# Shape Factor Analysis Logs



30-06-12  
Shape Factor Analysis Logs

